

NACRE II: an update of the NACRE compilation of charged-particle-induced thermonuclear reaction rates for nuclei with mass number $A < 16$

Y. Xu^{a,1}, K. Takahashi^{a,b}, S. Goriely^a, M. Arnould^{a,*}

^a*Institut d'Astronomie et d'Astrophysique, Université Libre de Bruxelles, Belgium*

^b*GSI Helmholtzzentrum für Schwerionenforschung, Darmstadt, Germany*

M. Ohta^{c,d}, H. Utsunomiya^d

^c*Hirao School of Management, Konan University, Kobe, Japan*

^d*Department of Physics, Konan University, Kobe, Japan*

Abstract

An update of the NACRE compilation [Angulo et al., Nucl. Phys. A 656 (1999) 3] is presented. This new compilation, referred to as NACRE II, reports thermonuclear reaction rates for 34 charged-particle induced, two-body exoergic reactions on nuclides with mass number $A < 16$, of which fifteen are particle-transfer reactions and the rest radiative capture reactions. When compared with NACRE, NACRE II features in particular (1) the addition to the experimental data collected in NACRE of those reported later, preferentially in the major journals of the field by early 2013, and (2) the adoption of potential models as the primary tool for extrapolation to very low energies of astrophysical S -factors, with a systematic evaluation of uncertainties.

As in NACRE, the rates are presented in tabular form for temperatures in the $10^6 \lesssim T \leq 10^{10}$ K range. Along with the 'adopted' rates, their low and high limits are provided. The new rates are available in electronic form as part of the Brussels Library (BRUSLIB) of nuclear data. The NACRE II rates also supersede the previous NACRE rates in the Nuclear Network Generator (NETGEN) for astrophysics. [<http://www.astro.ulb.ac.be/databases.html>.]

Keywords: thermonuclear reaction rates, nuclear astrophysics, potential model, dwba model

PACS: 24.50.+g; 24.30.-v; 25.10.+s

*Corresponding author. E-mail address: marnould@ulb.ac.be (M. Arnould)

¹Current address: Cyclotron Institute, Texas A&M University, College Station, TX 77843, USA

1. Introduction

The series of publications of William A. Fowler and his collaborators, starting with their pioneering work in 1967 [1] and extending up to 1988 [2] (often referred to as CF88), demonstrated in the most vivid way the pivotal role played by compilations of charged-particle induced thermonuclear reaction rates at sub-Coulomb energies in the fields of stellar structure and evolution models as well as of nucleosynthesis investigations.

The so-called NACRE (Nuclear Astrophysics Compilation of REactions) database [3] marked the beginning of a second generation of such astrophysics-oriented compilations. Since its publication in 1999, the compilation has indeed been used in great many astrophysical model calculations. Its aim was to supersede the previous compilations not only by using newly available experimental data as inputs, but also by introducing fundamentally new aspects to their format. Among others, NACRE featured (1) explicit references to the sources of the experimental data (and to some theoretical works) considered; (2) a documentation on the procedure of evaluation of those data; (3) the assessment of uncertainties in the reaction rates, with the lower and higher limits being presented along with the 'adopted' values, and (4) a tabular presentation of the rates for temperatures in the $10^6 \lesssim T \leq 10^{10}$ K range. (See [3] for more details).

Slightly more than half of the CF88 rates were re-compiled in NACRE on the basis of a careful evaluation of experimental data that became available by mid-June 1998. Comprised in NACRE is an ensemble of 86 charged-particle induced reactions on stable targets up to Si involved in Big Bang nucleosynthesis and in the non-explosive H- and He-burning modes, complemented with a limited number of reactions of special astrophysical significance on the unstable ^3H , ^7Be , ^{13}N , ^{22}Na and ^{26}Al nuclides.²

Since NACRE, many cross sections of astrophysical interest have been measured or re-measured, and additional efforts have been put forth toward better predictions of the required reaction rates. In particular: thermonuclear reaction rates of relevance to the Big Bang nucleosynthesis have been re-evaluated with the use of the R-matrix method [4]; the current status of experimental and theoretical studies of astrophysical *S*-factors of solar fusion reactions have been thoroughly surveyed [5]; an extended re-evaluation of reaction rates of charged-particle induced reactions on nuclei with mass number in the $14 \leq A \leq 40$ range together with the associated uncertainties has been prepared with the help of a Monte-Carlo simulation [6 - 9].

In parallel to those developments, it was thought in 2004 that the time was ripe for an update and an extension of NACRE. This project, referred to as NACRE II, was launched through a formal collaboration between the Konan University (Kobe, Japan) and the Université Libre de Bruxelles (Brussels, Belgium). Several preliminary accounts of NACRE II have appeared sporadically [10 - 16].³ In the meantime, the initial work programme has been adapted as much as possible in order to minimize the overlap with the other compilation works. The consequent compilation has a scope and/or pursues a course different from those of [4, 5], and complements the most recent compilation

²The NACRE homepage <http://pntpmp.ulb.ac.be/Nacre> is also accessible through the BRUSLIB website <http://www-astro.ulb.ac.be>.

³The Konan-ULB Collaboration formally ended at the end of March, 2009. An unfortunate incident, however, incapacitated the compilation work from being completed at that time. The NACRE-II project was resumed in the present form in September, 2009.

[6 - 9] by considering reactions on 'target' nuclides with mass numbers $A < 16$. More specifically: the current version of NACRE II surveys 34 two-body exoergic reactions (15 particle transfer and 19 radiative capture reactions), and adopts potential models to phenomenologically describe and extrapolate resonant and non-resonant reaction cross sections at low energies of interest.

Section 2 briefly reviews the theoretical models underlying the present compilation, and the procedure followed for evaluating the reaction rates. Section 3 is composed of subsections, each of which is designated for the results for a specific reaction. Section 4 presents a short summary. Appendices supplement the main text with the tables of the adopted values of the model parameters, and of the reverse two-body reaction rates.

2. The Method

2.1. The quantities in quest

The thermonuclear reaction rates of a two-body reaction $A(a, b)B$, which are in quest for astrophysical modellings, are canonically expressed by the Maxwellian-averaged rate $\langle \sigma v \rangle$ times the Avogadro number N_A (e.g. [17, 18]),

$$N_A \langle \sigma v \rangle = N_A \frac{(8/\pi)^{1/2}}{\mu^{1/2}(k_B T)^{3/2}} \int_0^\infty E \sigma(E) \exp[-E/(k_B T)] dE, \quad (1)$$

where $\sigma(E)$ is the reaction cross section at the centre-of-mass incident energy $E = \mu v^2/2$ with v being the relative velocity and $\mu = m_A m_a / (m_A + m_a)$ the reduced mass with m_A and m_a standing for the masses of target (A) and projectile (a) nuclei, while k_B is the Boltzmann constant and T is the temperature.

In dealing with charged-particle induced reactions at very low energies below the Coulomb barrier, it is more convenient, and indeed customary, to introduce the astrophysical S -factor, $S(E)$, which is classically defined as

$$S(E) = E \sigma(E) \exp[2\pi\eta], \quad (2)$$

where $\eta = Z_A Z_a e^2 / (\hbar v)$ is the Sommerfeld parameter, with $Z_A Z_a e^2$ being the product of the nuclear charges of A and a . This definition allows the S -factor to exhibit a much weaker energy dependence at low energies than that of the cross section itself, easing the comparison between predictions and experimental data, as well as the extrapolation at lower energies.

In practice, the rate is commonly expressed in $\text{cm}^3 \text{mol}^{-1} \text{s}^{-1}$, such that

$$N_A \langle \sigma v \rangle = 3.73 \times 10^{10} \hat{\mu}^{-1/2} T_9^{-3/2} \int_0^\infty E \sigma(E) \exp[-11.605 E/T_9] dE, \quad (3)$$

when E and $\sigma(E)$ are in units of MeV and barn, $\hat{\mu}$ denotes the reduced mass in atomic mass unit (amu = $M_{\text{atm}}(^{12}\text{C})/12 = 931.494 \text{ MeV}/c^2$), and T_9 is the temperature in units of 10^9 K . Correspondingly, η in Eq. (2) equals to $0.1575 Z_A Z_a (\hat{\mu}/E)^{1/2}$.

A quick reference to the energy around which the integrand of Eq. (1) becomes maximum can be made when the S -factor is constant or nearly so, leading to the so-called Gamow peak energy

$$E_0 = (\hat{\mu}/2)^{1/3} (\pi e^2 Z_A Z_a k_B T / \hbar)^{2/3}, \quad (4)$$

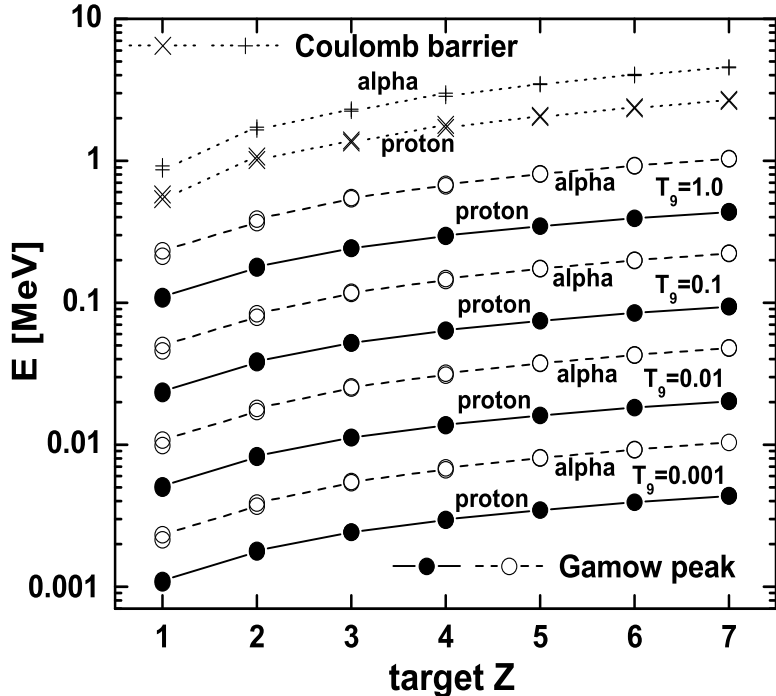


Figure 1: Gamow peak energies for proton- and α -induced reactions at temperatures of $10^6 - 10^9$ K in comparison with the Coulomb barrier heights against the atomic numbers Z of the targets. Except ${}^3\text{H}$, all the isotopes considered here are stable. Just for illustration, the Coulomb barriers are evaluated at the radii of $1.1 \times (A_A^{1/3} + A_a^{1/3})$ fm, where A_A and A_a are the target and projectile mass numbers.

the values of which are plotted in Fig. 1 for proton- and α -induced reactions in the temperature range of $10^6 \sim 10^9$ K. The concept of the Gamow peak loses its significance at higher temperatures as its width increases approximately as $0.7\sqrt{e_0 T_9}$ MeV, where e_0 is E_0 in MeV. The heights of the corresponding Coulomb barriers are added for comparison. It is clear that the reaction cross sections at energies far below the Coulomb barrier are generally in quest. They are next to impossible to measure in the laboratory, and thus have to be obtained by extrapolation from the values measured at higher energies, preferably with the help of some theoretical considerations.

2.2. Reaction mechanisms

Two extreme mechanisms are considered for low-energy nuclear reactions: the "compound nucleus process" and the "direct reaction process" (with the so-called "pre-equilibrium process" lying in between). In the former, the projectile merges with the target to excite many degrees of freedom that have time to statistically equilibrate. This first stage, the formation of the compound nucleus, is followed by its decays by particle or photon emissions. The radiative captures of thermal neutrons are typical examples. The

observed resonances are very narrow, reflecting the long times needed for the formation (and decays) of the compound nucleus.

As opposed to the compound nucleus process, the direct reaction proceeds via the excitation of only a few degrees of freedom on a much shorter time scale reflecting the time taken by the projectile to traverse the target. This process has been traditionally associated with energies that are high enough for the mean-free path of the incident particle to be comparable with the size of the nucleus. In these conditions, the particle ejection occurs preferentially at forward angles. It has become clear, however, that the direct reaction process is also important, and often dominant, in charged-particle induced reactions at the very low energies of astrophysical interest (e.g. [19]). Given the difficulty to penetrate the Coulomb barrier, the reaction may occur before the projectile could tunnel through deep inside the target nucleus. The formation of a compound state is suppressed accordingly, which is reinforced in very light nuclei by the paucity of quasi-bound states.

2.3. The model of our choice: the potential model

There are a few different approaches for describing the nuclear reactions of astrophysical interest at sub-Coulomb barrier energies. What may be considered as two extremes among oft-used ones are the R-matrix method on the purely phenomenological side and the so-called "microscopic cluster models" such as the resonating group method or the generator coordinate method on the side closer to first principles. Both approaches have been subject to much scrutiny in the last decades. In between the two extremes lies the potential model. All of these and some other models clearly have advantages and disadvantages (see [19 - 21] for concise summaries). Furthermore, some *ab initio* many-body approaches have also been applied in certain cases, the references for which shall be noted in the respective subsections in Sect. 3.

In the present work, we adopt the potential model as the major tool for supplementing the experimental data. Doing so, we hope that most of the non-resonant as well as resonant contributions to cross sections at very low energies could be effectively described by a direct reaction model. In practice, we adopt the zero-range Distorted-Wave Born Approximation (DWBA) for particle transfer reactions, and an extended "Direct Capture" model for radiative capture reactions. In what follows, we reserve the term "Potential Model (PM)" exclusively for radiative capture reactions, whereas the term "DWBA" is used for transfer reactions.

2.3.1. The radial wave functions

Various wave functions requested in the potential models that follow are obtained by solving two-body Schrödinger equations, the radial parts of which may be expressed in the relative coordinate r as

$$\left[\frac{d^2}{dr^2} - \frac{L(L+1)}{r^2} + \frac{2\mu}{\hbar^2} \{E - V(r)\} \right] \psi = 0. \quad (5)$$

Here, $V(r)$ is a central potential that consists of the nuclear and Coulomb parts ($V = V_N + V_C$; see 2.5.1), L is the relative orbital angular momentum, μ is the reduced mass, and ψ represents the resulting radial wave function, which vanishes at the origin. [We will *not explicitly* include spin-orbit couplings into V_N .]

For the sake of clarity, we will replace ψ by χ in the case of scattering problems ($E > 0$) and by ϕ in eigen-value problems ($E < 0$). For scattering states ($E = \hbar^2 k^2 / 2\mu$ with the wave number k), the radial wave functions $\chi_L(k, r)$ behave asymptotically at large distances where V_N is negligible as

$$\chi_L(k, r) \longrightarrow \frac{i}{2} [H_L^{(-)}(kr) - S_{kL} H_L^{(+)}(kr)] e^{i\delta_L^c} \quad \text{as } r \rightarrow \infty, \quad (6)$$

where $H_L^{(\mp)}(kr) = [G_L(kr) \mp iF_L(kr)]$ are the incoming $(-)$ and the outgoing $(+)$ Coulomb wave functions expressed in terms of the regular and the irregular Coulomb wave functions $F_L(kr)$ and $G_L(kr)$, the Coulomb phase shift is denoted by δ_L^c , and $S_{kL} = e^{2i\delta_L}$ is the scattering matrix for the elastic scattering with δ_L being the phase shift by the nuclear potential. Thus, the right-hand side of Eq. (6) becomes $\exp[i(\delta_L^c + \delta_L)][\cos(\delta_L)F_L(kr) + \sin(\delta_L)G_L(kr)]$.

For bound states, the radial wave functions must vanish at infinity and be normalised:

$$\phi_{nL}(r) \longrightarrow 0 \quad \text{as } r \rightarrow \infty; \quad \int_0^\infty |\phi_{nL}(r)|^2 dr = 1, \quad (7)$$

where n standing for the radial quantum number has to be chosen appropriately.

2.3.2. The DWBA cross section for transfer reactions

For the transfer reaction $A(a, b)B$, two processes are considered: the stripping ($a = x+b, A+x = B$) and the pickup ($a+x = b, A = B+x$). Of interest in this compilation the former includes (d,n), (d,p) and (α ,n) and the latter (p,d) and (p, α) reactions. We treat them as reactions transferring p, n, τ (${}^3\text{He}$ nucleus) or t (${}^3\text{H}$ nucleus). The transfer is specified by the spin s , the orbital angular momentum l and the total angular momentum j . The triangular relations $\mathbf{l} = \mathbf{j} - \mathbf{s}$, $\mathbf{j} = \mathbf{J}_B - \mathbf{J}_A$ and $\mathbf{s} = \mathbf{J}_a - \mathbf{J}_b$ hold, where J_A, J_a, J_b and J_B are the spins of the four participating nuclei. The residual state is usually, but not limited to, the ground state of the nucleus B .

If the interaction of the nuclei A and a is described by a potential just like in the elastic scattering, the particle transfer is understood to occur as the result of the residual interaction. The DWBA treats it as a perturbation, and obtains the transition matrix element by sandwiching it between the distorted waves in the initial and the final channels.

For simplicity, we adopt the zero-range approximation, namely for the interaction between the transferred particle and the core of the projectile (in a stripping) or ejectile (in a pickup). Furthermore, we do not explicitly include spin-orbit couplings in the distorted waves. Then, the differential cross section, with the normalisation of Eq. (6), becomes (e.g. [22, 23])

$$\frac{d\sigma(\theta)}{d\Omega} = \frac{1}{4\pi} C_{\alpha,\beta} \frac{1}{EE_f} \frac{k_f}{k} \frac{m_B^2}{m_A^2} \sum_{slj} \frac{S_F D_0^2}{(2s+1)} \sum_m |t(\theta)|^2, \quad (8)$$

where the coefficient $C_{\alpha,\beta}$ equals to $(2J_B + 1)/(2J_A + 1)$ for a stripping reaction, and to $(2J_b + 1)/(2J_a + 1)$ for a pickup reaction. The quantities $E (\equiv E_i)$ and E_f are the centre-of-mass energies in the entrance and exit channels, $k (\equiv k_i)$ and k_f are the corresponding

wave numbers, m_A and m_B are the masses of the target A and the residue B , S_F is the spectroscopic factor, and D_0 measures the strength of the zero-range interaction.

Finally, the amplitude $t(\theta)$ is, with the choice of the beam direction as the z -axis, given by

$$t(\theta) = \sum_{l_i, l_f} c_{l_f}^{|m|} P_{l_f}^{|m|}(\cos\theta) T^{if}, \quad (9)$$

where the summations run over the relative orbital angular momenta in the entrance and the exit channels, l_i and l_f . The triangular relation $\mathbf{l} = \mathbf{l}_f - \mathbf{l}_i$ holds, but $l_i + l_f + l$ must be even. In front of the associated Legendre polynomial P_L^M , the coefficient $c_L^M = [(2L+1)(L-M)!/(L+M)!]^{1/2}$ is factored out for convenience. The amplitude T^{if} is given by

$$T^{if} = c_{i,f} \int \chi_{l_f}(k_f, \frac{m_A}{m_B}r) \frac{\phi_{nl}^{js}(r)}{r} \chi_{l_i}(k, r) dr, \quad (10)$$

where

$$c_{i,f} = i^{l_i-l_f} \langle l_i l_f | m0m \rangle \langle l_i l_f l | 000 \rangle (2l_i + 1)(2l_f + 1)^{1/2}/(2l + 1) \quad (11)$$

with $\langle j_1 j_2 J | m_1 m_2 M \rangle$ denoting the Clebsch-Gordan coefficients. The radial wave functions, χ_{l_i} and χ_{l_f} , are the solutions of Eq. (5) for the scattering states in the entrance and the exit channels, respectively. The sandwiched $\phi_{nl}^{js}(r)/r$ is the radial form factor related to the stripped or picked-up species bound in the nucleus B or A , respectively.

The integration of Eq. (8) over the solid angle provides the cross section

$$\sigma_{J_B^\pi}(E) = C_{\alpha,\beta} \frac{1}{EE_f} \frac{k_f}{k} \frac{m_B^2}{m_A^2} \sum_{slj} \frac{S_F D_0^2}{2s+1} \sum_m \sum_{l_f} \left| \sum_{l_i} T^{if} \right|^2. \quad (12)$$

A special care must be taken if the entrance or exit channel is composed of identical nuclei (e.g. [24]). As long as only one set of slj values is considered, the necessary modification can be done by replacing $|t(\theta)|^2$ in Eq. (8) by $|t(\theta)|^2 + |t(\pi-\theta)|^2 + C_{\text{symm}} \text{Re}[t(\theta)t^*(\pi-\theta)]$, where C_{symm} depends on $slj(m)$, the spins of the three participating species, and on the even/oddness of the mass number of the identical species [25].

2.3.3. The PM cross section for radiative capture reactions

In the radiative capture reaction $A(a, \gamma)B$, the transition from the initial scattering state $A + a$ forms the nucleus B with accompanying γ -ray emission. Of interest in this compilation are (p, γ) , (d, γ) and (α, γ) reactions⁴

The PM calculates the transition matrix element between the initial and the final states in a perturbational manner by sandwiching the electromagnetic operators in the long wave-length limit. The consideration of electric dipole (E1), magnetic dipole (M1)

⁴The following formalism (adapted from [20, 26]) is basically an extension of the canonical "Direct Capture" model [27]. Along a similar vein, a systematic potential model analysis of radiative neutron- and proton-capture reactions to the daughter ground states has been carried out recently [28].

and electric quadrupole (E2) operators suffices for the current purpose. The "final state" is either the ground state of the nucleus B if fed directly or, more generally, one of its excited states before the secondary γ -ray cascade, which may be specified by its spin $J_f (\equiv J_B)$ and parity π_f . Correspondingly, we denote the total angular momentum and the parity of the initial state by J_i and π_i . The spin-parity selection rules for the transition between these states can be expressed by the triangular relation $\mathbf{J}_i = \mathbf{J}_f - \lambda$, with λ being the multi-polarity (1 for E1 and M1; 2 for E2), and $\pi_i \pi_f = -$ for E1, and + for M1 and E2.

The partial cross section to a given final state can be written as

$$\begin{aligned} \sigma_{J_f^\pi}(E) &= \frac{2J_f + 1}{(2J_A + 1)(2J_a + 1)} \frac{1}{Ek} \\ &\times \sum_{I_f, J_i, l_i, I_i} S_F \{ c_1 k_\gamma^3 (|M_{E1}|^2 + |M_{M1}|^2) + c_2 k_\gamma^5 |M_{E2}|^2 \}, \end{aligned} \quad (13)$$

where $c_\lambda = 4\pi(\lambda + 1)(2\lambda + 1)/\{\lambda[(2\lambda + 1)!!]^2\}$, k_γ is the wave number of the emitted photon, and S_F is the spectroscopic factor. The summations run over the channel spin I_i , orbital angular momentum l_i , and J_i of the initial state, and over the final channel spin I_f , provided that the spin-parity selection rules are obeyed.

The matrix elements consist of the part related to the radial moment, and those related to the internal moments, if any, of the nucleus A or a :

$$\begin{aligned} M_{E1} &= \mathcal{M}_{E1} \\ M_{M1} &= \mathcal{M}_{M1} + \mathcal{M}_{M1}^{\text{int}}(A) + \mathcal{M}_{M1}^{\text{int}}(a) \\ M_{E2} &= \mathcal{M}_{E2} + \mathcal{M}_{E2}^{\text{int}}(A) + \mathcal{M}_{E2}^{\text{int}}(a). \end{aligned} \quad (14)$$

The radial parts of the $E\lambda$ and $M1$ matrix elements are given by

$$\begin{aligned} \mathcal{M}_{E\lambda} &= e[Z_A \left(\frac{m_a}{m_A + m_a} \right)^\lambda + Z_a \left(\frac{-m_A}{m_A + m_a} \right)^\lambda] \delta_{I_i I_f} C_\lambda^{if} < l_i \lambda l_f |000 > \mathcal{I}_\lambda^{if} \\ \mathcal{M}_{M1} &= \mu_N \frac{Z_A m_a^2 + Z_a m_A^2}{m_A m_a (m_A + m_a)} \delta_{I_i I_f} \delta_{l_i l_f} C_1^{if} [l_i(l_i + 1)(2l_i + 1)]^{1/2} \mathcal{I}_0^{if}, \end{aligned} \quad (15)$$

where $\delta_{\kappa\kappa'}$ stands for the Kronecker symbol,

$$C_\lambda^{if} = (-)^{J_i + I_i + \lambda + l_f} i^{l_i - l_f} [(2J_i + 1)(2l_i + 1)]^{1/2} \left\{ \begin{array}{ccc} J_i & J_f & \lambda \\ l_f & l_i & I_i \end{array} \right\}, \quad (16)$$

and

$$\mathcal{I}_\nu^{if} = \int \phi_{n_f l_f}(r) r^\nu \chi_{l_i}(E, r) dr. \quad (17)$$

In the above, the quantity with the curly brackets is the $6j$ symbol. An additional triangular relation $\mathbf{l}_i = \mathbf{l}_f - \lambda$ holds. $\mathcal{M}_{E\lambda}$ vanishes when $l_i + l_f + \lambda$ is an odd number, and so does \mathcal{M}_{M1} when $l_i = 0$. The quantum numbers n_f and l_f have to be appropriately chosen in consideration of the Pauli principle.

The E2 and M1 matrix elements related to the internal moments of the nucleus A are

$$\mathcal{M}_{E2}^{\text{int}}(A) = \sqrt{5/4} e Q_{2,A} \delta_{l_i l_f} D_2^{if} \mathcal{I}_0^{if}, \quad \mathcal{M}_{M1}^{\text{int}}(A) = \sqrt{3} \mu_{1,A} \delta_{l_i l_f} D_1^{if} \mathcal{I}_0^{if}, \quad (18)$$

where $eQ_{2,A}$ and $\mu_{1,A}$ are the electric quadrupole and the magnetic dipole moments of nucleus A , respectively, and

$$D_\lambda^{if} = (-)^{J_A+J_a-J_f-l_f} \left[(2J_i + 1)(2J_A + 1)(2I_i + 1)(2I_f + 1) \right]^{1/2} \times \left\{ \begin{array}{ccc} J_i & \lambda & J_f \\ I_f & l_f & I_i \end{array} \right\} \left\{ \begin{array}{ccc} J_A & J_a & J_A \\ I_i & \lambda & I_f \end{array} \right\} / \langle J_A \lambda J_A | J_A 0 J_A \rangle. \quad (19)$$

The internal terms related to the partner nucleus a can be obtained by shuffling the suffices A and a in Eqs.(18-19). For the internal terms, the additional triangular relation is $\mathbf{I}_i = \mathbf{I}_f - \lambda$.

For a reaction between identical nuclides, the even-oddness of l_i is to be limited for a given I_i value [24]. In nuclei composed of the same number of neutrons and protons, E1 transitions are inhibited between isospin-zero states [29]. It is worth noting that the effective charge appearing in Eq. (15) vanishes if the ratios of the masses are replaced by that of the mass numbers, A_A and A_a . The residual contribution owing to the isospin impurity can effectively be taken into account by the inclusion of the proper masses together with the renormalisation factor S_F (e.g. [30]).

2.4. Selecting the experimental data

The primary ensemble of experimental low-energy cross section data of current interest comprises those included in NACRE and supplementary ones that have become available to the present authors, preferentially, but not limited to, those published in major refereed journals of the field by early 2013. Some material that was apparently overlooked by NACRE is also added to the list.

Generally speaking, we take the selected experimental data on cross sections and associated errors at face value since the availability of information required to do otherwise (e.g. [31]) is often quite limited. [Attempts of a stricter evaluation can be found in the literature for some specific reactions (e.g. [5, 6, 32 - 34].] In some cases, however, we omit from the analysis those data points which deviate very much from other measurements.

A distinct exception to the above practice concerns some S -factors increasing dramatically toward the lowest energy end. The conventional wisdom attributes this observation to the so-called "laboratory screening" effect (Sect. 2.7.1). We simply disregard those parts of the S -factor data which exhibit that tendency. The specific selection of low-energy data for fitting and reaction rate calculation is presented in Sect. 3 for each reaction.

We do not refer in this work to any differential quantities even when they have been measured.

2.5. Fitting procedure

The actual computations of the DWBA cross sections have been made with the well-known code DWUCK4 [23] albeit with certain modifications required to meet our goal, whereas a code of our own has been used for the PM cross sections. The choice of the form of the nuclear potential differs significantly from the DWBA to the PM analyses, and so does the concrete procedure of parameter fitting. This reflects by and large our preference for purely empirical approaches based on pragmatism to less phenomenological (thus often less flexible) ones. Later in Sect. 2.9, we will briefly discuss the question of the soundness of the present approach.

2.5.1. The Coulomb and nuclear potentials of choice

We adopt the commonly used Coulomb potential

$$\begin{aligned} V_C(r) &= \frac{Z_A Z_a e^2}{r} && \text{for } r \geq R_C \\ &= \frac{Z_A Z_a e^2}{2R_C} \left[3 - \left(\frac{r}{R_C} \right)^2 \right] && \text{for } r \leq R_C, \end{aligned} \quad (20)$$

which assumes a uniform charge distribution inside the radius R_C . The nuclear potential we adopt can be most generally written as a sum of the real Woods-Saxon potential and the surface absorption imaginary part:

$$V_N(r) = V_R f(x_R) + i V_S \frac{df}{dx}(x_S), \quad (21)$$

where

$$f(x_\kappa) = [1 + e^{x_\kappa}]^{-1} \quad \text{and} \quad x_\kappa = \frac{(r - R_\kappa)}{a_\kappa}, \quad (22)$$

with κ referring to the real (R) and surface imaginary (S) terms. The procedure adopted to select the potential strengths V_κ , the radius R_κ and the diffuseness a_κ depends on the types of reactions, as shall be described in the following.

2.5.2. DWBA fitting for transfer reactions

A cut-off energy for the DWBA fit on the high-energy side is normally set at $E_{\text{cm}} \simeq 1$ MeV. This choice is justified as long as the transfer reactions of the current interest are concerned because their S -factors are experimentally known even to relatively low energies, being dominated *either* by non-resonant contributions *or* by the contribution(s) from relatively broad resonance(s) if any. This is in a sharp contrast to the cases of radiative capture reactions (see Sect. 2.5.3). In exceptional cases the possible contributions from the sub-threshold resonances may have to be considered, however (see Sect. 2.7.2).

If applied to the entrance and exit channels and to the form factor, the potential form given by Eqs. (20-22) introduces clearly too many parameters. Just for the practical purpose of reproducing the measured cross section data, one may, however, reduce the number of parameters drastically without causing much damage. First of all, we generally retain a shallow imaginary part of the nuclear potential only for the entrance channel, which takes into account the weak absorption to the exit channel by particle transfer. Next, we parametrise the radius parameters as

$$R_\kappa^{(c)} = r_\kappa^{(c)} A_{t,c}^{1/3}, \quad (23)$$

where the subscript κ distinguishes the Coulomb (C), the real Woods-Saxon (R) and the surface imaginary (S) potentials, the superscript c is put for the entrance channel i , the form factor x and the exit channel f , and $A_{t,c}$ stands for the mass number of the heaviest nucleus (the "target" or the "core") in the channel c . We generally adopt $r_\kappa^{(c)}$ -values extrapolated from those for the global potentials found elsewhere [35 - 37]. The same source is used for the diffuseness parameter $a_\kappa^{(c)}$. Although those values may not adequately apply to very light nuclei, the practice is by and large justified in the

spirit of the "equivalent potential". Namely, by re-shuffling the potential depths, quite similar results are obtained with the radius and diffuseness varied within reasonable ranges. The depth of the (real) potential for the form factor, $V_R^{(x)}$, is determined so as to reproduce the measured binding energy of the particle x in the $B + x$ system for pickup and $A + x$ system for stripping reactions. All in all, we are left in almost all cases only with $V_R^{(i)}$, $V_S^{(i)}$, and $V_R^{(f)}$ as adjustable potential parameters. As for the absolute value of the cross section, we treat $S_F D_0^2$ as an adjustable parameter, rather than relying separately on the estimates of spectroscopic factors and of the zero-range interaction strengths found in the literature.

In case of non-resonant reactions, namely, if no trace of resonances is observed in the energy range of interest, the same potential is used for all the orbital angular momenta $l_i (= 0 - 2)$. When a resonance coinciding with a known level (with spin-parity J_R^π) is found in that energy range, the DWBA fit automatically picks an l_i value that suits to the formation of the resonance. For the same potential, the (consequently non-resonant) contributions from other waves are negligible. If that l_i forms a degenerate resonance with different J^π values, however, J_R^π must be projected out, especially when another J^π would lead to a lower l_f in the exit channel. This applies also to the cases in which the data exhibit more than one resonance at close energies.

In general, the optimal values of the adjustable parameters have been derived by applying to the S -factors the standard χ^2 fit technique. A "fit-by-eye" (linear or logarithmic) is used occasionally, however.

2.5.3. PM fitting for radiative capture reactions

Radiative capture cross sections have been measured rarely below $E_{\text{cm}} \sim 0.1$ MeV. This casts doubt upon the notion that the cross sections at the lowest energy range could simply be the tail of a resonance, if at all. Rather, they may well be dominated by non-resonant contributions. Under these circumstances, we are forced to adopt a strategy of parametrisation that is quite different from that we use for transfer reactions. Namely, we assign a real potential for each given set of l_i and J_i . In particular, we try to fit the resonances, if any, in order to deduce the non-resonant contributions simultaneously. As a consequence, the cut-off energy for the fit on the high energy side varies with each reaction and also depends on the model capability. In order to reduce the number of parameters, we take the same set of radius parameter values for both the initial (i) and final (f) states. This is in sharp contrast to the procedure used for transfer reactions. In stressing the difference, we set

$$R_R^{(i,f)} = R_C^{(i,f)} \equiv R_0, \quad a_R^{(i,f)} \equiv a_0, \quad \text{and} \quad R_0 = r_0 [A_A^{1/3} + A_a^{1/3}]. \quad (24)$$

Similarly we rewrite $V_R^{(c)}$ as $V_0^{(c)}$. For the final (bound) state, we determine the depth, $V_0^{(f)}$, by matching the binding energy of the particle inserted into the final nucleus B . Hence, we are left, for a set of l_i and J_i , with three potential parameters, $V_0^{(i)}$, r_0 and a_0 , and the renormalisation constant, S_F .

The measured cross sections (or S -factors) reveal in most cases one or more resonances in the energy range of astrophysical interest. The first step we take is to reproduce the excitation energy and width of each resonance (with the spin-parity J_R^π) by adjusting the potential parameters. By varying $V_0^{(i)}$ and a_0 with a rather arbitrarily chosen r_0

and an appropriately chosen l_i , this can generally be accomplished for not extremely narrow resonances with widths in excess of a few tenths of keV. As the first trial, we can make use of information on the excited levels in the literature. In other words, we mimic the phase-shift analysis for the elastic scattering. If necessary, the widths are altered so as to reproduce the cross section data of our immediate interest. The height of the resonance is then adjusted with S_F to match the measured value. Finally, the non-resonant contributions are calculated with combinations of J_i and l_i that were not used up for the resonances. They are added to the resonant contributions with S_F values that must be adjusted to reproduce the cross section observed in the lowest energy region without disturbing the fit in the resonance region.

The optimal values of the adjustable parameters are first derived by applying to the S -factors the standard χ^2 fit. In many cases, however, an overall iterative re-adjustment becomes due, for which a "fit-by-eye" (linear or logarithmic) technique is often helpful.

2.5.4. Nuclear data

The nuclear mass, m , in use in Sects. 2.1 and 2.3 may be replaced by the measured "atomic mass" less the summed rest mass of the electrons bound to the neutral atom. The electron binding energies need to be considered only in a limited number of very low energy phenomena such as the "laboratory electron screening" (Sect. 2.7.1). As far as the reactions of current interest are concerned, even the neglect of the electron rest mass does not introduce significant errors. [It may be worth noting here that the conversion of the mass density to the number density of stellar matter can be most conveniently done with the use of atomic masses [1].] The relevant atomic masses are well known [38].

Information on the properties of nuclear ground state and excited levels is in most cases available (e.g. in [39 - 41]). The required quantities include the spin, parity and excitation energy for each level. For our PM analysis of resonant radiative capture reactions, the total and γ -widths, and the γ -ray branching ratios in the literature are additionally taken as the trial input data for fixing the widths and heights of the resonances. Nuclear magnetic dipole ($\mu_{1,A}$) and electric quadrupole ($Q_{2,A}$) moments appearing in Eq. (18) are taken from [42].

2.6. The Breit-Wigner formula as a supplement

The potential models chosen above are inappropriate for, or fail in, describing certain resonances. First of all, this is clearly the case with very narrow resonances that must be understood in terms of compound nucleus formation, the cross sections near the resonance energy E_R being given by the Breit-Wigner formula

$$\sigma_R^{(i,f)} = \frac{\pi}{k_i^2} \omega \frac{\Gamma_i \Gamma_f}{(E - E_R)^2 + (\Gamma/2)^2}, \quad (25)$$

where $\omega = (2J_R + 1)/((2J_A + 1)(2J_a + 1)$, and Γ_i, Γ_f and Γ are the entrance partial, exit partial and total widths, respectively.

The integrated cross section from Eq. (25) is $(2\pi^2/k_i^2)\omega\gamma$. Here, the quantity $\omega\gamma = \Gamma_i \Gamma_f / \Gamma$ can be experimentally derived in relation to the "thick target yield", and is useful for evaluating the contribution to the reaction rates from a very narrow resonance (Sect. 2.8.2).

For a relatively broad resonance, the energy dependences of the widths can be approximately introduced such that Eq. (25) may be extended to a wider energy range. Namely, one rewrites, for an entrance channel,

$$\Gamma_i(E) = (2k_i a)v_{l_i}(E)\gamma_W^2\theta_i^2. \quad (26)$$

in terms of the penetrability $v_l(E) = 1/[F_l(ka)^2 + G_l(ka)^2]$ ([24]) and the reduced width $\theta_i^2(\leq 1)$ in units of the Wigner limit $\gamma_W^2 = 3\hbar^2/(2\mu a^2)$, where a is the channel radius [18]. The exit partial width for a transfer reaction can be computed similarly with a suitable shift in energetics. For a radiative capture with the multi-polarity λ , one may take $\Gamma_\gamma(E) = \Gamma_\gamma(E_R)[(E+q)/(E_R+q)]^{2\lambda+1}$ with q being the Q -value. The above formalism will be applied for the evaluation of possible contributions of sub-threshold resonances (Sect. 2.7.2).

Alternatively, the resonance shape and height of our model cross sections may be made to coincide nearly with those given by Eq. (25) by adjusting the fit parameters. This is useful when the dominant (and not very narrow) elastic scattering width is known but, for the reaction, only $\omega\gamma$ is measured.

2.7. Signatures of specific phenomena

In order to warrant a reliable extrapolation to the lowest energy region of the experimentally available S -factors, one has to pay special attention to a few phenomena as in the following.

2.7.1. The laboratory electron screening

In ordinary laboratory experiments, the targets are atomic or molecular. As such, the nuclear charge of a target is screened by the bound electrons in the eyes of the projectile. The cross sections, or more visibly the S -factors, get enhanced at very low energies when compared with those in the case of the target being a bare nucleus. That is the so-called laboratory electron screening.⁵

Since the light species of our interest are most likely fully ionised in stellar interiors, we must question the enhanced segments of the measured data. A quick estimate of the laboratory screening can be made by shifting the Coulomb barrier by a constant amount U_e , leading to an approximate enhancement factor of $\exp(\pi\eta U_e/E)$. In particular, U_e in the adiabatic (as opposed to sudden) approximation can be given as the difference of the atomic binding energy summed for the two separate species and that of the combined "molecular" state with the same number of bound electrons. More advanced dynamical treatments of the screening in the ${}^2\text{H} + \text{d}$ reaction indicate that the adiabatic U_e can indeed lead to a good measure for the maximum effect at low energies [43, 44]. On the other hand, various observations appear to indicate that the behaviour of the very low energy S -factors depends on the environmental conditions (e.g. [45]).

An indirect approach, the so-called "Trojan horse method" (THM), is meant to avoid the screening effect altogether (e.g. [46] for a brief summary).⁶

⁵The screening effect owing to the ionisation (or "free") electrons may have an important effect on reaction rates in stellar environments, particularly at high densities. This problem is not tackled here.

⁶Speaking of the indirect methods ([47, 48] for reviews), we note here that the "asymptotic normalisation constant" (ANC) derived from the analysis of suitable experiments gives information on the $S(0)$ -value for reaction in a very-loosely bound system.

Under these circumstances, we disregard in the fit procedure those parts of the measured S -factors whose behaviours are "abnormal" and may indicate that screening is in play. This is in contrast to some R-matrix fits that attempt to extract U_e simultaneously (e.g. [49]). We instead limit ourselves to display in Sect. 3 an adiabatic screening correction made to the S -factors in a few cases just to guide the eye.

2.7.2. Sub-threshold resonances

Another cause for possible enhancements at the lowest energies of the S -factors concerns the "tails" of sub-threshold states (e.g. [18]). This problem has been discussed extensively and most often in the framework of R-matrix analyses along with indirect measurements. In general, however, the quantitative estimates of the consequent enhancements of the S -factors remain more or less uncertain.

The simple models adopted for this compilation cannot treat the problem in a satisfactory manner. When relevant cross section enhancements are experimentally alluded or theoretically expected, we just explore them by a simple procedure [18] in which the Breit-Wigner formula (Sect. 2.6) is applied to the tail distribution of the culprit sub-threshold resonance. The key unknown quantity is $\Gamma_i(E)$, whereas $\Gamma_f(E)$ can usually be normalised to the experimental value at $E_R < 0$. The strength and the slope of that tail distribution may be adjusted by selecting different values for the reduced width θ^2 and the channel radius a (see e.g. [50]). If a is parametrised like R_0 in Eq. (24), r_{a0} may be in the approximate $1.4 \sim 1.9$ fm range.

2.7.3. Interference of resonances

In a limited number of cases, two or more resonances with the same J^π could be attributed to an l_i value. The S -factors in consideration of interference between two resonances (R1 and R2) are given by

$$S(E) = S_{R1}(E) + S_{R2}(E) + 2\sqrt{S_{R1}(E)S_{R2}(E)}\cos(\delta_{l,R1}(E) - \delta_{l,R2}(E)), \quad (27)$$

where $\delta_{l,R1}$ and $\delta_{l,R2}$ are the respective phase shifts. We select the overall sign of the interference term by inspecting the observed behaviours of the S -factors in the tail regions of the resonances.

2.8. The rate evaluation

Following the traditional practice [2, 3], we present the thermonuclear reaction rates in the temperature range of $10^6 \lesssim T \leq 10^{10}$ K. We summarise here the general procedure to evaluate the rates and their uncertainties. Comments on the specifics in individual cases are added in Sect. 3 along with the results.

2.8.1. Combining the measured and model S -factors

We search for the model parameter values that "best" reproduce the experimental S -factor data in a certain range of centre-of-mass energy, $[E_1, E_3]$, chosen for each reaction (see Sect. 2.5). The rates are then computed with the model and observed S -factor values in the $[E_0, E_2]$ and $[E_2, E_4]$ ranges, respectively, where $E_0 \approx 0 < E_1 < E_2 < E_3 < E_4$. This procedure generally defines the rates labelled as "adopted". In some cases, the lack of experimental data at energies beyond E_4 makes it necessary to extrapolate the S -factors by the model. In certain cases, one has even to resort to a statistical treatment

of compound nucleus reactions in order to compute the rates at very high temperatures (see Sect. 2.8.3).

The evaluation of the uncertainties in the $[E_0, E_2]$ range is not always straightforward, and is specific to each reaction. It depends on how to interpret a scatter (or even a conflict) among the experimental S -factors that is more or less large. It also depends on how sensitive the extrapolation to the $[E_0, E_1]$ range is to the equally good fits with different sets of parameter values. This is of particular concern in the analysis of observed resonances. For transfer reactions with a relatively broad resonance, sets of parameter values that reproduce the data near the resonance as well as in the "best" fit, but differ significantly in the tail region, are often used to define the "high" and "low" S -factor values in the $[E_0, E_2]$ range. In other cases, the upper and lower envelopes of the experimental data are used for the fit. The uncertainties regarding a relatively narrow resonance observed in a radiative capture reaction are often evaluated by allowing for 10 - 20 % errors on the height (or γ -width) of the resonance.

The integration over the $[E_2, E_4]$ range is made with the use of linear fits of the S -factor data points of interest in appropriately segmented energy domains. This method, rather than the local linear interpolation adopted in NACRE, avoids unwanted ripples in the computed rates. The reaction rates "low" and "high" include the experimental uncertainties in the $[E_2, E_4]$ range.

2.8.2. Extremely narrow resonances

In some reactions, resonances with very narrow widths ($\ll 1$ keV) may come into play, to which the potential model is inadequate to apply. With the cross sections unresolved, the experimental information available is the resonance strength $\omega\gamma$ deduced from the thick-target yields in relation to the background cross sections (see Sect. 2.6). The additional contribution to the thermonuclear reaction rates (3) from a very narrow resonance is in good approximation given by

$$N_A < \sigma v >^{(R)} = 1.54 \times 10^{11} \hat{\mu}^{-3/2} (\omega\gamma) T_9^{-3/2} \exp[-11.605 E_R / T_9], \quad (28)$$

where $\omega\gamma$ and E_R are in units of MeV.

2.8.3. Reaction rates at very high temperatures

The estimates of certain reaction rates at temperatures in excess of a few times 10^9 K can get progressively uncertain. This is primarily because the available cross section data may be incomplete for a reaction that may involve a considerable number of compound nuclear resonances at high excitation energies. If that is suspected, the cross sections derived by the state-of-the-art nuclear reaction code TALYS [51] may be consulted. This method is clearly more advanced, and can be better controlled, than the extrapolations based on integrated Hauser-Feshbach rates as in NACRE.

At high temperatures, the thermal population of the low-lying states of the *targets* may also come into play. The Hauser-Feshbach predictions [51] of the ratios of the reaction rates calculated for the thermalised targets relative to those for the ground states imply that the effects are generally small for the systems of interest here.

2.8.4. Forward and reverse reaction rates in astrophysical environments

All of the reactions of interest in this compilation may be expressed as

$$n_1 + n_2 \longrightarrow n_3 + n_4 \quad \text{or} \quad \{n_1 n_2 n_3 n_4\}, \quad (29)$$

15

where n_k refers to the numbers of *different* nuclear species k . The norms are $\{1111\}$ for transfer and $\{1110\}$ for radiative capture reactions that involve four different nuclear species.

The forward and the inverse reaction rates per unit volume are then given by

$$P_{12} = \rho N_A \Lambda_{12 \rightarrow 34} \quad P_{34} = \rho N_A \Lambda_{34 \rightarrow 12}, \quad (30)$$

where ρ is the matter density. Denoting the number fractions as $Y_k \equiv X_k/A_k$ (with X_k being the mass fraction normalised to $\sum_k X_k = 1$),

$$\Lambda_{12 \rightarrow 34} = \frac{N_A \langle \sigma v \rangle_{12}}{n_1!} Y_1^{n_1} Y_2^{n_2} \rho, \quad (31)$$

$$\Lambda_{34 \rightarrow 12} = \frac{N_A \langle \sigma v \rangle_{12} \times REV}{n_3!} Y_3^{n_3} Y_4^{n_4} \rho^{n_3+n_4-1}, \quad (32)$$

where

$$REV \equiv \frac{x_1 x_2}{x_3 x_4} \exp \left[-\frac{Q}{k_B T} \right] \left[\frac{k_B T}{2\pi\hbar^2 N_A^{5/3}} \right]^{(3/2)(n_1+n_2-n_3-n_4)}, \quad (33)$$

with $x_k = (g_k A_k^{3/2})^{n_k} / n_k!$, where $g_k = (2J_k + 1)G$, J_k and G being the ground-state spin and the partition function, and where Q is the Q -value for the forward reaction. The rates of the reverse two-body reactions are given explicitly in Appendix B. With these notations, the contributions to the time variation dY_k/dt of, e.g., the forward reaction are $-n_k \Lambda_{12 \rightarrow 34}$ for $k = 1, 2$, and $+n_k \Lambda_{12 \rightarrow 34}$ for $k = 3, 4$.

2.9. Critical assessment

Given the purpose of this compilation, we shall not be much devoured by the question of the applicability of the present potential-model approach to each reaction. Nonetheless, a brief discussion on some issues at stake may be due. A sequence of critical questions may be summarised as follows. Is the reaction a direct process? If so, is the DWBA or PM applicable? If so, are the values of the parameters and the goodness of the fit acceptable? In many cases, in fact, we work on the answers to these questions in the reversed order. Namely, if a good fit is achieved with the use of the potential parameter values in "reasonable" ranges, then we answer to the first two questions positively, although there may be many uncomfortable aspects left in the sense of theoretical nuclear physics.

As mentioned earlier, the potential models (PM and DWBA) are capable of dealing not only with non-resonant reactions at low energies below the Coulomb barrier, but also with reactions forming relatively broad resonances. The present study will indeed reveal (Sect. 3) that most resonances with their widths as narrow as of the order of 1 keV for radiative captures and of several tens of keV for transfer reactions could still be described by the PM and DWBA, respectively, to a more or less satisfactory extent without much manipulation of the potential parameter values. One way of judging the "reliability" of the models is through that of the potential parameter values derived from the fit. Whereas the "soundness" of the parameter values can always be checked, their "uniqueness" can hardly be warranted. For example, one may be able to find many different sets of parameter values that lead to similarly good fits to existing experimental data, which often come with large (or small but conflicting) errors. In order to constrain the spreads

to a manageable level, we have limited the number of adjustable parameters (of DWBA in particular). We stress here that we do not pretend aiming at the construction of a standard (or global) potential of any sort.

For transfer reactions, we have adopted the zero-range DWBA. Its "validity" in the light of a microscopic cluster model was studied for the $^{13}\text{C}(\alpha,\text{n})$ reaction at $E_{\text{cm}} \lesssim 5$ MeV [52]. With some clear shortcomings of DWBA set aside, it was expectedly found that the zero-range DWBA could reproduce quite well the shapes (not amplitudes, though) of the S -factors of the microscopic model as long as the potential parameters were fit to the same phase-shifts. This gives a sort of support for the present approach to an observed resonance, in which the model parameters are adjusted so as to reproduce the shape *and* the height of the resonance. We also note that some numerical experiments have shown that the use of the finite-range DWBA cannot bring notable improvements *as far as the empirical fits are concerned*, even for the multi-nucleon transfers considered in the present compilation. Both in $^9\text{Be}(\alpha,\text{n})$ and $^{11}\text{B}(\text{p},\alpha)$ reactions, for example, the finite-range corrections to $S(E)/S(0)$ *for a given potential* do not exceed 10 % even at $E \simeq E_R$.

In conclusion: Even when the applicability of the present method is stretched too far, our primary aim of a reproduction of experimental cross section data and its extrapolation would be met at least in a sense similar to oft-used polynomial fits. However, large uncertainties in extrapolation would be unavoidable when the experimental data are not enough to constrain the parameter values. This is particularly the case when sub-threshold resonances are involved. Similarly, the non-resonant components may, in some cases, not be constrained well enough as one wishes.

3. The results

The results for the 34 two-body, exoergic reactions listed in Table 1 are presented. Each subsection discusses 1) the available experimental data; 2) the model (PM or DWBA) astrophysical S -factor; and 3) the thermonuclear reaction rates.

The astrophysical S -factors are plotted versus the centre-of-mass energy, E_{cm} . The solid curve represents the "adopted" model S -factors, with the two dashed ones setting their boundaries, "low" and "high". If not specified otherwise, the $S(0)$ -values are those at about 0.5 - 1.0 keV (c.f. [53]). Other compilations in comparison are: [NACRE] (i.e. [3] extrapolation by various methods), [BBN04] (i.e. [4], R-matrix), [RAD10] (i.e. [28], potential model), and [SUN11] (i.e. [5], various methods).

The reaction rates are given versus T_9 in the same mesh as the one used by NACRE, and are graphically compared with those of NACRE (or CF88 [2] in two cases).

Figure captions may contain additional information such as on the selection of the experimental data, and on the possible cause of the differences between the present and previous results. The origin of these differences is, however, often hard to pin down as the details of the procedures taken by NACRE have meanwhile weathered out.

Additional references are given at the end of the subsections. The lists are, however, not meant to be exhaustive. The analytic form of REV [Eq. (33)] is attached to the rate tables. Recall that REV is dimensionless for a transfer reaction and is in mol/cm³ for a capture reaction.

Table 1: List of compiled reactions. Q is the Q -value. The first entry of Figures indicates Figure# that depicts the S -factors, and the second the reaction rates in comparison with the previous values. The entries of Tables indicate the Table# of the reaction rates, the model parameter values (Appendix A) and the reverse reaction rates (Appendix B) in that order.

subsection	reaction	Q (MeV)	Figures	Tables
3.1	$^2\text{H}(\text{p}, \gamma)^3\text{He}$	+ 5.493	2, 3	2, 51, 72
3.2	$^2\text{H}(\text{d}, \gamma)^4\text{He}$	+ 23.847	4, 5	3, 52, 72
3.3	$^2\text{H}(\text{d}, \text{n})^3\text{He}$	+ 3.269	6, 7	4, 36, 70
3.4	$^2\text{H}(\text{d}, \text{p})^3\text{H}$	+ 4.033	8, 9	5, 37, 70
3.5	$^2\text{H}(\alpha, \gamma)^6\text{Li}$	+ 1.474	10, 11	6, 53, 72
3.6	$^3\text{H}(\text{d}, \text{n})^4\text{He}$	+ 17.589	12, 13	7, 38, 70
3.7	$^3\text{H}(\alpha, \gamma)^7\text{Li}$	+ 2.467	14, 15	8, 54, 72
3.8	$^3\text{He}(\text{d}, \text{p})^4\text{He}$	+ 18.353	16-18, 19	9, 39, 70
3.9	$^3\text{He}(\tau, 2\text{p})^4\text{He}$	+ 12.860	20, 21	10, 40, -
3.10	$^3\text{He}(\alpha, \gamma)^7\text{Be}$	+ 1.586	22, 23	11, 55, 72
3.11	$^6\text{Li}(\text{p}, \gamma)^7\text{Be}$	+ 5.606	24-26, 27	12, 56, 72
3.12	$^6\text{Li}(\text{p}, \alpha)^3\text{He}$	+ 4.020	28, 29	13, 41, 70
3.13	$^7\text{Li}(\text{p}, \gamma)^8\text{Be}(2\alpha)^\dagger$	+ 17.347	30-32, 33	14, 57, -
3.14	$^7\text{Li}(\text{p}, \alpha)^4\text{He}$	+ 17.347	34, 35	15, 42, 70
3.15	$^7\text{Li}(\alpha, \gamma)^{11}\text{B}$	+ 8.665	36, 37	16, 58, 74
3.16	$^7\text{Be}(\text{p}, \gamma)^8\text{B}$	+ 0.137	38-40, 41	17, 59, 73-74
3.17	$^7\text{Be}(\alpha, \gamma)^{11}\text{C}$	+ 7.545	42, 43	18, 60, 74
3.18	$^9\text{Be}(\text{p}, \gamma)^{10}\text{B}$	+ 6.586	44, 45	19, 61, 74
3.19	$^9\text{Be}(\text{p}, \text{d})^8\text{Be}(2\alpha)^\dagger$	+ 0.651	46, 47	20, 43, -
3.20	$^9\text{Be}(\text{p}, \alpha)^6\text{Li}$	+ 2.125	48, 49	21, 44, 71
3.21	$^9\text{Be}(\alpha, \text{n})^{12}\text{C}$	+ 5.701	50, 51	22, 45, 71
3.22	$^{10}\text{B}(\text{p}, \gamma)^{11}\text{C}$	+ 8.689	52, 53	23, 62, 74
3.23	$^{10}\text{B}(\text{p}, \alpha)^7\text{Be}$	+ 1.145	54, 55	24, 46, 71
3.24	$^{11}\text{B}(\text{p}, \gamma)^{12}\text{C}$	+ 15.957	56, 57	25, 63, 74
3.25	$^{11}\text{B}(\alpha, \gamma)^8\text{Be}(2\alpha)^\dagger$	+ 8.682	58, 59	26, 47, -
3.26	$^{11}\text{B}(\alpha, \text{n})^{14}\text{N}$	+ 0.158	60, 61	27, 48, 71
3.27	$^{12}\text{C}(\text{p}, \gamma)^{13}\text{N}$	+ 1.943	62, 63	28, 64, 75
3.28	$^{12}\text{C}(\alpha, \gamma)^{16}\text{O}$	+ 7.162	64-68, 69	29, 65, 75
3.29	$^{13}\text{C}(\text{p}, \gamma)^{14}\text{N}$	+ 7.551	70-71, 72	30, 66, 75
3.30	$^{13}\text{C}(\alpha, \text{n})^{16}\text{O}$	+ 2.216	73-75, 76	31, 49, 71
3.31	$^{13}\text{N}(\text{p}, \gamma)^{14}\text{O}$	+ 4.627	77, 78	32, 67, 75
3.32	$^{14}\text{N}(\text{p}, \gamma)^{15}\text{O}$	+ 7.297	79-81, 82	33, 68, 75
3.33	$^{15}\text{N}(\text{p}, \gamma)^{16}\text{O}$	+ 12.127	83, 84	34, 69, 75
3.34	$^{15}\text{N}(\text{p}, \alpha)^{12}\text{C}$	+ 4.965	85, 86	35, 50, 71

[†] Q applies to the (2α) final state

3.1. ${}^2\text{H}(\text{p}, \gamma) {}^3\text{He}$

The experimental data sets referred to in NACRE are GR62 [54], GR63 [55], WA63 [56][†], BE64 [57][†], FE65 [58][†], ST65 [59][†], GE67 [60], WO67 [61], TI73 [62][†], SC95a [63] and MA97 [64], covering the $0.01 \lesssim E_{\text{cm}} \lesssim 20$ MeV range. [65] was superseded by MA97. Added are the post-NACRE data sets CA02 [66] and BY08a [67], the former extending the range down to $E_{\text{cm}} \simeq 0.0025$ MeV. SC95a [63] has been corrected by SC96 [68] for an error. [[†]from the inverse ${}^3\text{He}(\gamma, \text{p}) {}^2\text{H}$.]

Figure 2 compares the PM and experimental S -factors. The data in the $E_{\text{cm}} \lesssim 2$ MeV range are used for the PM fit. The s- and p-wave captures, leading to M1 and E1 transitions, contribute predominantly at low energies. The adopted parameter values are given in Table 51. The resulting $S(0) = 0.21 \pm 0.04$ eV b. In comparison, $S(0) = 0.20 \pm 0.07$ eV b [NACRE, quadratic polynomial], 0.223 ± 0.010 eV b [BBN04], 0.14 eV b [RAD10], and 0.214 ± 0.017 eV b [SUN11, quadratic polynomial].

Table 2 gives the reaction rates at $0.001 \leq T_9 \leq 10$, for which the PM-predicted and the experimental cross sections below and above $E_{\text{cm}} \simeq 0.1$ MeV are used, respectively. Figure 3 compares the present and the NACRE rates.

See [69] for an *ab initio* calculation.

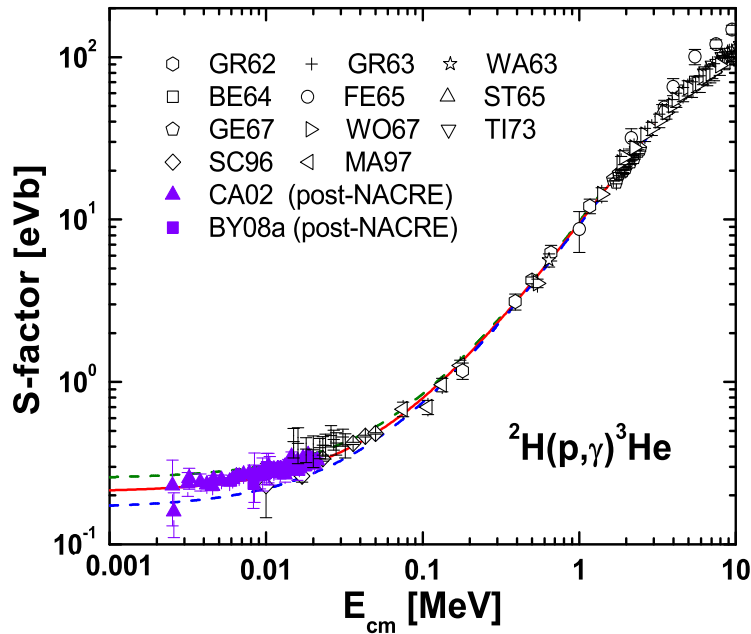


Figure 2: The S -factor for ${}^2\text{H}(\text{p}, \gamma) {}^3\text{He}$.

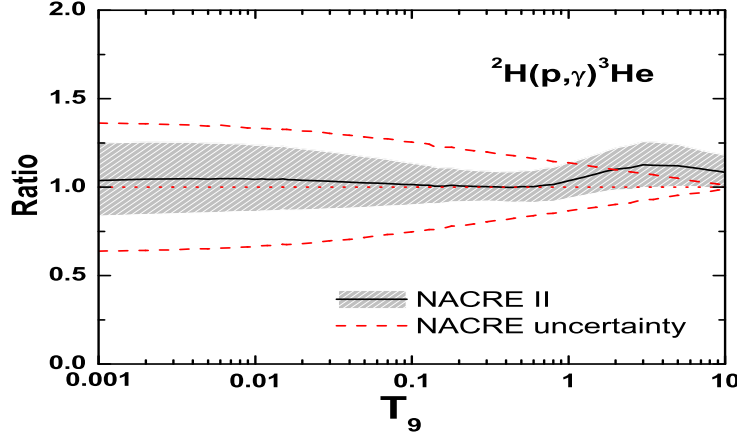


Figure 3: ${}^2\text{H}(\text{p}, \gamma){}^3\text{He}$ rates in units of the NACRE (adopt) values.

Table 2: ${}^2\text{H}(\text{p}, \gamma){}^3\text{He}$ rates in $\text{cm}^3 \text{mol}^{-1} \text{s}^{-1}$

T_9	adopted	low	high	T_9	adopted	low	high
0.001	1.35E-11	1.09E-11	1.62E-11	0.14	1.15E+01	1.03E+01	1.27E+01
0.002	1.87E-08	1.51E-08	2.25E-08	0.15	1.33E+01	1.20E+01	1.47E+01
0.003	6.07E-07	4.93E-07	7.27E-07	0.16	1.52E+01	1.37E+01	1.67E+01
0.004	5.38E-06	4.38E-06	6.43E-06	0.18	1.93E+01	1.75E+01	2.12E+01
0.005	2.52E-05	2.06E-05	3.01E-05	0.2	2.37E+01	2.16E+01	2.60E+01
0.006	8.15E-05	6.67E-05	9.71E-05	0.25	3.62E+01	3.31E+01	3.94E+01
0.007	2.07E-04	1.70E-04	2.47E-04	0.3	5.01E+01	4.59E+01	5.44E+01
0.008	4.47E-04	3.68E-04	5.31E-04	0.35	6.52E+01	5.98E+01	7.08E+01
0.009	8.55E-04	7.04E-04	1.01E-03	0.4	8.13E+01	7.45E+01	8.84E+01
0.01	1.49E-03	1.23E-03	1.77E-03	0.45	9.84E+01	9.00E+01	1.07E+02
0.011	2.43E-03	2.01E-03	2.87E-03	0.5	1.16E+02	1.06E+02	1.27E+02
0.012	3.73E-03	3.09E-03	4.40E-03	0.6	1.54E+02	1.40E+02	1.69E+02
0.013	5.47E-03	4.54E-03	6.45E-03	0.7	1.95E+02	1.77E+02	2.14E+02
0.014	7.73E-03	6.42E-03	9.10E-03	0.8	2.38E+02	2.16E+02	2.61E+02
0.015	1.06E-02	8.80E-03	1.24E-02	0.9	2.84E+02	2.57E+02	3.12E+02
0.016	1.41E-02	1.17E-02	1.65E-02	1.	3.32E+02	2.99E+02	3.64E+02
0.018	2.33E-02	1.95E-02	2.74E-02	1.25	4.57E+02	4.12E+02	5.03E+02
0.02	3.60E-02	3.02E-02	4.22E-02	1.5	5.91E+02	5.31E+02	6.52E+02
0.025	8.59E-02	7.25E-02	1.00E-01	1.75	7.30E+02	6.54E+02	8.07E+02
0.03	1.66E-01	1.41E-01	1.93E-01	2.	8.73E+02	7.79E+02	9.68E+02
0.04	4.35E-01	3.73E-01	5.01E-01	2.5	1.17E+03	1.04E+03	1.30E+03
0.05	8.62E-01	7.44E-01	9.86E-01	3.	1.46E+03	1.30E+03	1.63E+03
0.06	1.45E+00	1.26E+00	1.65E+00	3.5	1.76E+03	1.56E+03	1.97E+03
0.07	2.20E+00	1.93E+00	2.50E+00	4.	2.07E+03	1.84E+03	2.30E+03
0.08	3.11E+00	2.74E+00	3.51E+00	5.	2.67E+03	2.39E+03	2.95E+03
0.09	4.17E+00	3.69E+00	4.69E+00	6.	3.27E+03	2.95E+03	3.60E+03
0.1	5.37E+00	4.77E+00	6.02E+00	7.	3.86E+03	3.50E+03	4.23E+03
0.11	6.71E+00	5.98E+00	7.49E+00	8.	4.45E+03	4.05E+03	4.86E+03
0.12	8.18E+00	7.31E+00	9.10E+00	9.	5.02E+03	4.58E+03	5.48E+03
0.13	9.77E+00	8.76E+00	1.08E+01	10.	5.59E+03	5.10E+03	6.08E+03

$$\text{REV} = 1.63 \times 10^{10} T_9^{3/2} \exp(-63.752/T_9)$$

3.2. $^2\text{H}(\text{d}, \gamma)^4\text{He}$

The experimental data sets referred to in NACRE are ZU63 [70], ME69 [71][†], WI85 [72][‡], WE86 [73] and BA87 [74][‡], covering the $0.025 \lesssim E_{\text{cm}} \lesssim 5.4$ MeV range. Added is the post-NACRE data point ZH09 [75]^{††} at $E_{\text{cm}} \simeq 0.007$ MeV. [[†]re-calculated from the reverse $^4\text{He}(\gamma, \text{d})^2\text{H}$ cross sections; [‡]normalised to the σ_{dp} fit of [3]; ^{††}normalised to the extrapolated σ_{dp} of [76]]

Figure 4 compares the PM and experimental S -factors. No clear signature of electron screening has been detected. The data sets (but WI85 and WE86) in the $E_{\text{cm}} \lesssim 2$ MeV range are used for the PM fit. The main contribution at low energies is expected to come from the E2 transition resulting from $l_i = 2$ (with $I_i = 0, 2$), whereas the E1 transition with $l_i = 1$ (with $I_i = 1$) is isospin-forbidden. In order to reproduce the S -factor observed at the lowest energies, a D-state ($l_f = 2$) admixture in the ground state ^4He (consequently, E2 transition with $l_i = 0$) is invoked (e.g. [78]). The adopted parameter values are given in Table 52. The resulting $S(0) = 5.8^{+1.0}_{-1.5}$ meV b.

Table 3 gives the reaction rates at $0.001 \leq T_9 \leq 10$, for which the PM-predicted and the experimental cross sections below and above $E_{\text{cm}} \simeq 0.2$ MeV are used, respectively. Figure 5 compares the present and the NACRE rates.

See [77] for an *ab initio* calculation.

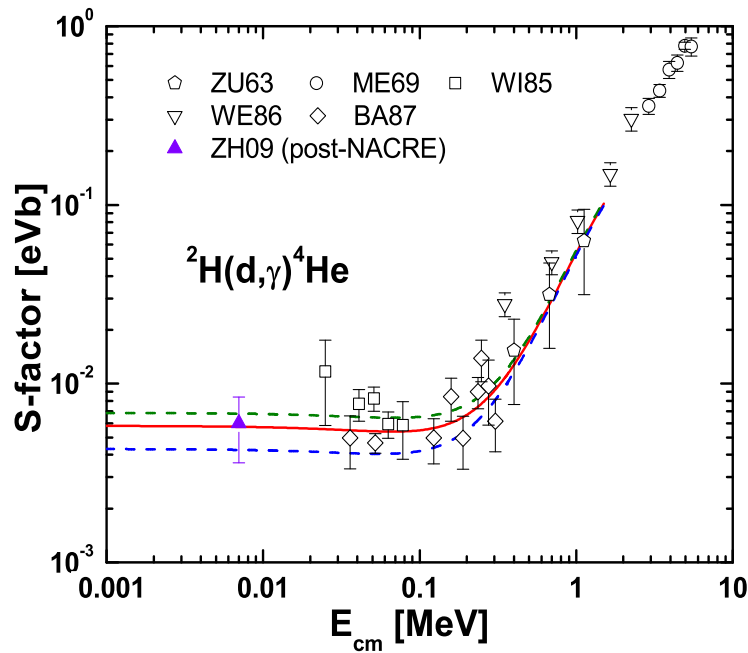


Figure 4: The S -factor for $^2\text{H}(\text{d}, \gamma)^4\text{He}$. Both WI85 and WE86 are not considered in the fit because of their inexplicable energy-dependences (cf. [77]).

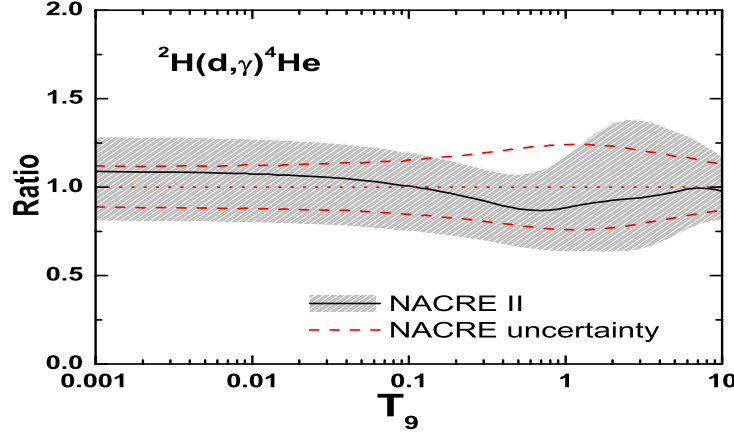


Figure 5: ${}^2\text{H}(\text{d}, \gamma){}^4\text{He}$ rates in units of the NACRE (adopt) values.

Table 3: ${}^2\text{H}(\text{d}, \gamma){}^4\text{He}$ rates in $\text{cm}^3 \text{mol}^{-1} \text{s}^{-1}$

T_9	adopted	low	high	T_9	adopted	low	high
0.001	1.46E-15	1.08E-15	1.72E-15	0.14	4.57E-02	3.41E-02	5.45E-02
0.002	6.02E-12	4.47E-12	7.12E-12	0.15	5.26E-02	3.93E-02	6.27E-02
0.003	3.30E-10	2.45E-10	3.90E-10	0.16	5.98E-02	4.47E-02	7.13E-02
0.004	4.05E-09	3.01E-09	4.79E-09	0.18	7.48E-02	5.60E-02	8.93E-02
0.005	2.39E-08	1.77E-08	2.83E-08	0.2	9.06E-02	6.79E-02	1.08E-01
0.006	9.19E-08	6.82E-08	1.09E-07	0.25	1.32E-01	9.96E-02	1.58E-01
0.007	2.68E-07	1.99E-07	3.18E-07	0.3	1.76E-01	1.33E-01	2.11E-01
0.008	6.47E-07	4.80E-07	7.66E-07	0.35	2.21E-01	1.67E-01	2.66E-01
0.009	1.36E-06	1.01E-06	1.61E-06	0.4	2.67E-01	2.02E-01	3.23E-01
0.01	2.57E-06	1.90E-06	3.04E-06	0.45	3.15E-01	2.37E-01	3.82E-01
0.011	4.47E-06	3.31E-06	5.29E-06	0.5	3.63E-01	2.73E-01	4.44E-01
0.012	7.28E-06	5.41E-06	8.62E-06	0.6	4.65E-01	3.47E-01	5.78E-01
0.013	1.13E-05	8.36E-06	1.33E-05	0.7	5.74E-01	4.25E-01	7.27E-01
0.014	1.67E-05	1.24E-05	1.98E-05	0.8	6.92E-01	5.07E-01	8.92E-01
0.015	2.38E-05	1.77E-05	2.82E-05	0.9	8.18E-01	5.94E-01	1.07E+00
0.016	3.29E-05	2.44E-05	3.90E-05	1.	9.54E-01	6.86E-01	1.27E+00
0.018	5.83E-05	4.33E-05	6.91E-05	1.25	1.33E+00	9.38E-01	1.85E+00
0.02	9.52E-05	7.07E-05	1.13E-04	1.5	1.76E+00	1.22E+00	2.51E+00
0.025	2.52E-04	1.87E-04	2.99E-04	1.75	2.23E+00	1.53E+00	3.25E+00
0.03	5.27E-04	3.91E-04	6.25E-04	2.	2.75E+00	1.88E+00	4.05E+00
0.04	1.52E-03	1.13E-03	1.80E-03	2.5	3.92E+00	2.67E+00	5.81E+00
0.05	3.19E-03	2.37E-03	3.79E-03	3.	5.27E+00	3.62E+00	7.74E+00
0.06	5.57E-03	4.14E-03	6.62E-03	3.5	6.80E+00	4.76E+00	9.81E+00
0.07	8.65E-03	6.44E-03	1.03E-02	4.	8.50E+00	6.07E+00	1.20E+01
0.08	1.24E-02	9.22E-03	1.47E-02	5.	1.23E+01	9.17E+00	1.67E+01
0.09	1.68E-02	1.25E-02	1.99E-02	6.	1.66E+01	1.28E+01	2.17E+01
0.1	2.16E-02	1.61E-02	2.58E-02	7.	2.12E+01	1.67E+01	2.69E+01
0.11	2.71E-02	2.02E-02	3.22E-02	8.	2.58E+01	2.08E+01	3.20E+01
0.12	3.29E-02	2.45E-02	3.92E-02	9.	3.04E+01	2.49E+01	3.70E+01
0.13	3.91E-02	2.92E-02	4.66E-02	10.	3.48E+01	2.88E+01	4.18E+01

$$\text{REV} = 4.53 \times 10^{10} T_9^{3/2} \exp(-276.74/T_9)$$

3.3. ${}^2\text{H}(\text{d}, \text{n}){}^3\text{He}$

The experimental data sets referred to in NACRE are SC72 [79], KR87a [80], BR90 [76] and GR95 [81], covering the $0.007 \lesssim E_{\text{cm}} \lesssim 3.1$ MeV range. [82-85] were apparently superseded by KR87a. Added are the post-NACRE data sets HO01 [86], LE06a [87], BY08b [88] and TU11 [89][†], extending the range down to $E_{\text{cm}} \simeq 0.002$ MeV. GA58 [90] is also included (cf. [33], however). [[†]THM via $\text{d}({}^3\text{He}, \text{n}{}^3\text{He})\text{p}$]

Figure 6 compares the DWBA and experimental S -factors. The data in the $0.004 \lesssim E_{\text{cm}} \lesssim 1$ MeV range are used for the DWBA fit. The symmetry of the entrance channel allows even and odd values of l_i for $I_i = 0, 2$ and $= 1$, respectively. The adopted parameter values are given in Table 36. The resulting $S(0) = 55.5 \pm 6.0$ keVb. In comparison, $S(0) = 55$ keVb [NACRE, quadratic polynomial], and 52.4 ± 3.5 keVb [BBN04].

Table 4 gives the reaction rates at $0.001 \leq T_9 \leq 10$, for which the DWBA-predicted and the experimental cross sections below and above $E_{\text{cm}} \simeq 0.1$ MeV are used, respectively. Figure 7 compares the present and the NACRE rates.

See [77] for an *ab initio* calculation; [91] for a second-order DWBA calculation.

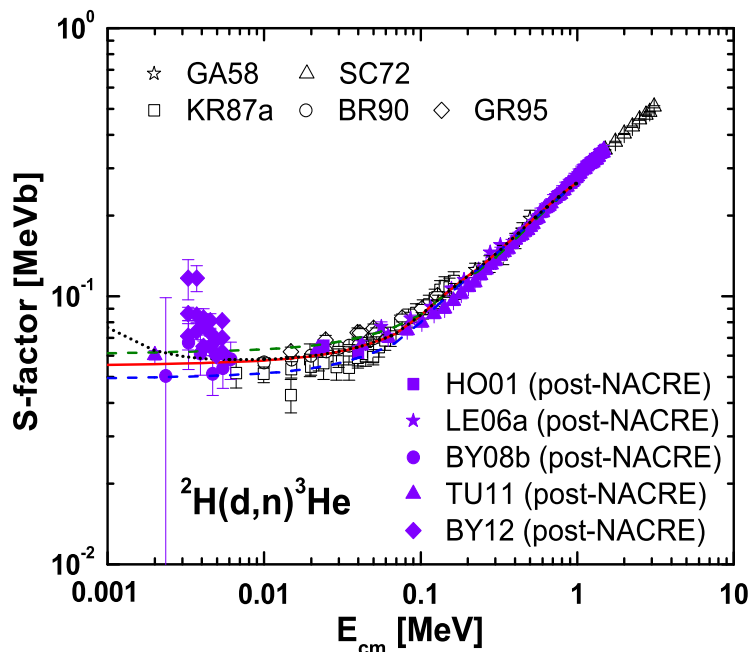


Figure 6: The S -factor for ${}^2\text{H}(\text{d}, \text{n}){}^3\text{He}$. The dotted line indicates an adiabatic screening correction ($U_e = 20.4$ eV) to the 'adopt' curve (solid line). A most recent data set BY12 [45] revealing in experiments with deuterated metals the extent and scatter of the enhanced S -factors at low energies is added just for comparison.

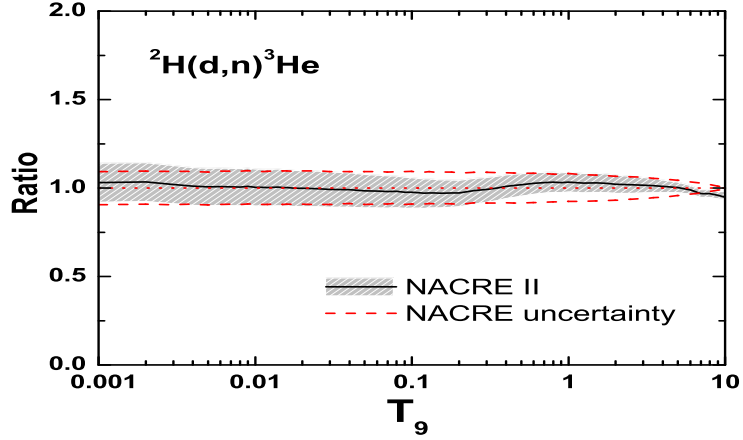


Figure 7: ${}^2\text{H}(\text{d}, \text{n}) {}^3\text{He}$ rates in units of the NACRE (adopt) values.

Table 4: ${}^2\text{H}(\text{d}, \text{n}) {}^3\text{He}$ rates in $\text{cm}^3 \text{mol}^{-1} \text{s}^{-1}$.

T_9	adopted	low	high	T_9	adopted	low	high
0.001	1.43E-08	1.28E-08	1.58E-08	0.14	5.48E+05	5.01E+05	5.92E+05
0.002	5.95E-05	5.31E-05	6.57E-05	0.15	6.38E+05	5.83E+05	6.88E+05
0.003	3.23E-03	2.89E-03	3.57E-03	0.16	7.32E+05	6.70E+05	7.89E+05
0.004	3.95E-02	3.53E-02	4.36E-02	0.18	9.36E+05	8.59E+05	1.01E+06
0.005	2.34E-01	2.09E-01	2.58E-01	0.2	1.16E+06	1.06E+06	1.24E+06
0.006	9.01E-01	8.05E-01	9.95E-01	0.25	1.77E+06	1.64E+06	1.90E+06
0.007	2.64E+00	2.36E+00	2.91E+00	0.3	2.46E+06	2.28E+06	2.63E+06
0.008	6.38E+00	5.70E+00	7.04E+00	0.35	3.20E+06	2.97E+06	3.41E+06
0.009	1.34E+01	1.20E+01	1.48E+01	0.4	3.98E+06	3.70E+06	4.23E+06
0.01	2.54E+01	2.27E+01	2.80E+01	0.45	4.78E+06	4.46E+06	5.08E+06
0.011	4.44E+01	3.97E+01	4.89E+01	0.5	5.59E+06	5.23E+06	5.93E+06
0.012	7.25E+01	6.49E+01	7.99E+01	0.6	7.25E+06	6.80E+06	7.67E+06
0.013	1.12E+02	1.01E+02	1.24E+02	0.7	8.90E+06	8.38E+06	9.40E+06
0.014	1.67E+02	1.49E+02	1.84E+02	0.8	1.05E+07	9.95E+06	1.11E+07
0.015	2.39E+02	2.14E+02	2.63E+02	0.9	1.22E+07	1.15E+07	1.28E+07
0.016	3.31E+02	2.96E+02	3.64E+02	1.	1.37E+07	1.30E+07	1.45E+07
0.018	5.88E+02	5.27E+02	6.48E+02	1.25	1.76E+07	1.66E+07	1.85E+07
0.02	9.64E+02	8.64E+02	1.06E+03	1.5	2.12E+07	2.01E+07	2.23E+07
0.025	2.58E+03	2.31E+03	2.84E+03	1.75	2.46E+07	2.34E+07	2.59E+07
0.03	5.44E+03	4.88E+03	5.97E+03	2.	2.79E+07	2.65E+07	2.93E+07
0.04	1.60E+04	1.44E+04	1.75E+04	2.5	3.39E+07	3.23E+07	3.55E+07
0.05	3.40E+04	3.07E+04	3.73E+04	3.	3.93E+07	3.76E+07	4.10E+07
0.06	6.04E+04	5.45E+04	6.60E+04	3.5	4.43E+07	4.25E+07	4.60E+07
0.07	9.52E+04	8.61E+04	1.04E+05	4.	4.87E+07	4.70E+07	5.05E+07
0.08	1.38E+05	1.25E+05	1.51E+05	5.	5.65E+07	5.48E+07	5.81E+07
0.09	1.89E+05	1.72E+05	2.06E+05	6.	6.26E+07	6.10E+07	6.42E+07
0.1	2.48E+05	2.25E+05	2.69E+05	7.	6.73E+07	6.58E+07	6.88E+07
0.11	3.13E+05	2.85E+05	3.40E+05	8.	7.27E+07	7.11E+07	7.44E+07
0.12	3.86E+05	3.51E+05	4.17E+05	9.	7.72E+07	7.54E+07	7.89E+07
0.13	4.64E+05	4.23E+05	5.02E+05	10.	8.13E+07	8.03E+07	8.40E+07

$\text{REV} = 1.73 \exp(-37.936/T_9)$

3.4. ${}^2\text{H}(\text{d}, \text{p}) {}^3\text{H}$

The experimental data sets referred to in NACRE are SC72 [79], KR87a [80], BR90 [76] and GR95 [81], covering the $0.0016 \lesssim E_{\text{cm}} \lesssim 3.1$ MeV range. [82, 83, 85, 92] were apparently superseded by KR87a. Added are the post-NACRE data sets LE06a [87] and TU11 [89][†]. [[†]from $\text{d}({}^3\text{He}, \text{p}{}^3\text{H})\text{p}$ (THM); [93] (THM) is not considered because of the stated "preliminary" nature of the data.]

Figure 8 compares the DWBA and experimental S -factors. GR95 using a D_2 gas target appears to indicate a modest electron screening effect, if at all, at the lowest energies. In contrast, measurements with deuterated metal targets indicate huge cross section enhancements at low energies (see RA02 [94] in Fig. 8). The data in the $0.004 \lesssim E_{\text{cm}} \lesssim 1$ MeV range are used for the DWBA fit. The symmetry of the entrance channel allows even and odd values of l_i for $I_i = 0, 2$ and $= 1$, respectively. The adopted parameter values are given in Table 37. The present $S(0) = 56.2^{+4.9}_{-4.7}$ keV b. In comparison, $S(0) = 56$ keV b [NACRE, quadratic polynomial], and 57.1 ± 0.8 keV b [BBN04].

Table 5 gives the reaction rates at $0.001 \leq T_9 \leq 10$, for which the DWBA-predicted and experimental cross sections below and above $E_{\text{cm}} \simeq 0.1$ MeV are used, respectively. Figure 9 compares the present and the NACRE rates.

See the ${}^2\text{H}(\text{d}, \text{n}) {}^3\text{He}$ counterpart in Sect. 3.3.

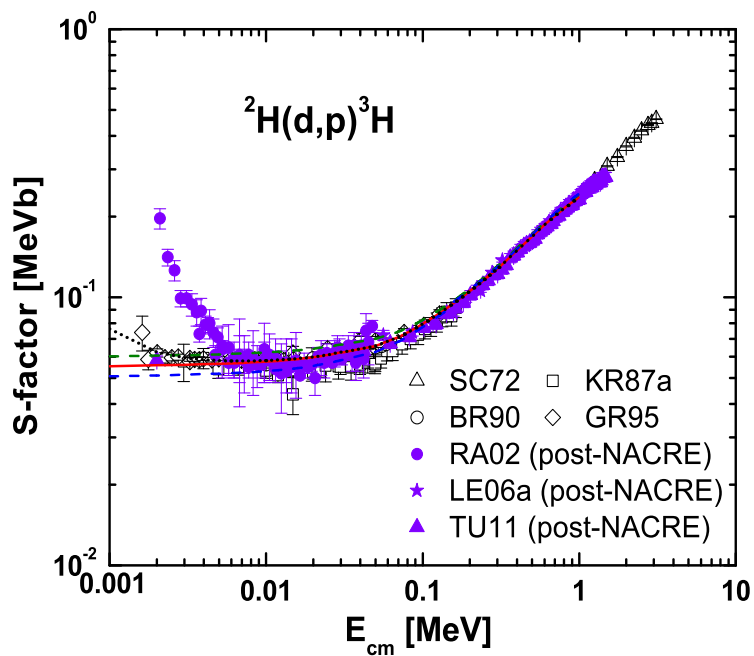


Figure 8: The S -factor for ${}^2\text{H}(\text{d}, \text{p}) {}^3\text{H}$. The dotted line indicates an adiabatic screening correction ($U_e = 20.4$ eV) to the 'adopt' curve (solid line). RA02 [94] with a TaD target is added just to exhibit the hugely enhanced S -factors at low energies.

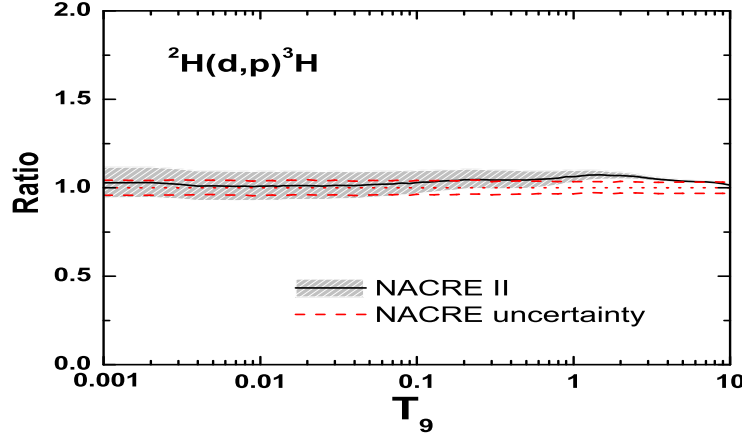


Figure 9: ${}^2\text{H}(\text{d}, \text{p}) {}^3\text{H}$ rates in units of the NACRE (adopt) values.

Table 5: ${}^2\text{H}(\text{d}, \text{p}) {}^3\text{H}$ rates in $\text{cm}^3 \text{mol}^{-1} \text{s}^{-1}$

T_9	adopted	low	high	T_9	adopted	low	high
0.001	1.45E-08	1.33E-08	1.57E-08	0.14	5.57E+05	5.26E+05	5.91E+05
0.002	6.02E-05	5.52E-05	6.54E-05	0.15	6.47E+05	6.12E+05	6.87E+05
0.003	3.27E-03	3.00E-03	3.55E-03	0.16	7.42E+05	7.02E+05	7.87E+05
0.004	4.00E-02	3.67E-02	4.34E-02	0.18	9.44E+05	8.95E+05	1.00E+06
0.005	2.36E-01	2.17E-01	2.57E-01	0.2	1.16E+06	1.10E+06	1.23E+06
0.006	9.12E-01	8.38E-01	9.89E-01	0.25	1.75E+06	1.66E+06	1.84E+06
0.007	2.67E+00	2.45E+00	2.90E+00	0.3	2.38E+06	2.26E+06	2.51E+06
0.008	6.46E+00	5.94E+00	7.00E+00	0.35	3.04E+06	2.89E+06	3.20E+06
0.009	1.36E+01	1.25E+01	1.47E+01	0.4	3.72E+06	3.54E+06	3.91E+06
0.01	2.57E+01	2.37E+01	2.79E+01	0.45	4.41E+06	4.20E+06	4.63E+06
0.011	4.49E+01	4.13E+01	4.87E+01	0.5	5.11E+06	4.87E+06	5.36E+06
0.012	7.34E+01	6.76E+01	7.96E+01	0.6	6.52E+06	6.23E+06	6.82E+06
0.013	1.14E+02	1.05E+02	1.23E+02	0.7	7.93E+06	7.61E+06	8.27E+06
0.014	1.69E+02	1.56E+02	1.83E+02	0.8	9.34E+06	8.99E+06	9.71E+06
0.015	2.42E+02	2.23E+02	2.62E+02	0.9	1.07E+07	1.04E+07	1.11E+07
0.016	3.35E+02	3.09E+02	3.63E+02	1.	1.21E+07	1.17E+07	1.25E+07
0.018	5.96E+02	5.49E+02	6.45E+02	1.25	1.54E+07	1.50E+07	1.59E+07
0.02	9.77E+02	9.01E+02	1.06E+03	1.5	1.86E+07	1.81E+07	1.90E+07
0.025	2.62E+03	2.41E+03	2.83E+03	1.75	2.15E+07	2.11E+07	2.19E+07
0.03	5.51E+03	5.10E+03	5.95E+03	2.	2.43E+07	2.38E+07	2.47E+07
0.04	1.62E+04	1.50E+04	1.74E+04	2.5	2.94E+07	2.89E+07	2.98E+07
0.05	3.46E+04	3.21E+04	3.72E+04	3.	3.40E+07	3.35E+07	3.44E+07
0.06	6.14E+04	5.71E+04	6.59E+04	3.5	3.82E+07	3.77E+07	3.86E+07
0.07	9.68E+04	9.02E+04	1.04E+05	4.	4.21E+07	4.17E+07	4.25E+07
0.08	1.41E+05	1.31E+05	1.50E+05	5.	4.91E+07	4.88E+07	4.95E+07
0.09	1.93E+05	1.80E+05	2.06E+05	6.	5.54E+07	5.51E+07	5.58E+07
0.1	2.52E+05	2.37E+05	2.69E+05	7.	6.10E+07	6.07E+07	6.14E+07
0.11	3.19E+05	3.00E+05	3.40E+05	8.	6.59E+07	6.55E+07	6.63E+07
0.12	3.92E+05	3.69E+05	4.17E+05	9.	7.00E+07	6.96E+07	7.03E+07
0.13	4.72E+05	4.45E+05	5.02E+05	10.	7.33E+07	7.29E+07	7.36E+07

$\text{REV} = 1.73 \exp(-46.799/T_9)$

3.5. ${}^2\text{H}(\alpha, \gamma) {}^6\text{Li}$

The experimental data sets referred to in NACRE are RO81 [95], KI91 [96][†] and MO94 [97], covering the $0.07 \lesssim E_{\text{cm}} \lesssim 8.3$ MeV range. No new cross section data are found, but HA10 [98][‡] is additionally considered. [[†]from Coulomb break-up (digital data given in the NACRE home page). [‡]potential-model analysis after Coulomb break-up experiments.]

Figure 10 compares the PM and experimental S -factors. The data in the $E_{\text{cm}} \lesssim 3$ MeV range are used for the PM fit. They exhibit the 3^+ and 2^+ resonances at $E_R \simeq 0.71$ and 3.89 MeV. As discussed in HA10 in detail, Coulomb break-up experiments get progressively unreliable at lower energies because of the larger nuclear break-up contributions to be separated. Below $E_{\text{cm}} \simeq 0.7$ MeV, therefore, we adopt the model analysis of HA10 to guide the extrapolation (see Fig. 10). The quasi-orthogonality between the $J_i = 1^+$ scattering state and the 1^+ ground state of ${}^6\text{Li}$ suppresses M1 transitions (s-wave) at low energies. Isospin-forbidden E1 transitions (p-wave) thus dominate at very low energies, but are surpassed by the E2 transitions (d-wave) at higher energies. The adopted parameter values are given in Table 53. The present $S(0) = 2.2^{+0.9}_{-1.2}$ meV b.

Table 6 gives the reaction rates at $0.002 \leq T_9 \leq 10$, for which the PM-predicted and the experimental cross sections below and above $E_{\text{cm}} \simeq 0.7$ MeV are used, respectively. Figure 11 compares the present and the NACRE rates.

See [99] for an *ab initio* calculation

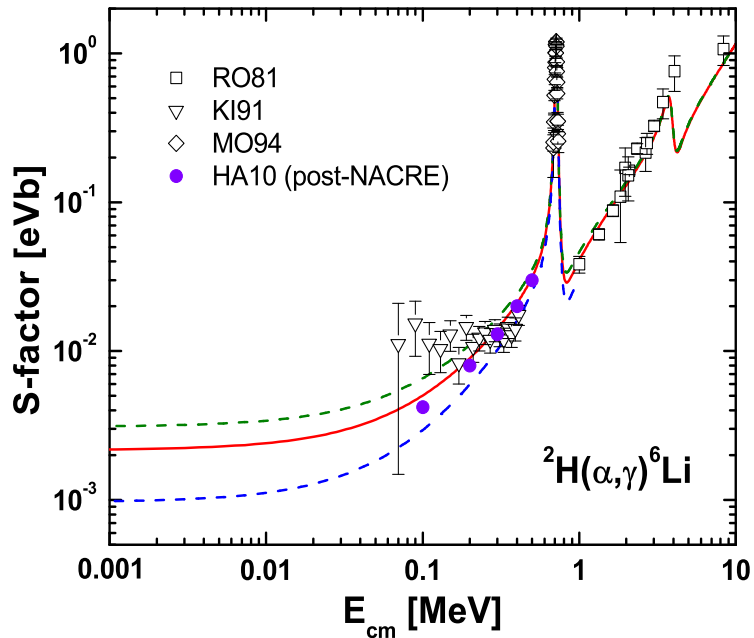


Figure 10: The S -factor for ${}^2\text{H}(\alpha, \gamma) {}^6\text{Li}$. Note that HA10 points between E_{cm} 0.1 and 0.5 are read off from the S -factor *curve* of the potential model analysis after the Coulomb break-up experiments (see text), which gives $S(0) \simeq 1.9$ meV b.

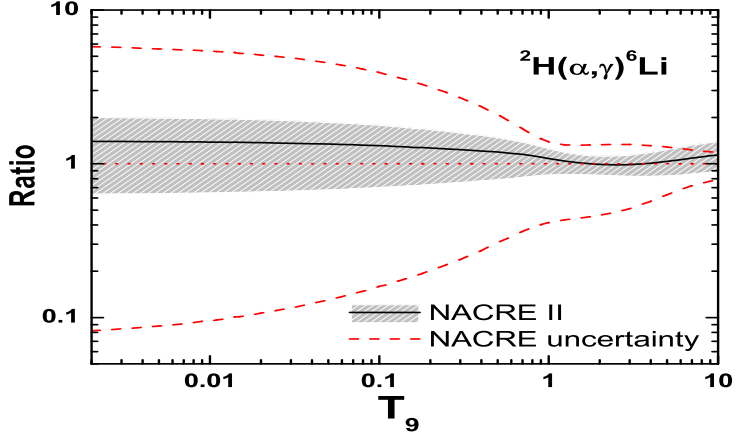


Figure 11: ${}^2\text{H}(\alpha, \gamma){}^6\text{Li}$ rates in units of the NACRE (adopt) values. Much larger uncertainties in NACRE stem from the adoption of the various estimates of the E1 contributions in early studies, and in particular of KI91 for the upper limit.

Table 6: ${}^2\text{H}(\alpha, \gamma){}^6\text{Li}$ rates in $\text{cm}^3\text{mol}^{-1}\text{s}^{-1}$

T_9	adopted	low	high	T_9	adopted	low	high
0.002	2.98E-23	1.35E-23	4.26E-23	0.15	1.13E-04	6.29E-05	1.50E-04
0.003	4.01E-20	1.83E-20	5.72E-20	0.16	1.49E-04	8.40E-05	1.99E-04
0.004	3.73E-18	1.71E-18	5.32E-18	0.18	2.46E-04	1.41E-04	3.26E-04
0.005	9.34E-17	4.29E-17	1.33E-16	0.2	3.80E-04	2.20E-04	4.99E-04
0.006	1.09E-15	5.00E-16	1.54E-15	0.25	9.10E-04	5.43E-04	1.18E-03
0.007	7.67E-15	3.55E-15	1.09E-14	0.3	1.79E-03	1.09E-03	2.30E-03
0.008	3.85E-14	1.78E-14	5.46E-14	0.35	3.09E-03	1.93E-03	3.94E-03
0.009	1.50E-13	6.98E-14	2.13E-13	0.4	4.89E-03	3.12E-03	6.16E-03
0.01	4.84E-13	2.26E-13	6.86E-13	0.45	7.24E-03	4.70E-03	9.05E-03
0.011	1.35E-12	6.30E-13	1.91E-12	0.5	1.02E-02	6.75E-03	1.27E-02
0.012	3.33E-12	1.56E-12	4.71E-12	0.6	1.84E-02	1.26E-02	2.24E-02
0.013	7.48E-12	3.52E-12	1.06E-11	0.7	3.04E-02	2.15E-02	3.65E-02
0.014	1.55E-11	7.31E-12	2.19E-11	0.8	4.78E-02	3.51E-02	5.66E-02
0.015	3.01E-11	1.42E-11	4.25E-11	0.9	7.26E-02	5.50E-02	8.48E-02
0.016	5.51E-11	2.61E-11	7.77E-11	1.	1.06E-01	8.29E-02	1.23E-01
0.018	1.61E-10	7.65E-11	2.26E-10	1.25	2.36E-01	1.93E-01	2.69E-01
0.02	4.04E-10	1.93E-10	5.68E-10	1.5	4.28E-01	3.59E-01	4.84E-01
0.025	2.55E-09	1.23E-09	3.58E-09	1.75	6.67E-01	5.64E-01	7.53E-01
0.03	1.04E-08	5.07E-09	1.46E-08	2.	9.32E-01	7.92E-01	1.05E+00
0.04	8.06E-08	3.99E-08	1.12E-07	2.5	1.49E+00	1.26E+00	1.70E+00
0.05	3.45E-07	1.74E-07	4.77E-07	3.	2.03E+00	1.71E+00	2.34E+00
0.06	1.05E-06	5.34E-07	1.44E-06	3.5	2.57E+00	2.13E+00	2.99E+00
0.07	2.54E-06	1.31E-06	3.49E-06	4.	3.10E+00	2.54E+00	3.64E+00
0.08	5.29E-06	2.77E-06	7.23E-06	5.	4.22E+00	3.39E+00	5.04E+00
0.09	9.85E-06	5.21E-06	1.34E-05	6.	5.50E+00	4.36E+00	6.63E+00
0.1	1.68E-05	8.98E-06	2.28E-05	7.	6.98E+00	5.49E+00	8.46E+00
0.11	2.69E-05	1.45E-05	3.63E-05	8.	8.67E+00	6.79E+00	1.05E+01
0.12	4.08E-05	2.22E-05	5.49E-05	9.	1.05E+01	8.23E+00	1.28E+01
0.13	5.92E-05	3.25E-05	7.94E-05	10.	1.25E+01	9.79E+00	1.53E+01
0.14	8.29E-05	4.59E-05	1.11E-04				

$$\text{REV} = 1.53 \times 10^{10} T_9^{3/2} \exp(-17.104/T_9) / [1.0 + 2.333 \exp(-25.369/T_9)]$$

3.6. ${}^3\text{H}(\text{d}, \text{n}) {}^4\text{He}$

The experimental data sets referred to in NACRE are BR51a [100], AR52 [101], CO52 [102], AR54 [83], HE55 [103], GA56 [104], BA57 [105], GO61 [106], KO66 [107], MC73 [108], MA75 [109], JA84 [110] and BR87a [111], covering the $0.005 \lesssim E_{\text{cm}} \lesssim 9.6$ MeV range. No new cross section data are found.

Figure 12 compares the DWBA and experimental S -factors. The data in the $E_{\text{cm}} \lesssim 1$ MeV range are used for the DWBA fit. They exhibit the $3/2^+$ resonance at $E_R \simeq 0.05$ MeV. The adopted parameter values are given in Table 38. The present $S(0) = 11 \pm 1$ MeV b. In comparison, $S(0) = 11.7 \pm 0.2$ MeV b [BBN04].

Table 7 gives the reaction rates at $0.001 \leq T_9 \leq 10$, for which the DWBA-predicted and the experimental cross sections below and above $E_{\text{cm}} \simeq 0.01$ MeV are used, respectively. Figure 13 compares the present and the NACRE rates.

See [112] for an *ab initio* calculation.

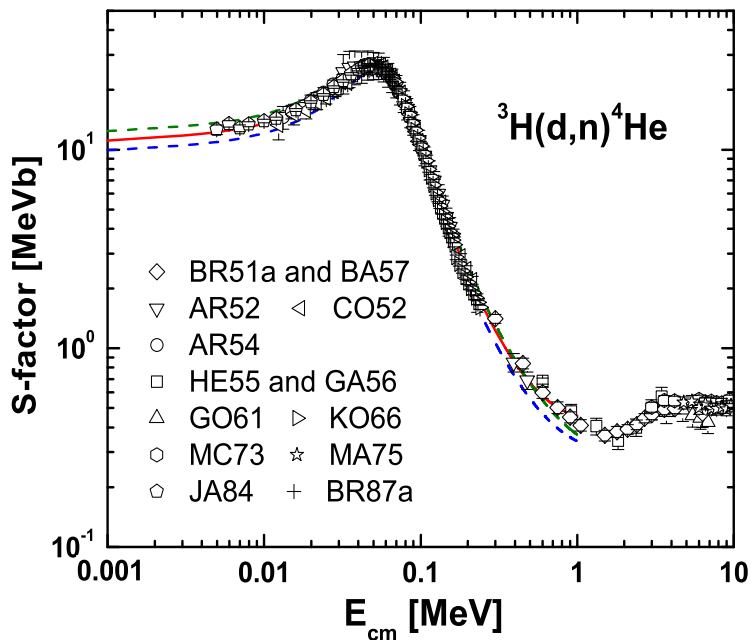


Figure 12: The S -factor for ${}^3\text{H}(\text{d}, \text{n}) {}^4\text{He}$.

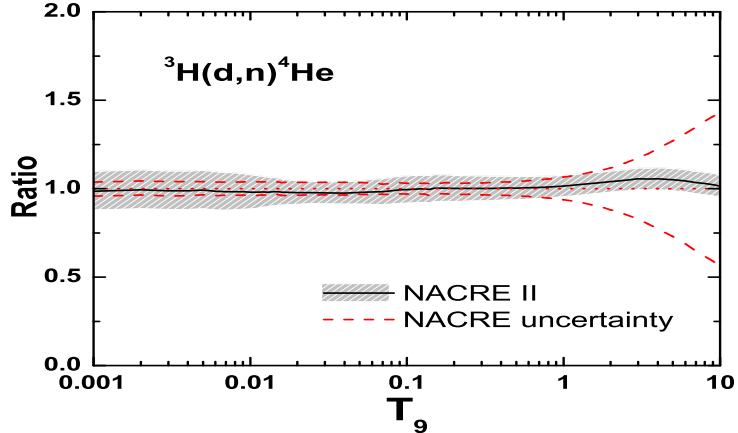


Figure 13: ${}^3\text{H}(\text{d}, \text{n}){}^4\text{He}$ rates in units of the NACRE (adopt) values. The origin of the NACRE large uncertainties diverging at the highest temperatures is unknown.

Table 7: ${}^3\text{H}(\text{d}, \text{n}){}^4\text{He}$ rates in $\text{cm}^3\text{mol}^{-1}\text{s}^{-1}$.

T_9	adopted	low	high	T_9	adopted	low	high
0.001	1.87E-07	1.67E-07	2.09E-07	0.14	1.05E+08	9.66E+07	1.13E+08
0.002	1.37E-03	1.22E-03	1.53E-03	0.15	1.21E+08	1.12E+08	1.31E+08
0.003	9.98E-02	8.90E-02	1.11E-01	0.16	1.38E+08	1.28E+08	1.49E+08
0.004	1.47E+00	1.31E+00	1.64E+00	0.18	1.73E+08	1.60E+08	1.85E+08
0.005	9.93E+00	8.86E+00	1.10E+01	0.2	2.06E+08	1.91E+08	2.21E+08
0.006	4.24E+01	3.78E+01	4.71E+01	0.25	2.83E+08	2.63E+08	3.04E+08
0.007	1.35E+02	1.20E+02	1.50E+02	0.3	3.47E+08	3.23E+08	3.72E+08
0.008	3.49E+02	3.12E+02	3.87E+02	0.35	3.98E+08	3.70E+08	4.25E+08
0.009	7.80E+02	7.01E+02	8.62E+02	0.4	4.36E+08	4.07E+08	4.66E+08
0.01	1.56E+03	1.41E+03	1.71E+03	0.45	4.65E+08	4.34E+08	4.96E+08
0.011	2.85E+03	2.59E+03	3.12E+03	0.5	4.85E+08	4.53E+08	5.17E+08
0.012	4.87E+03	4.44E+03	5.31E+03	0.6	5.10E+08	4.77E+08	5.42E+08
0.013	7.85E+03	7.19E+03	8.53E+03	0.7	5.19E+08	4.86E+08	5.51E+08
0.014	1.21E+04	1.11E+04	1.31E+04	0.8	5.19E+08	4.87E+08	5.50E+08
0.015	1.79E+04	1.65E+04	1.93E+04	0.9	5.13E+08	4.82E+08	5.44E+08
0.016	2.56E+04	2.37E+04	2.75E+04	1.	5.04E+08	4.74E+08	5.34E+08
0.018	4.81E+04	4.48E+04	5.16E+04	1.25	4.76E+08	4.48E+08	5.04E+08
0.02	8.30E+04	7.74E+04	8.87E+04	1.5	4.47E+08	4.21E+08	4.73E+08
0.025	2.47E+05	2.32E+05	2.63E+05	1.75	4.19E+08	3.95E+08	4.43E+08
0.03	5.70E+05	5.34E+05	6.06E+05	2.	3.94E+08	3.71E+08	4.17E+08
0.04	1.93E+06	1.81E+06	2.06E+06	2.5	3.52E+08	3.32E+08	3.72E+08
0.05	4.62E+06	4.30E+06	4.93E+06	3.	3.19E+08	3.00E+08	3.37E+08
0.06	8.98E+06	8.34E+06	9.63E+06	3.5	2.92E+08	2.75E+08	3.09E+08
0.07	1.52E+07	1.41E+07	1.64E+07	4.	2.70E+08	2.54E+08	2.86E+08
0.08	2.34E+07	2.16E+07	2.52E+07	5.	2.37E+08	2.23E+08	2.52E+08
0.09	3.35E+07	3.09E+07	3.61E+07	6.	2.14E+08	2.01E+08	2.27E+08
0.1	4.52E+07	4.17E+07	4.88E+07	7.	1.97E+08	1.84E+08	2.09E+08
0.11	5.85E+07	5.40E+07	6.30E+07	8.	1.83E+08	1.72E+08	1.95E+08
0.12	7.30E+07	6.73E+07	7.86E+07	9.	1.73E+08	1.62E+08	1.84E+08
0.13	8.84E+07	8.16E+07	9.52E+07	10.	1.64E+08	1.54E+08	1.75E+08

REV = $5.54 \exp(-204.12/T_9)$

3.7. ${}^3\text{H}(\alpha, \gamma) {}^7\text{Li}$

The experimental data sets referred to in NACRE are GR61 [113], BU87 [114], and BR94 [115], covering the $0.05 \lesssim E_{\text{cm}} \lesssim 1.2$ MeV range. [116] was rejected. Added is the post-NACRE data set TO01 [117][†]. [[†]from Coulomb break-up]

Figure 14 compares the PM and experimental S -factors. All the data sets but TO01 are used in the whole E_{cm} range for the PM fit. The transitions to the ground and the first excited states of ${}^7\text{Li}$ are considered inclusively. The adopted parameter values are given in Table 54. The present $S(0) = 98^{+11}_{-8}$ eV b. In comparison, $S(0) = 100$ eV b [NACRE, E -dependence of [118]], and 95 ± 5 eV b [BBN04].

Table 8 gives the reaction rates at $0.002 \leq T_9 \leq 10$, for which the PM-predicted cross sections in the $E_{\text{cm}} \lesssim 0.3$ MeV and $E_{\text{cm}} \gtrsim 1.2$ MeV ranges, and the experimental ones in the $0.3 \lesssim E_{\text{cm}} \lesssim 1.2$ MeV range are used, respectively. Figure 15 compares the present and the NACRE rates.

See [119] for an *ab initio* calculation.

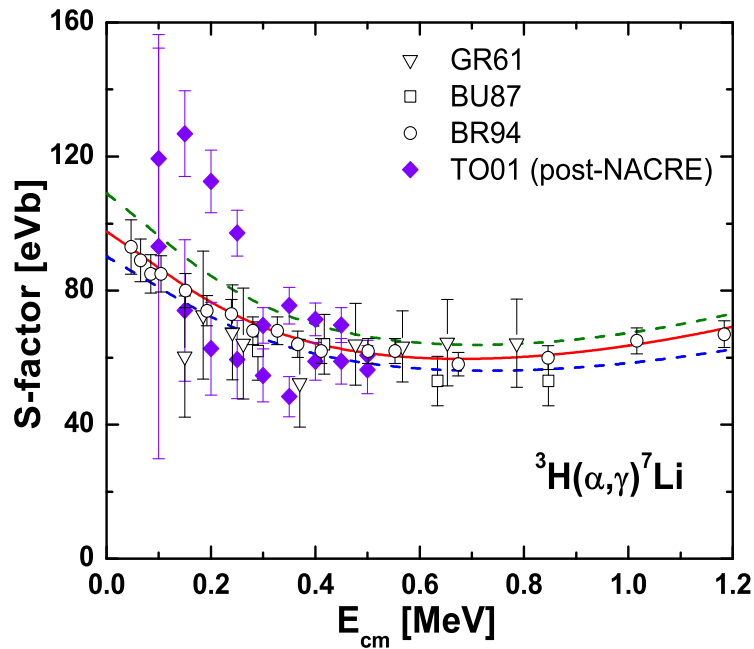


Figure 14: The S -factor for ${}^3\text{H}(\alpha, \gamma) {}^7\text{Li}$. TO01 is shown just for comparison and has not been used in the fit.

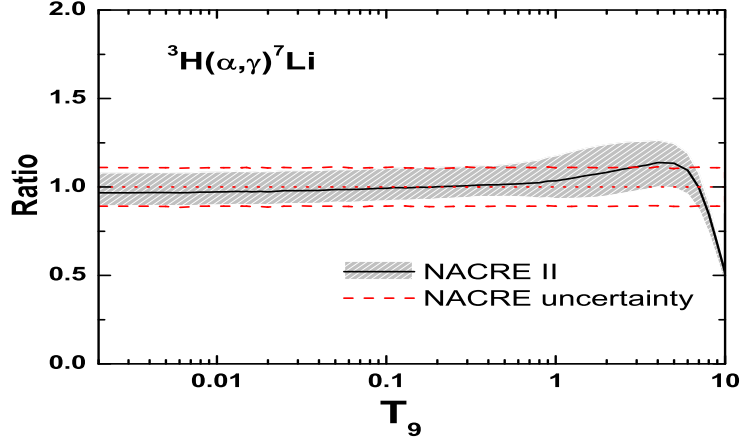


Figure 15: ${}^3\text{H}(\alpha, \gamma) {}^7\text{Li}$ rates in units of the NACRE (adopt) values. The sharp decrease of the ratio at the highest temperatures results from the rapid increase of the S -factors at high energies [118] adopted by NACRE.

Table 8: ${}^3\text{H}(\alpha, \gamma) {}^7\text{Li}$ rates in $\text{cm}^3\text{mol}^{-1}\text{s}^{-1}$

T_9	adopted	low	high	T_9	adopted	low	high
0.002	7.06E-21	6.52E-21	7.88E-21	0.15	6.64E-01	6.18E-01	7.38E-01
0.003	1.79E-17	1.65E-17	2.00E-17	0.16	8.76E-01	8.15E-01	9.73E-01
0.004	2.48E-15	2.29E-15	2.77E-15	0.18	1.43E+00	1.33E+00	1.58E+00
0.005	8.21E-14	7.59E-14	9.17E-14	0.2	2.16E+00	2.01E+00	2.40E+00
0.006	1.18E-12	1.09E-12	1.32E-12	0.25	4.93E+00	4.60E+00	5.46E+00
0.007	9.87E-12	9.12E-12	1.10E-11	0.3	9.14E+00	8.54E+00	1.01E+01
0.008	5.68E-11	5.25E-11	6.34E-11	0.35	1.49E+01	1.39E+01	1.65E+01
0.009	2.49E-10	2.30E-10	2.77E-10	0.4	2.21E+01	2.06E+01	2.44E+01
0.01	8.85E-10	8.18E-10	9.88E-10	0.45	3.07E+01	2.86E+01	3.40E+01
0.011	2.68E-09	2.48E-09	2.99E-09	0.5	4.06E+01	3.79E+01	4.51E+01
0.012	7.15E-09	6.61E-09	7.98E-09	0.6	6.39E+01	5.93E+01	7.13E+01
0.013	1.72E-08	1.59E-08	1.92E-08	0.7	9.12E+01	8.41E+01	1.02E+02
0.014	3.78E-08	3.49E-08	4.22E-08	0.8	1.22E+02	1.11E+02	1.37E+02
0.015	7.73E-08	7.15E-08	8.62E-08	0.9	1.55E+02	1.41E+02	1.75E+02
0.016	1.49E-07	1.37E-07	1.66E-07	1.	1.90E+02	1.72E+02	2.16E+02
0.018	4.72E-07	4.36E-07	5.26E-07	1.25	2.85E+02	2.54E+02	3.26E+02
0.02	1.27E-06	1.18E-06	1.42E-06	1.5	3.87E+02	3.42E+02	4.44E+02
0.025	9.25E-06	8.56E-06	1.03E-05	1.75	4.92E+02	4.32E+02	5.65E+02
0.03	4.17E-05	3.86E-05	4.65E-05	2.	5.99E+02	5.24E+02	6.86E+02
0.04	3.70E-04	3.42E-04	4.12E-04	2.5	8.15E+02	7.13E+02	9.28E+02
0.05	1.73E-03	1.60E-03	1.92E-03	3.	1.03E+03	9.04E+02	1.17E+03
0.06	5.55E-03	5.14E-03	6.18E-03	3.5	1.25E+03	1.11E+03	1.40E+03
0.07	1.40E-02	1.30E-02	1.56E-02	4.	1.46E+03	1.28E+03	1.62E+03
0.08	3.00E-02	2.78E-02	3.34E-02	5.	1.86E+03	1.63E+03	2.04E+03
0.09	5.68E-02	5.27E-02	6.32E-02	6.	2.27E+03	1.99E+03	2.42E+03
0.1	9.83E-02	9.12E-02	1.09E-01	7.	2.51E+03	2.19E+03	2.73E+03
0.11	1.58E-01	1.47E-01	1.76E-01	8.	2.74E+03	2.38E+03	2.96E+03
0.12	2.41E-01	2.24E-01	2.68E-01	9.	2.91E+03	2.51E+03	3.13E+03
0.13	3.50E-01	3.26E-01	3.90E-01	10.	3.02E+03	2.61E+03	3.25E+03
0.14	4.90E-01	4.56E-01	5.45E-01				

$$\text{REV} = 1.11 \times 10^{10} T_9^{3/2} \exp(-28.625/T_9) / [1.0 + 0.5 \exp(-5.543/T_9)]$$

3.8. ${}^3\text{He}(\text{d}, \text{p}) {}^4\text{He}$

This reaction is not included in NACRE, but is present in CF88. The experimental data sets adopted here are KR87a [80], SC89 [120], GE99 [121], CO00 [122], AL01 [123], and LA05 [124][†], covering the $0.005 \lesssim E_{\text{cm}} \lesssim 1$ MeV range. [125, 126] are superseded by AL01. [[†]from ${}^6\text{Li}({}^3\text{He}, \text{p}\alpha) {}^4\text{He}$ (THM).]

Figure 16 compares the DWBA and the experimental S -factors, whereas Figs. 17 and 18 summarise the pre- and post-CF88 experimental data sets, respectively. Many post-CF88 measurements below $E_{\text{cm}} \simeq 0.02$ MeV look highly contaminated by electron screening (see Fig. 18; also see [136]). Only the data in the $0.02 \lesssim E_{\text{cm}} \lesssim 1$ MeV range are used for the DWBA fit. They exhibit the $3/2^+$ resonance at $E_R \simeq 0.21$ MeV. The adopted parameter values are given in Table 39. The present $S(0) = 5.9 \pm 0.5$ MeV b. In comparison, $S(0) = 5.9 \pm 0.3$ MeV b [BBN04].

Table 9 gives the reaction rates at $0.001 \leq T_9 \leq 10$, for which the DWBA-predicted and the experimental cross sections below and above $E_{\text{cm}} \simeq 0.05$ MeV are used, respectively. Figure 19 compares the present and the CF88 rates.

See [112] for an *ab initio* calculation.

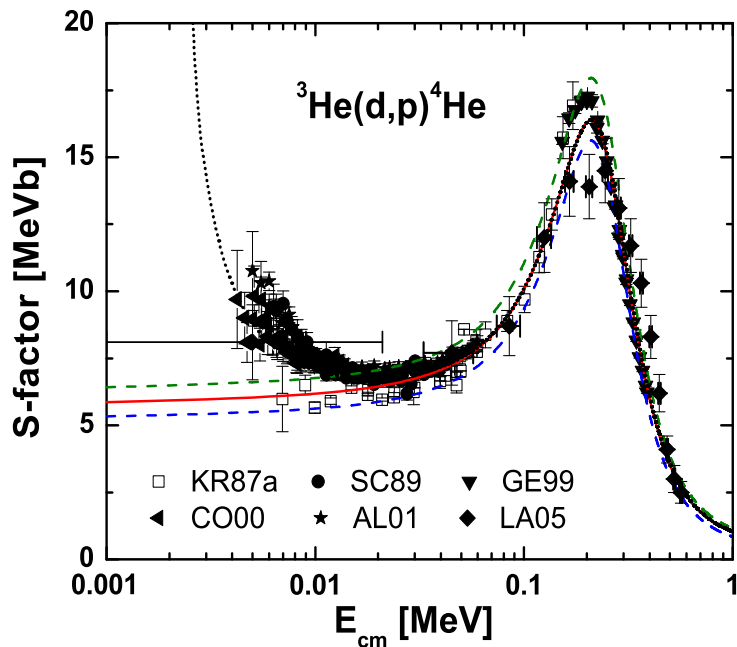


Figure 16: The S -factor for ${}^3\text{He}(\text{d}, \text{p}) {}^4\text{He}$. The dotted line indicates an adiabatic screening correction ($U_e = 119$ eV) to the 'adopt' curve (solid line).

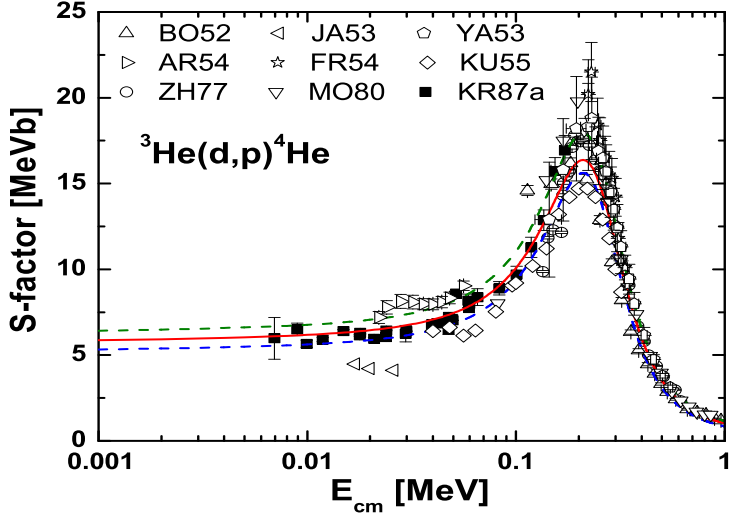


Figure 17: The pre-CF88 experimental S -factor data sets for ${}^3\text{He}(\text{d}, \text{p}) {}^4\text{He}$: BO52 [127], JA53 [128], YA53 [129], AR54 [83], FR54 [130], KU55 [131], ZH77 [132], MO80 [133], and KR87a [80]. The DWBA curves are added to guide the eye. CF88 relies on KR87a at low energies. See [134, 135] for data above $E_{\text{cm}} \gtrsim 1$ MeV.

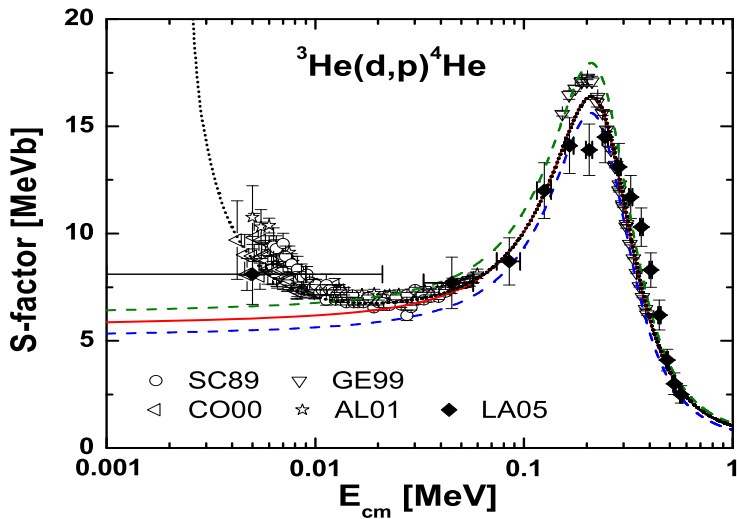


Figure 18: The post-CF88 experimental S -factor data sets for ${}^3\text{He}(\text{d}, \text{p}) {}^4\text{He}$. The DWBAhe3ag and screening correction curves are added to guide the eyes. Recall that the LA05 data points are from THM, but one at the lowest energy is not considered in our analysis because of its large uncertainties.

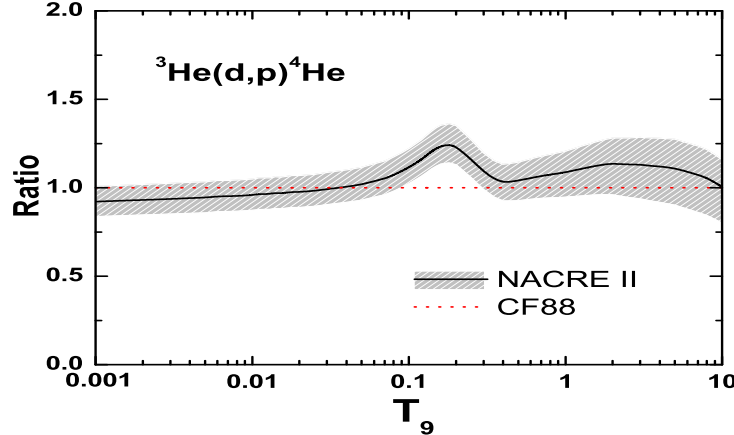


Figure 19: ${}^3\text{He}(\text{d}, \text{p}) {}^4\text{He}$ rates in units of the CF88 values.

Table 9: ${}^3\text{He}(\text{d}, \text{p}) {}^4\text{He}$ rates in $\text{cm}^3 \text{mol}^{-1} \text{s}^{-1}$.

T_9	adopted	low	high	T_9	adopted	low	high
0.001	3.54E-19	3.21E-19	3.87E-19	0.14	2.88E+05	2.64E+05	3.15E+05
0.002	6.14E-13	5.58E-13	6.72E-13	0.15	3.85E+05	3.53E+05	4.22E+05
0.003	6.36E-10	5.78E-10	6.96E-10	0.16	5.03E+05	4.61E+05	5.51E+05
0.004	5.02E-08	4.56E-08	5.49E-08	0.18	8.07E+05	7.40E+05	8.84E+05
0.005	1.11E-06	1.01E-06	1.22E-06	0.2	1.22E+06	1.11E+06	1.33E+06
0.006	1.18E-05	1.07E-05	1.29E-05	0.25	2.77E+06	2.53E+06	3.04E+06
0.007	7.74E-05	7.04E-05	8.47E-05	0.3	5.19E+06	4.71E+06	5.69E+06
0.008	3.64E-04	3.31E-04	3.99E-04	0.35	8.51E+06	7.68E+06	9.34E+06
0.009	1.35E-03	1.23E-03	1.48E-03	0.4	1.27E+07	1.14E+07	1.39E+07
0.01	4.15E-03	3.78E-03	4.54E-03	0.45	1.76E+07	1.57E+07	1.93E+07
0.011	1.11E-02	1.01E-02	1.21E-02	0.5	2.31E+07	2.06E+07	2.54E+07
0.012	2.64E-02	2.40E-02	2.89E-02	0.6	3.53E+07	3.13E+07	3.89E+07
0.013	5.74E-02	5.22E-02	6.29E-02	0.7	4.83E+07	4.26E+07	5.33E+07
0.014	1.16E-01	1.05E-01	1.26E-01	0.8	6.12E+07	5.37E+07	6.77E+07
0.015	2.18E-01	1.98E-01	2.39E-01	0.9	7.35E+07	6.42E+07	8.15E+07
0.016	3.89E-01	3.54E-01	4.26E-01	1.	8.49E+07	7.39E+07	9.43E+07
0.018	1.08E+00	9.87E-01	1.19E+00	1.25	1.09E+08	9.40E+07	1.21E+08
0.02	2.62E+00	2.38E+00	2.87E+00	1.5	1.27E+08	1.08E+08	1.42E+08
0.025	1.52E+01	1.39E+01	1.67E+01	1.75	1.39E+08	1.18E+08	1.56E+08
0.03	5.82E+01	5.30E+01	6.37E+01	2.	1.48E+08	1.25E+08	1.67E+08
0.04	4.07E+02	3.71E+02	4.46E+02	2.5	1.57E+08	1.31E+08	1.78E+08
0.05	1.62E+03	1.48E+03	1.77E+03	3.	1.61E+08	1.33E+08	1.83E+08
0.06	4.63E+03	4.23E+03	5.07E+03	3.5	1.61E+08	1.32E+08	1.83E+08
0.07	1.07E+04	9.80E+03	1.17E+04	4.	1.59E+08	1.30E+08	1.82E+08
0.08	2.14E+04	1.96E+04	2.35E+04	5.	1.53E+08	1.24E+08	1.76E+08
0.09	3.85E+04	3.52E+04	4.22E+04	6.	1.46E+08	1.18E+08	1.68E+08
0.1	6.38E+04	5.85E+04	6.99E+04	7.	1.38E+08	1.11E+08	1.59E+08
0.11	9.94E+04	9.11E+04	1.09E+05	8.	1.31E+08	1.05E+08	1.51E+08
0.12	1.47E+05	1.35E+05	1.61E+05	9.	1.24E+08	9.85E+07	1.42E+08
0.13	2.09E+05	1.92E+05	2.29E+05	10.	1.17E+08	9.27E+07	1.34E+08

REV = $5.54 \exp(-212.99/T_9)$

3.9. ${}^3\text{He}({}^3\text{He}, 2\text{p}){}^4\text{He}$

The experimental data sets referred to in NACRE are WA66 [137], BA67 [138], DW71 [139], DW74 [140], BR87b [141], KR87b [142] and JU98 [143], covering the $0.02 \lesssim E_{\text{cm}} \lesssim 12$ MeV range. [144] was superseded by JU98. Added are the post-NACRE data sets BO99 [145] and KU04 [146], extending the range down to $E_{\text{cm}} \simeq 0.016$ MeV.

Figure 20 compares the DWBA and experimental S -factors. JU98 and BO99 look contaminated by electron screening at the lowest energies. The data in the $0.03 \lesssim E_{\text{cm}} \lesssim 1$ MeV range are used for the DWBA fit. The two-protons in the exit channel are treated as a point-like spinless particle. The adopted parameter values are given in Table 40. The present $S(0) = 5.3 \pm 0.5$ MeV b. In comparison, $S(0) = 5.18$ MeV b [NACRE, quadratic polynomial], and 5.21 ± 0.27 MeV b [SUN11, quadratic polynomial].

Table 10 gives the reaction rates at $0.003 \leq T_9 \leq 10$, for which the DWBA-predicted and the experimental cross sections below and above $E_{\text{cm}} \simeq 0.1$ MeV are used, respectively. Figure 21 compares the present and the NACRE rates.

See [147] for a large scale cluster model calculation; [148] for a DWBA analysis.

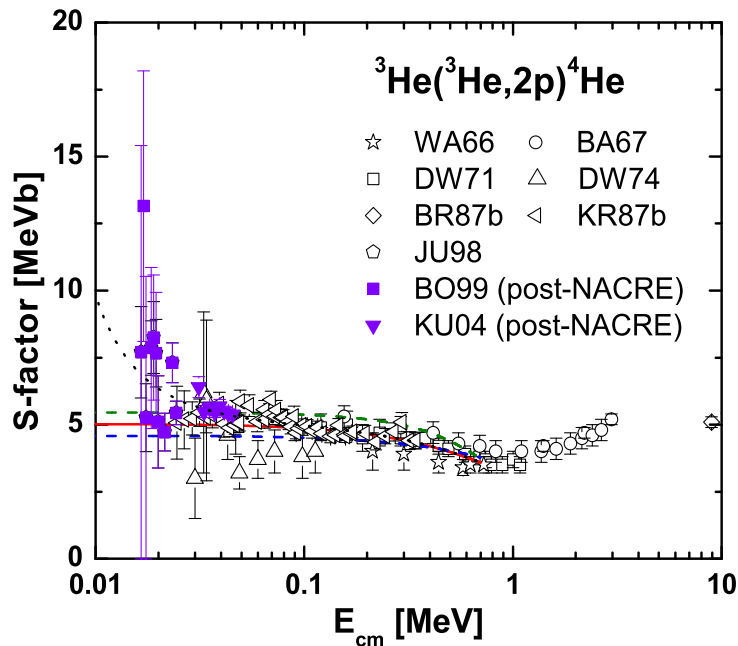


Figure 20: The S -factor for ${}^3\text{He}({}^3\text{He}, 2\text{p}){}^4\text{He}$. The dotted line indicates an adiabatic screening correction ($U_e = 241$ eV) to the 'adopt' curve (solid line). DW74 is not included in the fit.

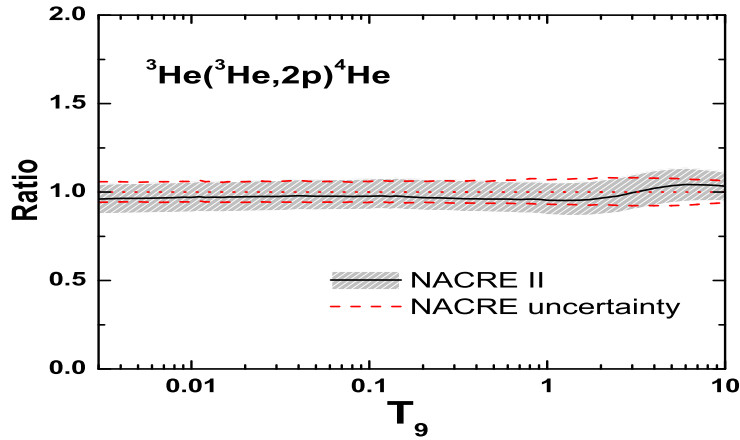


Figure 21: ${}^3\text{He}({}^3\text{He},2\text{p}){}^4\text{He}$ rates in units of the NACRE (adopt) values.

Table 10: ${}^3\text{He}({}^3\text{He},2\text{p}){}^4\text{He}$ rates in units of $\text{cm}^3\text{mol}^{-1}\text{s}^{-1}$.

T_9	adopted	low	high	T_9	adopted	low	high
0.003	2.80E-25	2.55E-25	3.04E-25	0.15	1.74E+01	1.61E+01	1.92E+01
0.004	5.55E-22	5.07E-22	6.04E-22	0.16	2.71E+01	2.51E+01	3.00E+01
0.005	1.22E-19	1.12E-19	1.33E-19	0.18	5.96E+01	5.52E+01	6.59E+01
0.006	7.48E-18	6.83E-18	8.14E-18	0.2	1.17E+02	1.08E+02	1.30E+02
0.007	1.99E-16	1.82E-16	2.17E-16	0.25	4.50E+02	4.16E+02	4.98E+02
0.008	2.98E-15	2.72E-15	3.24E-15	0.3	1.24E+03	1.15E+03	1.38E+03
0.009	2.93E-14	2.68E-14	3.19E-14	0.35	2.79E+03	2.58E+03	3.09E+03
0.01	2.09E-13	1.91E-13	2.28E-13	0.4	5.40E+03	4.99E+03	5.98E+03
0.011	1.17E-12	1.07E-12	1.27E-12	0.45	9.42E+03	8.70E+03	1.04E+04
0.012	5.34E-12	4.89E-12	5.82E-12	0.5	1.52E+04	1.40E+04	1.68E+04
0.013	2.08E-11	1.90E-11	2.27E-11	0.6	3.30E+04	3.04E+04	3.64E+04
0.014	7.08E-11	6.47E-11	7.71E-11	0.7	6.10E+04	5.61E+04	6.73E+04
0.015	2.15E-10	1.97E-10	2.35E-10	0.8	1.01E+05	9.24E+04	1.11E+05
0.016	5.95E-10	5.44E-10	6.48E-10	0.9	1.53E+05	1.40E+05	1.69E+05
0.018	3.59E-09	3.28E-09	3.91E-09	1.	2.19E+05	2.01E+05	2.42E+05
0.02	1.68E-08	1.54E-08	1.84E-08	1.25	4.46E+05	4.06E+05	4.93E+05
0.025	3.71E-07	3.40E-07	4.05E-07	1.5	7.60E+05	6.90E+05	8.40E+05
0.03	3.91E-06	3.58E-06	4.27E-06	1.75	1.16E+06	1.05E+06	1.28E+06
0.04	1.19E-04	1.10E-04	1.31E-04	2.	1.64E+06	1.49E+06	1.81E+06
0.05	1.35E-03	1.24E-03	1.48E-03	2.5	2.83E+06	2.56E+06	3.13E+06
0.06	8.49E-03	7.82E-03	9.32E-03	3.	4.30E+06	3.89E+06	4.74E+06
0.07	3.68E-02	3.39E-02	4.04E-02	3.5	6.01E+06	5.43E+06	6.60E+06
0.08	1.23E-01	1.13E-01	1.35E-01	4.	7.92E+06	7.16E+06	8.69E+06
0.09	3.40E-01	3.14E-01	3.74E-01	5.	1.22E+07	1.11E+07	1.34E+07
0.1	8.13E-01	7.52E-01	8.95E-01	6.	1.70E+07	1.54E+07	1.85E+07
0.11	1.74E+00	1.61E+00	1.92E+00	7.	2.21E+07	2.01E+07	2.40E+07
0.12	3.41E+00	3.15E+00	3.76E+00	8.	2.73E+07	2.50E+07	2.96E+07
0.13	6.21E+00	5.75E+00	6.85E+00	9.	3.27E+07	2.99E+07	3.53E+07
0.14	1.07E+01	9.86E+00	1.18E+01	10.	3.80E+07	3.49E+07	4.09E+07

3.10. ${}^3\text{He}(\alpha, \gamma){}^7\text{Be}$

The experimental data sets referred to in NACRE are HO59 [149], PA63 [150][†], NA69 [151], KR82 [152][‡], RO83 [153], AL84 [154], OS84 [155] and HI88 [156], covering the $0.1 \lesssim E_{\text{cm}} \lesssim 1.5$ MeV range. Added are the post-NACRE data sets NA04 [157], BE06 [158], BR07 [159], CO07 [160], GY07 [161], CO08 [162] and DI09 [163], extending the range to $0.07 \lesssim E_{\text{cm}} \lesssim 3$ MeV. Most recently, BO13 [164] and KO13 [165] have become available. [[†]taken in part from NA69; [‡]modified following HI88.]

Figure 22 compares the PM and experimental S -factors. All the data sets but PA63 in the whole E_{cm} range are used for the PM fit. The transitions to the ground and the first excited states of ${}^7\text{Be}$ are considered inclusively. The adopted parameter values are given in Table 55. The present $S(0) = 0.56^{+0.05}_{-0.07}$ keV b. In comparison, $S(0) = 0.54 \pm 0.09$ keV b [NACRE, E -dependence of [118]], 0.51 ± 0.04 [BBN04] keV b, and 0.56 ± 0.04 keV b of [SUN11, E -dependence of [99]].

Table 11 gives the reaction rates at $0.005 \leq T_9 \leq 10$, for which the PM-predicted and the experimental cross sections below and above $E_{\text{cm}} \simeq 0.5$ MeV are used, respectively. Figure 23 compares the present and the NACRE rates.

See [119] for an *ab initio* calculation.

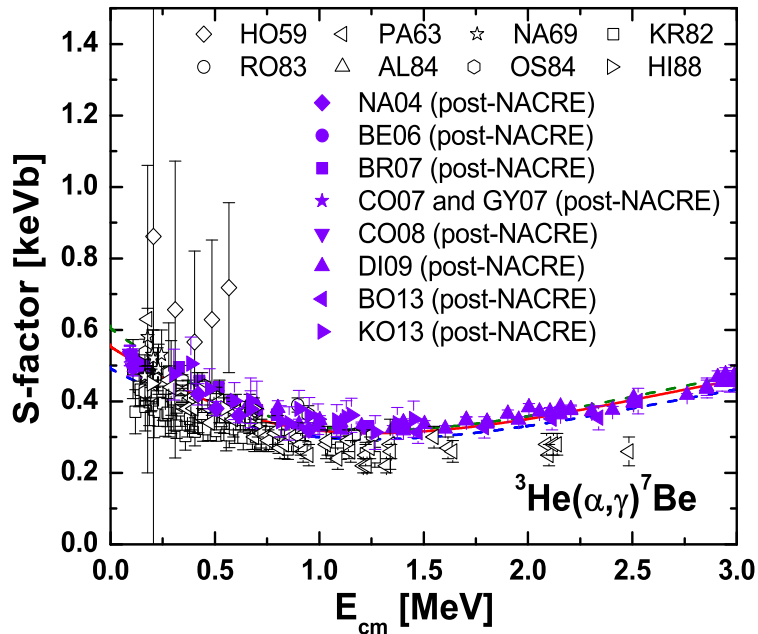


Figure 22: The S -factor for ${}^3\text{He}(\alpha, \gamma){}^7\text{Be}$. PA63 is not included in the fit.

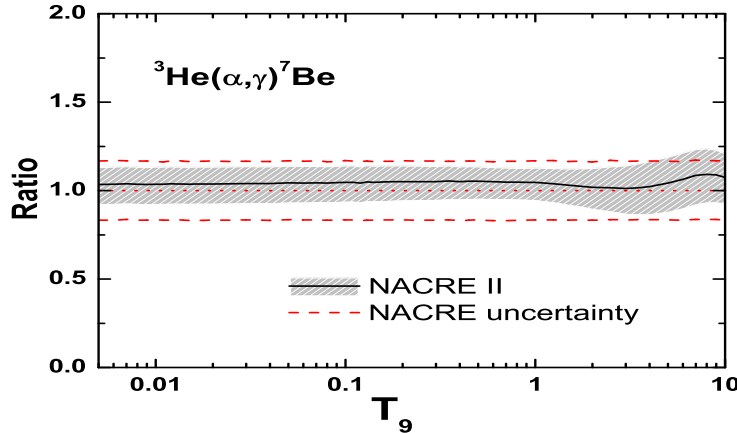


Figure 23: ${}^3\text{He}(\alpha, \gamma){}^7\text{Be}$ rates in units of the NACRE (adopt) values.

Table 11: ${}^3\text{He}(\alpha, \gamma){}^7\text{Be}$ rates in $\text{cm}^3\text{mol}^{-1}\text{s}^{-1}$

T_9	adopted	low	high	T_9	adopted	low	high
0.005	5.14E-25	4.57E-25	5.62E-25	0.16	9.98E-04	8.93E-04	1.08E-03
0.006	3.79E-23	3.37E-23	4.14E-23	0.18	2.28E-03	2.04E-03	2.47E-03
0.007	1.17E-21	1.04E-21	1.28E-21	0.2	4.62E-03	4.14E-03	5.02E-03
0.008	1.99E-20	1.77E-20	2.17E-20	0.25	1.89E-02	1.70E-02	2.05E-02
0.009	2.17E-19	1.93E-19	2.37E-19	0.3	5.49E-02	4.93E-02	5.94E-02
0.01	1.70E-18	1.51E-18	1.86E-18	0.35	1.28E-01	1.15E-01	1.38E-01
0.011	1.03E-17	9.13E-18	1.12E-17	0.4	2.54E-01	2.29E-01	2.74E-01
0.012	5.03E-17	4.48E-17	5.50E-17	0.45	4.54E-01	4.09E-01	4.89E-01
0.013	2.09E-16	1.86E-16	2.28E-16	0.5	7.44E-01	6.72E-01	8.02E-01
0.014	7.51E-16	6.68E-16	8.20E-16	0.6	1.67E+00	1.51E+00	1.80E+00
0.015	2.40E-15	2.14E-15	2.63E-15	0.7	3.16E+00	2.86E+00	3.39E+00
0.016	6.96E-15	6.20E-15	7.60E-15	0.8	5.30E+00	4.79E+00	5.70E+00
0.018	4.56E-14	4.06E-14	4.98E-14	0.9	8.17E+00	7.38E+00	8.79E+00
0.02	2.30E-13	2.05E-13	2.51E-13	1.	1.18E+01	1.07E+01	1.27E+01
0.025	5.86E-12	5.21E-12	6.39E-12	1.25	2.44E+01	2.19E+01	2.64E+01
0.03	6.88E-11	6.12E-11	7.50E-11	1.5	4.19E+01	3.73E+01	4.57E+01
0.04	2.46E-09	2.19E-09	2.69E-09	1.75	6.40E+01	5.66E+01	7.02E+01
0.05	3.11E-08	2.77E-08	3.39E-08	2.	9.04E+01	7.93E+01	9.98E+01
0.06	2.14E-07	1.91E-07	2.33E-07	2.5	1.54E+02	1.34E+02	1.72E+02
0.07	9.92E-07	8.85E-07	1.08E-06	3.	2.32E+02	1.98E+02	2.61E+02
0.08	3.50E-06	3.13E-06	3.82E-06	3.5	3.21E+02	2.73E+02	3.64E+02
0.09	1.02E-05	9.06E-06	1.11E-05	4.	4.21E+02	3.56E+02	4.79E+02
0.1	2.53E-05	2.26E-05	2.76E-05	5.	6.53E+02	5.49E+02	7.44E+02
0.11	5.62E-05	5.02E-05	6.11E-05	6.	9.15E+02	7.71E+02	1.04E+03
0.12	1.14E-04	1.02E-04	1.24E-04	7.	1.19E+03	1.01E+03	1.36E+03
0.13	2.13E-04	1.90E-04	2.31E-04	8.	1.47E+03	1.26E+03	1.67E+03
0.14	3.75E-04	3.35E-04	4.07E-04	9.	1.74E+03	1.49E+03	1.96E+03
0.15	6.25E-04	5.59E-04	6.80E-04	10.	1.99E+03	1.71E+03	2.24E+03

$$\text{REV} = 1.11 \times 10^{10} T_9^{3/2} \exp(-18.407/T_9) / [1.0 + 0.5 \exp(-4.979/T_9)]$$

3.11. ${}^6\text{Li}(\text{p},\gamma){}^7\text{Be}$

The experimental data set referred to in NACRE is SW79 [166], covering the $0.14 \lesssim E_{\text{cm}} \lesssim 1$ MeV range. Added here are BA55 [167], OS83 [168], BR92 [169][†], PA99 [170], and a most recent "surprise" HE12 [171] extending the range down to $E_{\text{cm}} \simeq 0.03$ MeV. [172] was rejected because of the unusually low cross section. [[†](p, γ_1) partial cross sections]

Figure 24 compares the PM and experimental S -factors, where the PM curves are selected from those in Figs. 25 and 26. The transitions to the ground and the first excited states of ${}^7\text{Be}$ are considered inclusively. The corresponding parameter values are given in Table 56. Note that the HE12 cross sections have been re-normalised by a factor of 1.17 [175]. Waiting for the confirmation of the HE12 data, we retain the uppermost PM curve in Fig. 25 as the upper limits. The present $S(0) = 73^{+56}_{-11}$ eV b. In comparison, $S(0) = 107$ eV b [NACRE from [176]], and 99.5 eV b [RAD10].

Table 12 gives the reaction rates at $0.001 \leq T_9 \leq 10$. The PM S -factors below $E_{\text{cm}} \simeq 0.07$, 0.1 and 0.2 MeV in "low", "adopt" and "high" cases, respectively, and above $E_{\text{cm}} \simeq 1$ MeV are used to supplement the experimental data. Figure 27 compares the present and the NACRE rates.

See [177] for a cluster model calculation.

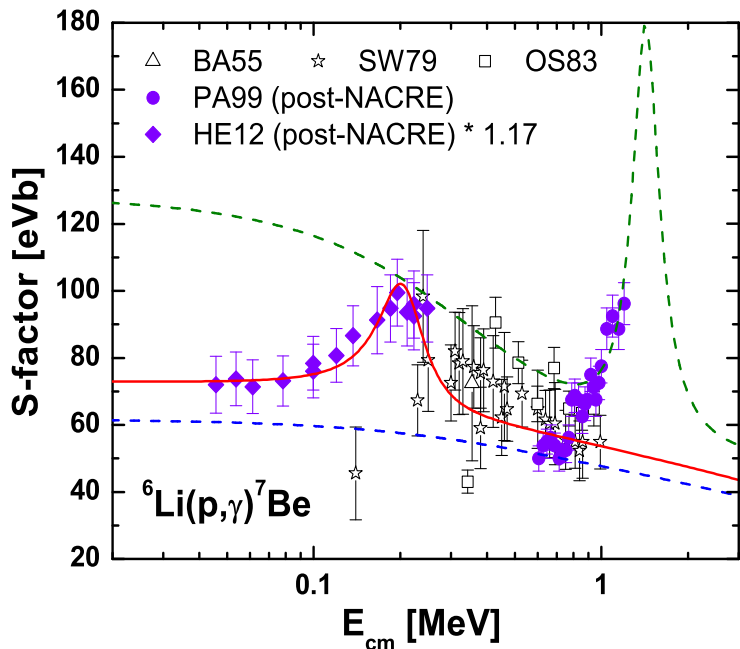


Figure 24: The S -factor for ${}^6\text{Li}(\text{p},\gamma){}^7\text{Be}$. See Figs. 25 and 26 for details.

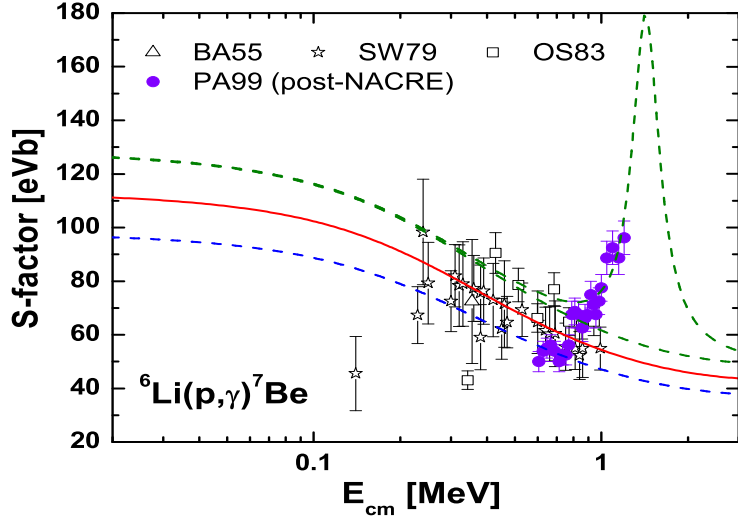


Figure 25: The S -factor for ${}^6\text{Li}(\text{p}, \gamma) {}^7\text{Be}$. The "preliminary" data set PA99 could not be substantiated, but it appears to reveal the tail of a $5/2^-$ resonance at $E_{\text{cm}} \simeq 1.6$ MeV that is evident in ${}^6\text{Li}(\text{p}, \alpha) {}^3\text{He}$. Thus, it is used to set the upper limits. We note that all the previous theoretical estimates led to $dS/dE < 0$ at low energies, and so did an experimental one [173]. Exceptionally, a positive dS/dE had been claimed by an experimental study [174].

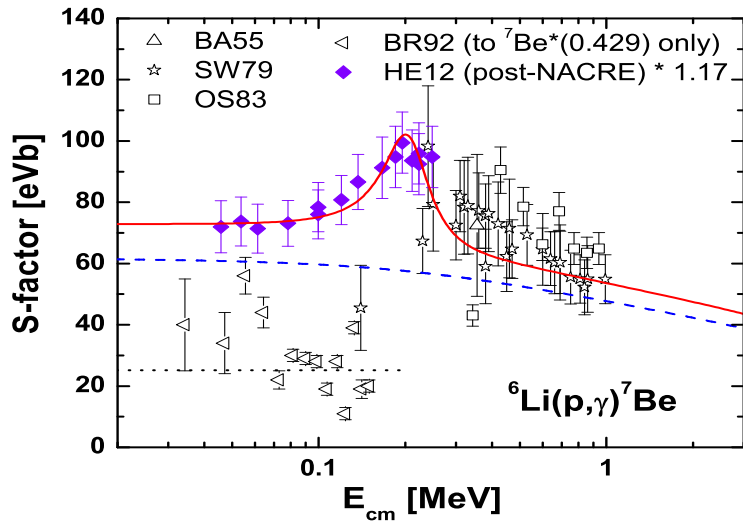


Figure 26: The S -factor for ${}^6\text{Li}(\text{p}, \gamma) {}^7\text{Be}$. The upper curve represents an artificial PM fit to the low-energy tail distribution of HE12 (with a re-normalisation factor of 1.17 [175]) by *assuming* an s-wave ($3/2^+$) resonance at $E_{\text{cm}} \simeq 0.2$ MeV. The dotted line is the mean partial S -factor of BR92 for the (p, γ_1) channel which is known to be about 40 % of the total. It is utilised to set the lower asymptotic bound for the S -factors at low energies (dashed line).

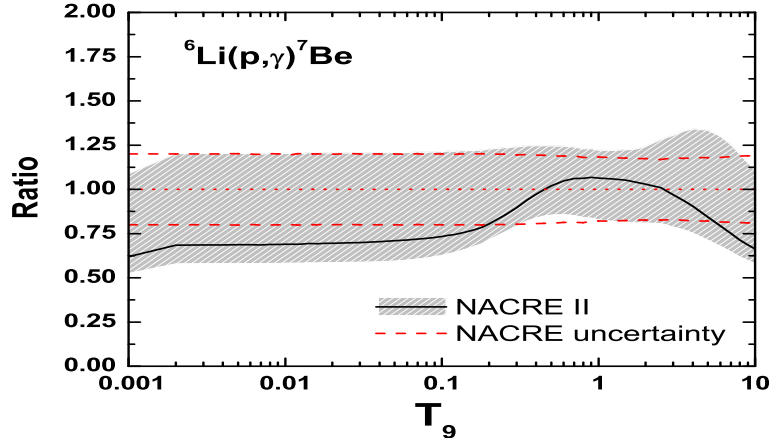


Figure 27: ${}^6\text{Li}(\text{p}, \gamma){}^7\text{Be}$ rates in units of the NACRE (adopt) values. The use of HE12 (re-normalised) has expectedly reduced the ratios at low temperatures. The decrease at the highest temperatures reflects the steep increase of the NACRE S -factors as extrapolated from [176].

Table 12: ${}^6\text{Li}(\text{p}, \gamma){}^7\text{Be}$ rates in $\text{cm}^3\text{mol}^{-1}\text{s}^{-1}$

T_9	adopted	low	high	T_9	adopted	low	high
0.001	2.23E-29	1.89E-29	3.92E-29	0.14	3.07E-01	2.67E-01	4.94E-01
0.002	5.38E-22	4.55E-22	9.45E-22	0.15	4.25E-01	3.72E-01	6.79E-01
0.003	1.91E-18	1.62E-18	3.36E-18	0.16	5.74E-01	5.03E-01	9.08E-01
0.004	3.28E-16	2.77E-16	5.75E-16	0.18	9.74E-01	8.59E-01	1.51E+00
0.005	1.26E-14	1.07E-14	2.21E-14	0.2	1.54E+00	1.36E+00	2.35E+00
0.006	2.04E-13	1.72E-13	3.57E-13	0.25	3.85E+00	3.42E+00	5.58E+00
0.007	1.87E-12	1.58E-12	3.27E-12	0.3	7.73E+00	6.82E+00	1.07E+01
0.008	1.16E-11	9.82E-12	2.03E-11	0.35	1.34E+01	1.17E+01	1.78E+01
0.009	5.44E-11	4.59E-11	9.49E-11	0.4	2.11E+01	1.82E+01	2.70E+01
0.01	2.05E-10	1.73E-10	3.57E-10	0.45	3.07E+01	2.60E+01	3.83E+01
0.011	6.52E-10	5.50E-10	1.14E-09	0.5	4.21E+01	3.53E+01	5.15E+01
0.012	1.82E-09	1.53E-09	3.16E-09	0.6	7.00E+01	5.72E+01	8.31E+01
0.013	4.53E-09	3.82E-09	7.89E-09	0.7	1.03E+02	8.30E+01	1.21E+02
0.014	1.03E-08	8.71E-09	1.80E-08	0.8	1.41E+02	1.12E+02	1.63E+02
0.015	2.18E-08	1.84E-08	3.80E-08	0.9	1.83E+02	1.43E+02	2.10E+02
0.016	4.32E-08	3.64E-08	7.51E-08	1.	2.26E+02	1.76E+02	2.60E+02
0.018	1.45E-07	1.22E-07	2.51E-07	1.25	3.43E+02	2.65E+02	3.95E+02
0.02	4.09E-07	3.44E-07	7.08E-07	1.5	4.64E+02	3.59E+02	5.40E+02
0.025	3.25E-06	2.74E-06	5.62E-06	1.75	5.85E+02	4.56E+02	6.92E+02
0.03	1.57E-05	1.32E-05	2.71E-05	2.	7.04E+02	5.53E+02	8.50E+02
0.04	1.55E-04	1.30E-04	2.65E-04	2.5	9.32E+02	7.45E+02	1.19E+03
0.05	7.80E-04	6.54E-04	1.33E-03	3.	1.14E+03	9.28E+02	1.54E+03
0.06	2.66E-03	2.24E-03	4.51E-03	3.5	1.34E+03	1.10E+03	1.90E+03
0.07	7.06E-03	5.95E-03	1.19E-02	4.	1.52E+03	1.26E+03	2.25E+03
0.08	1.58E-02	1.33E-02	2.64E-02	5.	1.84E+03	1.55E+03	2.91E+03
0.09	3.10E-02	2.63E-02	5.15E-02	6.	2.11E+03	1.80E+03	3.46E+03
0.1	5.53E-02	4.73E-02	9.15E-02	7.	2.34E+03	2.02E+03	3.91E+03
0.11	9.18E-02	7.88E-02	1.51E-01	8.	2.54E+03	2.20E+03	4.27E+03
0.12	1.44E-01	1.24E-01	2.34E-01	9.	2.71E+03	2.36E+03	4.56E+03
0.13	2.14E-01	1.85E-01	3.47E-01	10.	2.86E+03	2.50E+03	4.79E+03

$$\text{REV} = 1.19 \times 10^{10} T_9^{3/2} \exp(-65.054/T_9) [1.0 + 2.333 \exp(-25.369/T_9)] / [1.0 + 0.5 \exp(-4.979/T_9)]$$

3.12. ${}^6\text{Li}(\text{p}, \alpha){}^3\text{He}$

The experimental data sets referred to in NACRE are MA56 [178], GE66 [179], FA64 [180], SP71 [181], GO74 [182], LI77 [183], EL79 [184], SH79 [185], KW89 [186] and EN92 [187], covering the $0.01 \lesssim E_{\text{cm}} \lesssim 12$ MeV range. [188] was rejected. Added are the post-NACRE data sets TU03 [189][†], CR05 [190] and CR08 [191]. [[†]from $d({}^6\text{Li}, \alpha){}^3\text{He}$ (THM)]

Figure 28 compares the DWBA and experimental S -factors. Some measurements below $E_{\text{cm}} \simeq 0.05$ MeV look contaminated by electron screening (see CR05, and [192]). The data in the $0.05 \lesssim E_{\text{cm}} \lesssim 1$ MeV range are used for the DWBA fit. The adopted parameter values are given in Table 41. The present $S(0) = 3.1 \pm 0.4$ MeV b. In comparison, $S(0) = 2.97$ MeV b [NACRE, from KW89].

Table 13 gives the reaction rates at $0.001 \leq T_9 \leq 10$, for which the DWBA-predicted and the experimental cross sections below and above $E_{\text{cm}} \simeq 0.1$ MeV are used, respectively. Figure 29 compares the present and the NACRE rates.

See [177] for a cluster model calculation.

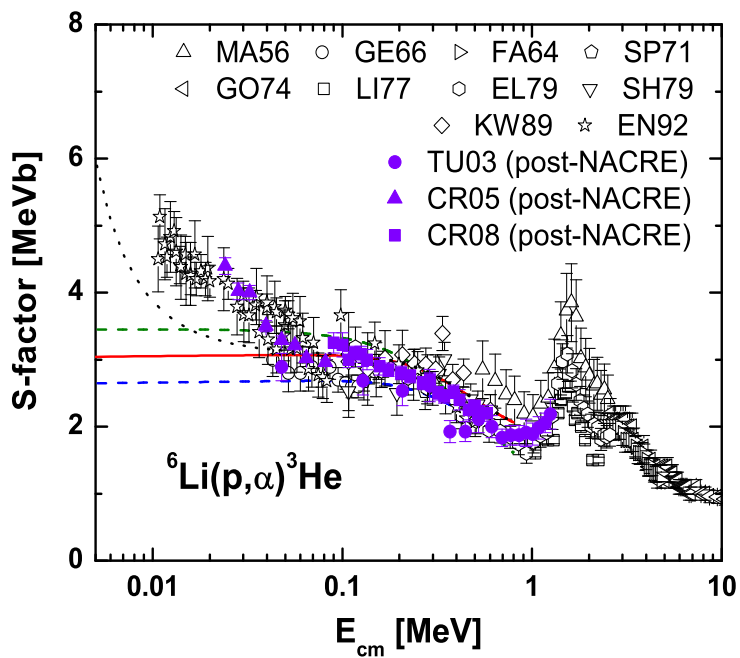


Figure 28: The S -factor for ${}^6\text{Li}(\text{p}, \alpha){}^3\text{He}$. The dotted line indicates an adiabatic screening correction ($U_e = 173$ eV) to the solid ('adopted') line. Of CR05, only the data points obtained with metallic Li are shown.

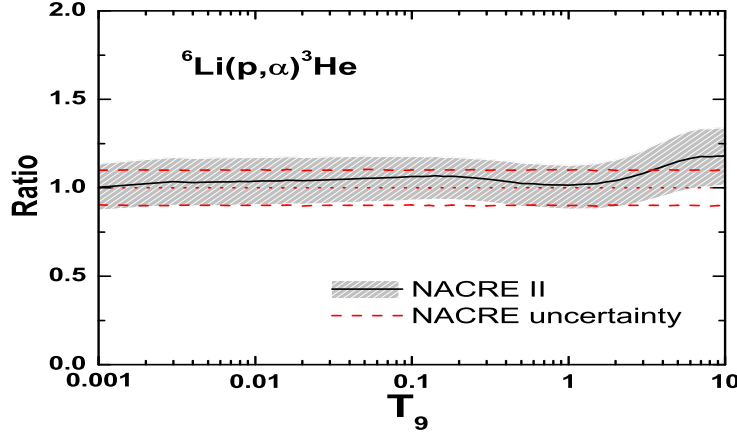


Figure 29: ${}^6\text{Li}(\text{p}, \alpha){}^3\text{He}$ rates in units of the NACRE (adopt) values.

Table 13: ${}^6\text{Li}(\text{p}, \alpha){}^3\text{He}$ rates in units of $\text{cm}^3\text{mol}^{-1}\text{s}^{-1}$.

T_9	adopted	low	high	T_9	adopted	low	high
0.001	1.00E-24	8.72E-25	1.14E-24	0.14	1.26E+04	1.10E+04	1.39E+04
0.002	2.24E-17	1.95E-17	2.54E-17	0.15	1.74E+04	1.52E+04	1.92E+04
0.003	8.03E-14	6.99E-14	9.09E-14	0.16	2.33E+04	2.04E+04	2.57E+04
0.004	1.37E-11	1.19E-11	1.55E-11	0.18	3.90E+04	3.41E+04	4.29E+04
0.005	5.28E-10	4.60E-10	5.98E-10	0.2	6.05E+04	5.30E+04	6.67E+04
0.006	8.53E-09	7.42E-09	9.65E-09	0.25	1.45E+05	1.27E+05	1.60E+05
0.007	7.83E-08	6.82E-08	8.86E-08	0.3	2.78E+05	2.43E+05	3.07E+05
0.008	4.87E-07	4.24E-07	5.50E-07	0.35	4.65E+05	4.06E+05	5.15E+05
0.009	2.28E-06	1.98E-06	2.57E-06	0.4	7.07E+05	6.18E+05	7.85E+05
0.01	8.58E-06	7.47E-06	9.69E-06	0.45	1.00E+06	8.76E+05	1.12E+06
0.011	2.73E-05	2.38E-05	3.09E-05	0.5	1.35E+06	1.18E+06	1.50E+06
0.012	7.61E-05	6.63E-05	8.59E-05	0.6	2.20E+06	1.91E+06	2.44E+06
0.013	1.90E-04	1.65E-04	2.14E-04	0.7	3.22E+06	2.80E+06	3.58E+06
0.014	4.33E-04	3.77E-04	4.89E-04	0.8	4.38E+06	3.81E+06	4.87E+06
0.015	9.15E-04	7.97E-04	1.03E-03	0.9	5.67E+06	4.92E+06	6.29E+06
0.016	1.81E-03	1.58E-03	2.04E-03	1.	7.05E+06	6.11E+06	7.83E+06
0.018	6.07E-03	5.29E-03	6.84E-03	1.25	1.08E+07	9.32E+06	1.20E+07
0.02	1.71E-02	1.49E-02	1.93E-02	1.5	1.48E+07	1.28E+07	1.65E+07
0.025	1.37E-01	1.19E-01	1.54E-01	1.75	1.90E+07	1.63E+07	2.11E+07
0.03	6.61E-01	5.76E-01	7.43E-01	2.	2.33E+07	1.99E+07	2.59E+07
0.04	6.50E+00	5.68E+00	7.29E+00	2.5	3.21E+07	2.74E+07	3.59E+07
0.05	3.28E+01	2.86E+01	3.66E+01	3.	4.13E+07	3.51E+07	4.63E+07
0.06	1.12E+02	9.75E+01	1.25E+02	3.5	5.07E+07	4.31E+07	5.70E+07
0.07	2.96E+02	2.59E+02	3.30E+02	4.	6.01E+07	5.11E+07	6.78E+07
0.08	6.59E+02	5.76E+02	7.33E+02	5.	7.83E+07	6.66E+07	8.86E+07
0.09	1.29E+03	1.13E+03	1.44E+03	6.	9.48E+07	8.07E+07	1.07E+08
0.1	2.31E+03	2.02E+03	2.56E+03	7.	1.09E+08	9.30E+07	1.24E+08
0.11	3.82E+03	3.34E+03	4.22E+03	8.	1.21E+08	1.03E+08	1.37E+08
0.12	5.95E+03	5.20E+03	6.57E+03	9.	1.31E+08	1.12E+08	1.49E+08
0.13	8.83E+03	7.73E+03	9.75E+03	10.	1.39E+08	1.19E+08	1.58E+08

$$\text{REV} = 1.07 \exp(-46.648/T_9) [1.0 + 2.333 \exp(-25.369/T_9)]$$

3.13. ${}^7\text{Li}(\text{p},\gamma){}^8\text{Be}$

The experimental data sets referred to in NACRE are PE63 [193][†], RI63 [194][†], and ZA95a [195], covering $0.09 \lesssim E_{\text{cm}} \lesssim 10$ MeV range. No new cross section data are found. [[†]normalised to ZA95a]

Figure 30 compares the PM and experimental S -factors. At $E_{\text{cm}} \lesssim 2$ MeV, the partial S -factors for the transitions to the ground and the first excited states are used for the PM fit (Figs. 31 and 32). The data exhibit the (interfering) 1^+ resonances at $E_R \simeq 0.38$ and 0.90 MeV. Whereas the cross section data at low energies could be well described by the essentially pure s-wave contributions, the observed anisotropies imply a significant mixture of p-wave contributions to (p,γ_0) cross sections [197-200]. Furthermore, $dS/dE < 0$ for the ground- and first-excited-state transitions have been asserted [196]. Given the difficulty of finding an explanation that is consistent with all these experimental findings in the low-energy range, we allow for relatively large uncertainties in the PM fits. The adopted parameter values are given in Table 57. The present total $S(0) = 1.3^{+0.4}_{-0.2}$ keV b. In comparison, $S(0) = 1.5 \pm 0.2$ keV b [NACRE, from [174]].

Table 14 gives the reaction rates at $0.001 \leq T_9 \leq 10$, for which the PM-predicted and the experimental cross sections below and above $E_{\text{cm}} \simeq 0.3$ MeV are used, respectively. Figure 33 compares the present and the NACRE rates.

See [201] for a potential model analysis.

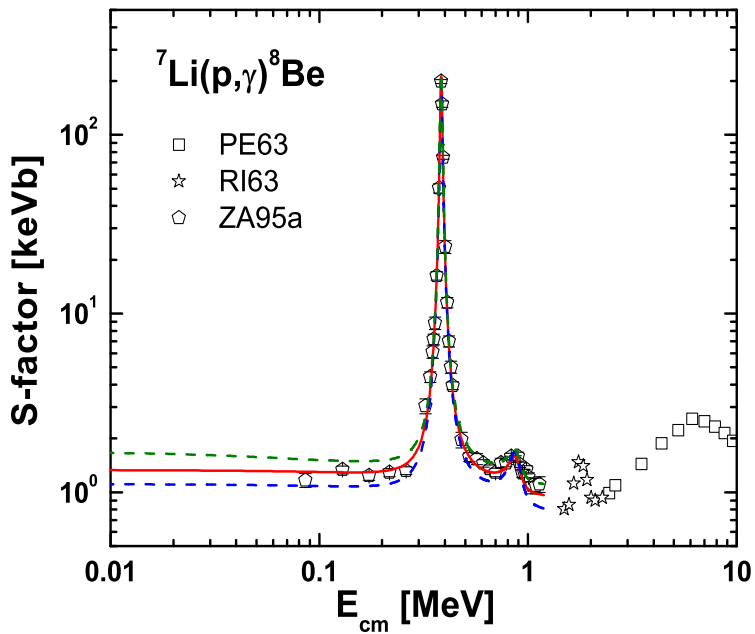


Figure 30: The S -factor for ${}^7\text{Li}(\text{p},\gamma){}^8\text{Be}$.

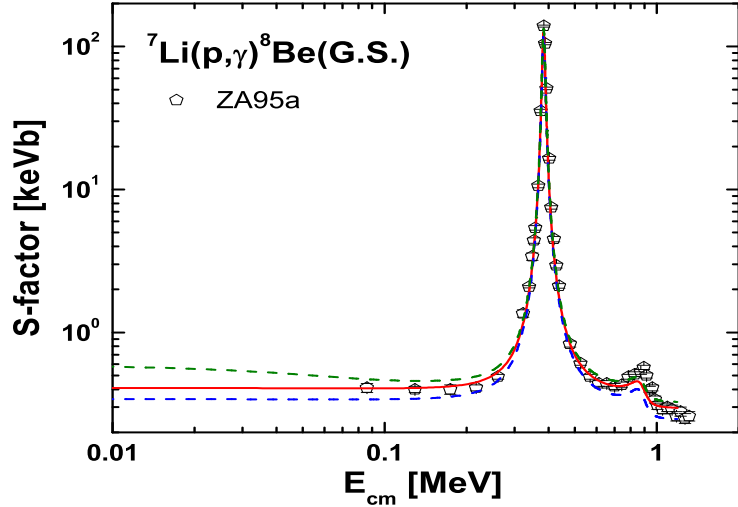


Figure 31: The partial S -factor for the ${}^7\text{Li}(p, \gamma){}^8\text{Be}$ transition to the 0^+ ground state. A modest contribution from the sub-threshold "halo-like" 2^+ state at -0.63 MeV with a very large channel radius ([196]) has been added to the upper limit. The M1 transitions via the 1^+ resonances are too weak to explain the observed extent of the p-wave mixture at the low energies. [A potential can be found that gives essentially the same shape of the S -factors for the s- (1^- ; E1) and p- ($2+$; E2) contributions. See Table 57 for an example, which gives about 25% p-wave non-resonant contributions to the (p, γ_0) channel.]

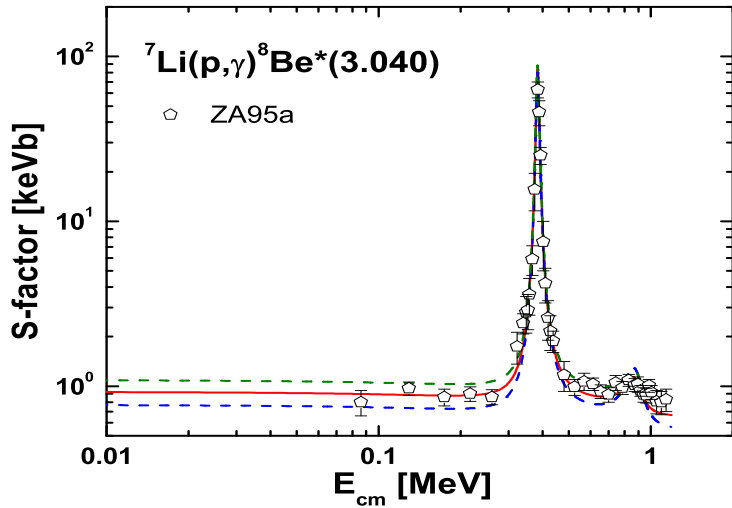


Figure 32: The partial S -factor for the ${}^7\text{Li}(p, \gamma){}^8\text{Be}$ transition to the 2^+ first excited state at $E_x = 3.040$ MeV. ZA95a is the difference of the unresolved $(p, \gamma_0 + \gamma_1)$ in Fig. 30 and (p, γ_0) in Fig. 31.

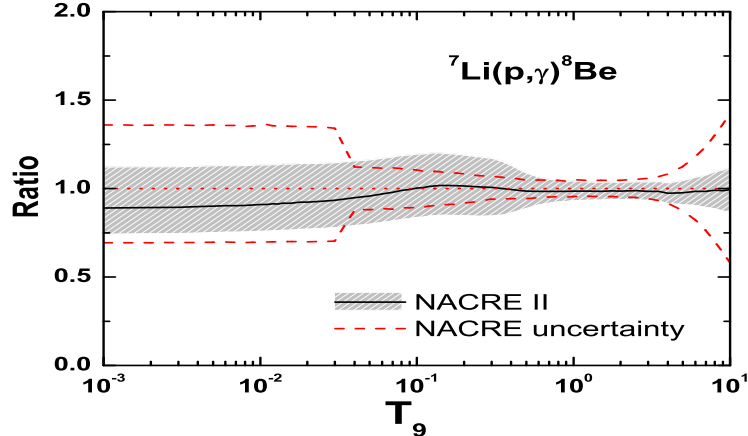


Figure 33: ${}^7\text{Li}(\text{p},\gamma){}^8\text{Be}$ rates in units of the NACRE (adopt) values. The use of PM lowers the upper uncertainty when compared with the NACRE guess.

Table 14: ${}^7\text{Li}(\text{p},\gamma){}^8\text{Be}$ rates in $\text{cm}^3\text{mol}^{-1}\text{s}^{-1}$

T_9	adopted	low	high	T_9	adopted	low	high
0.001	2.50E-28	2.08E-28	3.15E-28	0.14	4.79E+00	4.00E+00	5.66E+00
0.002	6.16E-21	5.14E-21	7.75E-21	0.15	6.63E+00	5.53E+00	7.82E+00
0.003	2.32E-17	1.93E-17	2.91E-17	0.16	8.92E+00	7.44E+00	1.05E+01
0.004	4.12E-15	3.44E-15	5.17E-15	0.18	1.50E+01	1.25E+01	1.77E+01
0.005	1.63E-13	1.36E-13	2.04E-13	0.2	2.35E+01	1.96E+01	2.76E+01
0.006	2.68E-12	2.24E-12	3.36E-12	0.25	5.77E+01	4.82E+01	6.74E+01
0.007	2.50E-11	2.09E-11	3.13E-11	0.3	1.17E+02	9.81E+01	1.36E+02
0.008	1.57E-10	1.31E-10	1.97E-10	0.35	2.18E+02	1.85E+02	2.51E+02
0.009	7.44E-10	6.20E-10	9.28E-10	0.4	3.97E+02	3.44E+02	4.52E+02
0.01	2.83E-09	2.36E-09	3.53E-09	0.45	7.10E+02	6.28E+02	7.94E+02
0.011	9.08E-09	7.57E-09	1.13E-08	0.5	1.22E+03	1.10E+03	1.35E+03
0.012	2.55E-08	2.12E-08	3.17E-08	0.6	3.07E+03	2.83E+03	3.32E+03
0.013	6.40E-08	5.34E-08	7.95E-08	0.7	6.22E+03	5.80E+03	6.66E+03
0.014	1.47E-07	1.22E-07	1.82E-07	0.8	1.06E+04	9.98E+03	1.13E+04
0.015	3.12E-07	2.60E-07	3.87E-07	0.9	1.60E+04	1.51E+04	1.70E+04
0.016	6.21E-07	5.17E-07	7.69E-07	1.	2.21E+04	2.09E+04	2.33E+04
0.018	2.09E-06	1.75E-06	2.59E-06	1.25	3.80E+04	3.60E+04	4.01E+04
0.02	5.96E-06	4.97E-06	7.36E-06	1.5	5.27E+04	5.00E+04	5.54E+04
0.025	4.81E-05	4.01E-05	5.92E-05	1.75	6.48E+04	6.15E+04	6.81E+04
0.03	2.35E-04	1.96E-04	2.89E-04	2.	7.42E+04	7.05E+04	7.79E+04
0.04	2.35E-03	1.96E-03	2.87E-03	2.5	8.64E+04	8.21E+04	9.09E+04
0.05	1.20E-02	9.98E-03	1.45E-02	3.	9.29E+04	8.80E+04	9.78E+04
0.06	4.11E-02	3.43E-02	4.97E-02	3.5	9.59E+04	9.06E+04	1.01E+05
0.07	1.10E-01	9.14E-02	1.32E-01	4.	9.71E+04	9.13E+04	1.03E+05
0.08	2.45E-01	2.05E-01	2.94E-01	5.	9.73E+04	9.05E+04	1.04E+05
0.09	4.84E-01	4.03E-01	5.78E-01	6.	9.66E+04	8.88E+04	1.04E+05
0.1	8.65E-01	7.22E-01	1.03E+00	7.	9.63E+04	8.73E+04	1.05E+05
0.11	1.44E+00	1.20E+00	1.71E+00	8.	9.66E+04	8.65E+04	1.07E+05
0.12	2.25E+00	1.87E+00	2.67E+00	9.	9.77E+04	8.62E+04	1.09E+05
0.13	3.35E+00	2.79E+00	3.96E+00	10.	9.93E+04	8.66E+04	1.12E+05

3.14. ${}^7\text{Li}(\text{p}, \alpha){}^4\text{He}$

The experimental data sets referred to in NACRE are CA62 [202], MA64 [203], FI67 [188], SP71 [181][†], RO86 [204], HA89 [205]^{†,‡}, and EN92 [187], covering the $0.011 \lesssim E_{\text{cm}} \lesssim 10$ MeV range. Added are the post-NACRE data sets LA01 [206]^{††}, CR05 [190] and CR09 [207], the first extending the range down to $E_{\text{cm}} \simeq 0.010$ MeV. [[†]corrected by NACRE for a factor of two; [‡]relative to ${}^6\text{Li}(\text{p}, \alpha)$; ^{††}from d(${}^7\text{Li}, \alpha\alpha$)n (THM).]

Figure 34 compares the DWBA and experimental S -factors. Some measurements below $E_{\text{cm}} \simeq 0.05$ MeV look contaminated by electron screening ([190] for details). The data in the $0.05 \lesssim E_{\text{cm}} \lesssim 1$ MeV range (exceptionally, all the LA01 data points by THM extending to the lower energies) are used for the DWBA fit. The symmetry of the exit channel allows even l_f , and thus odd l_i , only. The adopted parameter values are given in Table 42. The present $S(0) = 52^{+11}_{-8}$ keV b. In comparison, $S(0) = 59.3$ keV b [NACRE, from EN92], and 67 ± 4 keV b [BBN04].

Table 15 gives the reaction rates at $0.001 \leq T_9 \leq 10$, for which the DWBA-predicted and the experimental cross sections below and above $E_{\text{cm}} \simeq 0.05$ MeV are used, respectively. Figure 35 compares the present and the NACRE rates.

See [208, 209] for DWBA analyses; [210] on an invariance of the cross sections extracted from different Trojan horse reactions.

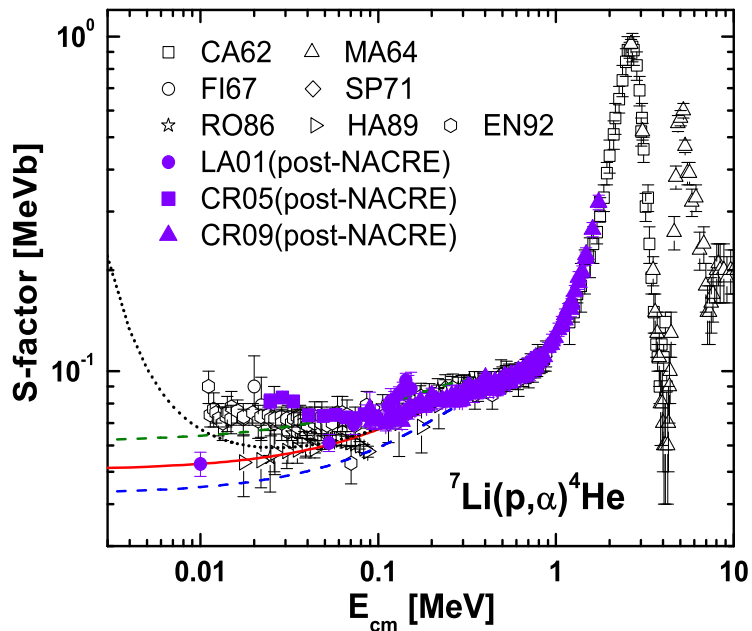


Figure 34: The S -factor for ${}^7\text{Li}(\text{p}, \alpha){}^4\text{He}$. The dotted line indicates an adiabatic screening correction ($U_e = 173$ eV) to the 'adopt' curve (solid line).

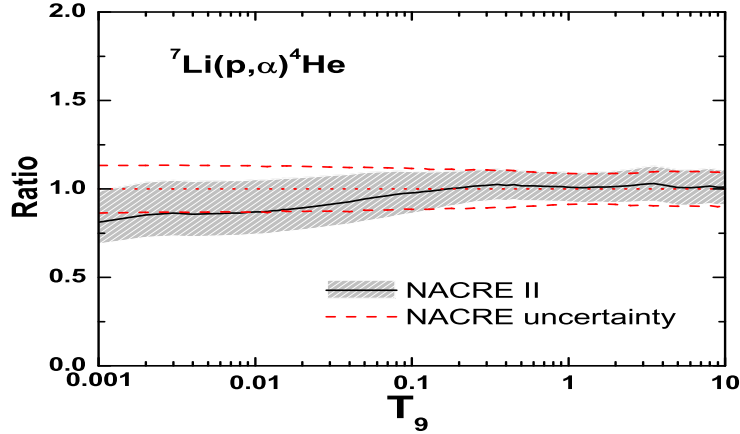


Figure 35: ${}^7\text{Li}(\text{p}, \alpha){}^4\text{He}$ rates in units of the NACRE (adopt) values. The adoption of LA01 (THM) reduces the rates at the lowest temperatures.

Table 15: Rates of ${}^7\text{Li}(\text{p}, \alpha){}^4\text{He}$ in units of $\text{cm}^3\text{mol}^{-1}\text{s}^{-1}$.

T_9	adopted	low	high	T_9	adopted	low	high
0.001	9.17E-27	7.79E-27	1.12E-26	0.14	2.60E+02	2.32E+02	2.87E+02
0.002	2.38E-19	2.02E-19	2.90E-19	0.15	3.62E+02	3.25E+02	4.00E+02
0.003	9.06E-16	7.71E-16	1.10E-15	0.16	4.92E+02	4.42E+02	5.42E+02
0.004	1.61E-13	1.37E-13	1.96E-13	0.18	8.42E+02	7.60E+02	9.25E+02
0.005	6.41E-12	5.45E-12	7.78E-12	0.2	1.34E+03	1.21E+03	1.46E+03
0.006	1.06E-10	9.02E-11	1.29E-10	0.25	3.35E+03	3.05E+03	3.66E+03
0.007	9.93E-10	8.46E-10	1.20E-09	0.3	6.73E+03	6.14E+03	7.31E+03
0.008	6.28E-09	5.36E-09	7.61E-09	0.35	1.17E+04	1.07E+04	1.27E+04
0.009	2.98E-08	2.55E-08	3.61E-08	0.4	1.84E+04	1.68E+04	1.99E+04
0.01	1.14E-07	9.74E-08	1.38E-07	0.45	2.68E+04	2.46E+04	2.91E+04
0.011	3.68E-07	3.15E-07	4.45E-07	0.5	3.71E+04	3.40E+04	4.02E+04
0.012	1.04E-06	8.89E-07	1.25E-06	0.6	6.31E+04	5.78E+04	6.83E+04
0.013	2.62E-06	2.25E-06	3.16E-06	0.7	9.58E+04	8.79E+04	1.04E+05
0.014	6.04E-06	5.18E-06	7.27E-06	0.8	1.35E+05	1.24E+05	1.46E+05
0.015	1.29E-05	1.11E-05	1.55E-05	0.9	1.79E+05	1.65E+05	1.94E+05
0.016	2.58E-05	2.22E-05	3.10E-05	1.	2.29E+05	2.10E+05	2.48E+05
0.018	8.80E-05	7.56E-05	1.05E-04	1.25	3.72E+05	3.41E+05	4.03E+05
0.02	2.53E-04	2.17E-04	3.01E-04	1.5	5.39E+05	4.93E+05	5.84E+05
0.025	2.09E-03	1.80E-03	2.47E-03	1.75	7.25E+05	6.63E+05	7.88E+05
0.03	1.04E-02	8.98E-03	1.23E-02	2.	9.31E+05	8.49E+05	1.01E+06
0.04	1.08E-01	9.30E-02	1.26E-01	2.5	1.40E+06	1.28E+06	1.53E+06
0.05	5.63E-01	4.88E-01	6.52E-01	3.	1.98E+06	1.79E+06	2.17E+06
0.06	1.98E+00	1.72E+00	2.28E+00	3.5	2.68E+06	2.42E+06	2.94E+06
0.07	5.40E+00	4.71E+00	6.17E+00	4.	3.51E+06	3.16E+06	3.85E+06
0.08	1.23E+01	1.08E+01	1.40E+01	5.	5.52E+06	4.97E+06	6.08E+06
0.09	2.47E+01	2.16E+01	2.78E+01	6.	7.86E+06	7.08E+06	8.65E+06
0.1	4.48E+01	3.94E+01	5.03E+01	7.	1.03E+07	9.29E+06	1.13E+07
0.11	7.53E+01	6.66E+01	8.42E+01	8.	1.27E+07	1.14E+07	1.40E+07
0.12	1.19E+02	1.06E+02	1.33E+02	9.	1.49E+07	1.35E+07	1.64E+07
0.13	1.79E+02	1.60E+02	1.99E+02	10.	1.70E+07	1.53E+07	1.86E+07

$$\text{REV} = 4.69 \exp(-201.32/T_9) [1.0 + 0.5 \exp(-5.543/T_9)]$$

3.15. ${}^7\text{Li}(\alpha, \gamma){}^{11}\text{B}$

No experimental cross section data are found. NACRE refers to the measured strengths of seven low-lying resonances [211, 212]. They have been supplemented by the data of [213]. The resonance assigned at 1.782 MeV is, however, discarded in the present work for the state was merely "inferred from the radiative capture cross section" ([211]).

Figure 36 presents the PM prediction of the S -factors. The $5/2^+, 3/2^-, 5/2^-$ and $7/2^+$ resonances at $E_R \simeq 0.61, 1.60, 1.67$ and 1.93 MeV [214] are considered. The observed γ and total widths are used to adjust the height of each resonance according to Eq.(25). The transitions to the ground and the first four excited states of ${}^{11}\text{B}$ are taken into account inclusively. The p-wave non-resonant ($J^\pi \neq 5/2^+$), and the $3/2^-$ sub-threshold resonance (at $E_R = -0.105$ MeV) contributions are additionally considered. The adopted parameter values are given in Table 58. The present $S(0.01 \text{ MeV}) = 6.0_{-2.0}^{+3.5} \text{ keV b}$.

Table 16 gives the reaction rates at $0.015 \leq T_9 \leq 10$, for which the PM-predicted cross sections are used. The very narrow resonances at $E_R \simeq 0.255$ and 0.518 MeV with measured strengths [212, 213] have also been taken into account. Figure 37 compares the present and the NACRE rates.

[215] for a cluster model calculation.

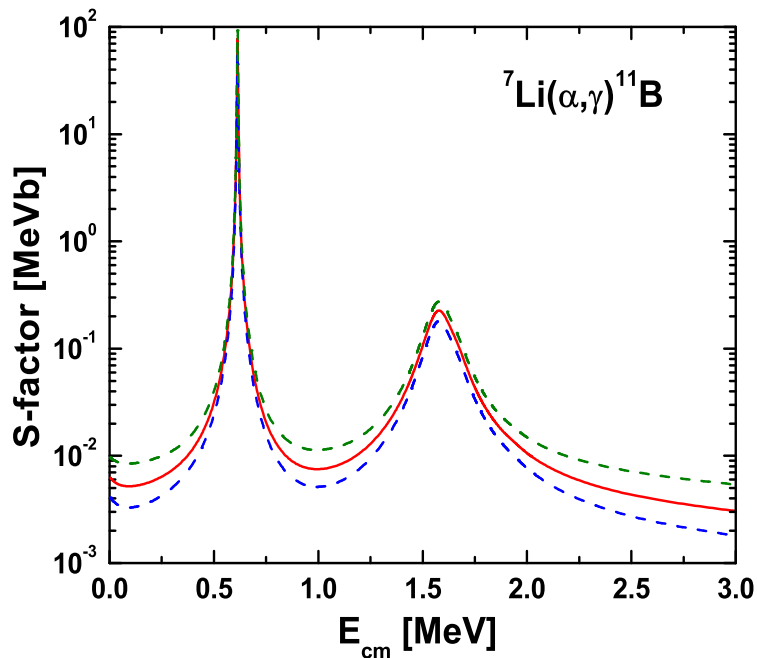


Figure 36: The S -factor for ${}^7\text{Li}(\alpha, \gamma){}^{11}\text{B}$.

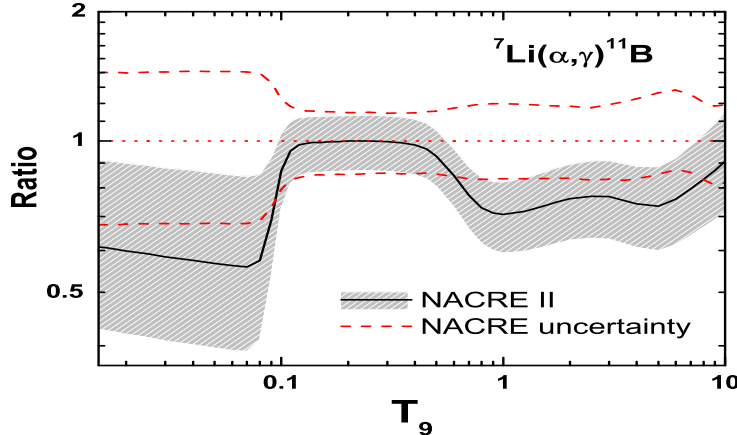


Figure 37: ${}^7\text{Li}(\alpha, \gamma){}^{11}\text{B}$ rates in units of the NACRE (adopt) values. The suppressed values at the lowest energies reflect the NACRE's large contributions from the tail of a $5/2^+$ resonance which is much wider than accepted now [214].

Table 16: ${}^7\text{Li}(\alpha, \gamma){}^{11}\text{B}$ rates in $\text{cm}^3 \text{mol}^{-1} \text{s}^{-1}$

T_9	adopted	low	high	T_9	adopted	low	high
0.015	1.73E-25	1.11E-25	2.76E-25	0.35	3.43E-01	2.93E-01	3.94E-01
0.016	8.64E-25	5.54E-25	1.38E-24	0.4	8.13E-01	6.93E-01	9.34E-01
0.018	1.48E-23	9.49E-24	2.37E-23	0.45	1.57E+00	1.34E+00	1.81E+00
0.02	1.71E-22	1.10E-22	2.74E-22	0.5	2.66E+00	2.26E+00	3.07E+00
0.025	2.30E-20	1.47E-20	3.69E-20	0.6	6.18E+00	5.21E+00	7.15E+00
0.03	9.61E-19	6.12E-19	1.55E-18	0.7	1.26E+01	1.05E+01	1.47E+01
0.04	2.20E-16	1.40E-16	3.57E-16	0.8	2.40E+01	1.98E+01	2.83E+01
0.05	1.05E-14	6.65E-15	1.70E-14	0.9	4.27E+01	3.49E+01	5.05E+01
0.06	1.99E-13	1.26E-13	3.23E-13	1.	7.02E+01	5.70E+01	8.34E+01
0.07	2.09E-12	1.33E-12	3.40E-12	1.25	1.80E+02	1.45E+02	2.15E+02
0.08	1.57E-11	1.03E-11	2.50E-11	1.5	3.37E+02	2.70E+02	4.04E+02
0.09	1.39E-10	1.03E-10	1.95E-10	1.75	5.20E+02	4.16E+02	6.24E+02
0.1	1.79E-09	1.46E-09	2.20E-09	2.	7.13E+02	5.70E+02	8.58E+02
0.11	2.00E-08	1.68E-08	2.34E-08	2.5	1.10E+03	8.78E+02	1.33E+03
0.12	1.60E-07	1.35E-07	1.85E-07	3.	1.48E+03	1.18E+03	1.80E+03
0.13	9.33E-07	7.94E-07	1.07E-06	3.5	1.87E+03	1.48E+03	2.27E+03
0.14	4.23E-06	3.60E-06	4.86E-06	4.	2.25E+03	1.78E+03	2.75E+03
0.15	1.56E-05	1.33E-05	1.79E-05	5.	2.97E+03	2.34E+03	3.67E+03
0.16	4.84E-05	4.13E-05	5.56E-05	6.	3.59E+03	2.81E+03	4.48E+03
0.18	3.17E-04	2.70E-04	3.64E-04	7.	4.10E+03	3.19E+03	5.17E+03
0.2	1.40E-03	1.19E-03	1.61E-03	8.	4.50E+03	3.47E+03	5.73E+03
0.25	1.93E-02	1.64E-02	2.22E-02	9.	4.79E+03	3.68E+03	6.17E+03
0.3	1.06E-01	9.00E-02	1.21E-01	10.	5.00E+03	3.81E+03	6.50E+03

$$\text{REV} = 4.02 \times 10^{10} T_9^{3/2} \exp(-100.56/T_9) [1.0 + 0.5 \exp(-5.543/T_9)] / [1.0 + 0.5 \exp(-24.657/T_9)]$$

3.16. ${}^7\text{Be}(\text{p}, \gamma){}^8\text{B}$

The experimental data sets referred to in NACRE are KA60 [216], PA66 [217], KA69 [218], VA70a [219], FI83a [220], FI83b [221] and HA98 [222], covering the $0.12 \lesssim E_{\text{cm}} \lesssim 9$ MeV range. [223] was omitted. Added are the post-NACRE data sets HA99 [224], HA01 [225], ST01 [226], BA03 [227], JU03 [228], SC06 [229][†] and JU10 [230], the second extending the range down to $E_{\text{cm}} \simeq 0.11$ MeV. [[†]from ${}^8\text{B}$ Coulomb break-up. The indirect Coulomb break-up experiments prior to SC06, starting from [231], are not considered here (see the review [232] for references).]

Figure 38 compares the PM and experimental S -factors. It is supplemented by Figs. 39 and 40. The data in the $E_{\text{cm}} \lesssim 3$ MeV range are used for the PM fit. They exhibit the 1^+ and 3^+ resonances at $E_R \simeq 0.64$ and 2.18 MeV. The adopted parameter values are given in Table 59. The present $S(0) = 20.8^{+1.9}_{-1.5}$ eV b. In comparison, $S(0) = 21 \pm 2$ eV b [NACRE, E -dependence of [233]], 20.8 ± 2.1 eV b [AD11, direct measurements only; E -dependence of [234]], and 19.4 eV b [RAD10], whereas an indirect derivation by the ANC method leads to $S(0) = 18.0 \pm 1.9$ eV b [235].

Table 17 gives the reaction rates at $0.003 \leq T_9 \leq 10$, for which the PM-predicted and the experimental cross sections below and above $E_{\text{cm}} \simeq 0.3$ MeV are used, respectively. Figure 41 compares the present and the NACRE rates.

See [236] for an *ab initio* calculation.

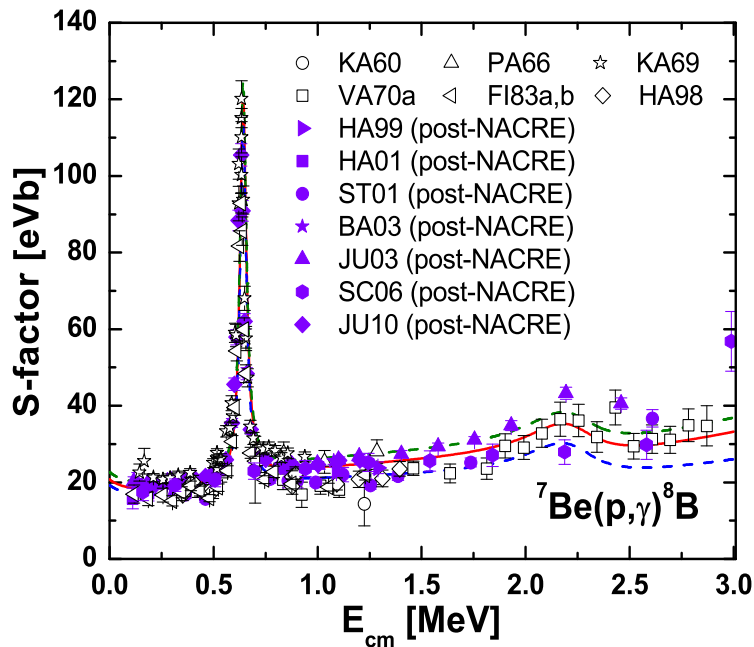


Figure 38: The S -factor for ${}^7\text{Be}(\text{p}, \gamma){}^8\text{B}$.

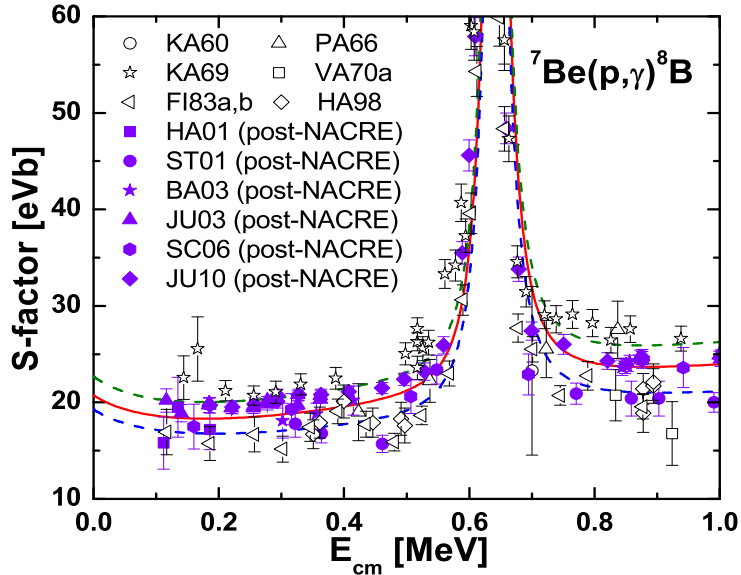


Figure 39: The S -factor for ${}^7\text{Be}(\text{p},\gamma){}^8\text{B}$ in the lowest energy range.

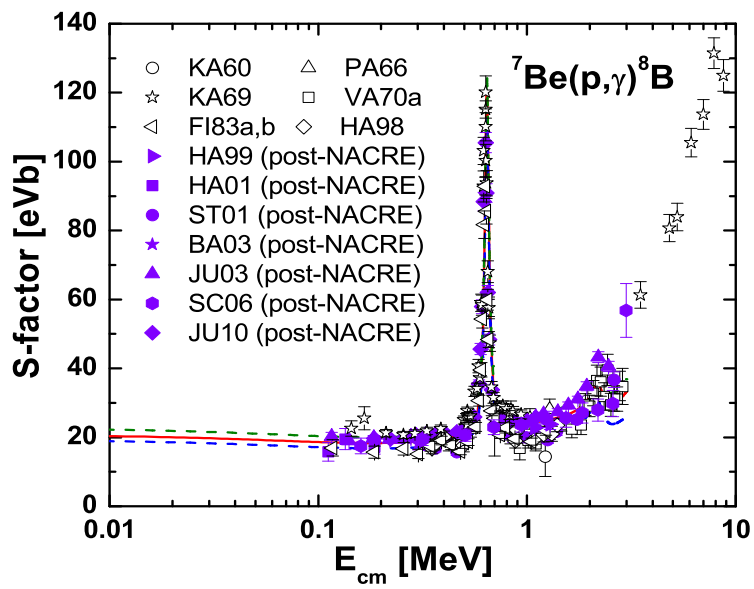


Figure 40: The S -factor for ${}^7\text{Be}(\text{p},\gamma){}^8\text{B}$ in the whole E_{cm} range (logarithmic scale).

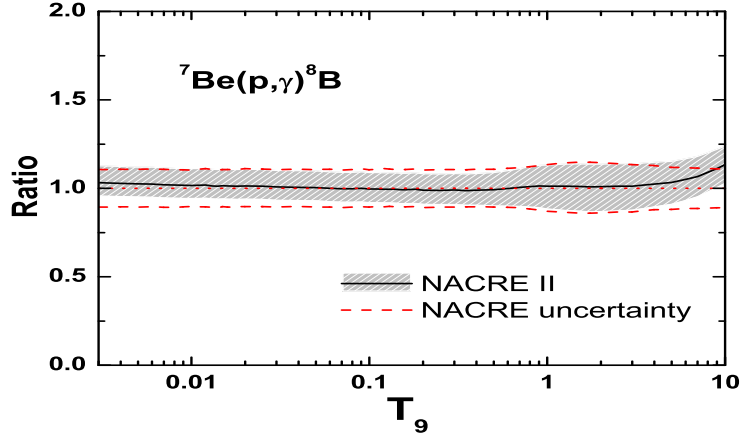


Figure 41: ${}^7\text{Be}(\text{p}, \gamma){}^8\text{B}$ rates in units of the NACRE (adopt) values.

Table 17: ${}^7\text{Be}(\text{p}, \gamma){}^8\text{B}$ rates in $\text{cm}^3\text{mol}^{-1}\text{s}^{-1}$

T_9	adopted	low	high	T_9	adopted	low	high
0.003	1.65E-24	1.53E-24	1.80E-24	0.15	3.61E-03	3.33E-03	3.95E-03
0.004	9.08E-22	8.42E-22	9.92E-22	0.16	5.21E-03	4.80E-03	5.70E-03
0.005	8.02E-20	7.44E-20	8.77E-20	0.18	9.94E-03	9.15E-03	1.09E-02
0.006	2.44E-18	2.26E-18	2.66E-18	0.2	1.73E-02	1.59E-02	1.89E-02
0.007	3.71E-17	3.44E-17	4.06E-17	0.25	5.23E-02	4.81E-02	5.72E-02
0.008	3.50E-16	3.25E-16	3.83E-16	0.3	1.21E-01	1.11E-01	1.32E-01
0.009	2.33E-15	2.16E-15	2.55E-15	0.35	2.35E-01	2.15E-01	2.57E-01
0.01	1.19E-14	1.10E-14	1.30E-14	0.4	4.06E-01	3.71E-01	4.44E-01
0.011	4.94E-14	4.58E-14	5.40E-14	0.45	6.44E-01	5.87E-01	7.06E-01
0.012	1.74E-13	1.61E-13	1.90E-13	0.5	9.58E-01	8.71E-01	1.05E+00
0.013	5.36E-13	4.97E-13	5.86E-13	0.6	1.86E+00	1.67E+00	2.05E+00
0.014	1.48E-12	1.37E-12	1.62E-12	0.7	3.18E+00	2.85E+00	3.52E+00
0.015	3.71E-12	3.44E-12	4.06E-12	0.8	5.03E+00	4.45E+00	5.58E+00
0.016	8.61E-12	7.98E-12	9.41E-12	0.9	7.46E+00	6.55E+00	8.31E+00
0.018	3.81E-11	3.53E-11	4.16E-11	1.	1.05E+01	9.19E+00	1.18E+01
0.02	1.37E-10	1.27E-10	1.49E-10	1.25	2.10E+01	1.81E+01	2.35E+01
0.025	1.76E-09	1.63E-09	1.92E-09	1.5	3.49E+01	3.01E+01	3.93E+01
0.03	1.23E-08	1.14E-08	1.34E-08	1.75	5.14E+01	4.42E+01	5.79E+01
0.04	2.06E-07	1.91E-07	2.25E-07	2.	6.97E+01	6.00E+01	7.86E+01
0.05	1.52E-06	1.40E-06	1.66E-06	2.5	1.09E+02	9.43E+01	1.23E+02
0.06	6.90E-06	6.38E-06	7.55E-06	3.	1.51E+02	1.31E+02	1.70E+02
0.07	2.30E-05	2.13E-05	2.52E-05	3.5	1.93E+02	1.68E+02	2.17E+02
0.08	6.20E-05	5.73E-05	6.78E-05	4.	2.37E+02	2.08E+02	2.66E+02
0.09	1.43E-04	1.32E-04	1.56E-04	5.	3.31E+02	2.91E+02	3.69E+02
0.1	2.93E-04	2.70E-04	3.20E-04	6.	4.33E+02	3.84E+02	4.81E+02
0.11	5.47E-04	5.05E-04	5.98E-04	7.	5.45E+02	4.87E+02	6.03E+02
0.12	9.49E-04	8.76E-04	1.04E-03	8.	6.68E+02	6.00E+02	7.36E+02
0.13	1.55E-03	1.43E-03	1.70E-03	9.	8.02E+02	7.24E+02	8.79E+02
0.14	2.42E-03	2.23E-03	2.64E-03	10.	9.43E+02	8.56E+02	1.03E+03

$$\begin{aligned} \text{REV} = & 1.31 \times 10^{10} T_9^{3/2} \exp(-1.596/T_9) [1.0 + 0.5 \exp(-4.979/T_9)] \\ & / [1.0 + 0.6 \exp(-8.982/T_9) + 1.4 \exp(-26.924/T_9)] \end{aligned}$$

3.17. ${}^7\text{Be}(\alpha, \gamma) {}^{11}\text{C}$

No experimental cross section data are found. NACRE refers to the measured strengths for the two lowest-lying resonances [212].

Figure 42 presents the PM S -factors. The $5/2^+, 3/2^-, 5/2^-$ and $7/2^+$ resonances at $E_R \simeq 1.16, 2.11, 2.24$ and 2.54 MeV [214] have been considered. The unknown γ -widths are obtained by scaling in transition energies from those known in ${}^{11}\text{B}$, but by allowing for large uncertainties. Along with the known total widths, they set the heights of the resonances through Eq. (25). The $7/2^-$ resonance at $E_R \simeq 2.43$ MeV, which does not have its counterpart in ${}^{11}\text{B}$, is included in the evaluation of the higher limit with the assumed γ -width of 1 eV. The transitions to the ground and the first three excited states of ${}^{11}\text{C}$ are considered inclusively. Non-resonant contributions are calculated with the same potential parameter values as those for the mirror ${}^7\text{Li}(\alpha, \gamma) {}^{11}\text{B}$ reaction. Significant contributions from the $3/2^+$ sub-threshold state at $E_R \simeq -0.044$ MeV are added (cf. [215]). The adopted parameter values are given in Table 60. The present $S(0.01 \text{ MeV}) = 1.2_{-0.8}^{+2.3} \text{ MeV b}$.

Table 18 gives the reaction rates at $0.02 \leq T_9 \leq 10$. Figure 43 compares the present and the NACRE rates. The very narrow resonances at $E_R \simeq 0.560$ and 0.877 MeV with measured strengths [212] are also taken into account.

See [215] for a cluster model calculation; [237] for a potential model analysis.

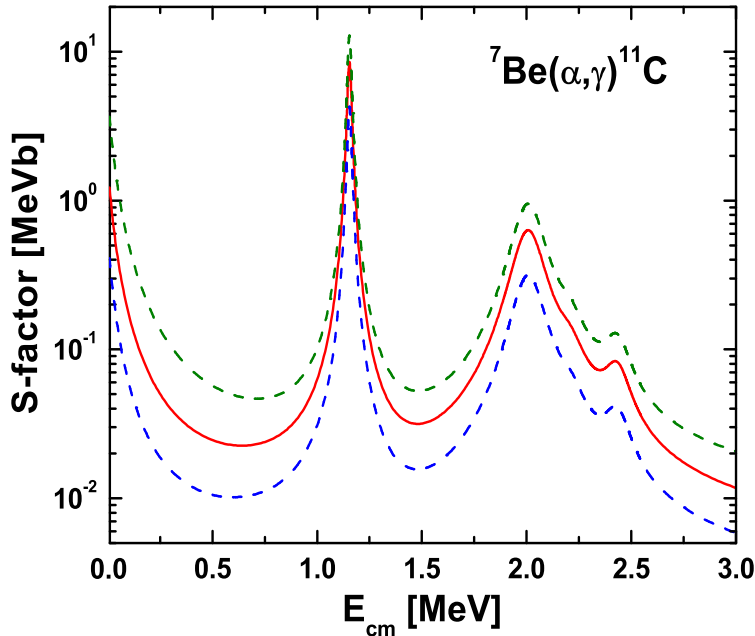


Figure 42: The S -factor for ${}^7\text{Be}(\alpha, \gamma) {}^{11}\text{C}$.

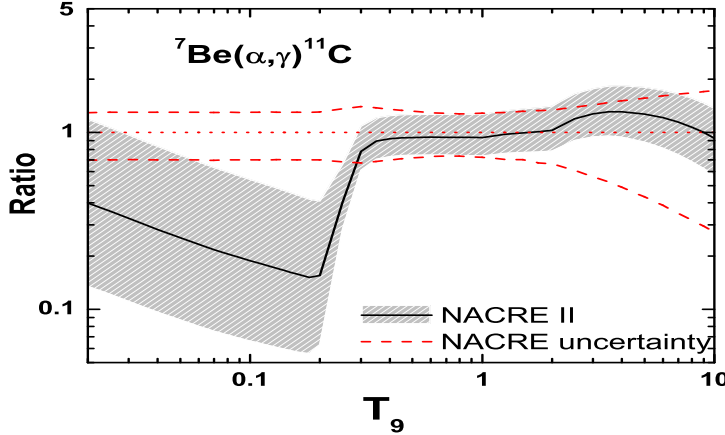


Figure 43: ${}^7\text{Be}(\alpha, \gamma) {}^{11}\text{C}$ rates in units of the NACRE (adopt) values. The reduction of the ratios at low temperatures reflect the NACRE apparent reliance on a cluster-model calculation [215] that predicts a much wider $5/2^+$ resonance than observed.

Table 18: ${}^7\text{Be}(\alpha, \gamma) {}^{11}\text{C}$ rates in $\text{cm}^3 \text{mol}^{-1} \text{s}^{-1}$

T_9	adopted	low	high	T_9	adopted	low	high
0.02	4.63E-27	1.57E-27	1.38E-26	0.45	2.17E-02	1.72E-02	2.92E-02
0.025	1.56E-24	5.30E-25	4.63E-24	0.5	7.87E-02	6.25E-02	1.06E-01
0.03	1.30E-22	4.42E-23	3.85E-22	0.6	5.31E-01	4.22E-01	7.15E-01
0.04	7.90E-20	2.70E-20	2.33E-19	0.7	2.05E+00	1.62E+00	2.76E+00
0.05	7.33E-18	2.52E-18	2.15E-17	0.8	5.63E+00	4.46E+00	7.59E+00
0.06	2.28E-16	7.86E-17	6.66E-16	0.9	1.25E+01	9.85E+00	1.68E+01
0.07	3.49E-15	1.21E-15	1.02E-14	1.	2.37E+01	1.87E+01	3.21E+01
0.08	3.29E-14	1.15E-14	9.55E-14	1.25	7.81E+01	6.11E+01	1.06E+02
0.09	2.18E-13	7.63E-14	6.29E-13	1.5	1.77E+02	1.37E+02	2.41E+02
0.1	1.10E-12	3.88E-13	3.17E-12	1.75	3.20E+02	2.46E+02	4.38E+02
0.11	4.53E-12	1.60E-12	1.30E-11	2.	4.97E+02	3.80E+02	6.82E+02
0.12	1.58E-11	5.61E-12	4.50E-11	2.5	9.09E+02	6.85E+02	1.25E+03
0.13	4.80E-11	1.71E-11	1.36E-10	3.	1.34E+03	9.92E+02	1.85E+03
0.14	1.31E-10	4.69E-11	3.69E-10	3.5	1.74E+03	1.27E+03	2.43E+03
0.15	3.24E-10	1.17E-10	9.11E-10	4.	2.11E+03	1.51E+03	2.95E+03
0.16	7.41E-10	2.69E-10	2.08E-09	5.	2.73E+03	1.90E+03	3.87E+03
0.18	3.23E-09	1.20E-09	8.93E-09	6.	3.22E+03	2.17E+03	4.61E+03
0.2	1.23E-08	4.98E-09	3.23E-08	7.	3.60E+03	2.35E+03	5.20E+03
0.25	6.37E-07	4.49E-07	1.04E-06	8.	3.89E+03	2.48E+03	5.66E+03
0.3	2.99E-05	2.34E-05	4.13E-05	9.	4.10E+03	2.56E+03	6.01E+03
0.35	5.11E-04	4.05E-04	6.93E-04	10.	4.24E+03	2.61E+03	6.26E+03
0.4	4.25E-03	3.37E-03	5.73E-03				

$$\text{REV} = 4.02 \times 10^{10} T_9^{3/2} \exp(-87.555/T_9) [1.0 + 0.5 \exp(-4.979/T_9)] / [1.0 + 0.5 \exp(-23.210/T_9)]$$

3.18. ${}^9\text{Be}(\text{p}, \gamma) {}^{10}\text{B}$

The experimental data sets referred to in NACRE are ME59 [238], HO64 [239], AU75 [240], PA89 [241] and ZA95b [242], covering the $0.07 \lesssim E_{\text{cm}} \lesssim 1.6$ MeV range. Among them, ME59 was omitted, and HO64, AU75 and PA89 were superseded by ZA95b. In the present work, all sets but ME59 are considered. No new cross section data are found.

Figure 44 compares the PM and experimental S -factors. The data in the $E_{\text{cm}} \lesssim 1$ MeV range are used for the PM fit. They exhibit the 1^- and 2^+ resonances at $E_R \simeq 0.29$ and 0.89 MeV. The transitions to the ground and the first three excited states of ${}^{10}\text{B}$ are considered inclusively. The adopted parameter values are given in Table 61. The present $S(0) = 1.2_{-0.2}^{+0.1}$ keV b. In comparison, $S(0) = 1$ keV b [NACRE from [242]], and 1.05 keV b [RAD10].

Table 19 gives the reaction rates at $0.003 \leq T_9 \leq 10$, for which the PM-predicted and the experimental cross sections below and above $E_{\text{cm}} \simeq 0.1$ MeV are used, respectively. The narrow 0^+ resonance at $E_R = 0.974$ MeV (with known $\omega\gamma$ [242]) is additionally considered, contributing to the rates marginally (up to 4 % at $T_9 > 3$). In the $E_{\text{cm}} \gtrsim 1.62$ MeV range, the S -factors are taken to be constant for simplicity. The impact of this assumption is very weak, as the contribution of that energy range to the rates amounts to about 5 % only, even at $T_9 = 10$. Figure 45 compares the present and the NACRE rates.

See [243] for an R-matrix fit.

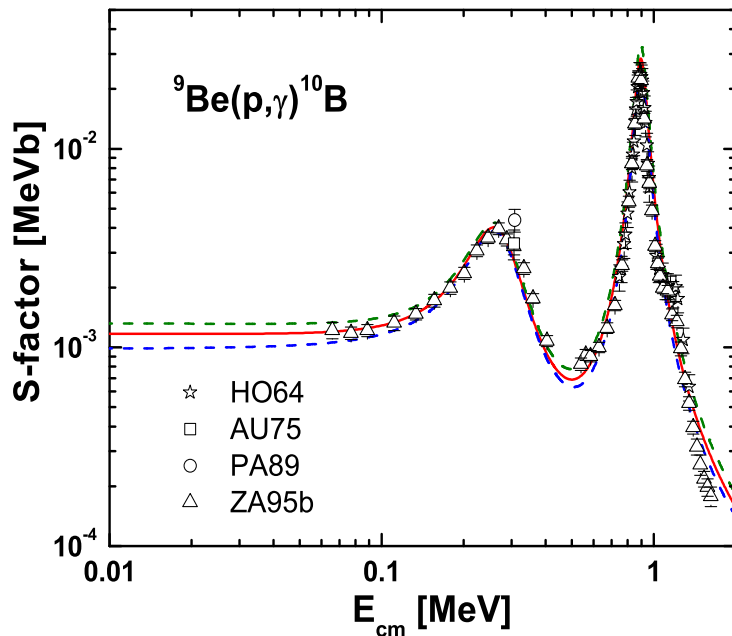


Figure 44: The S -factor for ${}^9\text{Be}(\text{p}, \gamma) {}^{10}\text{B}$.

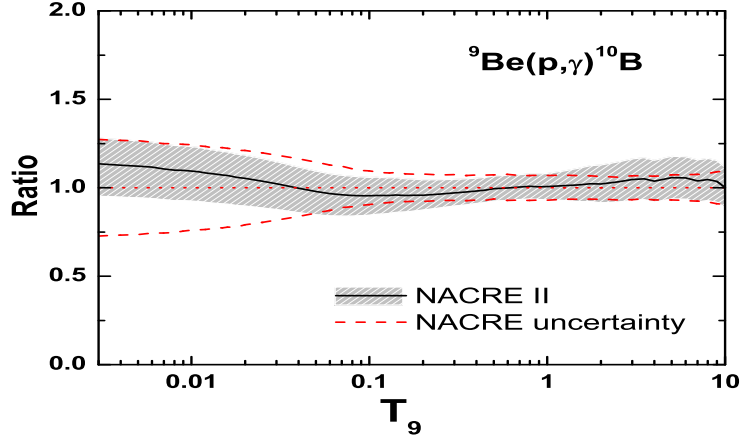


Figure 45: ${}^9\text{Be}(\text{p}, \gamma){}^{10}\text{B}$ rates in units of the NACRE (adopt) values. The use of PM limits the uncertainties when compared with NACRE.

Table 19: ${}^9\text{Be}(\text{p}, \gamma){}^{10}\text{B}$ rates in $\text{cm}^3 \text{mol}^{-1} \text{s}^{-1}$

T_9	adopted	low	high	T_9	adopted	low	high
0.003	4.64E-23	4.42E-23	5.09E-23	0.15	2.06E-01	1.92E-01	2.25E-01
0.004	2.73E-20	2.60E-20	3.00E-20	0.16	3.05E-01	2.84E-01	3.32E-01
0.005	2.54E-18	2.41E-18	2.78E-18	0.18	6.13E-01	5.70E-01	6.65E-01
0.006	8.00E-17	7.61E-17	8.78E-17	0.2	1.13E+00	1.05E+00	1.22E+00
0.007	1.26E-15	1.19E-15	1.38E-15	0.25	3.93E+00	3.65E+00	4.23E+00
0.008	1.21E-14	1.15E-14	1.33E-14	0.3	1.04E+01	9.65E+00	1.11E+01
0.009	8.25E-14	7.84E-14	9.05E-14	0.35	2.25E+01	2.10E+01	2.42E+01
0.01	4.29E-13	4.08E-13	4.71E-13	0.4	4.22E+01	3.93E+01	4.52E+01
0.011	1.81E-12	1.72E-12	1.99E-12	0.45	7.07E+01	6.57E+01	7.57E+01
0.012	6.47E-12	6.15E-12	7.10E-12	0.5	1.08E+02	1.01E+02	1.16E+02
0.013	2.02E-11	1.92E-11	2.22E-11	0.6	2.11E+02	1.96E+02	2.26E+02
0.014	5.64E-11	5.35E-11	6.18E-11	0.7	3.45E+02	3.21E+02	3.69E+02
0.015	1.43E-10	1.36E-10	1.57E-10	0.8	5.08E+02	4.72E+02	5.43E+02
0.016	3.35E-10	3.18E-10	3.68E-10	0.9	6.98E+02	6.48E+02	7.49E+02
0.018	1.51E-09	1.43E-09	1.66E-09	1.	9.24E+02	8.56E+02	9.93E+02
0.02	5.50E-09	5.22E-09	6.04E-09	1.25	1.71E+03	1.57E+03	1.85E+03
0.025	7.32E-08	6.94E-08	8.04E-08	1.5	2.93E+03	2.65E+03	3.20E+03
0.03	5.24E-07	4.96E-07	5.75E-07	1.75	4.62E+03	4.16E+03	5.09E+03
0.04	9.15E-06	8.65E-06	1.00E-05	2.	6.73E+03	6.01E+03	7.45E+03
0.05	6.94E-05	6.55E-05	7.62E-05	2.5	1.16E+04	1.03E+04	1.29E+04
0.06	3.24E-04	3.06E-04	3.56E-04	3.	1.65E+04	1.46E+04	1.85E+04
0.07	1.11E-03	1.04E-03	1.22E-03	3.5	2.09E+04	1.85E+04	2.34E+04
0.08	3.05E-03	2.86E-03	3.34E-03	4.	2.45E+04	2.16E+04	2.74E+04
0.09	7.16E-03	6.73E-03	7.86E-03	5.	2.94E+04	2.59E+04	3.29E+04
0.1	1.50E-02	1.40E-02	1.64E-02	6.	3.18E+04	2.80E+04	3.56E+04
0.11	2.85E-02	2.67E-02	3.13E-02	7.	3.27E+04	2.88E+04	3.66E+04
0.12	5.06E-02	4.73E-02	5.54E-02	8.	3.26E+04	2.88E+04	3.65E+04
0.13	8.47E-02	7.90E-02	9.25E-02	9.	3.20E+04	2.82E+04	3.58E+04
0.14	1.35E-01	1.26E-01	1.47E-01	10.	3.10E+04	2.74E+04	3.47E+04

$$\begin{aligned} \text{REV} = & 9.74 \times 10^9 T_9^{3/2} \exp(-76.429/T_9) \\ & \times [1.0 + 0.5 \exp(-19.543/T_9) + 1.5 \exp(-28.193/T_9)] \\ & / [1.0 + 0.429 \exp(-8.336/T_9) + 0.143 \exp(-20.194/T_9) + 0.429 \exp(-24.997/T_9)] \end{aligned}$$

3.19. ${}^9\text{Be}(\text{p}, \text{d}) {}^8\text{Be}$

The experimental data sets referred to in NACRE are NE51 [244], WE56 [245], HU72 [246], SI73 [247] and ZA97 [248], covering the $0.02 \lesssim E_{\text{cm}} \lesssim 10$ MeV range. No new cross section data are found. (For angular distribution in the $0.07 \lesssim E_{\text{cm}} \lesssim 0.29$ MeV range, see [249].) The enhancements of the S -factors below $E_{\text{cm}} = 0.03 \sim 0.04$ MeV are likely caused by electron screening as it is the case with ${}^9\text{Be}(\text{p}, \alpha) {}^4\text{He}$, for which THM has been applied (see Sect. 3.20).

Figure 46 compares the DWBA and experimental S -factors. The data in the $0.05 \lesssim E_{\text{cm}} \lesssim 1$ MeV range are used for the DWBA fit. They exhibit the 1^- resonance at $E_R \simeq 0.29$ MeV. The possible contribution from a $(4)^-$ sub-threshold state at $E_R \simeq -0.026$ MeV appears to be minor (see ZA97 and [249]). The adopted parameter values are given in Table 43. The present $S(0) = 15 \pm 4$ MeV b. In comparison, $S(0) = 17^{+25}_{-7}$ MeV b [NACRE, from SI73].

Table 20 gives the reaction rates at $0.002 \leq T_9 \leq 10$, for which the DWBA-predicted and the experimental cross sections below and above $E_{\text{cm}} \simeq 0.07$ MeV are used, respectively. Figure 47 compares the present and the NACRE rates.

See [250] for a DWBA analysis.

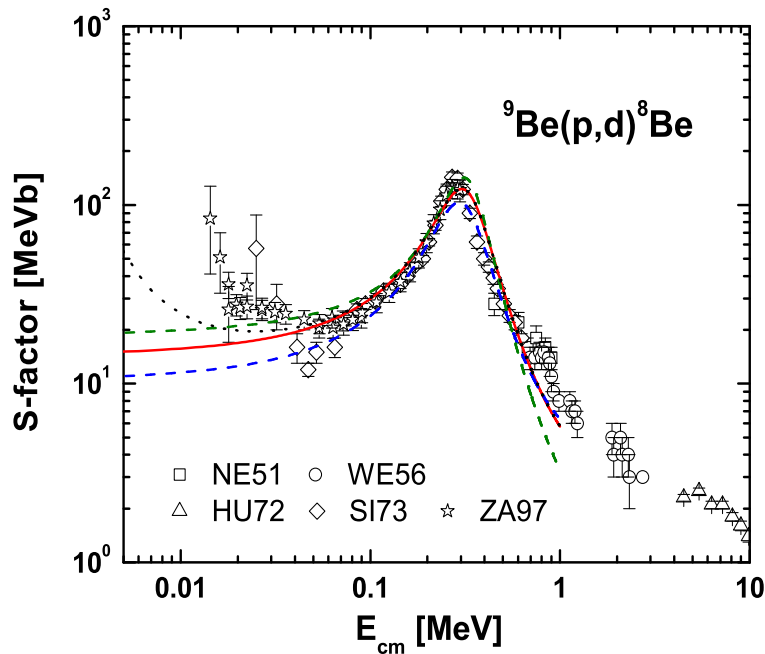


Figure 46: The S -factor for ${}^9\text{Be}(\text{p}, \text{d}) {}^8\text{Be}$. The dotted line indicates an adiabatic screening correction ($U_e = 264$ eV) to the 'adopt' curve (solid line).

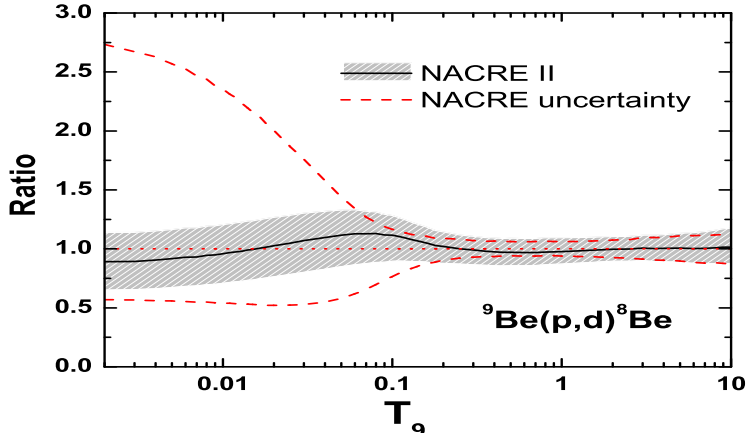


Figure 47: ${}^9\text{Be}(\text{p}, \text{d}) {}^8\text{Be}$ rates in units of the NACRE (adopt) values. The exclusion for the DWBA fit of the experimental data in the $E_{\text{cm}} \lesssim 0.05$ MeV range (see text) lowers the upper NACRE uncertainty.

Table 20: ${}^9\text{Be}(\text{p}, \text{d}) {}^8\text{Be}$ rates in units of $\text{cm}^3 \text{mol}^{-1} \text{s}^{-1}$.

T_9	adopted	low	high	T_9	adopted	low	high
0.002	2.38E-23	1.74E-23	3.04E-23	0.15	4.45E+03	3.74E+03	5.03E+03
0.003	5.95E-19	4.36E-19	7.60E-19	0.16	6.67E+03	5.64E+03	7.52E+03
0.004	3.55E-16	2.60E-16	4.52E-16	0.18	1.38E+04	1.18E+04	1.55E+04
0.005	3.33E-14	2.44E-14	4.22E-14	0.2	2.60E+04	2.24E+04	2.92E+04
0.006	1.06E-12	7.78E-13	1.34E-12	0.25	9.63E+04	8.38E+04	1.07E+05
0.007	1.68E-11	1.23E-11	2.12E-11	0.3	2.68E+05	2.35E+05	3.00E+05
0.008	1.64E-10	1.20E-10	2.06E-10	0.35	6.10E+05	5.36E+05	6.82E+05
0.009	1.12E-09	8.26E-10	1.41E-09	0.4	1.19E+06	1.05E+06	1.33E+06
0.01	5.87E-09	4.33E-09	7.38E-09	0.45	2.06E+06	1.81E+06	2.31E+06
0.011	2.50E-08	1.85E-08	3.13E-08	0.5	3.24E+06	2.86E+06	3.64E+06
0.012	8.99E-08	6.65E-08	1.13E-07	0.6	6.57E+06	5.82E+06	7.39E+06
0.013	2.83E-07	2.09E-07	3.53E-07	0.7	1.10E+07	9.79E+06	1.24E+07
0.014	7.94E-07	5.88E-07	9.90E-07	0.8	1.64E+07	1.45E+07	1.84E+07
0.015	2.03E-06	1.50E-06	2.53E-06	0.9	2.22E+07	1.98E+07	2.49E+07
0.016	4.78E-06	3.55E-06	5.94E-06	1.	2.84E+07	2.54E+07	3.18E+07
0.018	2.18E-05	1.62E-05	2.70E-05	1.25	4.41E+07	3.95E+07	4.92E+07
0.02	8.05E-05	5.99E-05	9.94E-05	1.5	5.88E+07	5.27E+07	6.54E+07
0.025	1.10E-03	8.23E-04	1.35E-03	1.75	7.19E+07	6.46E+07	7.98E+07
0.03	8.09E-03	6.07E-03	9.86E-03	2.	8.34E+07	7.49E+07	9.24E+07
0.04	1.48E-01	1.12E-01	1.78E-01	2.5	1.02E+08	9.14E+07	1.13E+08
0.05	1.17E+00	8.91E-01	1.39E+00	3.	1.16E+08	1.04E+08	1.28E+08
0.06	5.68E+00	4.36E+00	6.70E+00	3.5	1.26E+08	1.13E+08	1.41E+08
0.07	2.01E+01	1.56E+01	2.35E+01	4.	1.34E+08	1.19E+08	1.50E+08
0.08	5.70E+01	4.47E+01	6.62E+01	5.	1.46E+08	1.29E+08	1.64E+08
0.09	1.38E+02	1.09E+02	1.59E+02	6.	1.54E+08	1.34E+08	1.74E+08
0.1	2.95E+02	2.37E+02	3.39E+02	7.	1.59E+08	1.38E+08	1.81E+08
0.11	5.74E+02	4.66E+02	6.57E+02	8.	1.63E+08	1.41E+08	1.87E+08
0.12	1.04E+03	8.52E+02	1.18E+03	9.	1.65E+08	1.43E+08	1.91E+08
0.13	1.77E+03	1.46E+03	2.01E+03	10.	1.67E+08	1.44E+08	1.94E+08
0.14	2.86E+03	2.39E+03	3.24E+03				

3.20. ${}^9\text{Be}(\text{p},\alpha){}^6\text{Li}$

The experimental data sets referred to in NACRE are*: NE51 [244][†], DA52 [251][‡], MA59 [252][‡], BL63 [253]^{††}, YA64 [254], MO65 [255][†], SI73 [247] and ZA97 [248], covering the $0.014 \lesssim E_{\text{cm}} \lesssim 10$ MeV range. Added is the post-NACRE data set WE08 [256]^{‡, ‡‡}, extending the E_{cm} range down to $\simeq 0.012$ MeV. [^{*}(p,α_0), i.e. to the ground state of ${}^6\text{Li}$ with the Q -value of 2.125 MeV, if not marked otherwise; [†](re-)normalised (see NACRE); [‡](p,α_2), i.e. to the second excited state at 3.562 MeV) with MA59 normalised to DA52; ^{††}(p,α_1), i.e. to the first excited state at 2.186 MeV; ^{‡‡}from ${}^2\text{H}({}^9\text{Be},{}^6\text{Li}\alpha)\text{n}$ (THM).]

Figure 48 compares the DWBA and experimental S -factors. As inferred from WE08 using THM, the enhancements observed in other data sets below $E_{\text{cm}} \simeq 0.03 - 0.04$ MeV are likely caused by electron screening. The contribution from a sub-threshold resonance (SI73) appears to be minor (ZA97; see also [249]). The data in the $0.05 \lesssim E_{\text{cm}} \lesssim 1$ MeV range, and all the WE08 data, are used for the DWBA fit. They exhibit the 1^- resonance at $E_R \simeq 0.29$ MeV. The adopted parameter values are given in Table 44. The present $S(0) = 21^{+5}_{-13}$ MeV b. In comparison, $S(0) = 17^{+25}_{-7}$ MeV b [NACRE, from SI73].

Table 21 gives the reaction rates at $0.002 \leq T_9 \leq 10$, for which the DWBA-predicted and the experimental cross sections below and above $E_{\text{cm}} \simeq 0.07$ MeV are used, respectively. Figure 49 compares the present and the NACRE rates.

See BL63 for a DWBA analysis (also see [250]).

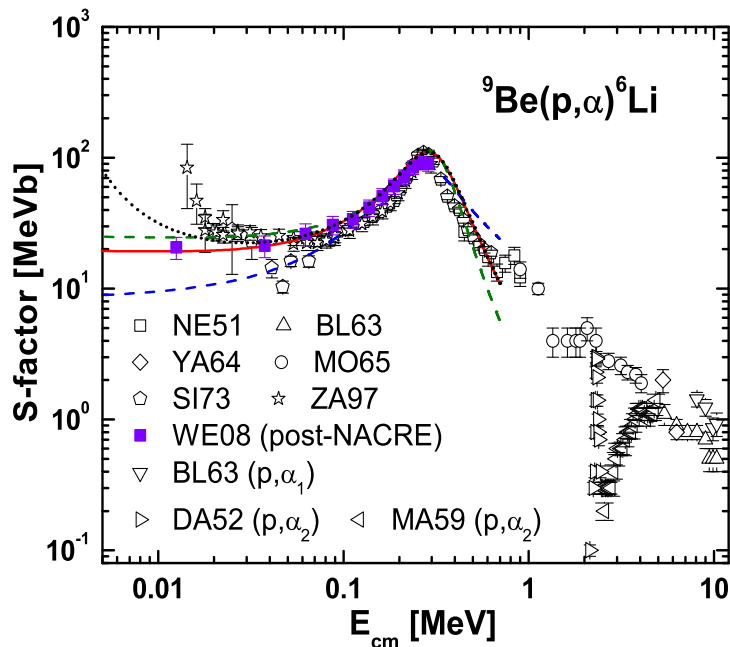


Figure 48: The S -factor for ${}^9\text{Be}(\text{p},\alpha){}^6\text{Li}$. The dotted line indicates an adiabatic screening correction ($U_e = 264$ eV) to the 'adopt' curve (solid line).

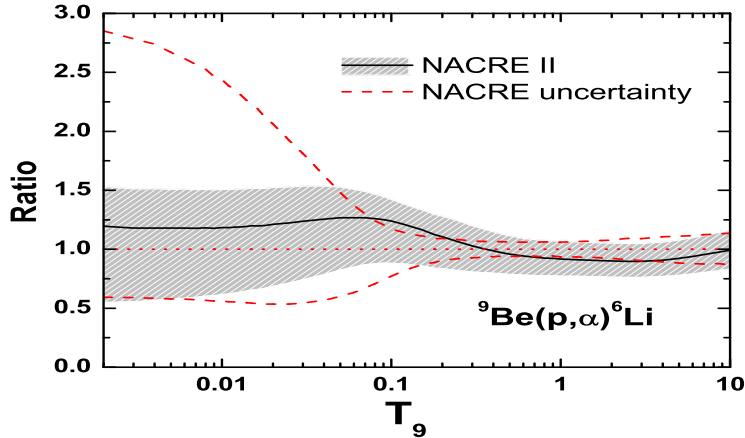


Figure 49: ${}^9\text{Be}(\text{p}, \alpha){}^6\text{Li}$ rates in units of the NACRE (adopt) values. The exclusion for the DWBA fit of the experimental data sets in the $E_{\text{cm}} \lesssim 0.05$ MeV range other than WE08 by THM (see text) lowers the upper NACRE uncertainty.

Table 21: ${}^9\text{Be}(\text{p}, \alpha){}^6\text{Li}$ rates in units of $\text{cm}^3 \text{mol}^{-1} \text{s}^{-1}$.

T_9	adopted	low	high	T_9	adopted	low	high
0.002	3.06E-23	1.41E-23	3.92E-23	0.15	4.88E+03	3.59E+03	5.59E+03
0.003	7.54E-19	3.55E-19	9.66E-19	0.16	7.30E+03	5.40E+03	8.38E+03
0.004	4.44E-16	2.13E-16	5.68E-16	0.18	1.49E+04	1.12E+04	1.72E+04
0.005	4.11E-14	2.01E-14	5.27E-14	0.2	2.79E+04	2.10E+04	3.23E+04
0.006	1.30E-12	6.44E-13	1.66E-12	0.25	9.92E+04	7.64E+04	1.16E+05
0.007	2.04E-11	1.03E-11	2.60E-11	0.3	2.64E+05	2.08E+05	3.08E+05
0.008	1.97E-10	1.01E-10	2.52E-10	0.35	5.77E+05	4.60E+05	6.72E+05
0.009	1.34E-09	6.93E-10	1.71E-09	0.4	1.09E+06	8.76E+05	1.26E+06
0.01	7.00E-09	3.65E-09	8.91E-09	0.45	1.82E+06	1.49E+06	2.12E+06
0.011	2.96E-08	1.56E-08	3.77E-08	0.5	2.81E+06	2.31E+06	3.26E+06
0.012	1.06E-07	5.64E-08	1.35E-07	0.6	5.51E+06	4.57E+06	6.39E+06
0.013	3.32E-07	1.78E-07	4.21E-07	0.7	9.06E+06	7.56E+06	1.05E+07
0.014	9.28E-07	5.02E-07	1.18E-06	0.8	1.32E+07	1.11E+07	1.54E+07
0.015	2.36E-06	1.29E-06	2.99E-06	0.9	1.78E+07	1.50E+07	2.07E+07
0.016	5.55E-06	3.05E-06	7.01E-06	1.	2.27E+07	1.91E+07	2.63E+07
0.018	2.51E-05	1.40E-05	3.17E-05	1.25	3.49E+07	2.95E+07	4.07E+07
0.02	9.22E-05	5.22E-05	1.16E-04	1.5	4.67E+07	3.96E+07	5.45E+07
0.025	1.25E-03	7.28E-04	1.56E-03	1.75	5.76E+07	4.89E+07	6.73E+07
0.03	9.09E-03	5.45E-03	1.13E-02	2.	6.75E+07	5.73E+07	7.89E+07
0.04	1.64E-01	1.03E-01	2.01E-01	2.5	8.46E+07	7.19E+07	9.89E+07
0.05	1.29E+00	8.40E-01	1.56E+00	3.	9.86E+07	8.37E+07	1.15E+08
0.06	6.25E+00	4.19E+00	7.44E+00	3.5	1.10E+08	9.35E+07	1.29E+08
0.07	2.21E+01	1.51E+01	2.59E+01	4.	1.20E+08	1.02E+08	1.40E+08
0.08	6.26E+01	4.36E+01	7.29E+01	5.	1.35E+08	1.14E+08	1.57E+08
0.09	1.51E+02	1.07E+02	1.75E+02	6.	1.45E+08	1.23E+08	1.70E+08
0.1	3.25E+02	2.31E+02	3.73E+02	7.	1.54E+08	1.29E+08	1.80E+08
0.11	6.33E+02	4.54E+02	7.25E+02	8.	1.60E+08	1.34E+08	1.87E+08
0.12	1.14E+03	8.28E+02	1.31E+03	9.	1.65E+08	1.38E+08	1.93E+08
0.13	1.95E+03	1.42E+03	2.23E+03	10.	1.69E+08	1.41E+08	1.97E+08
0.14	3.15E+03	2.30E+03	3.60E+03				

$$\text{REV} = 0.618 \exp(-24.660/T_9) / [1.0 + 2.333 \exp(-25.369/T_9)] \\ [1.0 + 0.5 \exp(-19.543/T_9) + 1.5 \exp(-28.193/T_9)]$$

3.21. ${}^9\text{Be}(\alpha, n){}^{12}\text{C}$

The experimental data sets referred to in NACRE are GI65 [257][†], VA70b [258], GE75 [259], SC92 [260], WR94 [261] and KU96 [262], covering the $0.02 \lesssim E_{\text{cm}} \lesssim 10$ MeV range. No new cross section data are found. [[†]measured neutrons include those by the break-up reaction ${}^9\text{Be}(\alpha, n\alpha){}^8\text{Be}_+$.]

Figure 50 compares model and experimental S -factors. The data in the $E_{\text{cm}} \lesssim 0.4$ MeV range are used for the DWBA fit. They exhibit the $5/2^-$ and $1/2^+$ resonances at $E_R \simeq 0.17$ and 0.35 MeV. The likely contribution to the low-energy S -factors from the $7/2^-$ resonance at 0.10 MeV is estimated by Eqs. (25) and (26) with $\theta_\alpha^2 = 0.1$ along with $\Gamma_{\text{cm}}(E_R)$ from [39] and the (α, n_0) and (α, n_1) branching ratios from [263]. For the upper limit, $\theta_\alpha^2 = 0.3$ is used so as to avoid conflicts with the data at higher energies. Furthermore, the same θ_α values are used to evaluate the possible contributions from the $3/2^-$ (s-wave) sub-threshold resonance at -0.751 MeV. For the lower limit, those contributions are assumed to be negligibly small. The adopted parameter values are given in Table 45. The present $S(0.01 \text{ MeV}) = 11.5 {}^{+16}_{-7.4} \times 10^3 \text{ MeV b}$.

Table 22 gives the reaction rates at $0.018 \leq T_9 \leq 10$, for which the predicted and the experimental cross sections below and above $E_{\text{cm}} \simeq 0.165$ MeV are used, respectively.

Figure 51 compares the present and the NACRE rates.

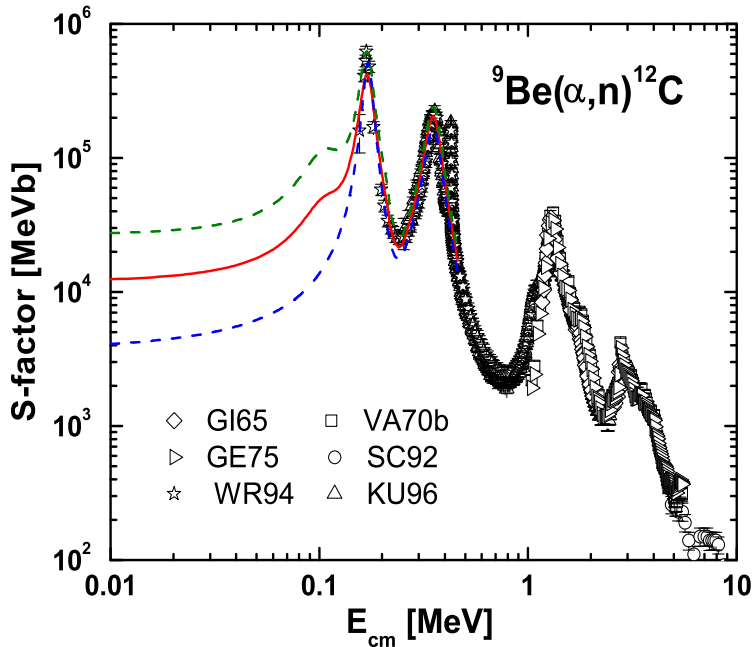


Figure 50: The S -factor for ${}^9\text{Be}(\alpha, n){}^{12}\text{C}$. GI65 data above $E_{\text{cm}} \simeq 3$ MeV are not used because of the possible contamination of break-up neutrons.

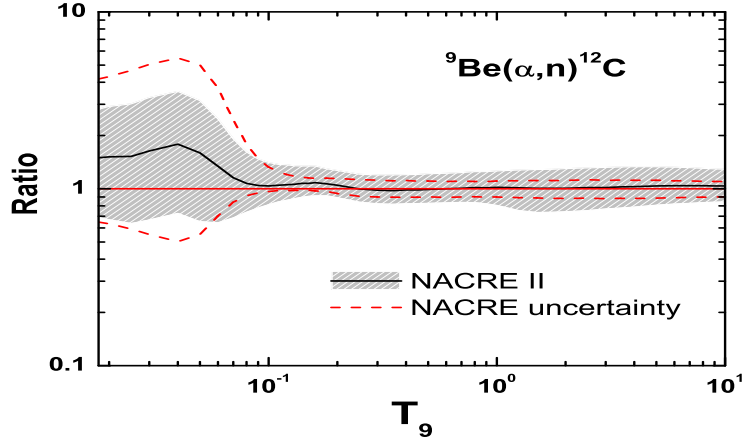


Figure 51: ${}^9\text{Be}(\alpha, \text{n}) {}^{12}\text{C}$ rates in units of the NACRE (adopt) values. The reduced upper limits at low temperatures result from a constraint imposed on the possible maximum contribution from the $7/2^-$ resonance (see text). The uncertainties at highest temperatures are slightly larger than in NACRE because of the less selective choice of the experimental data.

Table 22: ${}^9\text{Be}(\alpha, \text{n}) {}^{12}\text{C}$ rates in units of $\text{cm}^3 \text{mol}^{-1} \text{s}^{-1}$.

T_9	adopted	low	high	T_9	adopted	low	high
0.018	5.95E-25	2.73E-25	1.12E-24	0.4	1.22E+01	1.02E+01	1.49E+01
0.02	1.40E-23	6.17E-24	2.70E-23	0.45	3.30E+01	2.76E+01	4.04E+01
0.025	8.04E-21	3.35E-21	1.59E-20	0.5	7.37E+01	6.15E+01	9.03E+01
0.03	1.15E-18	4.69E-19	2.31E-18	0.6	2.49E+02	2.07E+02	3.05E+02
0.04	1.74E-15	7.06E-16	3.46E-15	0.7	6.05E+02	5.03E+02	7.42E+02
0.05	2.84E-13	1.16E-13	5.62E-13	0.8	1.23E+03	1.01E+03	1.51E+03
0.06	1.46E-11	7.00E-12	2.71E-11	0.9	2.27E+03	1.84E+03	2.80E+03
0.07	3.96E-10	2.35E-10	6.56E-10	1.	4.09E+03	3.24E+03	5.07E+03
0.08	6.33E-09	4.36E-09	9.51E-09	1.25	1.76E+04	1.31E+04	2.22E+04
0.09	6.28E-08	4.70E-08	8.82E-08	1.5	6.51E+04	4.75E+04	8.32E+04
0.1	4.19E-07	3.30E-07	5.64E-07	1.75	1.87E+05	1.37E+05	2.40E+05
0.11	2.04E-06	1.66E-06	2.66E-06	2.	4.28E+05	3.15E+05	5.52E+05
0.12	7.80E-06	6.45E-06	9.95E-06	2.5	1.40E+06	1.04E+06	1.81E+06
0.13	2.46E-05	2.06E-05	3.08E-05	3.	3.11E+06	2.35E+06	4.04E+06
0.14	6.66E-05	5.64E-05	8.23E-05	3.5	5.53E+06	4.21E+06	7.17E+06
0.15	1.60E-04	1.37E-04	1.97E-04	4.	8.57E+06	6.57E+06	1.11E+07
0.16	3.53E-04	3.03E-04	4.30E-04	5.	1.62E+07	1.26E+07	2.08E+07
0.18	1.42E-03	1.23E-03	1.70E-03	6.	2.54E+07	2.00E+07	3.23E+07
0.2	4.98E-03	4.28E-03	5.94E-03	7.	3.57E+07	2.84E+07	4.51E+07
0.25	7.67E-02	6.49E-02	9.25E-02	8.	4.66E+07	3.74E+07	5.85E+07
0.3	6.65E-01	5.58E-01	8.09E-01	9.	5.76E+07	4.66E+07	7.19E+07
0.35	3.44E+00	2.88E+00	4.20E+00	10.	6.85E+07	5.56E+07	8.50E+07

$$\text{REV} = 10.3 \exp(-66.163/T_9) [1.0 + 0.5 \exp(-19.543/T_9) + 1.5 \exp(-28.193/T_9)]$$

3.22. $^{10}\text{B}(\text{p},\gamma)^{11}\text{C}$

The experimental data sets referred to in NACRE are KU70 [264] and WI83 [265], covering the $0.09 \lesssim E_{\text{cm}} \lesssim 13$ MeV range. Added is the post-NACRE data set TO03 [266].

Figure 52 compares the model and experimental S -factors. The data for $E_{\text{cm}} \lesssim 1.0$ MeV are used for the PM fit. They exhibit the $3/2^-$ resonance at $E_R \simeq 0.96$ MeV. The transitions to the ground and the first five excited states of ^{11}C are considered inclusively. The S -factor data below $E_{\text{cm}} \simeq 0.2$ MeV are thought to reflect the tail of the $5/2^+$ resonance expected at $E_{\text{cm}} \simeq 0.010$ MeV. The extrapolation to the resonance peak region is performed in parallel to the $^{10}\text{B}(\text{p},\alpha)^7\text{Be}$ reaction, the S -factors of which are known to lower energies than in the (p,γ) case. In practice, we use the Breit-Wigner formula, Eqs. (25) and (26), with resonance energy and width that well reproduce the DWBA result. At $E_{\text{cm}} \lesssim 0.005$ MeV, a correction is made by directly scaling the DWBA results. No significant sub-threshold contributions (e.g. from the $7/2^+$ resonance at $E_R \simeq -0.034$ MeV) to the S -factors in the low-energy range are concordant with the experimental data at $E_{\text{cm}} \gtrsim 0.1$ MeV. The adopted parameter values are given in Table 62. The present $S(0.001\text{MeV}) = 0.13_{-0.09}^{+0.03}$ MeV b.

Table 23 gives the reaction rates at $0.004 \leq T_9 \leq 10$, for which the PM-predicted and the experimental cross sections below and above $E_{\text{cm}} \simeq 0.1$ MeV are used, respectively. Figure 53 compares the present and the NACRE rates.

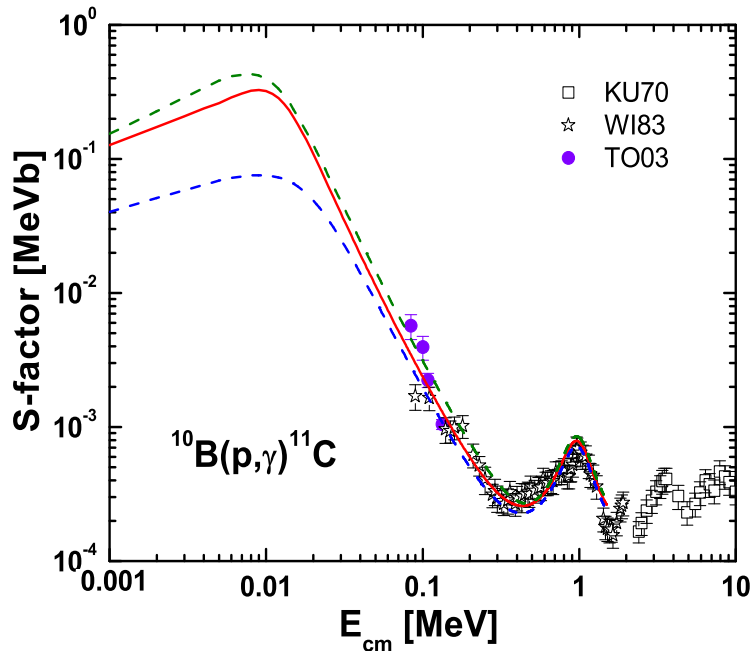


Figure 52: The S -factor for $^{10}\text{B}(\text{p},\gamma)^{11}\text{C}$.

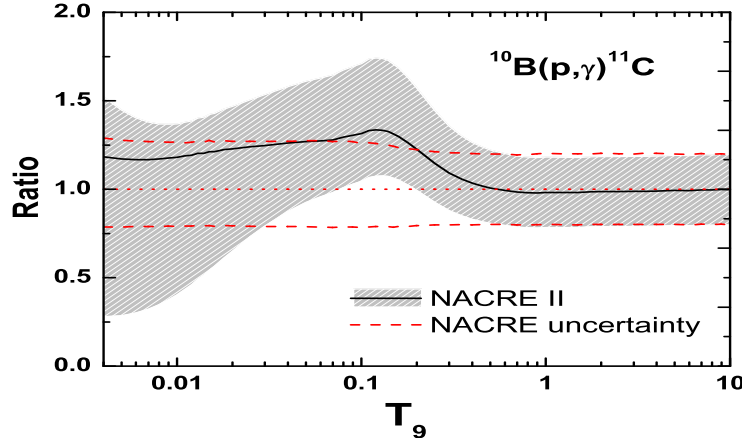


Figure 53: $^{10}\text{B}(\text{p}, \gamma)^{11}\text{C}$ rates in units of the NACRE (adopt) values. As for the large uncertainties at the lowest temperatures, see the caption to Fig. 55.

Table 23: $^{10}\text{B}(\text{p}, \gamma)^{11}\text{C}$ rates in $\text{cm}^3\text{mol}^{-1}\text{s}^{-1}$

T_9	adopted	low	high	T_9	adopted	low	high
0.004	1.71E-22	4.05E-23	2.21E-22	0.16	2.60E-02	2.10E-02	3.37E-02
0.005	3.29E-20	8.02E-21	4.07E-20	0.18	4.77E-02	3.87E-02	6.16E-02
0.006	1.72E-18	4.42E-19	2.06E-18	0.2	8.03E-02	6.50E-02	1.03E-01
0.007	3.87E-17	1.07E-17	4.56E-17	0.25	2.27E-01	1.83E-01	2.86E-01
0.008	4.89E-16	1.45E-16	5.71E-16	0.3	4.99E-01	4.02E-01	6.20E-01
0.009	4.07E-15	1.30E-15	4.73E-15	0.35	9.29E-01	7.47E-01	1.14E+00
0.01	2.48E-14	8.47E-15	2.87E-14	0.4	1.54E+00	1.24E+00	1.88E+00
0.011	1.19E-13	4.32E-14	1.38E-13	0.45	2.35E+00	1.89E+00	2.86E+00
0.012	4.69E-13	1.81E-13	5.45E-13	0.5	3.38E+00	2.71E+00	4.11E+00
0.013	1.59E-12	6.47E-13	1.85E-12	0.6	6.18E+00	4.95E+00	7.47E+00
0.014	4.74E-12	2.03E-12	5.54E-12	0.7	1.01E+01	8.10E+00	1.22E+01
0.015	1.27E-11	5.70E-12	1.49E-11	0.8	1.55E+01	1.24E+01	1.87E+01
0.016	3.13E-11	1.46E-11	3.68E-11	0.9	2.25E+01	1.80E+01	2.71E+01
0.018	1.52E-10	7.59E-11	1.80E-10	1.	3.15E+01	2.52E+01	3.79E+01
0.02	5.86E-10	3.10E-10	7.00E-10	1.25	6.41E+01	5.12E+01	7.70E+01
0.025	8.50E-09	5.02E-09	1.03E-08	1.5	1.13E+02	9.02E+01	1.36E+02
0.03	6.37E-08	4.05E-08	7.84E-08	1.75	1.78E+02	1.42E+02	2.14E+02
0.04	1.15E-06	7.98E-07	1.44E-06	2.	2.58E+02	2.07E+02	3.10E+02
0.05	8.72E-06	6.36E-06	1.11E-05	2.5	4.52E+02	3.61E+02	5.42E+02
0.06	4.00E-05	3.01E-05	5.12E-05	3.	6.70E+02	5.36E+02	8.04E+02
0.07	1.33E-04	1.02E-04	1.71E-04	3.5	8.94E+02	7.16E+02	1.07E+03
0.08	3.55E-04	2.76E-04	4.58E-04	4.	1.12E+03	8.94E+02	1.34E+03
0.09	8.07E-04	6.36E-04	1.05E-03	5.	1.55E+03	1.24E+03	1.86E+03
0.1	1.63E-03	1.30E-03	2.12E-03	6.	1.96E+03	1.57E+03	2.36E+03
0.11	3.00E-03	2.40E-03	3.91E-03	7.	2.37E+03	1.90E+03	2.84E+03
0.12	5.11E-03	4.11E-03	6.67E-03	8.	2.78E+03	2.22E+03	3.33E+03
0.13	8.21E-03	6.62E-03	1.07E-02	9.	3.18E+03	2.55E+03	3.82E+03
0.14	1.25E-02	1.01E-02	1.63E-02	10.	3.59E+03	2.88E+03	4.31E+03
0.15	1.84E-02	1.49E-02	2.39E-02				

$$\begin{aligned} \text{REV} = & 3.03 \times 10^{10} T_9^{3/2} \exp(-100.84/T_9) / [1.0 + 0.5 \exp(-23.210/T_9)] \\ & \times [1.0 + 0.429 \exp(-8.336/T_9) + 0.143 \exp(-20.194/T_9) + 0.429 \exp(-24.997/T_9)] \end{aligned}$$

3.23. $^{10}\text{B}(\text{p},\alpha)^7\text{Be}$

The experimental data sets referred to in NACRE are BU50 [267], BR51b [268], JE64 [269][†], SZ72 [270], RO79 [271], YO91 [272], KN93 [273] and AN93 [274], covering the $0.02 \lesssim E_{\text{cm}} \lesssim 6.4$ MeV range. Added are the post-NACRE data sets LA10 [275][‡] and PU10 [276][‡], extending the range down to $E_{\text{cm}} \simeq 0.004$ MeV. [277][‡] is superseded by LA10. Some data in the lowest energy range may possibly be contaminated by electron screening. [[†](p, α_1) also; [‡]from $^2\text{H}(^{10}\text{B}, \alpha^7\text{Be})\text{n}$ (THM).]

Figure 54 compares the DWBA and experimental S -factors. The data in the $E_{\text{cm}} \lesssim 0.1$ MeV range are used for the DWBA fit. They appear to exhibit the $5/2^+$ resonance, or its tail, expected at $E_{\text{cm}} \simeq 0.010$ MeV. The "low" curve results from the fit to PU10, albeit this data set (which is "still under study") requires a width of about 30 keV, twice as much as those obtained for the "adopt" and "high" curves here and by other methods. The adopted parameter values are given in Table 46. The present $S(0.001) = 1.3_{-0.9}^{+0.2} \times 10^3$ MeV b.

Table 24 gives the reaction rates at $0.003 \leq T_9 \leq 10$, for which the DWBA-predicted and the experimental cross sections below and above $E_{\text{cm}} \simeq 0.02$ MeV are used, respectively. Figure 55 compares the present and the NACRE rates.

See [279] for a DWBA analysis.

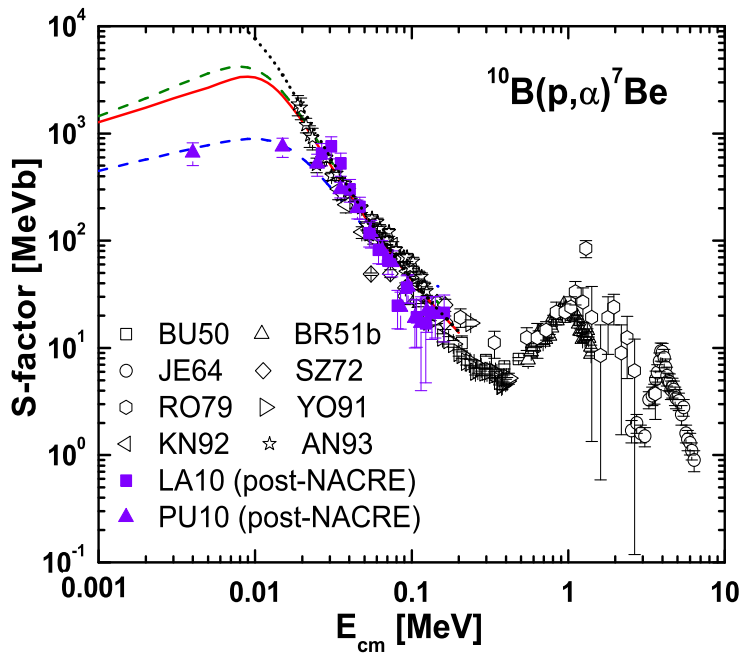


Figure 54: The S -factor for $^{10}\text{B}(\text{p},\alpha)^7\text{Be}$. The dotted line indicates an adiabatic screening correction ($U_e = 348$ eV) to the "adopt" curve (solid line). The recent data [278], not shown here, from the reverse $^7\text{Be}(\alpha, \text{p})^{10}\text{B}$ reaction imply (but with large uncertainties) less structured S -factors in the $0.3 \lesssim E_{\text{cm}} \lesssim 1.1$ MeV range, and some fine structures in the $2.3 \lesssim E_{\text{cm}} \lesssim 6.5$ MeV range.

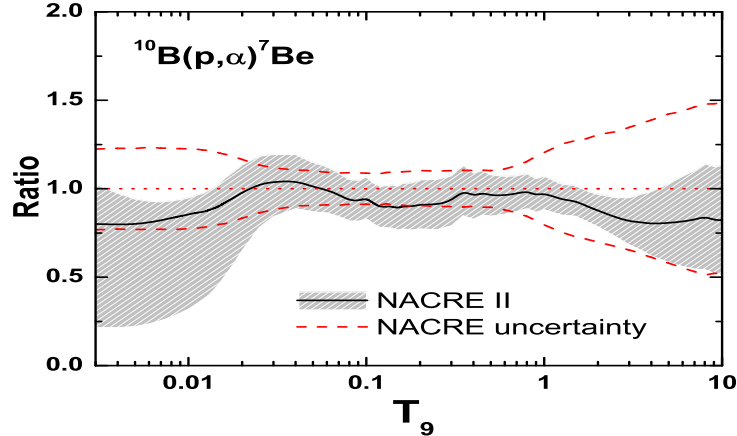


Figure 55: $^{10}\text{B}(\text{p}, \alpha)^7\text{Be}$ rates in units of the NACRE (adopt) values. The consideration of PU10 (THM) explains the large uncertainty at the lowest temperatures. What is seen at high temperatures may be the consequence of the different interpolation/integration techniques of high-energy data.

Table 24: $^{10}\text{B}(\text{p}, \alpha)^7\text{Be}$ rates in $\text{cm}^3 \text{mol}^{-1} \text{s}^{-1}$

T_9	adopted	low	high	T_9	adopted	low	high
0.003	1.00E-21	2.68E-22	1.28E-21	0.15	3.17E+02	2.73E+02	3.61E+02
0.004	1.78E-18	4.75E-19	2.17E-18	0.16	4.52E+02	3.88E+02	5.17E+02
0.005	3.43E-16	9.47E-17	4.04E-16	0.18	8.43E+02	7.17E+02	9.68E+02
0.006	1.80E-14	5.25E-15	2.07E-14	0.2	1.43E+03	1.21E+03	1.65E+03
0.007	4.11E-13	1.27E-13	4.64E-13	0.25	4.04E+03	3.41E+03	4.67E+03
0.008	5.26E-12	1.73E-12	5.87E-12	0.3	8.79E+03	7.45E+03	1.01E+04
0.009	4.43E-11	1.55E-11	4.92E-11	0.35	1.62E+04	1.39E+04	1.86E+04
0.01	2.72E-10	1.02E-10	3.03E-10	0.4	2.69E+04	2.32E+04	3.06E+04
0.011	1.31E-09	5.22E-10	1.46E-09	0.45	4.13E+04	3.59E+04	4.66E+04
0.012	5.22E-09	2.22E-09	5.86E-09	0.5	5.99E+04	5.26E+04	6.72E+04
0.013	1.78E-08	8.05E-09	2.01E-08	0.6	1.13E+05	1.00E+05	1.25E+05
0.014	5.32E-08	2.57E-08	6.05E-08	0.7	1.92E+05	1.72E+05	2.13E+05
0.015	1.44E-07	7.37E-08	1.64E-07	0.8	3.09E+05	2.77E+05	3.40E+05
0.016	3.54E-07	1.93E-07	4.07E-07	0.9	4.73E+05	4.26E+05	5.20E+05
0.018	1.74E-06	1.05E-06	2.01E-06	1.	6.98E+05	6.30E+05	7.66E+05
0.02	6.79E-06	4.49E-06	7.88E-06	1.25	1.60E+06	1.45E+06	1.76E+06
0.025	1.02E-04	7.76E-05	1.18E-04	1.5	3.12E+06	2.83E+06	3.41E+06
0.03	7.90E-04	6.39E-04	9.08E-04	1.75	5.32E+06	4.80E+06	5.83E+06
0.04	1.49E-02	1.27E-02	1.71E-02	2.	8.19E+06	7.33E+06	9.05E+06
0.05	1.18E-01	1.02E-01	1.34E-01	2.5	1.57E+07	1.36E+07	1.78E+07
0.06	5.66E-01	4.91E-01	6.41E-01	3.	2.50E+07	2.09E+07	2.91E+07
0.07	1.96E+00	1.71E+00	2.21E+00	3.5	3.53E+07	2.83E+07	4.22E+07
0.08	5.41E+00	4.73E+00	6.09E+00	4.	4.59E+07	3.55E+07	5.64E+07
0.09	1.27E+01	1.11E+01	1.43E+01	5.	6.68E+07	4.83E+07	8.54E+07
0.10	2.62E+01	2.29E+01	2.94E+01	6.	8.55E+07	5.87E+07	1.12E+08
0.11	4.90E+01	4.28E+01	5.53E+01	7.	1.01E+08	6.71E+07	1.36E+08
0.12	8.50E+01	7.39E+01	9.60E+01	8.	1.15E+08	7.38E+07	1.55E+08
0.13	1.38E+02	1.20E+02	1.57E+02	9.	1.25E+08	7.92E+07	1.71E+08
0.14	2.14E+02	1.85E+02	2.43E+02	10.	1.34E+08	8.36E+07	1.84E+08

$$\begin{aligned} \text{REV} = & 0.754 \exp(-13.285/T_9) / [1.0 + 0.5 \exp(-4.979/T_9)] \\ & \times [1.0 + 0.429 \exp(-8.336/T_9) + 0.143 \exp(-20.194/T_9) + 0.429 \exp(-24.997/T_9)] \end{aligned}$$

3.24. $^{11}\text{B}(\text{p},\gamma)^{12}\text{C}$

The experimental data sets referred to in NACRE are HU53 [280], AL64 [281] and SE65 [282], covering the $0.3 \lesssim E_{\text{cm}} \lesssim 9$ MeV range. Added is the post-NACRE data set KE00 [283], exploring the $0.07 \lesssim E_{\text{cm}} \lesssim 0.09$ MeV range.

Figure 56 compares the PM and experimental S -factors. The data in the $E_{\text{cm}} \lesssim 0.7$ MeV range are used for the PM fit. They suggest a 2^+ resonance at $E_R \simeq 0.15$ MeV, and exhibit the 2^- resonance[†] at $E_R \simeq 0.61$ MeV. For the former, the Breit-Wigner formula is used to fix its height, and the PM extrapolation then nicely goes through the KE00 data points. The transitions to the ground and the first excited states of ^{12}C are considered inclusively. The adopted parameter values are given in Table 63. The present $S(0) = 4.3^{+0.8}_{-0.6}$ keV b. In comparison, $S(0) = 3.3 \pm 0.5$ keV b [NACRE, from [174]]. [[†]This state at $E_x \simeq 16.57$ MeV decays to the ground state 100 % via an M2 transition [39]. Whereas this mode is not included in the formalism given in Sect. 2.3.3, the *shape* of the corresponding S -factor is determined essentially by the scattering state. It is therefore nearly independent of the multipolarities when the Q -value is as high as in the current case.]

Table 25 gives the reaction rates at $0.004 \leq T_9 \leq 10$, for which the PM-predicted and the experimental cross sections below and above $E_{\text{cm}} \simeq 0.2$ MeV are used, respectively. Figure 57 compares the present and the NACRE rates.

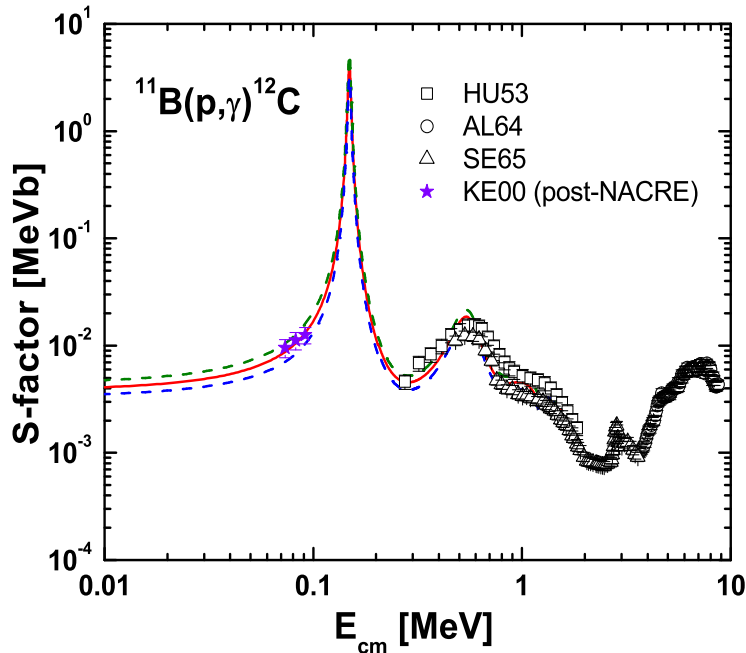


Figure 56: The S -factor for $^{11}\text{B}(\text{p},\gamma)^{12}\text{C}$.

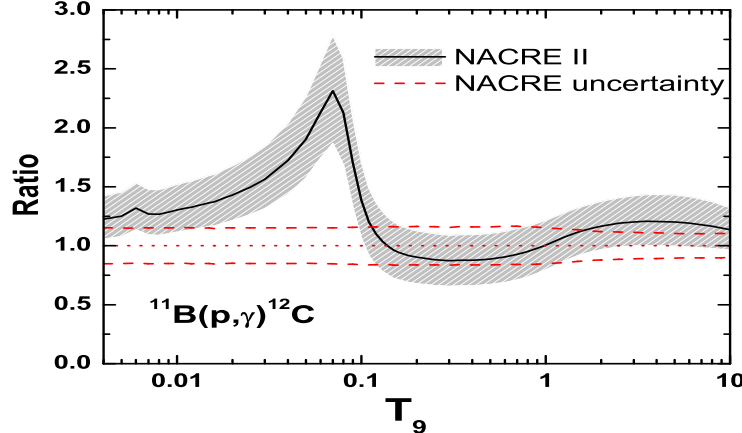


Figure 57: $^{11}\text{B}(\text{p}, \gamma)^{12}\text{C}$ rates in units of the NACRE (adopt) values. The peculiar increase of the ratio at $T_9 \lesssim 0.1$ reflects the improved S-factor shape of the low-energy tail of the 2^+ resonance.

Table 25: $^{11}\text{B}(\text{p}, \gamma)^{12}\text{C}$ rates in $\text{cm}^3\text{mol}^{-1}\text{s}^{-1}$

T_9	adopted	low	high	T_9	adopted	low	high
0.004	1.78E-24	1.53E-24	2.06E-24	0.16	1.95E+00	1.47E+00	2.44E+00
0.005	3.65E-22	3.15E-22	4.25E-22	0.18	5.29E+00	3.98E+00	6.61E+00
0.006	2.12E-20	1.83E-20	2.47E-20	0.2	1.16E+01	8.75E+00	1.45E+01
0.007	5.43E-19	4.67E-19	6.33E-19	0.25	4.63E+01	3.48E+01	5.78E+01
0.008	7.89E-18	6.77E-18	9.19E-18	0.3	1.12E+02	8.40E+01	1.39E+02
0.009	7.56E-17	6.49E-17	8.82E-17	0.35	2.03E+02	1.53E+02	2.54E+02
0.01	5.30E-16	4.54E-16	6.18E-16	0.4	3.12E+02	2.35E+02	3.89E+02
0.011	2.91E-15	2.49E-15	3.39E-15	0.45	4.29E+02	3.24E+02	5.35E+02
0.012	1.31E-14	1.12E-14	1.53E-14	0.5	5.49E+02	4.15E+02	6.83E+02
0.013	5.05E-14	4.32E-14	5.90E-14	0.6	7.83E+02	5.96E+02	9.71E+02
0.014	1.70E-13	1.45E-13	1.99E-13	0.7	1.01E+03	7.75E+02	1.25E+03
0.015	5.14E-13	4.39E-13	6.02E-13	0.8	1.24E+03	9.63E+02	1.53E+03
0.016	1.41E-12	1.20E-12	1.65E-12	0.9	1.50E+03	1.17E+03	1.82E+03
0.018	8.45E-12	7.19E-12	9.90E-12	1.	1.78E+03	1.41E+03	2.15E+03
0.02	3.95E-11	3.35E-11	4.63E-11	1.25	2.64E+03	2.14E+03	3.16E+03
0.025	8.70E-10	7.35E-10	1.02E-09	1.5	3.72E+03	3.05E+03	4.40E+03
0.03	9.26E-09	7.79E-09	1.09E-08	1.75	4.94E+03	4.08E+03	5.83E+03
0.04	2.96E-07	2.47E-07	3.51E-07	2.	6.24E+03	5.18E+03	7.36E+03
0.05	3.58E-06	2.96E-06	4.26E-06	2.5	8.87E+03	7.36E+03	1.05E+04
0.06	2.49E-05	2.04E-05	2.98E-05	3.	1.13E+04	9.40E+03	1.34E+04
0.07	1.28E-04	1.03E-04	1.54E-04	3.5	1.35E+04	1.12E+04	1.60E+04
0.08	5.79E-04	4.58E-04	7.04E-04	4.	1.54E+04	1.28E+04	1.83E+04
0.09	2.50E-03	1.94E-03	3.07E-03	5.	1.85E+04	1.53E+04	2.20E+04
0.1	9.84E-03	7.54E-03	1.22E-02	6.	2.09E+04	1.73E+04	2.48E+04
0.11	3.34E-02	2.54E-02	4.15E-02	7.	2.28E+04	1.90E+04	2.70E+04
0.12	9.67E-02	7.32E-02	1.20E-01	8.	2.47E+04	2.07E+04	2.91E+04
0.13	2.42E-01	1.83E-01	3.02E-01	9.	2.67E+04	2.25E+04	3.13E+04
0.14	5.36E-01	4.04E-01	6.68E-01	10.	2.89E+04	2.45E+04	3.36E+04
0.15	1.07E+00	8.05E-01	1.33E+00				

$$\text{REV} = 7.02 \times 10^{10} T_9^{3/2} \exp(-185.18/T_9) [1.0 + 0.5 \exp(-24.657/T_9)]$$

3.25. $^{11}\text{B}(\text{p},\alpha)^8\text{Be}$

The experimental data sets referred to in NACRE are SE65 [282], DA79 [284], BE87 [285], and AN93 [274], covering the $0.017 \lesssim E_{\text{cm}} \lesssim 3.5$ MeV range. For the $^{11}\text{B}(\text{p},\alpha_1)^8\text{Be}$ ($E_x \simeq 3.04$ MeV) channel, which is overwhelming, no new cross section data are found. The data below $E_{\text{cm}} \simeq 0.04$ MeV appear to be contaminated by electron screening, which seems to be supported by the recent data for the (p,α_0) channel [286][†].
[[†]from $^2\text{H}(^{11}\text{B},\alpha_0^8\text{Be})\text{n}$ (THM).]

Figure 58 compares the DWBA and experimental S -factors. The data in the $0.04 \lesssim E_{\text{cm}} \lesssim 1$ MeV range are used for the DWBA fit. They exhibit the 2^- resonance at $E_R \simeq 0.61$ MeV. The $0.1 \lesssim E_{\text{cm}} \lesssim 0.2$ MeV range containing the narrow 2^+ resonance at $E_R \simeq 0.15$ MeV is excluded in the fitting procedure. The adopted parameter values are given in Table 47. The present $S(0) = 210_{-30}^{+20}$ MeV b. In comparison, $S(0) = 187 \pm 30$ MeV b [NACRE, from AN93].

Table 26 gives the reaction rates at $0.003 \leq T_9 \leq 10$, for which the DWBA-predicted and the experimental cross sections below and above $E_{\text{cm}} \simeq 0.05$ MeV are used, respectively. The narrow resonance at $E_R \simeq 0.15$ MeV with measured strength [284, 287, 288] is also taken into account. Figure 59 compares the present and the NACRE rates.

See [279] for a DWBA analysis.

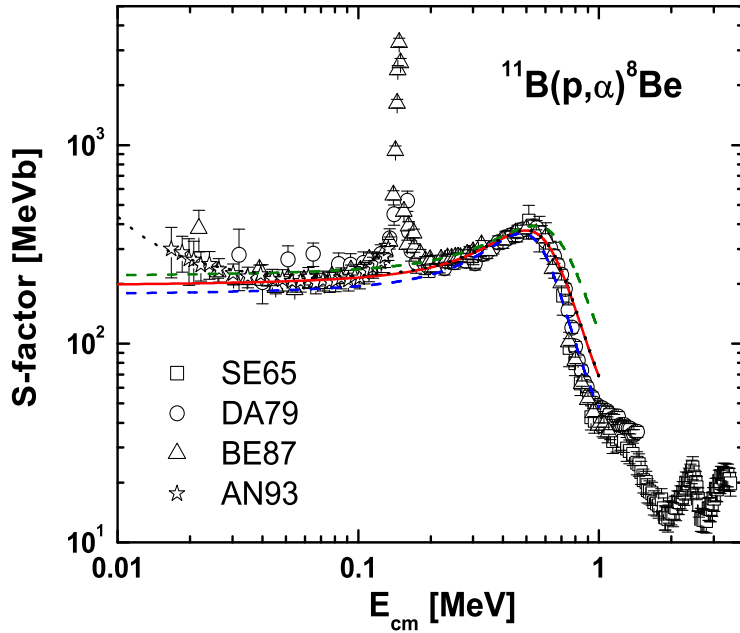


Figure 58: The S -factor for $^{11}\text{B}(\text{p},\alpha)^8\text{Be}$. The dotted line indicates an adiabatic screening correction ($U_e = 348$ eV) to the 'adopt' curve (solid line).

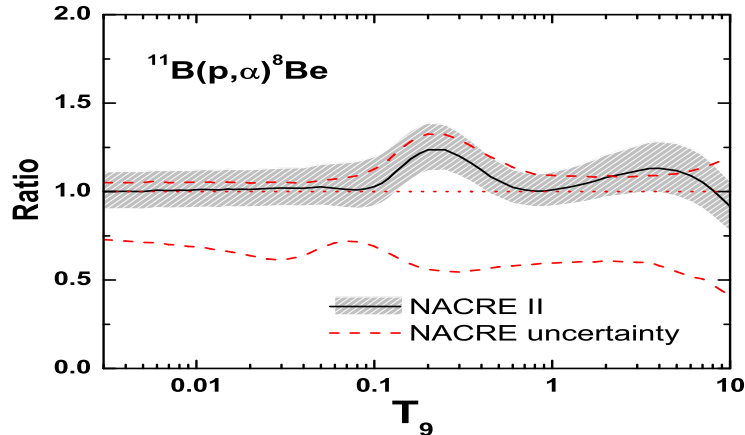


Figure 59: $^{11}\text{B}(\text{p}, \alpha)^8\text{Be}$ rates in units of the NACRE (adopt) values. The origin of the large (and asymmetric) uncertainty given in NACRE for the lower limits is unclear.

Table 26: $^{11}\text{B}(\text{p}, \alpha)^8\text{Be}$ rates in unit is $\text{cm}^3\text{mol}^{-1}\text{s}^{-1}$.

T_9	adopted	low	high	T_9	adopted	low	high
0.003	4.90E-23	4.41E-23	5.45E-23	0.15	2.22E+03	1.99E+03	2.52E+03
0.004	8.69E-20	7.83E-20	9.67E-20	0.16	3.69E+03	3.33E+03	4.19E+03
0.005	1.77E-17	1.59E-17	1.97E-17	0.18	8.96E+03	8.08E+03	1.01E+04
0.006	1.02E-15	9.17E-16	1.13E-15	0.2	1.87E+04	1.69E+04	2.09E+04
0.007	2.58E-14	2.33E-14	2.87E-14	0.25	7.35E+04	6.67E+04	8.21E+04
0.008	3.72E-13	3.35E-13	4.13E-13	0.3	1.92E+05	1.74E+05	2.13E+05
0.009	3.53E-12	3.18E-12	3.93E-12	0.35	3.97E+05	3.60E+05	4.40E+05
0.01	2.45E-11	2.21E-11	2.73E-11	0.4	7.13E+05	6.48E+05	7.89E+05
0.011	1.34E-10	1.20E-10	1.48E-10	0.45	1.17E+06	1.06E+06	1.29E+06
0.012	5.98E-10	5.38E-10	6.64E-10	0.5	1.80E+06	1.64E+06	1.99E+06
0.013	2.28E-09	2.05E-09	2.53E-09	0.6	3.75E+06	3.41E+06	4.12E+06
0.014	7.62E-09	6.87E-09	8.47E-09	0.7	6.82E+06	6.22E+06	7.49E+06
0.015	2.28E-08	2.06E-08	2.53E-08	0.8	1.12E+07	1.02E+07	1.23E+07
0.016	6.22E-08	5.60E-08	6.90E-08	0.9	1.70E+07	1.55E+07	1.87E+07
0.018	3.66E-07	3.30E-07	4.06E-07	1.	2.42E+07	2.20E+07	2.67E+07
0.02	1.68E-06	1.51E-06	1.87E-06	1.25	4.71E+07	4.27E+07	5.21E+07
0.025	3.55E-05	3.20E-05	3.94E-05	1.5	7.43E+07	6.71E+07	8.25E+07
0.03	3.62E-04	3.26E-04	4.02E-04	1.75	1.03E+08	9.26E+07	1.15E+08
0.04	1.06E-02	9.54E-03	1.18E-02	2.	1.31E+08	1.17E+08	1.46E+08
0.05	1.16E-01	1.04E-01	1.30E-01	2.5	1.80E+08	1.61E+08	2.03E+08
0.06	7.15E-01	6.43E-01	8.14E-01	3.	2.20E+08	1.95E+08	2.48E+08
0.07	3.06E+00	2.74E+00	3.51E+00	3.5	2.51E+08	2.22E+08	2.84E+08
0.08	1.02E+01	9.13E+00	1.18E+01	4.	2.75E+08	2.42E+08	3.12E+08
0.09	2.86E+01	2.56E+01	3.33E+01	5.	3.08E+08	2.69E+08	3.51E+08
0.1	7.13E+01	6.37E+01	8.31E+01	6.	3.30E+08	2.86E+08	3.77E+08
0.11	1.62E+02	1.45E+02	1.89E+02	7.	3.46E+08	2.97E+08	3.96E+08
0.12	3.43E+02	3.06E+02	3.96E+02	8.	3.57E+08	3.04E+08	4.10E+08
0.13	6.78E+02	6.07E+02	7.80E+02	9.	3.65E+08	3.09E+08	4.20E+08
0.14	1.26E+03	1.13E+03	1.44E+03	10.	3.70E+08	3.13E+08	4.28E+08

3.26. $^{11}\text{B}(\alpha, \text{n})^{14}\text{N}$

This reaction is not included in NACRE, but is present in CF88. The experimental data sets adopted here are VA75 [289], and WA91 [290], covering the $0.4 \lesssim E_{\text{cm}} \lesssim 6$ MeV range. [291] is superseded by WA91.

Figure 60 compares the DWBA and experimental S -factors. The data in the $E_{\text{cm}} \lesssim 0.8$ MeV range are used for the DWBA fit. They exhibit the $1/2^+$ and $3/2^+$ resonances at $E_R \simeq 0.45$ and 0.77 MeV, the former being almost degenerate in energy with the narrow $7/2^-$ resonance. The adopted parameter values are given in Table 48. The present $S(0.001 \text{ MeV}) = 7.5_{-3.1}^{+3.7} \times 10^2 \text{ MeV b}$.

Table 27 gives the reaction rates at $0.03 \leq T_9 \leq 10$, for which the DWBA-predicted and the experimental cross sections below and above $E_{\text{cm}} \simeq 0.4$ MeV are used, respectively. In addition to the one at $E_{\text{cm}} \simeq 0.45$ MeV mentioned above, the very narrow $1/2^-$ resonance at $E_R \simeq 0.30$ MeV with measured strength [290] is also taken into account. Figure 61 compares the present and the CF88 rates.

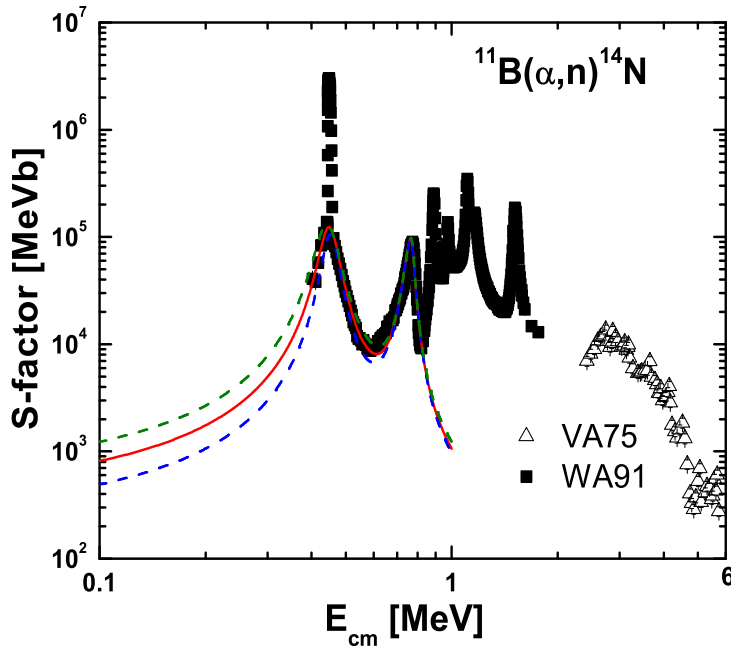


Figure 60: The S -factor for $^{11}\text{B}(\alpha, \text{n})^{14}\text{N}$. Note that the very narrow peak ($7/2^-$), not used for the fit, is shown overlapping with the broader $1/2^+$ resonance at $E_{\text{cm}} \simeq 0.44$ MeV.

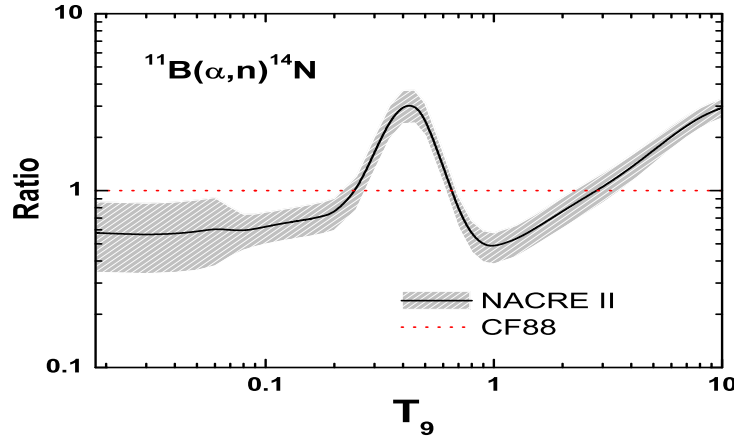


Figure 61: $^{11}\text{B}(\alpha, \text{n})^{14}\text{N}$ rates in units of the CF88 values. The difference from CF88 stems mostly from the inclusion of the new data set WA91.

Table 27: Rates of $^{11}\text{B}(\alpha, \text{n})^{14}\text{N}$ in units of $\text{cm}^3 \text{mol}^{-1} \text{s}^{-1}$.

T_9	adopted	low	high	T_9	adopted	low	high
0.03	2.75E-26	1.56E-26	4.25E-26	0.5	7.07E-01	5.44E-01	8.82E-01
0.04	1.04E-22	5.96E-23	1.62E-22	0.6	3.67E+00	2.84E+00	4.56E+00
0.05	3.77E-20	2.16E-20	5.85E-20	0.7	1.44E+01	1.12E+01	1.78E+01
0.06	3.65E-18	2.14E-18	5.59E-18	0.8	4.95E+01	3.87E+01	6.07E+01
0.07	2.82E-16	1.97E-16	3.85E-16	0.9	1.50E+02	1.18E+02	1.84E+02
0.08	2.32E-14	1.80E-14	2.88E-14	1.	4.02E+02	3.17E+02	4.89E+02
0.09	9.45E-13	7.49E-13	1.15E-12	1.25	2.79E+03	2.21E+03	3.38E+03
0.1	1.89E-11	1.50E-11	2.28E-11	1.5	1.12E+04	8.87E+03	1.36E+04
0.11	2.18E-10	1.74E-10	2.62E-10	1.75	3.15E+04	2.50E+04	3.81E+04
0.12	1.66E-09	1.32E-09	1.99E-09	2.	7.02E+04	5.57E+04	8.50E+04
0.13	9.16E-09	7.32E-09	1.10E-08	2.5	2.26E+05	1.79E+05	2.74E+05
0.14	3.94E-08	3.14E-08	4.73E-08	3.	5.16E+05	4.07E+05	6.29E+05
0.15	1.38E-07	1.10E-07	1.66E-07	3.5	9.71E+05	7.59E+05	1.19E+06
0.16	4.14E-07	3.30E-07	4.98E-07	4.	1.62E+06	1.25E+06	2.00E+06
0.18	2.55E-06	2.03E-06	3.07E-06	5.	3.55E+06	2.71E+06	4.46E+06
0.2	1.10E-05	8.74E-06	1.33E-05	6.	6.35E+06	4.78E+06	8.08E+06
0.25	1.88E-04	1.47E-04	2.31E-04	7.	9.88E+06	7.36E+06	1.27E+07
0.3	2.00E-03	1.55E-03	2.49E-03	8.	1.39E+07	1.03E+07	1.79E+07
0.35	1.46E-02	1.12E-02	1.82E-02	9.	1.81E+07	1.33E+07	2.35E+07
0.4	7.10E-02	5.46E-02	8.87E-02	10.	2.24E+07	1.64E+07	2.91E+07
0.45	2.51E-01	1.93E-01	3.14E-01				

$$\text{REV} = 3.67 \exp(-1.835/T_9) [1.0 + 0.5 \exp(-24.657/T_9)] / [1.0 + 0.333 \exp(-26.840/T_9)]$$

3.27. $^{12}\text{C}(\text{p},\gamma)^{13}\text{N}$

The experimental data sets referred to in NACRE are BA50 [292], HA50 [293], LA57a [294], VO63 [295][†] and RO74a [296][‡], covering the $0.07 \lesssim E_{\text{cm}} \lesssim 2.3$ MeV range. [297] was apparently superseded by VO63. Added is the post-NACRE data set BU08 [298]. [[†]*S*-factors re-calculated in the present work from the original cross section table; [‡]from $d\sigma/d\Omega$ at 0 and 90 degrees, used here in the $E_{\text{cm}} \gtrsim 0.63$ MeV range.]

Figure 62 compares the PM and experimental *S*-factors. The data in the $E_{\text{cm}} \lesssim 1$ MeV range are used for the PM fit. They exhibit the $1/2^+$ resonance at $E_R \simeq 0.42$ MeV. The adopted parameter values are given in Table 64. The present $S(0) = 1.4 \pm 0.5$ keV b. In comparison, $S(0) = 1.45 \pm 0.20$ keV b [NACRE from [296]], and 2.35 keV b [RAD10].

Table 28 gives the reaction rates at $0.006 \leq T_9 \leq 10$, for which the PM-predicted and the experimental cross sections below and above $E_{\text{cm}} \simeq 0.2$ MeV are used, respectively. Figure 63 compares the present and the NACRE rates.

See [299] for a cluster model calculation; [300] for a potential model fit.

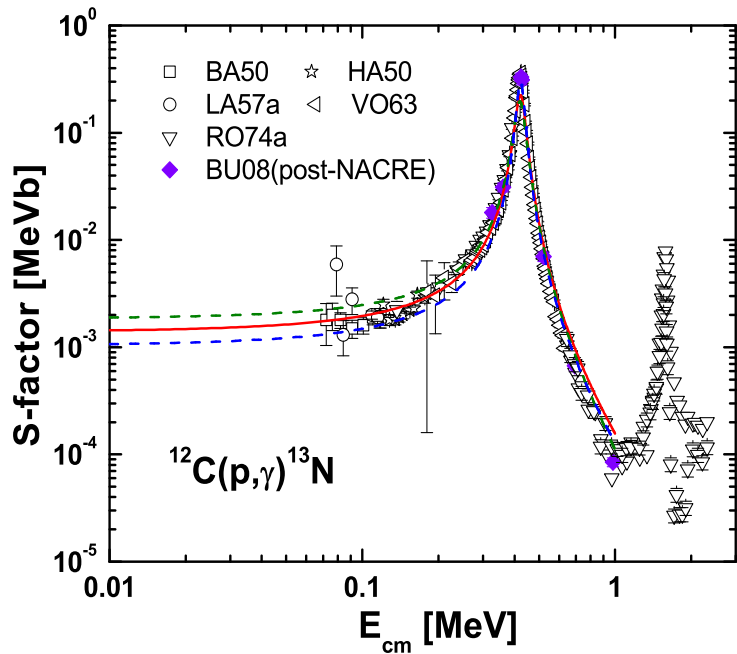


Figure 62: The *S*-factor for $^{12}\text{C}(\text{p},\gamma)^{13}\text{N}$. See the footnotes to VO63 and RO74a in the text.

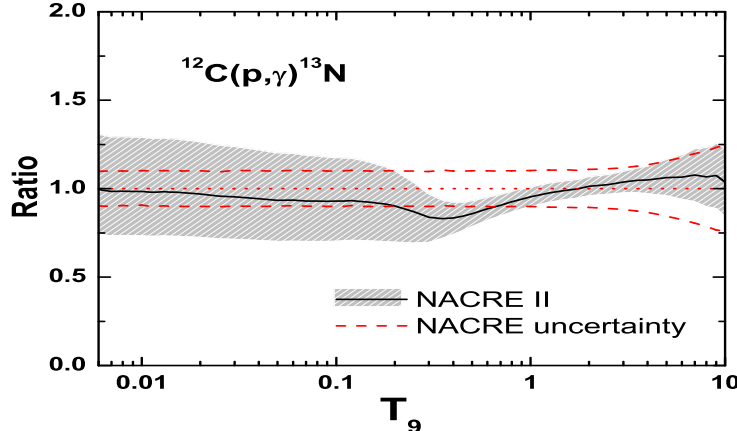


Figure 63: $^{12}\text{C}(\text{p},\gamma)^{13}\text{N}$ rates in units of the NACRE (adopt) values. The NACRE small uncertainty at low temperatures may not be warranted.

Table 28: $^{12}\text{C}(\text{p},\gamma)^{13}\text{N}$ rates in $\text{cm}^3 \text{mol}^{-1} \text{s}^{-1}$

T_9	adopted	low	high	T_9	adopted	low	high
0.006	1.21E-24	9.04E-25	1.60E-24	0.18	3.35E-03	2.57E-03	4.12E-03
0.007	4.75E-23	3.54E-23	6.24E-23	0.2	7.81E-03	6.04E-03	9.54E-03
0.008	9.85E-22	7.34E-22	1.29E-21	0.25	4.78E-02	3.81E-02	5.69E-02
0.009	1.28E-20	9.53E-21	1.68E-20	0.3	2.33E-01	1.94E-01	2.69E-01
0.01	1.16E-19	8.66E-20	1.52E-19	0.35	9.55E-01	8.26E-01	1.08E+00
0.011	7.99E-19	5.96E-19	1.05E-18	0.4	3.18E+00	2.83E+00	3.52E+00
0.012	4.40E-18	3.28E-18	5.77E-18	0.45	8.62E+00	7.79E+00	9.41E+00
0.013	2.02E-17	1.51E-17	2.65E-17	0.5	1.96E+01	1.79E+01	2.12E+01
0.014	8.01E-17	5.97E-17	1.05E-16	0.6	6.79E+01	6.30E+01	7.29E+01
0.015	2.79E-16	2.08E-16	3.65E-16	0.7	1.64E+02	1.53E+02	1.75E+02
0.016	8.75E-16	6.53E-16	1.14E-15	0.8	3.13E+02	2.93E+02	3.33E+02
0.018	6.60E-15	4.93E-15	8.62E-15	0.9	5.10E+02	4.79E+02	5.41E+02
0.02	3.76E-14	2.81E-14	4.90E-14	1.	7.43E+02	7.01E+02	7.88E+02
0.025	1.23E-12	9.17E-13	1.59E-12	1.25	1.41E+03	1.33E+03	1.49E+03
0.03	1.74E-11	1.31E-11	2.26E-11	1.5	2.06E+03	1.95E+03	2.17E+03
0.04	8.35E-10	6.26E-10	1.08E-09	1.75	2.62E+03	2.48E+03	2.76E+03
0.05	1.31E-08	9.82E-09	1.68E-08	2.	3.06E+03	2.90E+03	3.22E+03
0.06	1.07E-07	8.02E-08	1.37E-07	2.5	3.64E+03	3.45E+03	3.84E+03
0.07	5.70E-07	4.30E-07	7.29E-07	3.	3.94E+03	3.71E+03	4.18E+03
0.08	2.28E-06	1.72E-06	2.90E-06	3.5	4.08E+03	3.81E+03	4.35E+03
0.09	7.36E-06	5.57E-06	9.34E-06	4.	4.13E+03	3.82E+03	4.44E+03
0.1	2.03E-05	1.53E-05	2.56E-05	5.	4.12E+03	3.73E+03	4.52E+03
0.11	4.92E-05	3.73E-05	6.20E-05	6.	4.06E+03	3.58E+03	4.54E+03
0.12	1.08E-04	8.21E-05	1.36E-04	7.	3.97E+03	3.42E+03	4.52E+03
0.13	2.19E-04	1.67E-04	2.75E-04	8.	3.88E+03	3.27E+03	4.48E+03
0.14	4.16E-04	3.17E-04	5.19E-04	9.	3.78E+03	3.12E+03	4.43E+03
0.15	7.46E-04	5.69E-04	9.28E-04	10.	3.68E+03	2.99E+03	4.35E+03
0.16	1.28E-03	9.77E-04	1.58E-03				

$$\text{REV} = 8.85 \times 10^9 T_9^{3/2} \exp(-22.554/T_9) / [1.0 + \exp(-27.445/T_9)]$$

3.28. $^{12}\text{C}(\alpha, \gamma)^{16}\text{O}$

The experimental data sets referred to in NACRE are DY74 [301][†], RE87 [302]^{†,††}, KR88 [303][†] and OU96 [304][†], covering the $0.94 \lesssim E_{\text{cm}} \lesssim 3$ MeV range. Added are the post-NACRE data sets RO99 [305][†], GI01 [306][†], KU01 [307][†], FE04 [308][†], SC05 [309][‡], AS06 [310][†], MA09 [311][†], SC11 [312]^{††} and PL12 [313]^{†,‡,††}, extending the range to $0.89 \lesssim E_{\text{cm}} \lesssim 5$ MeV. KE82 [314]^{††}, KU02 [315]^{††}, and MA06 [316]^{††} are also considered. [[†]to g.s.; [‡]cascade; [‡]total.]

Figure 64 compares the PM and experimental S -factors. The partial S -factors for $E_{\text{cm}} \lesssim 4.5$ MeV of the transitions to the ground and the four excited states are used for the PM fit (Figs. 65-68). The $1^-, 2^+, 3^-$ and 4^+ resonances at $E_R \simeq 2.42, 2.68$ and $4.36, 4.43$, and 3.19 MeV are seen. Possible contributions from the 1^- and 2^+ sub-threshold states at $E_R \simeq -0.045$ and -0.245 MeV (and their interference to the respective resonances at 2.42 and 2.68 MeV) are also considered. The adopted parameter values are given in Table 65. The present $S_{E1}(0.3 \text{ MeV}) = 80 \pm 18 \text{ keV b}$, $S_{E2}(0.3 \text{ MeV}) = 61 \pm 19 \text{ keV b}$, and $S_{\text{casc}}(0.3 \text{ MeV}) = 6.5_{-2.2}^{+4.7} \text{ keV b}$, leading to the total $S(0.3 \text{ MeV}) = 148 \pm 27 \text{ keV b}$. These ranges overlap with such previous estimates as [NACRE], [317], and [318].

Table 29 gives the reaction rates at $0.06 \leq T_9 \leq 10$, for which the PM-predicted and the experimental cross sections below and above $E_{\text{cm}} \simeq 2$ MeV are used, respectively. Several very narrow resonances in the $5.28 \lesssim E_{\text{cm}} \lesssim 5.93$ MeV range with measured strengths [319] are also taken into account. Figure 69 compares the present and the NACRE rates.

See [320] for a critical review. See also [50, 317, 321-326] for indirect measurements (such as the ^{16}N β -delayed α -spectrum, the transfer reaction and the scattering).

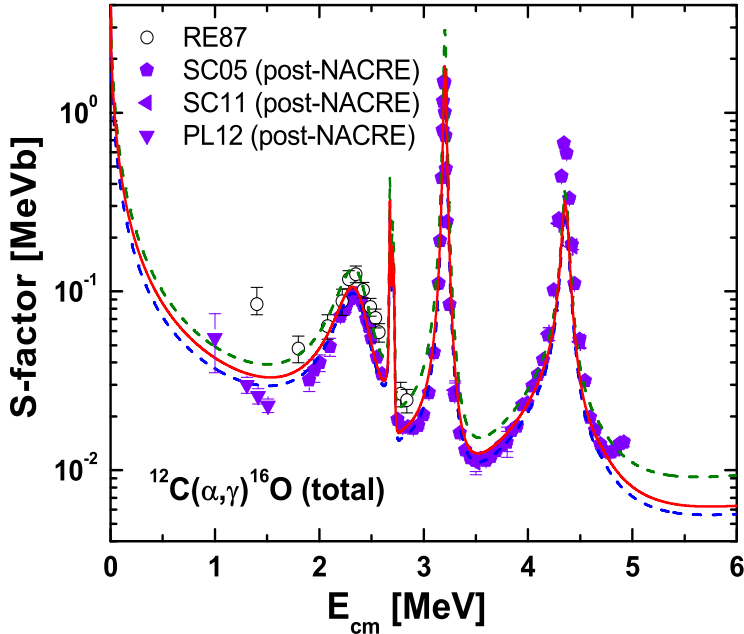


Figure 64: The S -factor for $^{12}\text{C}(\alpha, \gamma)^{16}\text{O}$. RE87 and SC11 refer to the sums of the partial S -factors with regard to the final states (for RE87, allow for some errors owing to the reading of the graphs).

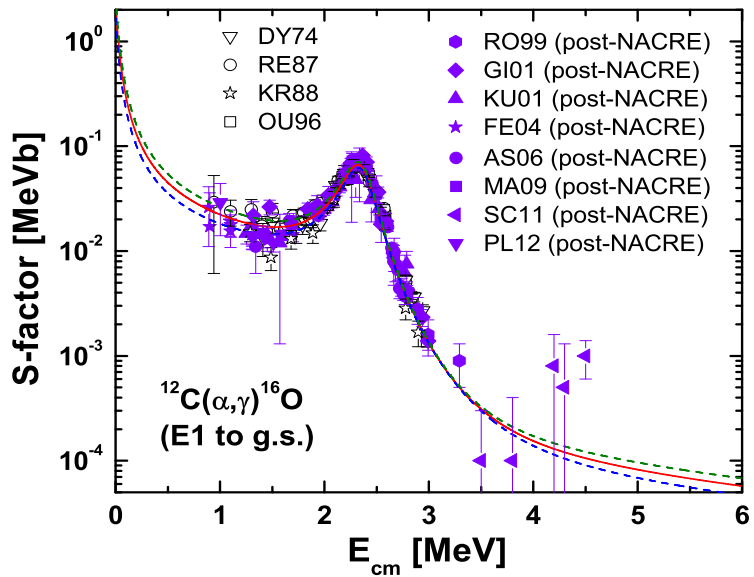


Figure 65: The E1 S -factor for the $^{12}\text{C}(\alpha, \gamma)^{16}\text{O}$ transition to the ground state.

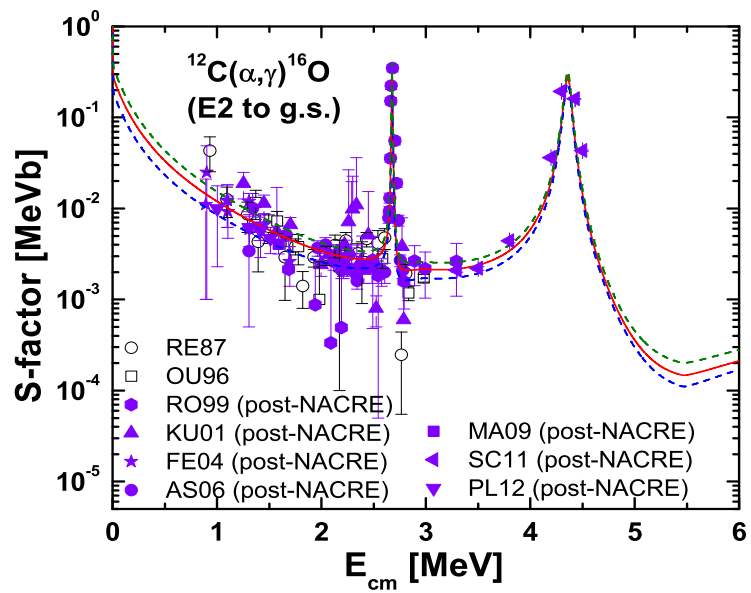


Figure 66: The E2 S -factor for the $^{12}\text{C}(\alpha, \gamma)^{16}\text{O}$ transition to the ground state.

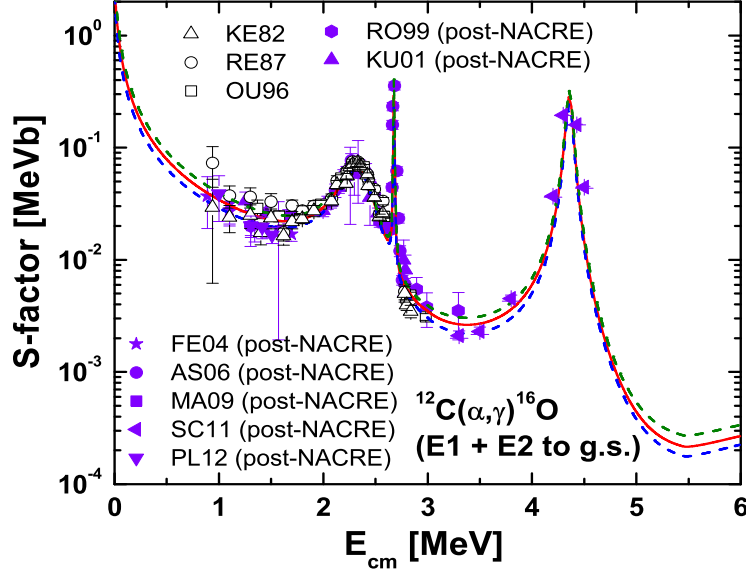


Figure 67: The S -factor for the $^{12}\text{C}(\alpha, \gamma)^{16}\text{O}$ E1 and E2 transitions to the ground state.

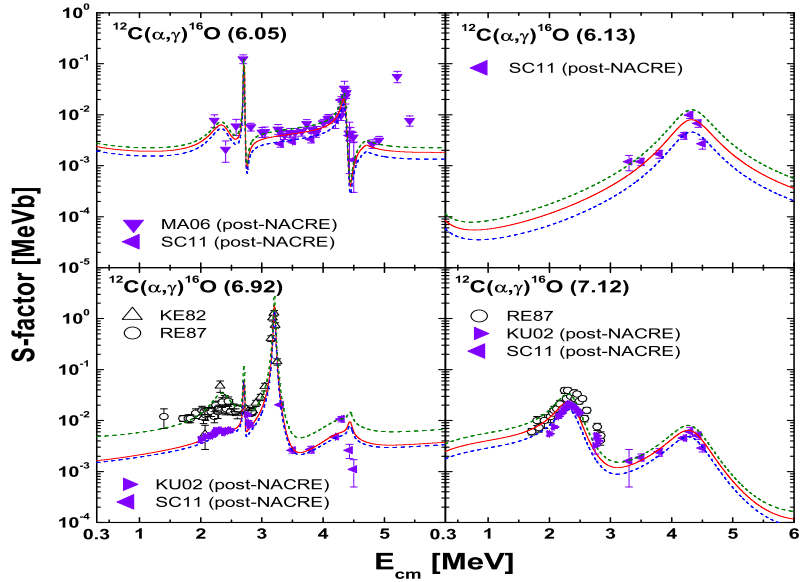


Figure 68: The "cascade" S -factors for the $^{12}\text{C}(\alpha, \gamma)^{16}\text{O}^*$ transitions to the 0^+ , 3^- , 2^+ and 1^- excited states at $E_x = 6.05$, 6.13 , 6.92 and 7.12 MeV. The present S -factors sum up to $6.6_{-2.0}^{+5.3}$ and $7.3_{-1.3}^{+8.2}$ keV b at $E_{\text{cm}} \simeq 1.0$ and 1.5 MeV, to be compared with 16 ± 8.5 and 7.0 ± 1.5 keV b of PL12 [313], respectively.

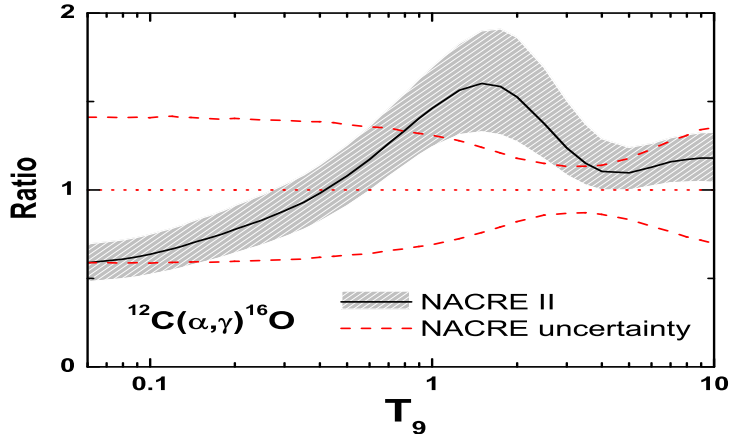


Figure 69: $^{12}\text{C}(\alpha, \gamma)^{16}\text{O}$ rates in units of the NACRE (adopt) values. The reduction at low temperatures owes mainly to the NACRE choice of a high $S_{\text{E}2}(0.3)$ -value (120 ± 60 keV b) taken from an R-matrix analysis [30] of the early data. The hump at $T_9 \simeq 2$ results from the present inclusion of the cascade transitions.

Table 29: $^{12}\text{C}(\alpha, \gamma)^{16}\text{O}$ rates in $\text{cm}^3 \text{mol}^{-1} \text{s}^{-1}$

T_9	adopted	low	high	T_9	adopted	low	high
0.06	6.00E-26	4.91E-26	7.09E-26	0.6	3.23E-08	2.74E-08	3.74E-08
0.07	2.98E-24	2.44E-24	3.52E-24	0.7	1.77E-07	1.51E-07	2.05E-07
0.08	7.43E-23	6.09E-23	8.75E-23	0.8	7.16E-07	6.12E-07	8.29E-07
0.09	1.12E-21	9.18E-22	1.32E-21	0.9	2.33E-06	1.99E-06	2.70E-06
0.1	1.15E-20	9.46E-21	1.36E-20	1.	6.45E-06	5.49E-06	7.48E-06
0.11	8.81E-20	7.24E-20	1.04E-19	1.25	4.99E-05	4.19E-05	5.83E-05
0.12	5.32E-19	4.38E-19	6.26E-19	1.5	2.45E-04	2.03E-04	2.91E-04
0.13	2.65E-18	2.18E-18	3.12E-18	1.75	9.13E-04	7.56E-04	1.10E-03
0.14	1.13E-17	9.27E-18	1.32E-17	2.	2.81E-03	2.34E-03	3.43E-03
0.15	4.18E-17	3.44E-17	4.91E-17	2.5	1.75E-02	1.49E-02	2.15E-02
0.16	1.38E-16	1.14E-16	1.63E-16	3.	7.19E-02	6.30E-02	8.75E-02
0.18	1.15E-15	9.49E-16	1.35E-15	3.5	2.23E-01	2.00E-01	2.66E-01
0.2	7.08E-15	5.86E-15	8.30E-15	4.	5.77E-01	5.22E-01	6.73E-01
0.25	2.67E-13	2.21E-13	3.12E-13	5.	2.75E+00	2.51E+00	3.11E+00
0.3	4.19E-12	3.49E-12	4.89E-12	6.	9.63E+00	8.72E+00	1.08E+01
0.35	3.75E-11	3.13E-11	4.37E-11	7.	2.60E+01	2.33E+01	2.90E+01
0.4	2.27E-10	1.90E-10	2.64E-10	8.	5.66E+01	5.05E+01	6.33E+01
0.45	1.03E-09	8.69E-10	1.20E-09	9.	1.05E+02	9.29E+01	1.17E+02
0.5	3.80E-09	3.21E-09	4.41E-09	10.	1.71E+02	1.51E+02	1.92E+02

$$\text{REV} = 5.14 \times 10^{10} T_9^{3/2} \exp(-83.114/T_9)$$

3.29. $^{13}\text{C}(\text{p},\gamma)^{14}\text{N}$

The experimental data sets referred to in NACRE are HE60a [297][†], HE61 [327][†] and KI94 [328]^{†,††}, covering the $0.1 \lesssim E_{\text{cm}} \lesssim 0.9$ MeV range. Added is the post-NACRE data set GE10 [329]^{†,††}. In the present work, HE60a is superseded by VO63 [295][†] (see Sect. 3.27). The data point WO52 [330][‡] is added at $E_{\text{cm}} = 0.12$ MeV. [[†]to g.s., ^{††}cascades, [‡]total, ^{††}in reverse kinematics]

Figure 70 compares the PM and experimental S -factors. The partial S -factors in the $E_{\text{cm}} \lesssim 0.8$ MeV range for the transitions to the ground and the six excited states are used for the PM fit (Fig. 71). The data exhibit the 1^- resonance at $E_R \simeq 0.51$ MeV. The GE10 data were not used in the PM fit because of their systematic deviation from the other data. The adopted parameter values are given in Table 66. The present $S(0) = 8.1_{-1.1}^{+1.2}$ keV b. In comparison, $S(0) = 7.0 \pm 1.5$ keV b [NACRE, R-matrix plus a background], and 6.22 keV b [RAD10].

Table 30 gives the reaction rates at $0.007 \leq T_9 \leq 10$, for which the PM-predicted cross sections and the measured resonance strengths in the $0.415 \lesssim E_{\text{cm}} \lesssim 2.881$ MeV range ([328, 331–336]) are used. Figure 72 compares the present and the NACRE rates.

See [337] for an R-matrix fit.

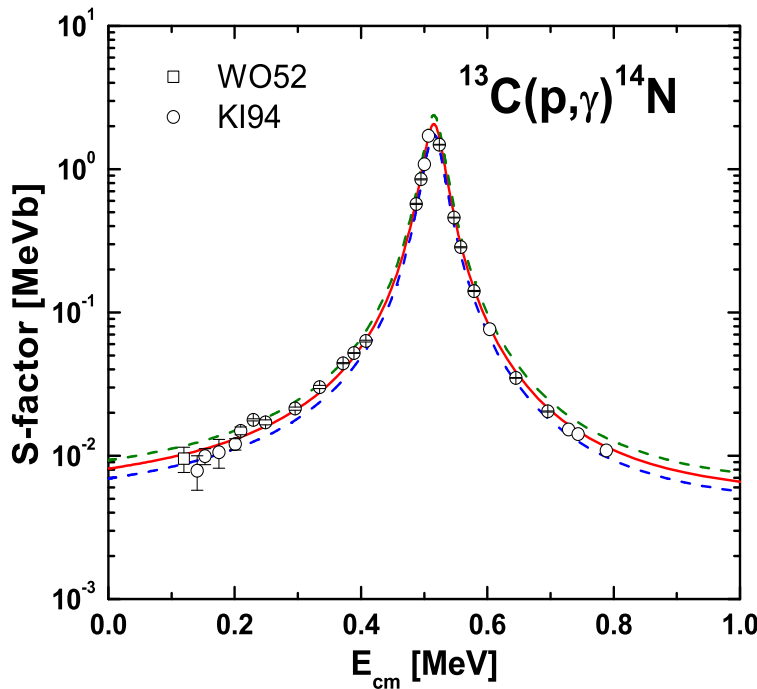


Figure 70: The S -factor for $^{13}\text{C}(\text{p},\gamma)^{14}\text{N}$. KI94 refers to the sum of the partial contributions (allow for some errors in reading the graphs). The PM results also correspond to the sum of the partial S -factors shown in Fig. 71. Note that in the NACRE S -factors for the "total" (inclusive) reaction are from KI94 and 1.18 times the HE60a and HE61 values for the ground-state transition.

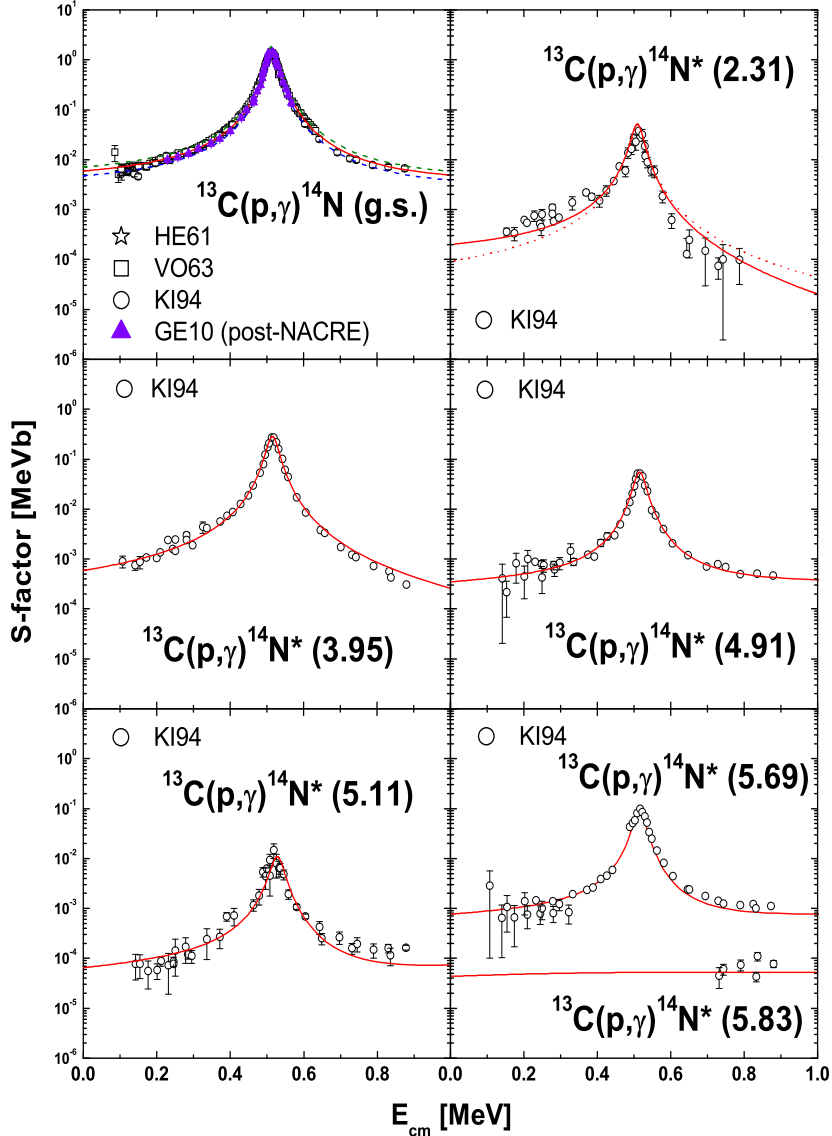


Figure 71: The partial S -factors for the $^{13}\text{C}(\text{p},\gamma)^{14}\text{N}$ transitions to the 1^+ ground state, and to the $0^+, 1^+, 0^-, 2^-, 1^-$ and 3^- excited states at $E_x = 2.31, 3.95, 4.91, 5.11, 5.69$ and 5.83 MeV. For the transitions to the first excited (2.31 MeV) state, the 1^- sub-threshold state at $E_R = -1.86$ MeV and the 1^- resonance at 0.51 MeV interfere. The dotted line represents the case without the interference. The effect of the interference is negligible for the ground-state transition. Not used in the fit, the data from the recent measurements in reverse kinematics GE10 [329] are added for comparison.

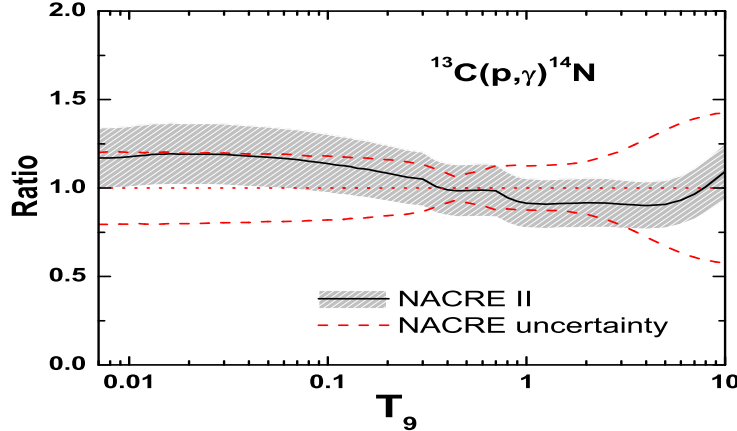


Figure 72: $^{13}\text{C}(\text{p}, \gamma)^{14}\text{N}$ rates in units of the NACRE (adopt) values.

Table 30: $^{13}\text{C}(\text{p}, \gamma)^{14}\text{N}$ rates in $\text{cm}^3\text{mol}^{-1}\text{s}^{-1}$

T_9	adopted	low	high	T_9	adopted	low	high
0.007	2.34E-22	2.00E-22	2.68E-22	0.18	1.42E-02	1.21E-02	1.63E-02
0.008	4.86E-21	4.15E-21	5.57E-21	0.2	3.18E-02	2.71E-02	3.64E-02
0.009	6.32E-20	5.39E-20	7.24E-20	0.25	1.63E-01	1.40E-01	1.87E-01
0.01	5.76E-19	4.92E-19	6.60E-19	0.3	6.10E-01	5.21E-01	6.99E-01
0.011	3.98E-18	3.40E-18	4.57E-18	0.35	1.98E+00	1.69E+00	2.26E+00
0.012	2.20E-17	1.88E-17	2.52E-17	0.4	5.97E+00	5.09E+00	6.86E+00
0.013	1.02E-16	8.67E-17	1.16E-16	0.45	1.66E+01	1.41E+01	1.91E+01
0.014	4.02E-16	3.44E-16	4.61E-16	0.5	4.14E+01	3.52E+01	4.76E+01
0.015	1.41E-15	1.20E-15	1.61E-15	0.6	1.80E+02	1.53E+02	2.07E+02
0.016	4.41E-15	3.76E-15	5.05E-15	0.7	5.32E+02	4.52E+02	6.13E+02
0.018	3.32E-14	2.84E-14	3.81E-14	0.8	1.20E+03	1.02E+03	1.38E+03
0.02	1.89E-13	1.62E-13	2.17E-13	0.9	2.24E+03	1.90E+03	2.59E+03
0.025	6.17E-12	5.27E-12	7.07E-12	1.	3.66E+03	3.11E+03	4.22E+03
0.03	8.77E-11	7.50E-11	1.01E-10	1.25	8.53E+03	7.24E+03	9.83E+03
0.04	4.18E-09	3.57E-09	4.79E-09	1.5	1.44E+04	1.22E+04	1.66E+04
0.05	6.49E-08	5.55E-08	7.44E-08	1.75	2.04E+04	1.73E+04	2.35E+04
0.06	5.25E-07	4.49E-07	6.01E-07	2.	2.58E+04	2.19E+04	2.98E+04
0.07	2.78E-06	2.38E-06	3.19E-06	2.5	3.46E+04	2.94E+04	3.98E+04
0.08	1.10E-05	9.42E-06	1.26E-05	3.	4.06E+04	3.45E+04	4.67E+04
0.09	3.52E-05	3.01E-05	4.04E-05	3.5	4.46E+04	3.80E+04	5.13E+04
0.1	9.60E-05	8.20E-05	1.10E-04	4.	4.74E+04	4.03E+04	5.45E+04
0.11	2.31E-04	1.97E-04	2.64E-04	5.	5.10E+04	4.34E+04	5.85E+04
0.12	5.01E-04	4.28E-04	5.74E-04	6.	5.35E+04	4.56E+04	6.13E+04
0.13	1.00E-03	8.58E-04	1.15E-03	7.	5.55E+04	4.73E+04	6.36E+04
0.14	1.88E-03	1.61E-03	2.15E-03	8.	5.71E+04	4.87E+04	6.55E+04
0.15	3.33E-03	2.84E-03	3.81E-03	9.	5.84E+04	4.97E+04	6.70E+04
0.16	5.61E-03	4.80E-03	6.43E-03	10.	5.93E+04	5.05E+04	6.80E+04

$$\text{REV} = 1.19 \times 10^{10} T_9^{3/2} \exp(-87.624/T_9) / [1.0 + 0.333 \exp(-26.840/T_9)]$$

3.30. $^{13}\text{C}(\alpha, \text{n})^{16}\text{O}$

The experimental cross section data sets referred to in NACRE are SE67 [338], DA68 [339], BA73 [340], DR93 [341] and BR93 [342], covering the $0.28 \lesssim E_{\text{cm}} \lesssim 4.5$ MeV range. Added are the post-NACRE data sets HA05 [343] and HE08 [344], the former extending the range up to $E_{\text{cm}} \simeq 6$ MeV.

Figure 73 compares the DWBA and experimental S -factors, which are extended in Figs. 74 and 75. The data for $E_{\text{cm}} \lesssim 0.9$ MeV are used for the DWBA fit. They exhibit the $3/2^+$ resonance at $E_R \simeq 0.84$ MeV. Possible contributions from the sub-threshold states, such as the $1/2^-$ and $1/2^+$ states at $E_R = -0.419$ and -0.003 MeV, are considered. The adopted parameter values are given in Table 49. The present $S(0.2 \text{ MeV}) = 1.5_{-0.4}^{+0.5} \times 10^6$ MeV b. In comparison, $S(0.2 \text{ MeV}) = 2.5 \times 10^6$ MeV b [NACRE, parametrised sub-threshold contribution].

Table 31 gives the reaction rates at $0.04 \leq T_9 \leq 10$, for which the DWBA-predicted and the experimental cross sections are used below and above $E_{\text{cm}} \simeq 0.4$ MeV, respectively. Figure 76 compares the present and the NACRE rates.

See [345] for a cluster model calculation; [52] for a DWBA analysis. Also see [346-351] for indirect measurements by α -transfer reactions in relation to the sub-threshold contributions.

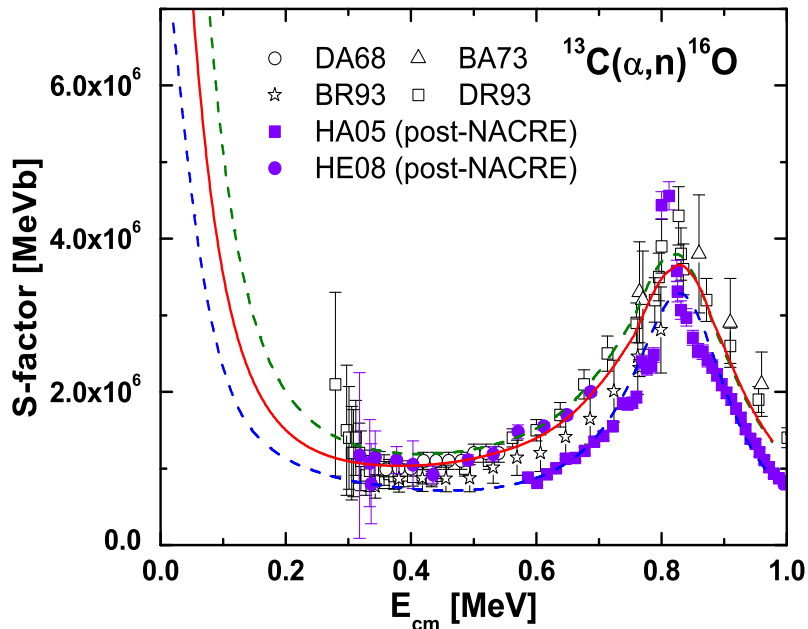


Figure 73: The S -factor for $^{13}\text{C}(\alpha, \text{n})^{16}\text{O}$.

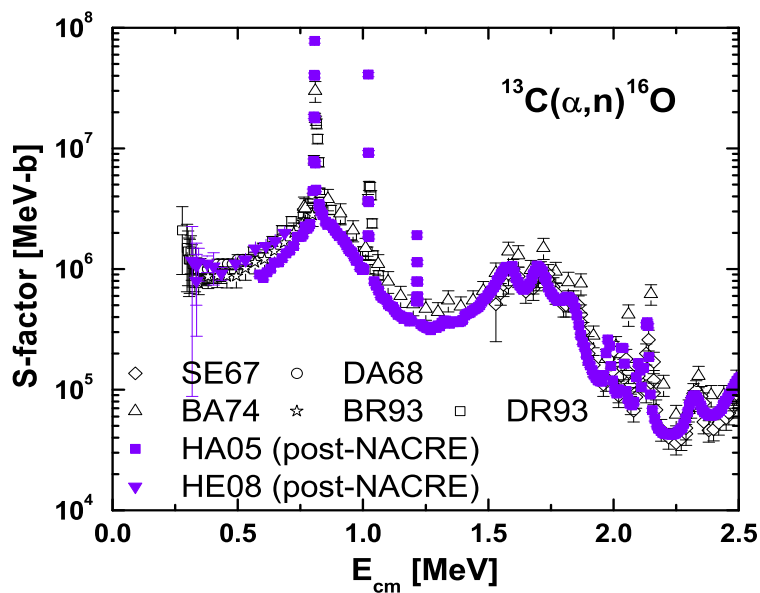


Figure 74: Experimental S -factor for $^{13}\text{C}(\alpha, \text{n})^{16}\text{O}$ below $E_{\text{cm}} = 3$ MeV.

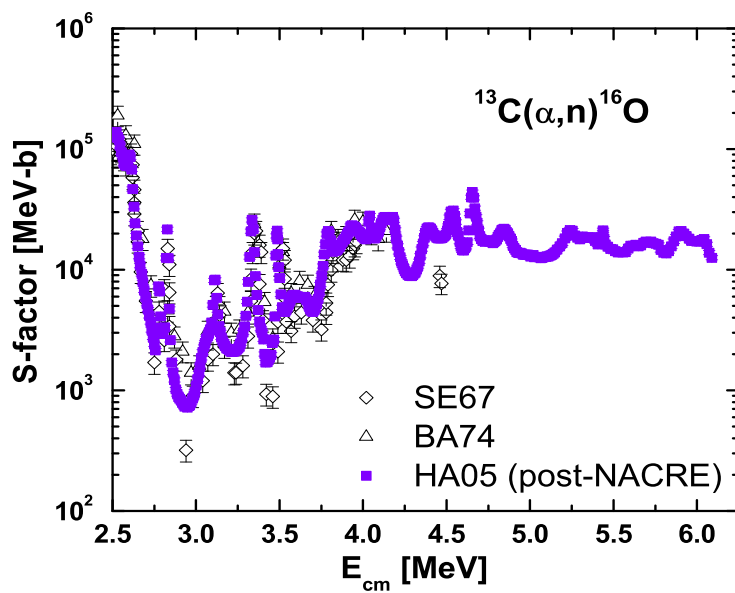


Figure 75: Experimental S -factor for $^{13}\text{C}(\alpha, \text{n})^{16}\text{O}$ above $E_{\text{cm}} = 3$ MeV.

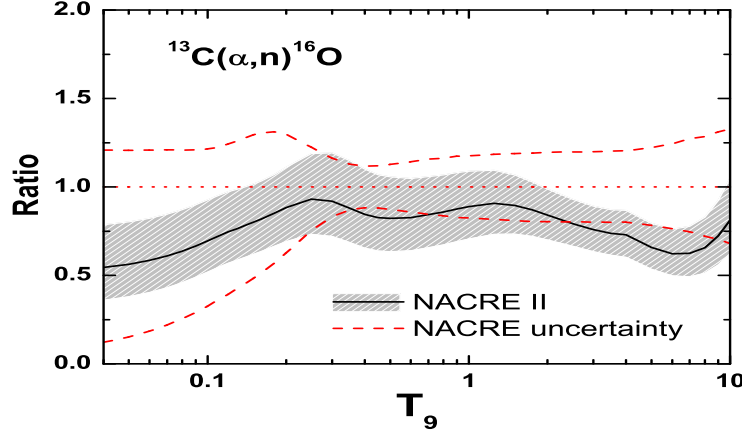


Figure 76: $^{13}\text{C}(\alpha, \text{n})^{16}\text{O}$ rates in units of the NACRE (adopt) values. The reduction at low temperatures owes mainly to the NACRE choice of a very steep S -factor assumed for the $1/2^+$ sub-threshold resonance contributions. For very high temperatures, we rely on the new experimental S factors at high energies [343], whereas NACRE adopts a Hauser-Feshbach rate calculation.

Table 31: $^{13}\text{C}(\alpha, \text{n})^{16}\text{O}$ rates in units of $\text{cm}^3\text{mol}^{-1}\text{s}^{-1}$.

T_9	adopted	low	high	T_9	adopted	low	high
0.04	2.91E-24	1.92E-24	4.20E-24	0.5	6.92E-02	5.34E-02	8.90E-02
0.05	1.82E-21	1.23E-21	2.60E-21	0.6	8.76E-01	6.78E-01	1.11E+00
0.06	2.45E-19	1.69E-19	3.44E-19	0.7	6.06E+00	4.72E+00	7.60E+00
0.07	1.22E-17	8.60E-18	1.69E-17	0.8	2.73E+01	2.14E+01	3.40E+01
0.08	3.06E-16	2.20E-16	4.19E-16	0.9	9.10E+01	7.18E+01	1.12E+02
0.09	4.65E-15	3.42E-15	6.29E-15	1.	2.44E+02	1.94E+02	2.99E+02
0.1	4.86E-14	3.62E-14	6.48E-14	1.25	1.57E+03	1.27E+03	1.89E+03
0.11	3.78E-13	2.86E-13	4.98E-13	1.5	6.04E+03	4.94E+03	7.20E+03
0.12	2.33E-12	1.77E-12	3.04E-12	1.75	1.73E+04	1.43E+04	2.05E+04
0.13	1.18E-11	9.09E-12	1.53E-11	2.	4.07E+04	3.39E+04	4.78E+04
0.14	5.15E-11	3.97E-11	6.58E-11	2.5	1.48E+05	1.24E+05	1.74E+05
0.15	1.96E-10	1.51E-10	2.48E-10	3.	3.70E+05	3.09E+05	4.35E+05
0.16	6.63E-10	5.15E-10	8.38E-10	3.5	7.24E+05	6.03E+05	8.55E+05
0.18	5.77E-09	4.49E-09	7.25E-09	4.	1.21E+06	9.99E+05	1.44E+06
0.2	3.72E-08	2.91E-08	4.68E-08	5.	2.54E+06	2.06E+06	3.06E+06
0.25	1.58E-06	1.24E-06	2.02E-06	6.	4.37E+06	3.49E+06	5.35E+06
0.3	2.89E-05	2.26E-05	3.74E-05	7.	6.87E+06	5.42E+06	8.55E+06
0.35	3.14E-04	2.45E-04	4.10E-04	8.	1.04E+07	8.09E+06	1.31E+07
0.4	2.43E-03	1.88E-03	3.17E-03	9.	1.53E+07	1.18E+07	1.96E+07
0.45	1.45E-02	1.12E-02	1.88E-02	10.	2.21E+07	1.69E+07	2.86E+07

REV = $5.79 \exp(-25.712/T_9)$

3.31. $^{13}\text{N}(\text{p},\gamma)^{14}\text{O}$

No experimental cross section data are found. The rates are dominated by the contribution of the 1^- resonance at $E_R \simeq 0.53$ MeV. NACRE refers to [352-354] for its total width, to [355, 356] for the γ -branching ratio, and to [353] for the γ -width. The Coulomb break-up measurements [357, 358] are rejected.

Figure 77 presents the PM prediction of the S -factors. The resonance energy and the widths of that 1^- state, and their uncertainties are taken from NACRE in order to fix the height of the resonance to normalise the PM S -factors. The non-resonant contributions are estimated from the same nuclear potentials as for $^{13}\text{C}(\text{p},\gamma)^{14}\text{N}$, and turn out to be insignificant at low temperatures. Note that the s-wave (0^-) transition is forbidden to the ^{14}O ground state, save the unlikely possibility of very strong (non-resonant) cascade transitions via the 1^- state from the higher energy range. Similarly, the E1 cascade transition, possibly from the third excited (0^+) state, is not included here. The adopted parameter values are given in Table 67. The present $S(0) = 3.8_{-0.8}^{+1.0}$ keV b. In comparison, $S(0) = 5.77$ keV b [RAD10].

Table 32 gives the reaction rates at $0.008 \leq T_9 \leq 10$. Figure 78 compares the present and the NACRE rates.

See [360] for a cluster model calculation; [300] for a potential model prediction.

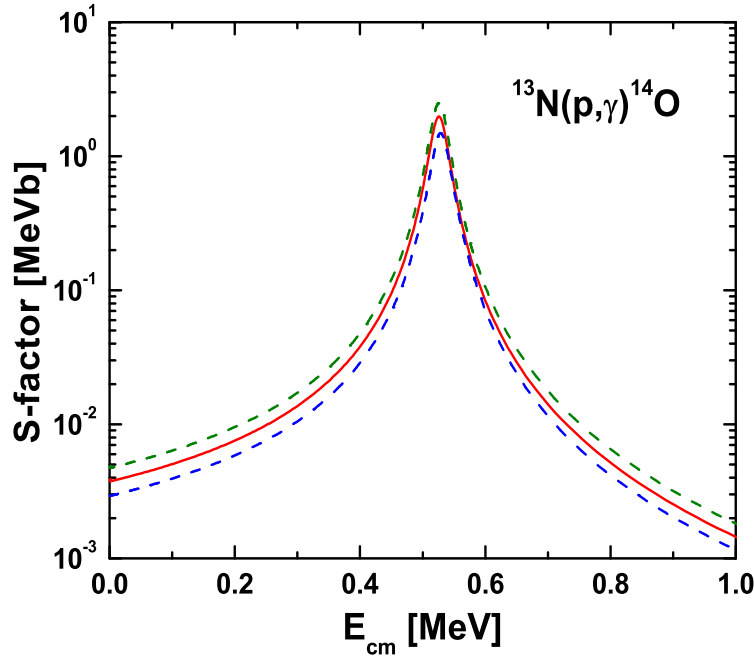


Figure 77: The S -factor of $^{13}\text{N}(\text{p},\gamma)^{14}\text{O}$.

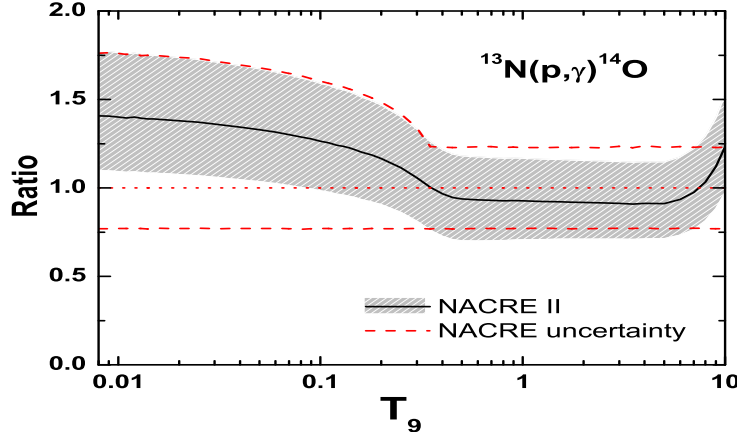


Figure 78: $^{13}\text{N}(\text{p}, \gamma)^{14}\text{O}$ rates in units of the NACRE (adopt) values. In the $1 \lesssim T_9 \lesssim 5$ range, the rates are basically determined by the 1^- resonance. The present rates in that range are slightly lower than NACRE, but agrees very well with those derived from the original experimental study [359]. The coincidence of the upper limits at low temperatures is accidental since NACRE (as well as [359]) introduces an unwarranted "interference" term (see [20]). At very high temperatures, some effects of the difference in the assumed non-resonant contributions are seen.

Table 32: $^{13}\text{N}(\text{p}, \gamma)^{14}\text{O}$ rates in $\text{cm}^3 \text{mol}^{-1} \text{s}^{-1}$.

T_9	adopted	low	high	T_9	adopted	low	high
0.008	1.48E-24	1.15E-24	1.86E-24	0.2	1.56E-03	1.21E-03	1.97E-03
0.009	2.56E-23	2.00E-23	3.22E-23	0.25	1.03E-02	7.96E-03	1.30E-02
0.01	2.98E-22	2.33E-22	3.76E-22	0.3	4.87E-02	3.74E-02	6.14E-02
0.011	2.55E-21	1.99E-21	3.22E-21	0.35	2.03E-01	1.54E-01	2.56E-01
0.012	1.71E-20	1.33E-20	2.15E-20	0.4	7.71E-01	5.80E-01	9.71E-01
0.013	9.34E-20	7.28E-20	1.18E-19	0.45	2.53E+00	1.89E+00	3.18E+00
0.014	4.32E-19	3.37E-19	5.44E-19	0.5	6.99E+00	5.23E+00	8.80E+00
0.015	1.74E-18	1.36E-18	2.19E-18	0.6	3.42E+01	2.57E+01	4.31E+01
0.016	6.20E-18	4.84E-18	7.81E-18	0.7	1.08E+02	8.14E+01	1.36E+02
0.018	5.89E-17	4.60E-17	7.42E-17	0.8	2.53E+02	1.92E+02	3.19E+02
0.02	4.10E-16	3.19E-16	5.16E-16	0.9	4.85E+02	3.69E+02	6.11E+02
0.025	1.99E-14	1.55E-14	2.50E-14	1.	8.07E+02	6.16E+02	1.02E+03
0.03	3.84E-13	2.99E-13	4.83E-13	1.25	1.94E+03	1.49E+03	2.44E+03
0.04	2.86E-11	2.23E-11	3.60E-11	1.5	3.33E+03	2.56E+03	4.19E+03
0.05	6.14E-10	4.78E-10	7.73E-10	1.75	4.74E+03	3.67E+03	5.97E+03
0.06	6.37E-09	4.96E-09	8.01E-09	2.	6.03E+03	4.68E+03	7.60E+03
0.07	4.13E-08	3.21E-08	5.19E-08	2.5	8.05E+03	6.26E+03	1.01E+04
0.08	1.93E-07	1.50E-07	2.43E-07	3.	9.31E+03	7.25E+03	1.17E+04
0.09	7.13E-07	5.55E-07	8.97E-07	3.5	1.00E+04	7.80E+03	1.26E+04
0.1	2.20E-06	1.71E-06	2.77E-06	4.	1.03E+04	8.05E+03	1.30E+04
0.11	5.90E-06	4.59E-06	7.42E-06	5.	1.03E+04	8.07E+03	1.30E+04
0.12	1.41E-05	1.10E-05	1.78E-05	6.	1.00E+04	7.85E+03	1.26E+04
0.13	3.10E-05	2.41E-05	3.90E-05	7.	9.74E+03	7.66E+03	1.22E+04
0.14	6.30E-05	4.90E-05	7.93E-05	8.	9.62E+03	7.58E+03	1.20E+04
0.15	1.20E-04	9.34E-05	1.51E-04	9.	9.67E+03	7.62E+03	1.20E+04
0.16	2.17E-04	1.69E-04	2.74E-04	10.	9.85E+03	7.78E+03	1.22E+04
0.18	6.25E-04	4.85E-04	7.86E-04				

$$\text{REV} = 3.57 \times 10^{10} T_9^{3/2} \exp(-53.697/T_9) [1.0 + \exp(-27.445/T_9)]$$

3.32. $^{14}\text{N}(\text{p},\gamma)^{15}\text{O}$

The experimental cross section data sets referred to in NACRE are LA57b [361], PI57 [362], HE63 [363] and SC87 [364][†], covering the $0.20 \lesssim E_{\text{cm}} \lesssim 3.3$ MeV range[‡]. Added are the post-NACRE data sets FO04 [366]^{††} IM05 [367], RU05 [368], BE06b [369], LE06b [370] and MA08 [371]^{†††}, extending the range down to $E_{\text{cm}} \simeq 0.07$ MeV. [[†]to be corrected for summing effects [365]; [‡]For $E_{\text{cm}} \gtrsim 1$ MeV, NACRE used resonance strengths; ^{††}to g.s. only.]

Figure 79 compares the PM and experimental total S -factors. The partial S -factors in the $E_{\text{cm}} \lesssim 1.5$ MeV range for the transitions to the ground and five excited states are used for the PM fit (Figs. 80 and 81). The data exhibit the $1/2^+$, $3/2^+$ and $1/2^+$ resonances at $E_{\text{cm}} \simeq 0.26$, 0.99 and 1.45 MeV, respectively. The possible contributions from the $3/2^+$ sub-threshold state at $E_R \simeq -0.50$ MeV are additionally considered. The adopted parameter values are given in Table 68. The present $S(0) = 1.8 \pm 0.2$ keV b. In comparison, $S(0) = 3.2 \pm 0.8$ keV b [NACRE], 1.47 keV b [RAD10], and 1.66 ± 0.12 keV b [SUN11, R-matrix].

Table 33 gives the reaction rates at $0.008 \leq T_9 \leq 10$, for which the PM and the experimental cross sections are used below and above $E_{\text{cm}} \lesssim 0.3$ MeV, respectively. Several very narrow resonances in the $2.18 \lesssim E_{\text{cm}} \lesssim 4.55$ MeV range with measured strengths [374 - 376] are also considered. Figure 82 compares the present and the NACRE rates.

See [377] for continuum shell model calculations.

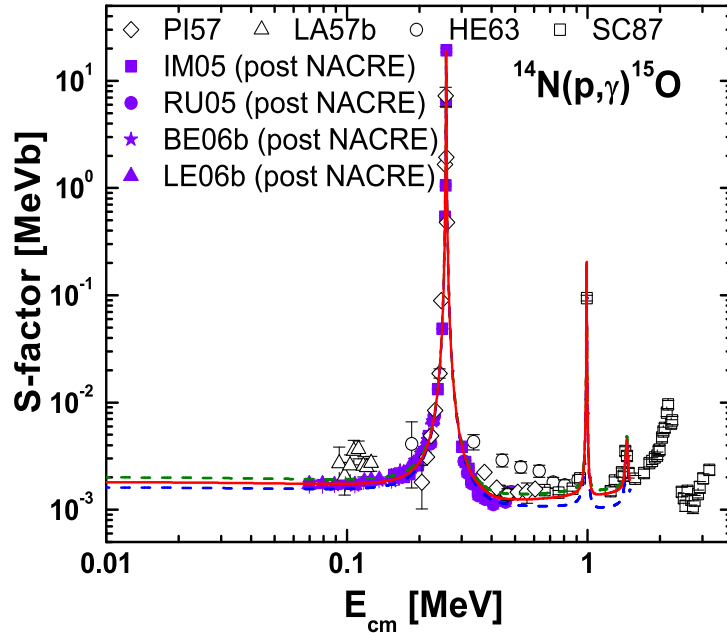


Figure 79: The total S -factor for $^{14}\text{N}(\text{p},\gamma)^{15}\text{O}$. The data sets SC87, IM05 and RU05 are the sums of the partial S -factors shown in Figs. 80 and 81. In the $E_{\text{cm}} \simeq 0.3$ MeV range, the PM fits are performed with the data shown here, whereas the sums of the partial S -factors are used at higher energies. See SC87 for data in the high-energy range.

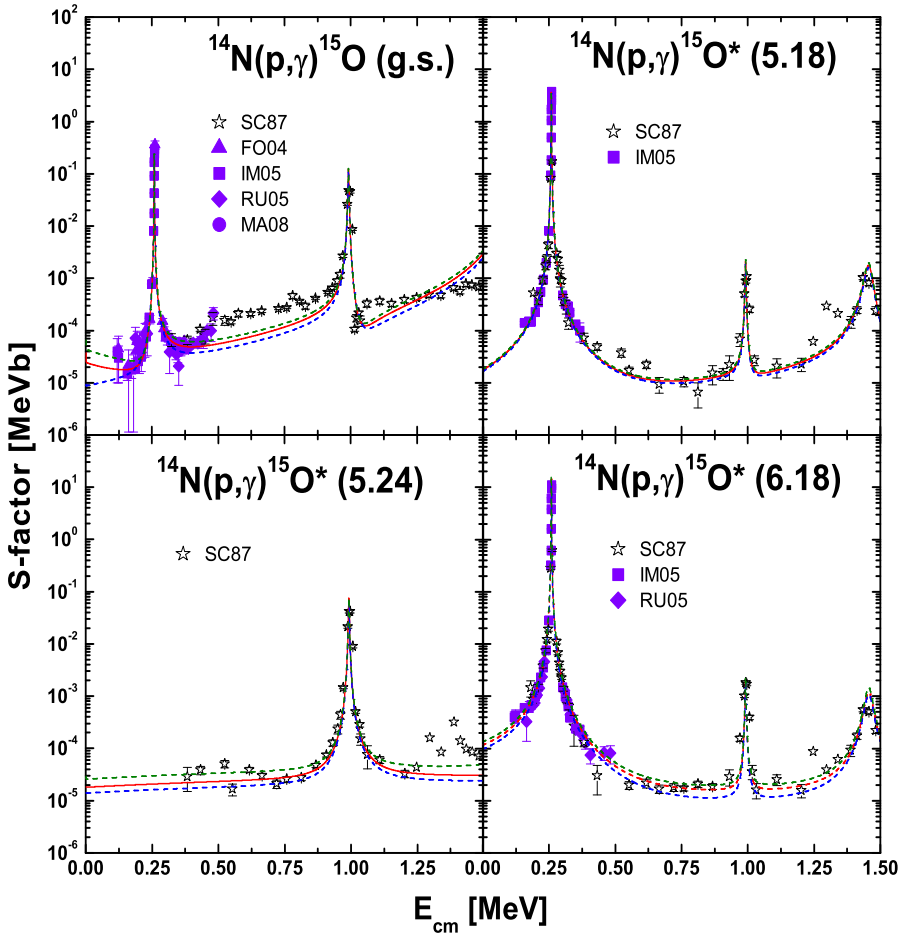


Figure 80: The partial S -factors for the $^{14}\text{N}(\text{p}, \gamma)^{15}\text{O}$ transitions to the $1/2^-$ ground state, and to the $1/2^+$, $5/2^+$ and $3/2^-$ excited states at $E_x = 5.183$, 5.241 and 6.176 MeV, respectively. For the ground-state transitions, PM clearly fails to reproduce the general trend of SC87 toward high energies, unless a twist of the potential parameter values were made. [In R-matrix fits, this trouble is avoided by the addition of a background pole of choice, typically at $5 \sim 6$ MeV with a width of comparable magnitude.] The present $S_{\text{g.s.}}(0) = 0.04 \pm 0.03$ keV b is on the lower side of the R-matrix values such as $0.08^{+0.13}_{-0.06}$ keV b [372] and 0.15 ± 0.07 keV b [373] in contrast, e.g., to 0.20 ± 0.05 keV b [371].

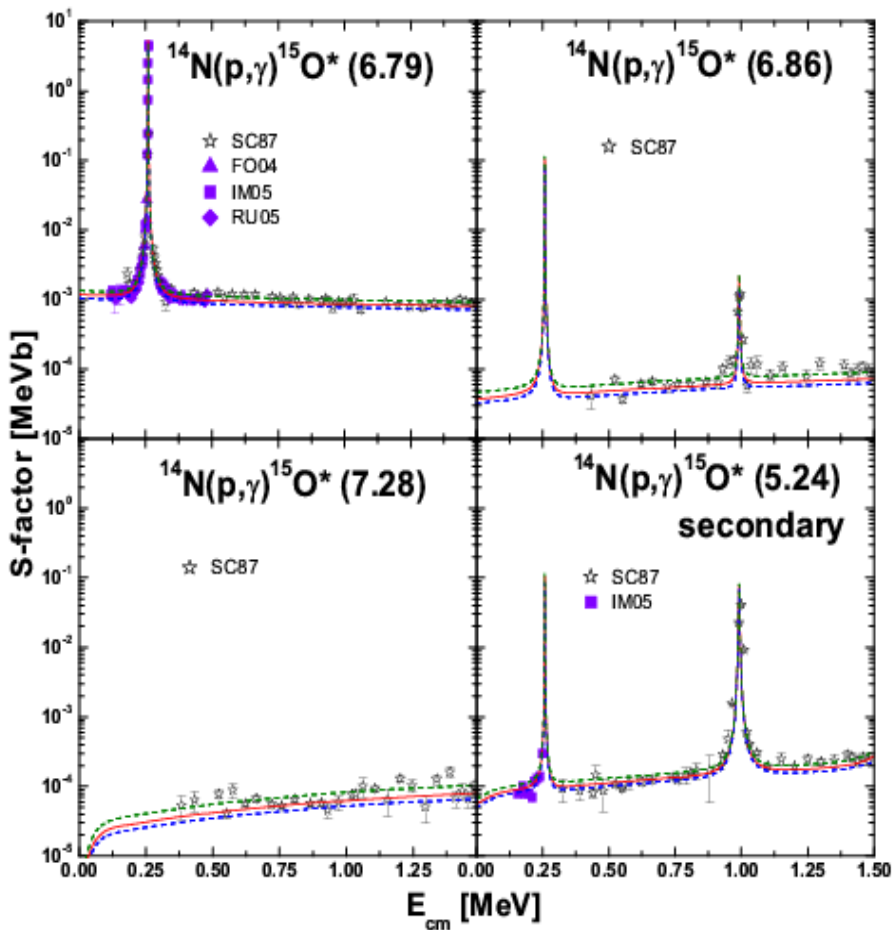


Figure 81: The partial S -factors for the $^{14}\text{N}(\text{p}, \gamma)^{15}\text{O}^*$ transitions to the $3/2^+$, $5/2^+$ and $7/2^+$ excited states at $E_x = 6.793$, 6.859 and 7.276 MeV, respectively, with the last two contributing to the secondary transitions from the $5/2^+$ state at $E_x = 5.241$ MeV.

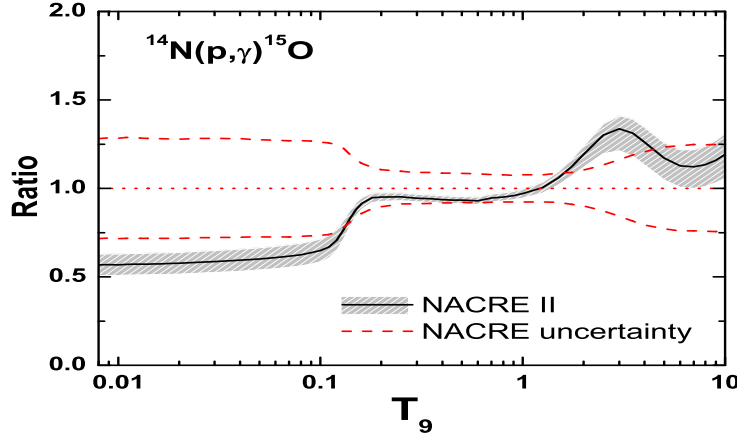


Figure 82: $^{14}\text{N}(\text{p}, \gamma)^{15}\text{O}$ rates in units of the NACRE (adopt) values. The use of the 'modern' data and the lower subthreshold contribution leads to the reductions of the ratios at the lowest energies. The increased ratios at $T_9 > 1$ reflect the seeming neglect by NACRE of the non-resonant contributions near the second resonance.

Table 33: $^{14}\text{N}(\text{p}, \gamma)^{15}\text{O}$ rates in $\text{cm}^3 \text{mol}^{-1} \text{s}^{-1}$

T_9	adopted	low	high	T_9	adopted	low	high
0.008	5.84E-25	5.21E-25	6.47E-25	0.2	7.85E-03	7.65E-03	8.05E-03
0.009	1.01E-23	9.03E-24	1.12E-23	0.25	1.09E-01	1.06E-01	1.11E-01
0.01	1.18E-22	1.05E-22	1.31E-22	0.3	6.05E-01	5.91E-01	6.19E-01
0.011	1.01E-21	9.01E-22	1.12E-21	0.35	2.00E+00	1.95E+00	2.04E+00
0.012	6.74E-21	6.02E-21	7.46E-21	0.4	4.77E+00	4.66E+00	4.88E+00
0.013	3.68E-20	3.28E-20	4.07E-20	0.45	9.20E+00	8.99E+00	9.41E+00
0.014	1.70E-19	1.52E-19	1.88E-19	0.5	1.53E+01	1.50E+01	1.57E+01
0.015	6.82E-19	6.09E-19	7.55E-19	0.6	3.18E+01	3.11E+01	3.25E+01
0.016	2.43E-18	2.17E-18	2.69E-18	0.7	5.18E+01	5.06E+01	5.31E+01
0.018	2.30E-17	2.05E-17	2.55E-17	0.8	7.31E+01	7.13E+01	7.48E+01
0.02	1.59E-16	1.42E-16	1.76E-16	0.9	9.39E+01	9.15E+01	9.62E+01
0.025	7.63E-15	6.82E-15	8.45E-15	1.	1.14E+02	1.10E+02	1.17E+02
0.03	1.45E-13	1.30E-13	1.61E-13	1.25	1.58E+02	1.53E+02	1.62E+02
0.04	1.06E-11	9.45E-12	1.17E-11	1.5	2.00E+02	1.92E+02	2.07E+02
0.05	2.21E-10	1.98E-10	2.45E-10	1.75	2.50E+02	2.37E+02	2.59E+02
0.06	2.24E-09	2.01E-09	2.47E-09	2.	3.11E+02	2.92E+02	3.24E+02
0.07	1.42E-08	1.27E-08	1.57E-08	2.5	4.81E+02	4.42E+02	5.05E+02
0.08	6.50E-08	5.83E-08	7.17E-08	3.	7.21E+02	6.53E+02	7.61E+02
0.09	2.36E-07	2.12E-07	2.60E-07	3.5	1.03E+03	9.26E+02	1.09E+03
0.1	7.20E-07	6.48E-07	7.92E-07	4.	1.40E+03	1.26E+03	1.49E+03
0.11	1.97E-06	1.78E-06	2.16E-06	5.	2.31E+03	2.06E+03	2.48E+03
0.12	5.21E-06	4.75E-06	5.66E-06	6.	3.37E+03	3.01E+03	3.65E+03
0.13	1.41E-05	1.31E-05	1.52E-05	7.	4.52E+03	4.03E+03	4.92E+03
0.14	4.02E-05	3.79E-05	4.25E-05	8.	5.70E+03	5.07E+03	6.22E+03
0.15	1.14E-04	1.09E-04	1.20E-04	9.	6.84E+03	6.08E+03	7.50E+03
0.16	3.11E-04	3.00E-04	3.23E-04	10.	7.93E+03	7.04E+03	8.71E+03
0.18	1.83E-03	1.77E-03	1.88E-03				

$$\text{REV} = 2.70 \times 10^{10} T_9^{3/2} \exp(-84.679/T_9) [1.0 + 0.333 \exp(-26.840/T_9)]$$

3.33. $^{15}\text{N}(\text{p},\gamma)^{16}\text{O}$

The experimental data set referred to in NACRE is RO74b [378], covering the $0.13 \lesssim E_{\text{cm}} \lesssim 2.3$ MeV range. Added are the post-NACRE data sets BE09 [379], LE10 [380] and CA11 [381], extending the range down to $E_{\text{cm}} \simeq 0.07$ MeV. HE60 [382], rejected in NACRE in favour of RO74b, is resurrected here by following the argument in [5], and is partially used.

Figure 83 compares the PM and experimental S -factors for the transitions to the ground state. The data for $E_{\text{cm}} \lesssim 1.3$ MeV are used for the PM fit. They exhibit the predominant broad 1^- resonances at $E_R \simeq 0.31$ and 0.96 MeV. The adopted parameter values are given in Table 69. The present $S(0) = 45^{+9}_{-7}$ keV b. In comparison, $S(0) = 64 \pm 6$ keV b [NACRE, from RO74b], 22.1 keV b [RAD10], and 36 ± 6 keV b [SUN11, R-matrix from [383]].

Table 34 gives the reaction rates at $0.007 \leq T_9 \leq 10$, for which the PM-predicted and the experimental cross sections are used below and above $E_{\text{cm}} \simeq 0.2$ MeV, respectively. The cascade transitions via two very narrow 2^- resonances as well as the 0^- and 3^- resonances in the $0.40 \lesssim E_R \lesssim 1.14$ MeV range ([319, 384-386]) are additionally considered for the rate calculations. Figure 84 compares the present and the NACRE rates.

See [386] for a very recent report on the partial S -factors of the cascade transitions.

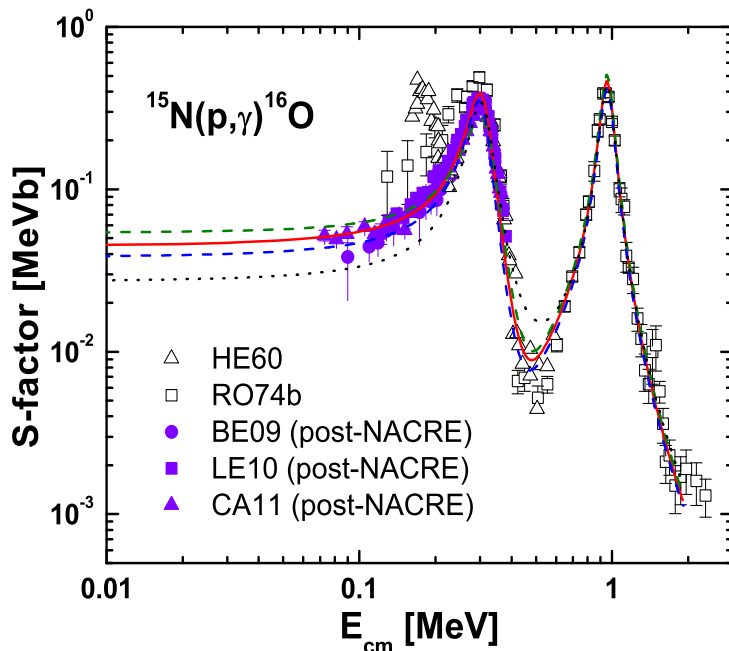


Figure 83: The S -factor for $^{15}\text{N}(\text{p},\gamma)^{16}\text{O}$. [See text for the contributions of the cascade transitions.] The dotted line corresponds to the solid ("adopt") curve without the interference between the two 1^- (s-wave) resonances. HE60 and RO74b data in the $E_{\text{cm}} \lesssim 0.3$ MeV range are not considered in the fit because of the clear deviations from the 'modern' data.

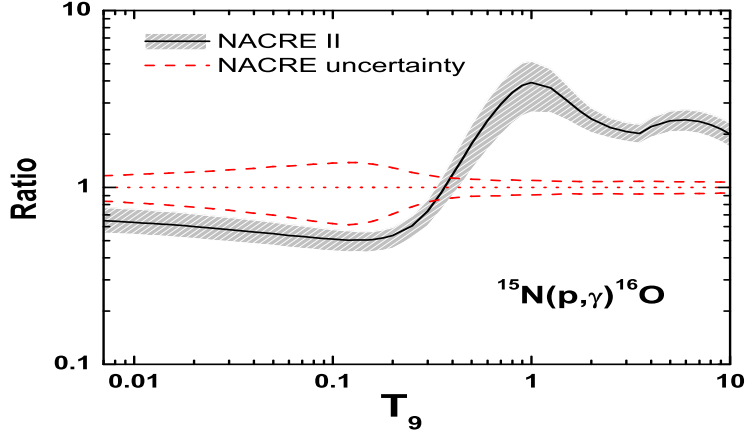


Figure 84: $^{15}\text{N}(\text{p}, \gamma)^{16}\text{O}$ rates in units of the NACRE (adopt) values. The use of the 'modern' data results in the reduced rates at the low temperatures. The enhancement of the ratio at $T_9 \gtrsim 1$ is owing to the contribution of the cascade transitions, which are not included in NACRE. The small hump around $T_9 \approx 6$ reflects a peculiar behaviour of unknown origin in the NACRE rates.

Table 34: $^{15}\text{N}(\text{p}, \gamma)^{16}\text{O}$ rates in $\text{cm}^3 \text{mol}^{-1} \text{s}^{-1}$

T_9	adopted	low	high	T_9	adopted	low	high
0.007	4.54E-25	3.87E-25	5.39E-25	0.18	7.00E-03	5.95E-03	7.77E-03
0.008	1.34E-23	1.14E-23	1.59E-23	0.2	1.88E-02	1.59E-02	2.09E-02
0.009	2.34E-22	2.00E-22	2.78E-22	0.25	1.48E-01	1.26E-01	1.68E-01
0.01	2.75E-21	2.35E-21	3.26E-21	0.3	7.72E-01	6.37E-01	8.96E-01
0.011	2.36E-20	2.02E-20	2.81E-20	0.35	2.95E+00	2.35E+00	3.54E+00
0.012	1.59E-19	1.36E-19	1.89E-19	0.4	8.85E+00	6.73E+00	1.09E+01
0.013	8.73E-19	7.46E-19	1.03E-18	0.45	2.17E+01	1.59E+01	2.75E+01
0.014	4.05E-18	3.47E-18	4.80E-18	0.5	4.55E+01	3.24E+01	5.85E+01
0.015	1.64E-17	1.40E-17	1.94E-17	0.6	1.41E+02	9.63E+01	1.85E+02
0.016	5.86E-17	5.01E-17	6.93E-17	0.7	3.16E+02	2.12E+02	4.19E+02
0.018	5.60E-16	4.78E-16	6.60E-16	0.8	5.79E+02	3.87E+02	7.72E+02
0.02	3.90E-15	3.34E-15	4.60E-15	0.9	9.30E+02	6.24E+02	1.24E+03
0.025	1.91E-13	1.63E-13	2.24E-13	1.	1.37E+03	9.33E+02	1.81E+03
0.03	3.70E-12	3.17E-12	4.34E-12	1.25	2.91E+03	2.10E+03	3.72E+03
0.04	2.78E-10	2.38E-10	3.24E-10	1.5	5.20E+03	4.02E+03	6.40E+03
0.05	5.97E-09	5.12E-09	6.94E-09	1.75	8.35E+03	6.78E+03	9.92E+03
0.06	6.21E-08	5.32E-08	7.17E-08	2.	1.23E+04	1.03E+04	1.42E+04
0.07	4.03E-07	3.45E-07	4.63E-07	2.5	2.18E+04	1.90E+04	2.47E+04
0.08	1.89E-06	1.62E-06	2.16E-06	3.	3.21E+04	2.82E+04	3.60E+04
0.09	6.98E-06	5.99E-06	7.95E-06	3.5	4.16E+04	3.66E+04	4.68E+04
0.1	2.16E-05	1.85E-05	2.44E-05	4.	5.00E+04	4.37E+04	5.64E+04
0.11	5.82E-05	5.00E-05	6.57E-05	5.	6.22E+04	5.38E+04	7.05E+04
0.12	1.40E-04	1.20E-04	1.58E-04	6.	6.90E+04	5.94E+04	7.87E+04
0.13	3.11E-04	2.67E-04	3.47E-04	7.	7.22E+04	6.17E+04	8.26E+04
0.14	6.41E-04	5.49E-04	7.14E-04	8.	7.29E+04	6.20E+04	8.37E+04
0.15	1.24E-03	1.06E-03	1.38E-03	9.	7.21E+04	6.11E+04	8.30E+04
0.16	2.30E-03	1.97E-03	2.55E-03	10.	7.03E+04	5.94E+04	8.12E+04

$$\text{REV} = 3.63 \times 10^{10} T_9^{3/2} \exp(-140.74/T_9)$$

3.34. $^{15}\text{N}(\text{p},\alpha)^{12}\text{C}$

The experimental data sets referred to in NACRE are SC52 [387], ZY79 [388] and RE82 [389], covering the $0.07 \lesssim E_{\text{cm}} \lesssim 1.5$ MeV range. Added is the post-NACRE data set LA07 [390][†], extending the range down to $E_{\text{cm}} \simeq 0.02$ MeV. [[†]from $^2\text{H}(^{15}\text{N},\alpha)^{12}\text{C}$ n (THM)]

Figure 85 compares the DWBA and experimental S -factors. The data for $E_{\text{cm}} \lesssim 1.1$ MeV are used for the DWBA fit. They exhibit the 1^- resonances at $E_R \simeq 0.31$ and 0.96 MeV. The adopted parameter values are given in Table 50. The present $S(0) = 67 \pm 14$ MeV b. In comparison, $S(0) = 64 \pm 6$ keV b [NACRE, from RE82], and 73 ± 5 MeV b [SUN11, R-matrix fit by [392]]. At the high-energy end, the data set [391] is added, and the S -factor from Hauser-Feshbach calculations [51] is used as a measure for the upper limit. In this energy range the $^{15}\text{N}(\text{p},\alpha_1\gamma)^{12}\text{C}^*$ (4.44 MeV, 2^+) becomes significant.

Table 35 gives the reaction rates at $0.005 \leq T_9 \leq 10$, for which the DWBA-predicted and the experimental cross sections below and above $E_{\text{cm}} \simeq 0.06$ MeV are used, respectively. The additional contributions from the two very narrow 2^- resonances at $E_R \lesssim 0.40$ and 0.84 MeV ([39]) are included.

Figure 86 compares the present and the NACRE rates.

See [392, 393] for discussions on the subtleties of R-matrix fits.

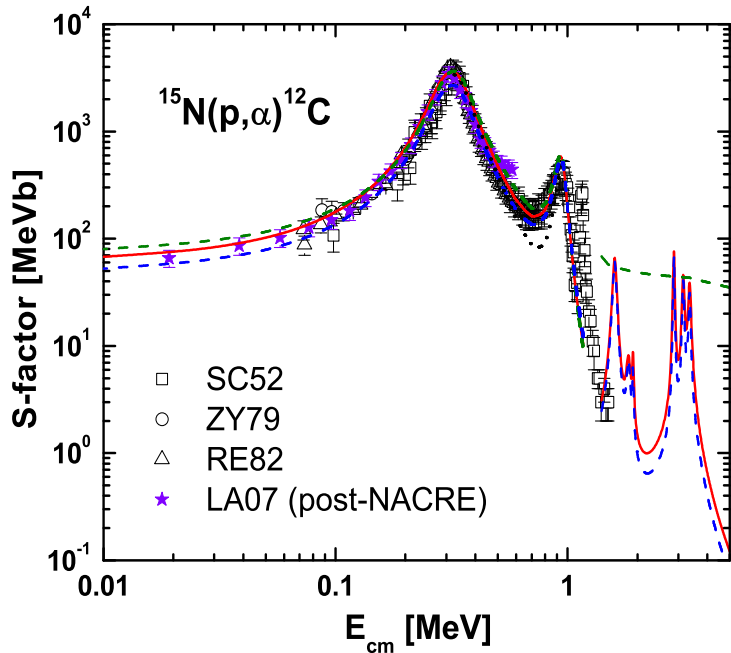


Figure 85: The S -factor for $^{15}\text{N}(\text{p},\alpha)^{12}\text{C}$. The dots showing a minimum at $E_{\text{cm}} \approx 0.7$ MeV correspond to the "adopt" case without the interference between the two 1^- resonances. In the low energy range, they closely follow the "low" curve. The curves displayed in the $E_{\text{cm}} \gtrsim 1.6$ MeV range are from [391] (structured curves), and the Hauser-Feshbach predictions [51] (upper, monotonous dashed line)

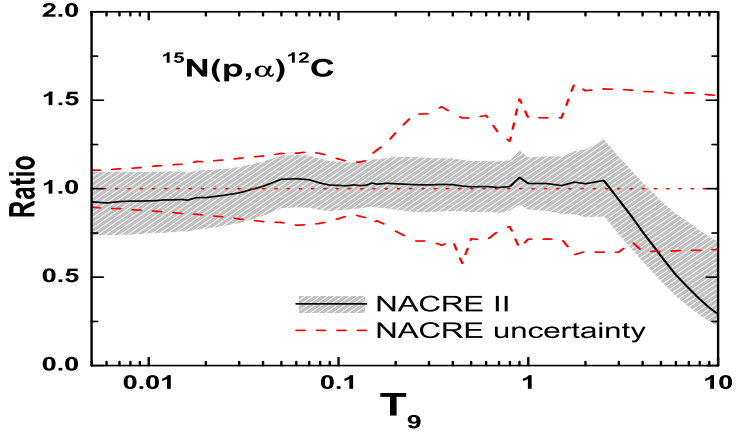


Figure 86: $^{15}\text{N}(\text{p}, \alpha)^{12}\text{C}$ rates in units of the NACRE (adopt) values. The large and systematic deviation at $T_9 \geq 2.5$ has its origin in the extrapolation made by NACRE with the help of the *rates* from a Hauser-Feshbach calculation. The zig-zagged fine structures in the NACRE rates are of unknown origin.

Table 35: $^{15}\text{N}(\text{p}, \alpha)^{12}\text{C}$ rates in $\text{cm}^3 \text{mol}^{-1} \text{s}^{-1}$

T_9	adopted	low	high	T_9	adopted	low	high
0.005	6.59E-26	5.22E-26	7.85E-26	0.16	1.00E+01	8.67E+00	1.14E+01
0.006	1.14E-23	9.07E-24	1.36E-23	0.18	3.38E+01	2.90E+01	3.86E+01
0.007	7.04E-22	5.59E-22	8.35E-22	0.2	9.91E+01	8.45E+01	1.14E+02
0.008	2.11E-20	1.67E-20	2.49E-20	0.25	9.00E+02	7.61E+02	1.04E+03
0.009	3.73E-19	2.97E-19	4.41E-19	0.3	4.76E+03	4.03E+03	5.49E+03
0.01	4.43E-18	3.54E-18	5.23E-18	0.35	1.70E+04	1.44E+04	1.95E+04
0.011	3.86E-17	3.09E-17	4.55E-17	0.4	4.58E+04	3.90E+04	5.26E+04
0.012	2.63E-16	2.10E-16	3.09E-16	0.45	1.00E+05	8.57E+04	1.15E+05
0.013	1.46E-15	1.17E-15	1.72E-15	0.5	1.90E+05	1.62E+05	2.18E+05
0.014	6.85E-15	5.50E-15	8.04E-15	0.6	4.97E+05	4.25E+05	5.69E+05
0.015	2.80E-14	2.25E-14	3.28E-14	0.7	9.92E+05	8.47E+05	1.14E+06
0.016	1.01E-13	8.14E-14	1.18E-13	0.8	1.66E+06	1.43E+06	1.91E+06
0.018	9.87E-13	7.96E-13	1.15E-12	0.9	2.50E+06	2.13E+06	2.87E+06
0.02	7.02E-12	5.68E-12	8.18E-12	1.	3.47E+06	2.96E+06	3.98E+06
0.025	3.60E-10	2.94E-10	4.17E-10	1.25	6.38E+06	5.40E+06	7.36E+06
0.03	7.30E-09	5.99E-09	8.41E-09	1.5	9.88E+06	8.28E+06	1.15E+07
0.04	5.95E-07	4.94E-07	6.79E-07	1.75	1.39E+07	1.14E+07	1.63E+07
0.05	1.38E-05	1.16E-05	1.56E-05	2.	1.82E+07	1.48E+07	2.17E+07
0.06	1.53E-04	1.29E-04	1.73E-04	2.5	2.71E+07	2.17E+07	3.33E+07
0.07	1.05E-03	8.89E-04	1.19E-03	3.	3.57E+07	2.80E+07	4.52E+07
0.08	5.20E-03	4.41E-03	5.91E-03	3.5	4.32E+07	3.35E+07	5.68E+07
0.09	2.03E-02	1.73E-02	2.31E-02	4.	4.93E+07	3.80E+07	6.79E+07
0.1	6.65E-02	5.71E-02	7.54E-02	5.	5.84E+07	4.44E+07	8.84E+07
0.11	1.90E-01	1.64E-01	2.15E-01	6.	6.40E+07	4.84E+07	1.08E+08
0.12	4.87E-01	4.21E-01	5.50E-01	7.	6.76E+07	5.08E+07	1.26E+08
0.13	1.14E+00	9.91E-01	1.29E+00	8.	6.98E+07	5.23E+07	1.43E+08
0.14	2.49E+00	2.17E+00	2.82E+00	9.	7.12E+07	5.31E+07	1.59E+08
0.15	5.13E+00	4.45E+00	5.81E+00	10.	7.19E+07	5.36E+07	1.74E+08

REV = $0.706 \times \exp(-57.625/T_9)$

4. Summary

The NACRE II update of NACRE reported in this work includes: (1) the collection of experimental data published, in the first instance, in the major journals of the field by early 2013; (2) the extrapolation of astrophysical S -factors to very low energies based on potential models, with a systematic evaluation of uncertainties; (3) the presentation in tabular form of adopted reaction rates along with their low and high limits for temperatures in the $10^6 \lesssim T \leq 10^{10}$ range. The new reaction rates are also available electronically as part of the regularly improved and enlarged Brussels Library (BRUSLIB) of nuclear data. The NACRE II rates also supersede the NACRE ones in the Nuclear Network Generator (NETGEN) for astrophysics (<http://www.astro.ulb.ac.be/databases.html>).

The authors are much obliged to anonymous referees for their careful reading of this long manuscript and for many valuable and constructive comments. This compilation was originally planned within the Konan-ULB convention "Construction of an Extended Nuclear Database for Astrophysics". The initiatives and the financial support by the Konan Board of Trustees and Professors H. Yoshizawa and Y. Sugimura are warmly thanked. It has also been supported by the Interuniversity Attraction Pole IAP 5/07 of the Belgian Federal Science Policy, and by the Communauté Française de Belgique (Actions de Recherche Concertées). The authors acknowledge with thanks the contributions to the early phase of this project by M. Aikawa, K. Arai, and M. Katsuma, and the help of G. L. Chen for the preparation of the reference list. Last but not least, their special thanks go to Alain Jorissen for his continued interest in the present work.

Appendix A

The adopted values of the potential parameters and of the overall renormalisation constants are collected here. The potential parameters are described in Sects. 2.5.1 - 2.5.3, and are given in units of MeV or fm. The overall renormalisation constant for transfer reactions is $D_0^2 S_F$ in Eq. (12). It is given in units of 10^4 MeV 2 fm 3 , which is denoted as $D_{t,4}$. [D_0^2 is known to be 1.55×10^4 MeV 2 fm 3 for (d,p) reactions.] The overall renormalisation constant for capture reactions is S_F in Eq. (13). We denote this dimensionless quantity as C_c in order to stress again the purely empirical nature of its determination. The asterisk on l_i in the non-resonant (N.R.) case means the exclusion of J^π value(s) that is(are) exhausted by the resonance capture(s). The sets of parameter values are in many cases not unique in that some different combinations may lead to fits that are equally good. On the other hand, the limitation of the applicability of the model in certain cases may be self-evident from derived "unreasonable" sets of parameter values. We also note that the values given below are often rounded, so that some fine tuning may be necessary to reproduce, for example, the resonance energy to the desired accuracy.

Transfer Reactions

Table 36: DWBA parameter values for ${}^2\text{H}(\text{d}, \text{n}) {}^3\text{He}$

N.R.	i: $d+{}^2\text{H}$						f: $n+{}^3\text{He}$			form f.: $p+{}^2\text{H}$		
	V_R	r_R	a_R	V_S	r_S	a_S	V_R	r_R	a_R	r_R	a_R	$\mathcal{D}_{t,4}$
ad	-78.25	1.17	0.81	-0.010	1.33	0.52	-35.11	1.02	0.68	0.98	0.68	3.96
lo	-79.97	r_C					-35.75			r_C		4.47
hi	-75.53	1.70					-34.03			5.73		3.71

Table 37: DWBA parameter values for ${}^2\text{H}(\text{d}, \text{p}) {}^3\text{H}$

N.R.	i: $d+{}^2\text{H}$						f: $p+{}^3\text{H}$			form f.: $n+{}^2\text{H}$		
	V_R	r_R	a_R	V_S	r_S	a_S	V_R	r_R	a_R	r_R	a_R	$\mathcal{D}_{t,4}$
ad	-78.95	1.17	0.81	-0.010	1.33	0.52	-34.45	1.02	0.68	0.98	0.68	4.18
lo	-81.20	r_C					-35.36	r_C				4.72
hi	-77.14	1.70					-33.75	3.62				3.74

Table 38: DWBA parameter values for ${}^3\text{H}(\text{d}, \text{n}) {}^4\text{He}$

R.R.	i: $d+{}^3\text{H}$						f: $n+{}^4\text{He}$			form f.: $p+{}^3\text{H}$		
	V_R	r_R	a_R	V_S	r_S	a_S	V_R	r_R	a_R	r_R	a_R	$\mathcal{D}_{t,4}$
R.R.	$l_i = s$	$[J^\pi, E_R] =$	$[3/2^+, 0.05]$									
ad	-67.92	1.17	0.81	-2.88	1.33	0.53	-12.75	1.05	0.687	1.02	0.68	0.95
lo	-67.92	r_C		-2.89			-29.11			r_C		0.39
hi	-67.92	1.70		-3.09			-90.31			3.62		0.41

Table 39: DWBA parameter values for ${}^3\text{He}(\text{d}, \text{p}) {}^4\text{He}$

R.R.	i: $d+{}^3\text{He}$						f: $p+{}^4\text{He}$			form f.: $n+{}^3\text{He}$		
	V_R	r_R	a_R	V_S	r_S	a_S	V_R	r_R	a_R	r_R	a_R	$\mathcal{D}_{t,4}$
R.R.	$l_i = s$	$[J^\pi, E_R] =$	$[3/2^+, 0.21]$									
ad	-68.71	1.17	0.81	-3.37	1.33	0.53	-39.16	1.05	0.68	1.02	0.68	0.51
lo	-68.82	r_C		-3.111			-73.06	r_C				0.36
hi	-68.72	1.70		-3.36			-27.49	2.76				0.70

Table 40: DWBA parameter values for ${}^3\text{He}({}^3\text{He}, 2\text{p}) {}^4\text{He}$

N.R.	i: $\tau+{}^3\text{He}$						f: $2p+{}^4\text{He}$			form f.: $n+{}^3\text{He}$		
	V_R	r_R	a_R	V_S	r_S	a_S	V_R	r_R	a_R	r_R	a_R	$\mathcal{D}_{t,4}$
ad	-41.65	0.97	0.82	-0.077	1.22	0.84	-89.98	1.17	0.81	1.02	0.68	2.08
lo	-45.65	r_C		-0.23			-93.24	r_C				1.93
hi	-42.98	1.32		-23.06			-90.22	1.70				3.85

Table 41: DWBA parameter values for ${}^6\text{Li}(\text{p}, \alpha){}^3\text{He}$

N.R.	i: $\text{p}+{}^6\text{Li}$						f: $\alpha+{}^3\text{He}$						form f.: $t+{}^3\text{He}$		
	V_R	r_R	a_R	V_S	r_S	a_S	V_R	r_R	a_R	r_R	a_R	$D_{t,4}$			
ad	-83.17	1.08	0.68	-51.25	1.31	0.52	-74.43	0.94	0.77	0.97	0.82	4.58			
lo	-82.18	r_C		-66.66			-24.48	r_C		r_C		22.2			
hi	-88.29	2.07		-68.26			-32.40	1.48		1.32		15.1			

Table 42: DWBA parameter values for ${}^7\text{Li}(\text{p}, \alpha){}^4\text{He}$

N.R.	i: $\text{p}+{}^7\text{Li}$						f: $\alpha+{}^4\text{He}$						form f.: $t+{}^4\text{He}$		
	V_R	r_R	a_R	V_S	r_S	a_S	V_R	r_R	a_R	r_R	a_R	$D_{t,4}$			
ad	-59.81	1.09	0.68	-0.083	1.31	0.52	-75.36	0.97	0.77	1.00	0.82	2.32			
lo	-61.88	r_C		-1.87			-73.35	r_C		r_C		3.78			
hi	-58.64	1.90		-0.082			-79.08	1.48		1.32		1.64			

Table 43: DWBA parameter values for ${}^9\text{Be}(\text{p}, \text{d}){}^8\text{Be}$

R.R.	i: $\text{p}+{}^9\text{Be}$						f: $d+{}^8\text{Be}$						form. f.: $n+{}^8\text{Be}$		
	V_R	r_R	a_R	V_S	r_S	a_S	V_R	r_R	a_R	r_R	a_R	$D_{t,4}$			
R.R.	$l_i = s$	$[J^\pi, E_R] = [1^-, 0.29]$													
ad	-73.78	1.11	0.68	-2.461	1.31	0.52	-72.14	1.17	0.81	1.10	0.61	0.80			
lo	-73.96	r_C		-2.492	1.309	0.52	-73.74	r_C		r_C		1.38			
hi	-73.67	1.69		-1.88			-70.03	1.48		1.31		0.34			

Table 44: DWBA parameter values for ${}^9\text{Be}(\text{p}, \alpha){}^6\text{Li}$

R.R.	i: $\text{p}+{}^9\text{Be}$						f: $\alpha+{}^6\text{Li}$						form f.: $t+{}^6\text{Li}$		
	V_R	r_R	a_R	V_S	r_S	a_S	V_R	r_R	a_R	r_R	a_R	$D_{t,4}$			
R.R.	$l_i = s$	$[J^\pi, E_R] = [1^-, 0.29]$													
ad	-73.99	1.11	0.68	-3.07	1.31	0.52	-22.07	1.01	0.78	1.04	0.82	2.98			
lo	-74.71	r_C		-3.64			-20.18	r_C		r_C		17.76			
hi	-73.30	1.69		-2.17			-23.47	1.48		1.31		0.81			

Table 45: DWBA parameter values for ${}^9\text{Be}(\alpha, \text{n}){}^{12}\text{C}$

R.R.	entrance channel i: $\alpha+{}^9\text{Be}$						exit channel f: $n+{}^{12}\text{C}$						form factor form f.: $\tau+{}^9\text{Be}$		
	V_R	r_R	a_R	V_S	r_S	a_S	V_R	r_R	a_R	r_R	a_R	$D_{t,4}$			
R.R.	$l_i = s$	$[J^\pi, E_R] = [5/2^-, 0.17]$													
ad	-56.63	1.04	0.78	-0.123	1.11	0.69	-98.75	1.13	0.68	1.07	0.82	6.46			
lo	-56.62	r_C		-0.091			-98.24			r_C		4.16			
hi	-56.63	1.48		-0.116			-99.70			1.30		9.02			
R.R.	$l_i = p$	$[J^\pi, E_R] = [1/2^+, 0.35]$													
ad	-37.00			0.303			-38.13					0.48			
lo	-36.27			0.302			-38.21					0.39			
hi	-37.11			0.303			-38.12					0.57			
R.R.	$l_i = d$	$[J^\pi, E_R] = [7/2^-, 0.105]$	(see text)												
SUB R.	$l_i = s$	$[J^\pi, E_R] = [3/2^-, -0.751]$	ad/lo/hi										$a = 5.1$	$\theta_\alpha^2 = 0.1/0.0/0.3$	

Table 46: DWBA parameter values for $^{10}\text{B}(\text{p}, \alpha)^7\text{Be}$

i: $p+^{10}\text{B}$						f: $\alpha+^7\text{Be}$			form f.: $t+^7\text{Be}$			
	V_R	r_R	a_R	V_S	r_S	a_S	V_R	r_R	a_R	r_R	a_R	$D_{t,4}$
R.R.	$l_i = s$	$[J^\pi, E_R] = [5/2^+, 0.01]$										
ad	-73.55	1.12	0.68	-0.143	1.31	0.52	-39.60	1.02	0.78	1.05	0.82	3.01
lo	-73.54			-0.226			-61.99					0.083
hi	-73.55	r_C		-0.140			-39.60	r_C		r_C		3.59
			1.63					1.48			1.30	

Table 47: DWBA parameter values for $^{11}\text{B}(\text{p}, \alpha)^8\text{Be}$

i: $p+^{11}\text{B}$						f: $\alpha+^8\text{Be}$			form f.: $t+^8\text{Be}$						
	V_R	r_R	a_R	V_S	r_S	a_S	V_R	r_R	a_R	V_S	r_S	a_S	r_R	a_R	$D_{t,4}$
R.R.	$l_i = s$	$[J^\pi, E_R] = [2^-, 0.61]$													
ad	-64.13	1.12	0.68	-4.04	1.31	0.52	-44.29	1.03	0.78	-1.110	1.10	0.69	0.98	0.82	17.87
lo	-64.67	r_C		-3.432			-45.65	r_C		-0.660			r_C		20.99
hi	-63.25	1.58		-4.49			-41.95	1.48		-0.120			1.30		13.21

Table 48: DWBA parameter values for $^{11}\text{B}(\alpha, n)^{14}\text{N}$

i: $\alpha+^{11}\text{B}$						f: $n+^{14}\text{N}$			form f.: $\tau+^{11}\text{B}$			
	V_R	r_R	a_R	V_S	r_S	a_S	V_R	r_R	a_R	r_R	a_R	$D_{t,4}$
R.R.	$l_i = p$	$[J^\pi, E_R] = [1/2^+, 0.44]$										
ad	-87.83	1.06	0.79	-0.349	1.12	0.70	-67.02	1.14	0.68	1.08	0.82	0.033
lo	-87.81	r_C		-0.300			-97.36			r_C		0.21
hi	-87.86	1.48		-0.410			-64.16			1.29		0.042
R.R.	$l_i = p$	$[J^\pi, E_R] = [3/2^+, 0.77]$										
all	-64.06			-0.401			-28.77					0.0077

Table 49: DWBA parameter values for the $^{13}\text{C}(\alpha, n)^{16}\text{O}$

i: $\alpha+^{13}\text{C}$						f: $n+^{16}\text{O}$			form f.: $\tau+^{13}\text{C}$			
	V_R	r_R	a_R	V_S	r_S	a_S	V_R	r_R	a_R	r_R	a_R	$D_{t,4}$
R.R.	$l_i = p$	$[J^\pi, E_R] = [3/2^+, 0.84]$										
ad	-62.67	1.07	0.79	-1.470	1.13	0.70	-65.57	1.14	0.68	1.1	0.82	18.6
lo		r_C								r_C		16.6
hi		1.48								1.29		19.7
SUB R.	$l_i = p$	$[J^\pi, E_R] = [1/2^+, -0.003]$	ad/lo/hi				$a = 7.5$	$\theta_\alpha^2 =$				
	$l_i = s$	$[J^\pi, E_R] = [1/2^-, -0.419]$										8./5./15. E-3 0.65/0.50/0.85

Table 50: DWBA parameter values for $^{15}\text{N}(\text{p}, \alpha)^{12}\text{C}$.

i: $p+^{15}\text{N}$						f: $\alpha+^{12}\text{C}$			form f.: $t+^{12}\text{C}$			
	V_R	r_R	a_R	V_S	r_S	a_S	V_R	r_R	a_R	r_R	a_R	$D_{t,4}$
R.R.	$l_i = p$	$[J^\pi, E_R] = [1^-, 0.31]$										
ad	-59.16	1.139	0.68	-0.93	1.30	0.53	-43.70	1.07	0.79	1.09	0.82	13.
lo	-59.17	r_C		-0.93			-43.69	r_C		r_C		16.
hi	-59.12	1.46		-0.88			-43.92	1.48		1.29		12.
R.R.	$l_i = p$	$[J^\pi, E_R] = [1^-, 0.96]$										
all	-54.87			-2.026			-44.10					0.26

Capture Reactions

Table 51: PM parameter values for ${}^2\text{H}(\text{p}, \gamma) {}^3\text{He}$

l_i	V_i	r_0	a_0	\mathcal{C}_c
N.R. sp	ad/lo/hi	-50.0/-48.0/-52.0	0.84	0.35

Table 52: PM parameter values for ${}^2\text{H}(\text{d}, \gamma) {}^4\text{He}$

l_i	V_i	r_0	a_0	\mathcal{C}_c
N.R. d	ad/lo/hi	-54.0/-52.2/-56.0	1.22/1.25/1.25	1.25
s				0.95/0.83/1.87 ($l_f = 0$) 0.035/0.023/0.081 ($l_f = 2$)

Table 53: PM parameter values for ${}^2\text{H}(\alpha, \gamma) {}^6\text{Li}$

l_i	$[J^\pi, E_R]$	V_i	r_0	a_0	\mathcal{C}_c
R.C.	d	[3 ⁺ , 0.711]	ad/lo/hi	-34.77	1.10
	d	[2 ⁺ , 3.892]		-77.67	0.70
N.R.	p		ad/lo/hi	-36.35	1.11
	d*				0.64 1.5/1.4/1.5

Table 54: PM parameter values for ${}^3\text{H}(\alpha, \gamma) {}^7\text{Li}$

	l_i	V_i	r_0	a_0	\mathcal{C}_c
N.R.	s/d	ad	-38.6/30.6	1.24	0.425/0.43
		lo	-39.6/36.3		0.42/0.52
		hi	-36.3		0.52 0.71/0.67

Table 55: PM parameter values for ${}^3\text{He}(\alpha, \gamma) {}^7\text{Be}$

	l_i	V_i	r_0	a_0	\mathcal{C}_c
N.R.	s/d	ad	-38.6/36.3	1.24	0.425/0.52
		lo	-39.6/36.3		0.42/0.52
		hi	-36.3		0.52 0.71/0.67

Table 56: PM parameter values for ${}^6\text{Li}(\text{p}, \gamma) {}^7\text{Be}$

	l_i	$[J^\pi, E_R]$	V_i	r_0	a_0	\mathcal{C}_c
R.C.	s	[3/2 ⁺ , 0.2](see text)	ad	-80.0	1.15	1.2
	p	[5/2 ⁻ , 1.6](see text)	hi	-74.5	0.65	0.2 0.03
N.R.	s*		ad	-50.0	0.90	0.50 0.37
	s		lo			0.165
	s		hi/(ad/lo) [†]	-85.0	1.10	0.45 0.68/(0.52/0.60) [†]

[[†]for Fig. 25 without PA99.]

Table 57: PM parameter values for ${}^7\text{Li}(\text{p}, \gamma){}^8\text{Be}$

	l_i	$[J^\pi, E_R]$	$\rightarrow E_x({}^8\text{B})$	V_i	r_0	a_0	C_c
R.C.	p	[1 ⁺ , 0.375]	$\rightarrow 0$	ad/lo/hi	-120.19	0.4926	0.059
			$\rightarrow 3.04$	all			4.0/3.8/4.2 (E-3)
	p	[1 ⁺ , 0.896]	$\rightarrow 0$		-67.9	0.658	0.17
			$\rightarrow 3.04$	ad/lo/hi			1.2/1.1/1.3 (E-3)
N.R.	s		$\rightarrow 0$	ad/lo/hi	-50.0	0.92	0.50
			$\rightarrow 3.04$				0.60/1.9/0.6 (E-4)
			or (see Fig.31):				8.7/7.3/9.6
SUB R.	s		$\rightarrow 0$	ad	-50.0	0.80	6.6
	p*		(E2)				18.0
SUB R.	p	[2 ⁺ , -0.629]	hi	$a =$	40.	$\theta_\alpha^2 =$	0.3

Table 58: PM parameter values for ${}^7\text{Li}(\alpha, \gamma){}^{11}\text{B}$

	l_i	$[J^\pi, E_R]$	V_i	r_0	a_0	C_c
R.C.	p	[5/2 ⁺ , 0.609]	ad/lo/hi	-55.55	0.70	0.40
	d	[3/2 ⁻ , 1.595]		-54.07	0.82	0.60
	d	[5/2 ⁻ , 1.665]		-35.75	1.08	0.16
	f	[7/2 ⁺ , 1.932]		-85.44	1.04	0.48
N.R.	p*		ad/lo/hi	-50.0	0.9	0.5
SUB R.	s	[3/2 ⁻ , -0.105]	ad/lo/hi	$a =$	40.	$\theta_\alpha^2 =$
						2.6/2.0/3.0 (E-3)

Table 59: PM parameter values for ${}^7\text{Be}(\text{p}, \gamma){}^8\text{B}$

	l_i	$[J^\pi, E_R]$	V_i	r_0	a_0	C_c
R.C.	p	[1 ⁺ , 0.633]	ad/lo/hi	-61.62	0.70	0.12
	p	[3 ⁺ , 2.183]		-96.0	0.656	1.73
N.R.	spd		ad	-50.00	0.92	0.60
			lo			0.45, 0.20, 0.25
			hi			0.42, 0.18, 0.18
						0.49, 0.22, 0.28

Table 60: PM parameter values for ${}^7\text{Be}(\alpha, \gamma){}^{11}\text{C}$

	l_i	$[J^\pi, E_R]$	V_i	r_0	a_0	C_c
R.C.	p	[5/2 ⁺ , 1.155]	ad/lo/hi	-56.94	0.70	0.40
	d	[3/2 ⁻ , 2.106]		-55.45	0.82	0.60
	d	[5/2 ⁻ , 2.236]		-36.24	1.08	0.16
	d	[7/2 ⁻ , 2.426]	hi	-94.33	0.93	0.10
N.R.	f	[7/2 ⁺ , 2.539]	ad/lo/hi	-85.70	1.04	0.48
	p*		ad/lo/hi	-50.0	0.9	0.5
						0.094/0.0075/0.0113
						1.7/0.9/3.4

Table 61: PM parameter values for ${}^9\text{Be}(\text{p}, \gamma){}^{10}\text{B}$

	l_i	$[J^\pi, E_R]$	V_i	r_0	a_0	C_c
R.C.	s	[1 ⁻ , 0.290]	ad/lo/hi	-31.8	0.40	2.6
	p	[2 ⁺ , 0.892]		-62.68	0.65	0.3
N.R.	s*		ad/lo/hi	-53.9/-56.9/-53.9	1.0	0.70
						0.30/1.9/0.36

Table 62: PM parameter values for $^{10}\text{B}(\text{p}, \gamma)^{11}\text{C}$

	l_i	$[J^\pi, E_R]$		V_i	r_0	a_0	\mathcal{C}_c
R.C.	s	$[5/2^+, 0.01]$	(see text)				
	p	$[3/2^-, 0.961]$	ad/lo/hi	-88.72	1.35	0.76	0.67/0.8/0.8
N.R.	p^*		all	-76.09	0.76	0.68	9.6

Table 63: PM parameter values for $^{11}\text{B}(\text{p}, \gamma)^{12}\text{C}$

	l_i	$[J^\pi, E_R]$		V_i	r_0	a_0	\mathcal{C}_c
R.C.	p	$[2^+, 0.149]$	ad/lo/high	-69.79	1.10	3.23	8.0/6.0/10.0
	s	$[2^-, 0.613]$	all	-38.82	1.10	0.60	(see text)
N.R.	s^*p^*/d		all	-62.0/75.0	1.10	0.60	1.00

Table 64: PM parameter values for $^{12}\text{C}(\text{p}, \gamma)^{13}\text{N}$

	l_i	$[J^\pi, E_R]$		V_i	r_0	a_0	\mathcal{C}_c
R.C.	s	$[1/2^+, 0.421]$	ad	-36.00	1.15	0.65	0.33
			lo	-57.57	0.90	0.50	0.29
			hi	-60.72	1.45	0.40	0.33

Table 65: PM parameter values for $^{12}\text{C}(\alpha, \gamma)^{16}\text{O}$

	l_i	$[J^\pi, E_R]$	$\rightarrow E_x(^{16}\text{O})$		V_i	r_0	a_0	\mathcal{C}_c
R.C.	p	$[1^-, 2.423]$	$\rightarrow 0$	ad/lo/hi	-55.67	1.15	0.30	31.4/29.7/33.0
			$\rightarrow 6.05$					66.0/57.8/74.3
			$\rightarrow 6.92$					18./18./230.
			$\rightarrow 7.12$					0.34/0.25/0.49
	d	$[2^+, 2.683]$	$\rightarrow 0$	ad/lo/hi	-99.86	0.337	0.021	6.0/3.0/3.0
			$\rightarrow 6.05$					120./90./150.
	g	$[4^+, 3.194]$	$\rightarrow 6.92$	ad/lo/hi	-85.48	1.0	0.4	1.8/2.5/5.0
	d	$[2^+, 4.358]$	$\rightarrow 0$	ad/lo/hi	-39.80	0.532	0.01	2.4/2.1/3.0
			$\rightarrow 6.05$					3.0/2.4/3.9
			$\rightarrow 6.92$					0.12/0.12/0.18
	f	$[3^-, 4.432]$	$\rightarrow 6.13$	ad/lo/hi	-65.75	1.0	0.39	5.5/3.1/8.6 E-3
			$\rightarrow 6.92$					90./130./300.
			$\rightarrow 7.12$					0.28/0.21/0.35
SUB R.	p	$[1^-, -0.045]$		add/lo/hi	$a =$	6.5	$\theta_\alpha^2 =$	0.008/0.006/0.010
	d	$[2^+, -0.245]$				7.5		0.019/0.013/0.025

Table 66: PM parameter values for $^{13}\text{C}(\text{p}, \gamma)^{14}\text{N}$

	l_i	$[J^\pi, E_R]$	$\rightarrow E_x(^{15}\text{O})$	V_i	r_0	a_0	C_c	
R.C.	s	$[1^-, 0.511]$	$\rightarrow 0$	ad/lo/hi	-25.82	0.58	0.04	0.28/0.18/0.37
			$\rightarrow 2.31$	all	-20.54	0.67	0.24	0.027
			$\rightarrow 3.95$		-25.82	0.58	0.04	0.28
			$\rightarrow 4.91$				1.0	
			$\rightarrow 5.11$				224.	
			$\rightarrow 5.69$				2.1	
N.R.	s*pd	$[1^-, 0.511]$	$\rightarrow 0$	ad/lo/hi	-30.48	1.12	0.39	1.0/0.8/1.2
			$\rightarrow 2.31$	all	-36.88	4.16	1.01	0.45
			$\rightarrow 3.95$			1.15	0.16	0.0015
			$\rightarrow 4.91$		-30.48	1.12	0.39	1.0
			$\rightarrow 5.11$		-34.48			0.05/1.0
			$\rightarrow 5.69$		-30.48		0.8	
			$\rightarrow 5.83$				0.5	

Table 67: PM parameter values for $^{13}\text{N}(\text{p}, \gamma)^{14}\text{O}$

	l_i	$[J^\pi, E_R]$	V_i	r_0	a_0	C_c	
R.C.	s	$[1^-, 0.528]$	ad/hi	-53.92	0.96	0.30	0.977/1.23
			lo	-53.91			0.775
N.R.	pd		ad/lo/hi	-30.48	1.12	0.39	1.0/0.8/1.2

Table 68: PM parameter values for $^{14}\text{N}(\text{p}, \gamma)^{15}\text{O}$

	l_i	$[J^\pi, E_R]$	$\rightarrow E_x(^{15}\text{O})$	V_i	r_0	a_0	C_c	
R.C.	s	$[1/2^+, 0.260]$	$\rightarrow 0$	all	-57.53	0.88	0.52	3.4 E-5
			$\rightarrow 5.18$	ad/lo/hi				6.0/5.8/6.3 E-6
			$\rightarrow 6.18$					2.4/2.1/2.7 E-5
			$\rightarrow 6.79$					8.6/8.2/8.9 E-5
			$\rightarrow 6.86$					1.7/1.4/1.9 E-7
			$\rightarrow 0$	ad/lo/hi	-57.78	0.88	0.36	3.4/3.2/3.6 E-3
d	$[3/2^+, 0.987]$		$\rightarrow 5.18$					1.7/1.5/1.9 E-5
			$\rightarrow 5.24$					6.1/5.5/6.5 E-4
			$\rightarrow 6.18$					1.7/1.5/1.9 E-5
			$\rightarrow 6.86$					1.7/1.2/1.9 E-5
			$\rightarrow 5.18$	ad/lo/hi	-57.07	0.88	0.64	5.0/4.5/5.5
			$\rightarrow 6.18$					5.0/4.5/6.0 E-3
N.R.	s*	$[1/2^+, 1.446]$	$\rightarrow 0$	ad,hi	-35.0	1.00	0.55	0.015
			$\rightarrow 5.18$	all				4.E-4
			$\rightarrow 6.18$	ad/lo/hi				0.8/0.5/1.0 E-3
			$\rightarrow 6.79$					7.8/7.5/8.0 E-2
			$\rightarrow 0$	ad/lo/hi	-40.0	1.00	0.55	11./11./12.
			$\rightarrow 5.24$					0.09/0.07/0.12
d	$[1/2^+, 1.446]$		$\rightarrow 6.79$					0.50/0.45/0.60
			$\rightarrow 6.86$					0.40/0.35/0.50
			$\rightarrow 7.28$					0.95/0.76/1.25
SUB R.	s	$[3/2^+, -0.504]$		add/lo/hi	$a =$	5.8	$\theta_p^2 =$	0.15/0.0/0.30

Table 69: PM parameter values for $^{15}\text{N}(\text{p}, \gamma)^{16}\text{O}$.

	l_i	$[J^\pi, E_R]$	V_i	r_0	a_0	C_c	
R.C.	s	$[1^-, 0.313]$	ad	-73.5	0.5	3.4	51.
			lo	-68.0	0.6	3.4	61.
			hi	-72.0	0.4	3.6	6.7
R.C.	s	$[1^-, 0.963]$	ad/lo/hi (see text)	-60.43	0.35	0.16	1.3/1.2/1.4
			cascades				
R.C.	s	$[2^-, 0.669]$	all	-26.66	0.57	0.43	0.012
			d	$[3^-, 1.138]$	all	-42.71	1.0

Appendix B

Tabulated here are the reverse (endoergic) reaction rates that are defined by the product $\text{REV} \times N_A < \sigma v >$ of REV [Eq.(33)] and the forward reaction rates $N_A < \sigma v >$. Recall that they have different dimensions for transfer and photo-disintegration processes. In particular, the direct comparison of photo-disintegration rates with the forward capture rates is meaningless. In contrast, REV is dimensionless as far as the two-body transfer reactions considered in this compilation are concerned. The cases in which the forward reactions lead to three-body systems or ${}^8\text{Be}$ are omitted. Only the rates derived with the use of the "adopted" forward reaction rates are shown.

Transfer reactions

Table 70: Backward two-body endoergic transfer reaction rates in $\text{cm}^3 \text{mol}^{-1} \text{s}^{-1}$

T_9	${}^3\text{H(p,d)}{}^2\text{H}$	${}^3\text{He(n,d)}{}^2\text{H}$	${}^3\text{He}(\alpha,p){}^6\text{Li}$	${}^4\text{He(n,d)}{}^3\text{H}$	${}^4\text{He(p,d)}{}^3\text{He}$	${}^4\text{He}(\alpha,p){}^7\text{Li}$
0.5		1.08E-26				
0.6	1.51E-27	4.36E-21	4.04E-28			
0.7	1.27E-22	4.48E-17	3.94E-23			
0.8	6.35E-19	4.62E-14	2.22E-19			
0.9	4.84E-16	1.04E-11	1.88E-16			
1.	9.91E-14	7.93E-10	4.16E-14			
1.25	1.47E-09	2.01E-06	7.17E-10			
1.5	9.08E-07	3.81E-04	4.94E-07			
1.75	9.05E-05	1.64E-02	5.39E-05			
2.	2.89E-03	2.79E-01	1.85E-03			
2.5	3.77E-01	1.51E+01	2.71E-01	6.77E-27	8.69E-29	7.37E-29
3.	9.88E+00	2.19E+02	7.81E+00	4.99E-21	1.31E-22	7.19E-23
3.5	1.03E+02	1.50E+03	8.85E+01	7.60E-17	3.32E-18	1.45E-18
4.	6.04E+02	6.41E+03	5.56E+02	1.03E-13	6.60E-15	2.57E-15
5.	7.32E+03	4.95E+04	7.54E+03	2.45E-09	2.68E-10	9.84E-11
6.	3.93E+04	1.94E+05	4.41E+04	1.99E-06	3.10E-07	1.18E-07
7.	1.32E+05	5.16E+05	1.58E+05	2.37E-04	4.67E-05	1.92E-05
8.	3.28E+05	1.10E+06	4.17E+05	8.41E-03	1.99E-03	8.77E-04
9.	6.68E+05	1.97E+06	8.96E+05	1.35E-01	3.62E-02	1.71E-02
10.	1.18E+06	3.17E+06	1.66E+06	1.24E+00	3.64E-01	1.85E-01

Table 71: Backward two-body endoergic transfer reaction rates in $\text{cm}^3 \text{mol}^{-1} \text{s}^{-1}$

T_9	${}^6\text{Li}(\alpha,p){}^9\text{Be}$	${}^7\text{Be}(\alpha,p){}^{10}\text{B}$	${}^{12}\text{C(n,}\alpha{})^9\text{Be}$	${}^{12}\text{C}(\alpha,p){}^{15}\text{N}$	${}^{14}\text{N}(\text{n,}\alpha{})^{11}\text{B}$	${}^{16}\text{O}(\text{n,}\alpha{})^{13}\text{C}$
0.08					9.30E-24	
0.09					4.85E-21	
0.1					7.44E-19	
0.11					4.55E-17	
0.12					1.39E-15	
0.13					2.49E-14	
0.14					2.94E-13	
0.15					2.46E-12	
0.16					1.59E-11	
0.18					3.50E-10	
0.2		1.53E-26			4.18E-09	
0.25		2.54E-20			4.48E-07	

(to continue)

T_9	${}^6\text{Li}(\alpha, \text{p}) {}^9\text{Be}$	${}^7\text{Be}(\alpha, \text{p}) {}^{10}\text{B}$	${}^{12}\text{C}(\text{n}, \alpha) {}^9\text{Be}$	${}^{12}\text{C}(\text{p}, \alpha) {}^{15}\text{N}$	${}^{14}\text{N}(\text{n}, \alpha) {}^{11}\text{B}$	${}^{16}\text{O}(\text{n}, \alpha) {}^{13}\text{C}$
0.3		3.88E-16			1.62E-05	
0.35	8.97E-26	4.00E-13			2.83E-04	
0.4	1.13E-21	7.64E-11			2.65E-03	
0.45	1.79E-18	4.70E-09			1.56E-02	1.29E-26
0.5	6.61E-16	1.30E-07			6.61E-02	1.86E-23
0.6	4.82E-12	2.06E-05			6.33E-01	1.24E-18
0.7	2.81E-09	8.28E-04			3.84E+00	3.92E-15
0.8	3.35E-07	1.43E-02		6.11E-26	1.83E+01	1.74E-12
0.9	1.39E-05	1.38E-01		2.75E-22	7.17E+01	2.06E-10
1.	2.74E-04	8.92E-01	7.77E-25	2.31E-19	2.35E+02	9.63E-09
1.25	5.84E-02	2.90E+01	1.87E-18	4.29E-14	2.36E+03	1.06E-05
1.5	2.09E+00	3.30E+02	4.68E-14	1.44E-10	1.21E+04	1.26E-03
1.75	2.70E+01	1.97E+03	7.33E-11	4.91E-08	4.05E+04	4.17E-02
2.	1.84E+02	7.78E+03	1.89E-08	3.94E-06	1.03E+05	6.15E-01
2.5	2.72E+03	5.54E+04	4.63E-05	1.87E-03	3.98E+05	2.93E+01
3.	1.64E+04	2.11E+05	8.47E-03	1.15E-01	1.03E+06	4.06E+02
3.5	5.93E+04	5.55E+05	3.52E-01	2.16E+00	2.11E+06	2.70E+03
4.	1.56E+05	1.15E+06	5.81E+00	1.93E+01	3.76E+06	1.13E+04
5.	6.02E+05	3.24E+06	3.03E+02	4.07E+02	9.04E+06	8.59E+04
6.	1.47E+06	6.47E+06	4.39E+03	3.05E+03	1.72E+07	3.48E+05
7.	2.80E+06	1.05E+07	3.05E+04	1.27E+04	2.81E+07	1.01E+06
8.	4.49E+06	1.54E+07	1.34E+05	3.67E+04	4.10E+07	2.42E+06
9.	6.49E+06	2.03E+07	4.27E+05	8.33E+04	5.50E+07	5.09E+06
10.	8.69E+06	2.55E+07	1.10E+06	1.60E+05	6.97E+07	9.78E+06

Photo-disintegrations

Table 72: Backward photodisintegration reaction rates in s^{-1}						
T_9	${}^3\text{He}(\gamma, \text{p}) {}^2\text{H}$	${}^4\text{He}(\gamma, \text{d}) {}^2\text{H}$	${}^6\text{Li}(\gamma, \alpha) {}^2\text{H}$	${}^7\text{Li}(\gamma, \alpha) {}^3\text{H}$	${}^7\text{Be}(\gamma, \text{p}) {}^6\text{Li}$	${}^7\text{Be}(\gamma, \alpha) {}^3\text{He}$
0.35			5.85E-15			4.25E-15
0.4			5.09E-12			7.38E-12
0.45			1.04E-09	2.43E-17		2.62E-09
0.5			7.68E-08	2.18E-14		3.00E-07
0.6			5.45E-05	6.29E-10		4.09E-04
0.7			6.66E-03	1.03E-06		7.81E-02
0.8			2.71E-01	2.80E-04		4.28E+00
0.9			5.29E+00	2.26E-02		1.01E+02
1.	1.11E-15		6.05E+01	7.79E-01	1.50E-16	1.32E+03
1.25	7.37E-10		5.76E+03	4.98E+02	1.41E-10	1.51E+05
1.5	6.16E-06		1.34E+05	4.02E+04	1.46E-06	3.93E+06
1.75	4.16E-03		1.34E+06	9.75E+05	1.12E-03	4.32E+07
2.	5.77E-01		7.79E+06	1.11E+07	1.70E-01	2.74E+08
2.5	6.34E+02		9.63E+07	3.61E+08	2.05E+02	4.01E+09
3.	7.30E+04		5.39E+08	3.95E+09	2.46E+04	2.64E+10
3.5	2.31E+06		1.94E+09	2.31E+10	7.90E+05	1.08E+11
4.	3.23E+07	2.77E-18	5.25E+09	8.99E+10	1.10E+07	3.28E+11
5.	1.41E+09	5.72E-12	2.33E+10	6.47E+11	4.69E+08	1.72E+12
6.	1.90E+10	1.03E-07	6.91E+10	2.62E+12	6.13E+09	5.70E+12
7.	1.29E+11	1.20E-04	1.62E+11	7.05E+12	4.05E+10	1.42E+13
8.	5.68E+11	2.51E-02	3.22E+11	1.54E+13	1.74E+11	2.92E+13
9.	1.85E+12	1.65E+00	5.69E+11	2.85E+13	5.59E+11	5.24E+13
10.	4.91E+12	4.78E+01	9.23E+11	4.70E+13	1.46E+12	8.50E+13

Table 73: Backward photodisintegration reaction rates in s^{-1}

T_9	${}^8\text{B}(\gamma,\text{p}){}^7\text{Be}$	T_9	${}^8\text{B}(\gamma,\text{p}){}^7\text{Be}$	T_9	${}^8\text{B}(\gamma,\text{p}){}^7\text{Be}$
0.04	1.01E-16	0.12	8.64E-01	0.3	1.27E+06
0.05	3.05E-12	0.13	4.43E+00	0.35	6.65E+06
0.06	3.72E-09	0.14	1.86E+01	0.4	2.48E+07
0.07	6.99E-07	0.15	6.56E+01	0.45	7.32E+07
0.08	3.98E-05	0.16	2.03E+02	0.5	1.82E+08
0.09	1.00E-03	0.18	1.40E+03	0.6	7.90E+08
0.1	1.42E-02	0.2	6.92E+03	0.7	2.49E+09
0.11	1.30E-01	0.25	1.44E+05	0.8	6.40E+09

Table 74: Backward photodisintegration reaction rates in s^{-1}

T_9	${}^8\text{B}(\gamma,\text{p}){}^7\text{Be}$	${}^{10}\text{B}(\gamma,\text{p}){}^9\text{Be}$	${}^{11}\text{B}(\gamma,\alpha){}^7\text{Li}$	${}^{11}\text{C}(\gamma,\text{p}){}^{10}\text{B}$	${}^{11}\text{C}(\gamma,\alpha){}^7\text{Be}$	${}^{12}\text{C}(\gamma,\text{p}){}^{11}\text{B}$
0.9	1.42E+10					
1.	2.80E+10					
1.25	1.08E+11	6.49E-14				
1.5	2.95E+11	3.89E-09	1.93E-16	4.01E-17	5.95E-13	
1.75	6.42E+11	1.12E-05	5.47E-12	1.18E-12	5.73E-09	
2.	1.20E+12	4.67E-03	1.22E-08	2.82E-09	5.72E-06	
2.5	3.13E+12	2.32E+01	6.26E-04	1.67E-04	9.52E-02	1.67E-17
3.	6.42E+12	7.02E+03	9.24E-01	2.73E-01	6.48E+01	6.42E-12
3.5	1.12E+13	4.22E+05	1.81E+02	5.66E+01	7.01E+03	6.53E-08
4.	1.79E+13	9.15E+06	9.82E+03	3.22E+03	2.42E+05	6.79E-05
5.	3.77E+13	6.88E+08	2.86E+06	9.89E+05	3.59E+07	1.20E+00
6.	6.77E+13	1.23E+10	1.33E+08	4.85E+07	1.05E+09	8.58E+02
7.	1.10E+14	9.82E+10	2.13E+09	8.33E+08	1.21E+10	9.76E+04
8.	1.65E+14	4.69E+11	1.74E+10	7.35E+09	7.71E+10	3.55E+06
9.	2.37E+14	1.60E+12	8.98E+10	4.13E+10	3.29E+11	6.06E+07
10.	3.24E+14	4.28E+12	3.37E+11	1.70E+11	1.06E+12	6.07E+08

Table 75: Backward photodisintegration reaction rates in s^{-1}

T_9	${}^{13}\text{N}(\gamma,\text{p}){}^{12}\text{C}$	${}^{14}\text{N}(\gamma,\text{p}){}^{13}\text{C}$	${}^{14}\text{O}(\gamma,\text{p}){}^{13}\text{N}$	${}^{15}\text{O}(\gamma,\text{p}){}^{14}\text{N}$	${}^{16}\text{O}(\gamma,\text{p}){}^{15}\text{N}$	${}^{16}\text{O}(\gamma,\alpha){}^{12}\text{C}$
0.4	2.32E-15					
0.45	3.94E-12					
0.5	1.58E-09					
0.6	1.32E-05					
0.7	8.64E-03					
0.8	1.13E+00		4.57E-17			
0.9	5.04E+01		1.81E-13			
1.	1.05E+03		1.38E-10			
1.25	2.54E+05	5.11E-17	2.14E-05	2.26E-17		
1.5	9.88E+06	1.34E-11	6.20E-02	3.02E-12	2.00E-17	
1.75	1.36E+08	1.01E-07	1.85E+01	1.51E-08	2.57E-13	
2.	9.70E+08	8.15E-05	1.33E+03	9.72E-06	3.47E-16	3.66E-10
2.5	1.54E+10	9.77E-01	5.34E+05	1.00E-01	1.11E-09	1.30E-05
3.	9.84E+10	5.19E+02	2.91E+07	5.58E+01	2.56E-05	1.78E-02
3.5	3.76E+11	4.66E+04	5.08E+08	5.66E+03	3.40E-02	3.65E+00
4.	1.04E+12	1.38E+06	4.35E+09	1.94E+05	7.61E+00	2.25E+02
5.	4.46E+12	1.66E+08	8.95E+10	3.08E+07	1.51E+04	9.54E+04
6.	1.22E+13	4.24E+09	6.88E+11	9.97E+08	2.39E+06	7.01E+06
7.	2.54E+13	4.45E+10	3.06E+12	1.27E+10	9.00E+07	1.73E+08
8.	4.49E+13	2.66E+11	9.76E+12	8.91E+10	1.37E+09	2.02E+09
9.	7.04E+13	1.09E+12	2.50E+13	4.16E+11	1.14E+10	1.42E+10
10.	1.01E+14	3.41E+12	5.51E+13	1.45E+12	6.23E+10	6.83E+10

References

- [1] W.A. Fowler, G.R. Caughlan, B.A. Zimmerman, Ann. Rev. Astron. Astrophys. 5 (1967) 525-570.
- [2] G.R. Caughlan, W.A. Fowler, At. Data Nucl. Data 40 (1988) 283-334.
- [3] C. Angulo, M. Arnould, M. Rayet, P. Descouvemont, D. Baye, C. Leclercq-Willain, A. Coc, S. Barhoumi, P. Auger, C. Rolfs, R. Kunz, J.W. Hammer, A. Mayer, T. Paradellis, S. Kossionides, C. Chronidou, K. Spyrou, S. Degl'Innocenti, G. Fiorentini, B. Ricci, S. Zavatarelli, C. Providencia, H. Wolters, J. Soares, C. Grama, J. Rahighi, A. Shotter, M. Lamehi-Rachti, Nucl. Phys. A 656 (1999) 3-183.
- [4] P. Descouvemont, A. Aour, C. Angulo, A. Coc, E. Vangioni-Flam, At. Data Nucl. Data 88 (2004) 203-236.
- [5] E.G. Adelberger, A. García, R.G.H. Robertson, K.A. Snover, A.B. Balantekin, K. Heeger, M.J. Ramsey-Musolf, D. Bemmerer, A. Junghans, C.A. Bertulani, J.-W. Chen, H. Costantini, P. Prati, M. Couder, E. Uberseder, M. Wiescher, R. Cyburt, B. Davids, S.J. Freedman, M. Gai, D. Gazit, L. Gialanella, G. Imbriani, U. Greife, M. Hass, W.C. Haxton, T. Itahashi, K. Kubodera, K. Langanke, D. Leitner, M. Leitner, P. Vetter, L. Winslow, L.E. Marcucci, T. Motobayashi, A. Mukhamedzhanov, R.E. Tribble, K.M. Nollett, F.M. Nunes, T.-S. Park, P.D. Parker, R. Schiavilla, E.C. Simpson, C. Spitaleri, F. Strieder, H.-P. Trautvetter, K. Suemmerer, S. Typel, Rev. Mod. Phys. 83 (2011), 195-245.
- [6] R. Longland, C. Iliadis, A.E. Champagne, J.R. Newton, C. Ugalde, A. Coc, R. Fitzgerald, Nucl. Phys. A 841 (2010) 1-30.
- [7] C. Iliadis, R. Longland, A.E. Champagne, A.Coc, R. Fitzgerald, Nucl. Phys. A 841 (2010) 31-250.
- [8] C. Iliadis, R. Longland, A.E. Champagne, A. Coc, Nucl. Phys. A 841 (2010) 251-322.
- [9] C. Iliadis, R. Longland, A.E. Champagne, A. Coc, Nucl. Phys. A 841 (2010) 323-388.
- [10] M. Aikawa, M. Arnould, S. Goriely, A. Jorissen, K. Takahashi, Astron. Astrophys. 441 (2005) 1195-1203.
- [11] M. Aikawa, K. Arai, M. Arnould, K.Takahashi, H. Utsunomiya, in: S. V. Harissopoulos, P. Demetriou, R. Julin (Eds.), Proc. Int. Conf. on Frontiers in Nuclear Structure, Astrophysics and Reactions (FINUSTAR), Kos, Greece, Sept. 12-17, 2005, AIP Conf. Proc. 831 (2006) 26-30.
- [12] M. Aikawa, K. Arai, M. Katsuma, K. Takahashi, M. Arnould, H. Utsunomiya, in: S. Kubono, W. Aoki, T. Kajino, T. Motobayashi, K. Nomoto (Eds.), Proc. Int. Symp. on Origin of Matter and Evolution of Galaxies (OMEQ05), Tokyo, Japan, Nov. 8-11, 2005, AIP Conf. Proc. 847 (2006) 359-361.
- [13] M. Katsuma, in: M. Arnould, M. Lewitowicz, H. Emling, H. Akimune, M. Ohta, H. Utsunomiya, T. Wada, T. Yamagata (Eds.), Proc. Tours Symp. on Nuclear Physics VI, Tours, France, Sept. 5-8, 2006, AIP Conf. Proc. 891 (2007) 355-363.
- [14] M. Katsuma, in: P. Demetriou, R. Julin, S.V. Harissopoulos (Eds.), Proc. Int. Conf. on Frontiers in Nuclear Structure, Astrophysics and Reactions (FINUSTAR 2), Crete, Greece, Sept. 10-14, 2007, AIP Conf. Proc. 1012 (2008) 365-367.
- [15] M. Arnould, M. Katsuma, in: O. Bersillon, F. Gunsing, E. Bauge, R.J. Jacqmin, S. Leray (Eds.), Proc. Int. Conf. on Nuclear Data for Science and Technology (ND2007), Nice, France, April 22-27, 2007, EDP Sci., Paris (2008) 5-10.
- [16] Y. Xu, S. Goriely, K. Takahashi, in: H. Susa, H. Utsunomiya, M. Arnould, S. Galès, T. Motobayashi, C. Scheidenberger (Eds.), Proc. Tours Symp. on Nuclear Physics VII, Kobe, Jaoan, Nov. 16-20, 2009, AIP Conf. Proc. 1238 (2010) 187-192.
- [17] D.D. Clayton, Principles of Stellar Evolution and Nucleosynthesis, McGraw - Hill, New York (1968).
- [18] C.E. Rolfs, W.S. Rodney, Cauldrons in the Cosmos, University of Chicago Press, Chicago (1988).
- [19] H. Oberhummer, G. Staudt, in: H. Oberhummer (Ed.), Nuclei in the Cosmos, Springer Verlag, Heidelberg (1991) 29-59.
- [20] P. Descouvemont, Theoretical Models for Nuclear Astrophysics, Nova Science Publishers, New York (2003).
- [21] P. Descouvemont, J. Phys. G Nucl. Partic. 35 (2008) 014006 [7 pages].
- [22] G.R. Satchler, Direct Nuclear Reactions, Clarendon Press, Oxford (1983).
- [23] P.D. Kunz, A DWBA Reaction Code DWUCK4, University of Colorado, Boulder (1987), unpublished: <http://spot.colorado.edu/kunz/DWBA.html>.
- [24] J.M. Blatt, V.F. Weisskopf, Theoretical Nuclear Physics, John Wiley & Sons, New York (1952).
- [25] P.J.A. Buttle, L.J.B. Goldfarb, Nucl. Phys. 78 (1966) 409-422.
- [26] B.M. Braizinha, Calculation of nuclear reaction rates in astrophysical processes, PhD thesis, Univ. Lisbon (2004) unpublished.
- [27] C. Rolfs, Nucl. Phys. A 217 (1973) 29-70.

- [28] J.T. Huang, C.A. Berutulani, V. Guimarães, At. Data Nucl. Data 96 (2010) 828-847.
- [29] J.M. Eisenberg, W. Greiner, Excitation Mechanisms of the Nucleus, North Holland Pub. Co., Amsterdam (1970).
- [30] F.C. Barker, T. Kajino, Aust. J. Phys. 44 (1991) 369-396.
- [31] D.L. Smith, Probability, Statistics, and Data Uncertainties in Nuclear Science and Technology, Am. Nucl. Soc., LaGrange park (1991).
- [32] R.H. Cyburt, B. Davids, B.K. Jennings, Phys. Rev. C 70 (2004) 045801 [9 pages].
- [33] R.H. Cyburt, Phys. Rev. D 70 (2004) 023504 [25 pages].
- [34] R.H. Cyburt, B. Davids, Phys. Rev. C 78 (2008) 064614 [7 pages].
- [35] A.J. Koning, J.P. Delaroche, Nucl. Phys. A 713 (2003) 231-310.
- [36] Y. Han, Y. Shi, Q. Shen, Phys. Rev. C, 74 (2006) 044615 [11 pages].
- [37] D.Y. Pang, P. Roussel-Chomaz, H. Savajols, R.L. Varner, R. Wolski, Phys. Rev. C 79 (2009) 024615 [21 pages]; Erratum: Phys. Rev. C 81 (2010) 019902.
- [38] G. Audi, A.H. Wapstra, C. Thibault, Nucl. Phys. A 729 (2003) 337-676.
- [39] R.B. Firestone, V.S. Shirley, Table of Isotopes, 8th ed. vol I, John Wiley & Sons, New York (1999).
- [40] R. Capote, M. Herman, P. Obložinský, P.G. Young, S. Goriely, T. Belgya, A.V. Ignatyuk, A.J. Koning, S. Hilaire, V.A. Plujko, M. Avrigeanu, O. Bersillon, M.B. Chadwick, T. Fukahori, Z. Ge, Y. Han, S. Kailas, J. Kopecky, V.M. Maslov, G. Reffo, M. Sin, E.Sh. Soukhanovskii, P. Talou, Nucl. Data Sheets 110 (2009) 3107-3214.
- [41] TUNL Nuclear Data Evaluation Project, 'Energy Levels of Light Nuclei, $A = 3 - 20$ ': <http://www.tunl.duke.edu/nucldata/>
- [42] P. Raghavan, Atm. Data Nucl. Data 42 (1989), 189-291.
- [43] T.D. Shopka, S.E. Koonin, K. Langanke, R. Seki, Phys. Rev. C 48 (1993) 837-890.
- [44] S. Kimura, N. Takigawa, M. Abe, D.M. Brink, Phys. Rev. C 67 (2003) 022801(R) [5 pages].
- [45] V.M. Bystritsky, Vit.M. Bystritskii, G.N. Dudkin, M. Filipowicz, S. Gazi, H. Huran, A.P. Kobzev, G.A. Mesyats, B.A. Nechaev, V.N. Padalko, S.S. Parzhitskii, F.M. Pen'kov, A.V. Philippov, V.L. Kaminskii, Yu.Zh. Tuleushev, J. Wozniak, Nucl. Phys. A 889 (2012) 93-104.
- [46] S. Romano, C. Spitaleri, S. Cherubini, V. Crucillà, M. Gulino, M. La Cofnata, L. Lamia, R.G. Pizzzone, S.M. Puglia, G.G. Rapisarda, M.I. Sergi, S. Tudisco, A. Tumino, R.E. Tribble, V.Z. Goldberg, A.M. Mukhamedzhanov, G. Tabacarum L. Trache, V. Kroha, V. Burjan, Z. Hons, J. Mrázek, E. somorjai, Z. Elekes, Z. Fülop, G. Gyürky, G. Kiss, A. Szanto de Toledo, N. Carlin, M.M. De Mousa, M.G. Del Santo, M.G. Munhoz, R. Liguori Neto, F. A. Aouza, A. A. Suaide, F. Szanto, J. Phys. G: Nucl. Part. Phys. 35 (2008) 014008 [7 pages].
- [47] S. Typel, EAS Pub. Ser. 27 (2007), 185-193.
- [48] A.M. Mukhamedzhanov, L.D. Blokhintsev, S. Brown, V. Burjan, S. Cherubini, V.Z. Goldberg, M. Gulino, B.F. Irgaziev, E. Johnson, K. Kemper, V. Kroha, M. La Cognata, L. Lamia, A. Momotyuk, R.G. Pizzone, B. Roeder, G. Rogachev, S. Romano, C. Spitaleri, R.E. Tribble, A. Tumino, Nucl. Phys. A 787 (2007) 321-328.
- [49] F.C. Barker, Nucl. Phys. A 707 (2002) 277-300.
- [50] A. Belhout, S. Ouichaoui, H. Beaumevieille, A. Boughrara, S. Fortier, J. Kiener, J.M. Maison, S.K. Mehdi, L. Rosier, J.P. Thibaud, A. Trabelsi, J. Vernotte, Nucl. Phys. A 793 (2007) 178-211.
- [51] S. Goriely, S. Hilaire, A. J. Koning, Astron. Astrophys. 487 (2008) 767-774.
- [52] A. Adachour, P. Descouvemont, Eur. Phys. J. A 23 (2005) 435-443.
- [53] D. Baye, E. Brainis, Phys. Rev. C 61 (2000) 025801 [10 pages].
- [54] G.M. Griffiths, E.A. Larson, L.P. Robertson, Can. J. Phys. 40 (1962) 402-411.
- [55] G.M. Griffiths, M. Lal, C.D. Scarfe, Can. J. Phys. 41 (1963) 724-736.
- [56] J.B. Warren, K.L. Erdman, L.P. Robertson, D.A. Axen, J.R. Macdonald, Phys. Rev. 132 (1963) 1691-1692.
- [57] B.L. Berman, L.J. Koester, Jr., J.H. Smith, Phys. Rev. 133 (1964) B117-B129.
- [58] V.N. Fetisov, A.N. Gorbunov, A.T. Varfolomeev, Nucl. Phys. 71 (1965) 305-342.
- [59] J.R. Stewart, R.C. Morrison, J.S. O'Connell, Phys. Rev. 138 (1965) B372-B381.
- [60] K.N. Geller, E.G. Muirhead, L.D. Cohen, Nucl. Phys. A 96 (1967) 397-400.
- [61] W. Wölfi, R. Bösch, J. Lang, R. Müller, P. Marmier, Helv. Phys. Acta 40 (1967) 946-972.
- [62] G. Ticconi, S.N. Gardiner, J.L. Matthews, R.O. Owens, Phys. Lett. B 46 (1973) 369-371.
- [63] G.J. Schmid, R.M. Chasteler, C.M. Laymon, H.R. Weller, R.M. Prior, D.R. Tilley, Phys. Rev. C 52 (1995) R1732-R1735.
- [64] L. Ma, H.J. Karwowski, C.R. Brune, Z. Ayer, T.C. Black, J.C. Blackmon, E.J. Ludwig, M. Viviani, A. Kievsky, R. Schiavilla, Phys. Rev. C 55 (1997) 588-596.
- [65] G.M. Bailey, G.M. Griffiths, M.A. Olivo, R.L. Helmer, Can. J. Phys. 48 (1970) 3059-3061.

- [66] C. Casella, H. Costantini, A. Lemut, B. Limata, R. Bonetti, C. Broggini, L. Campajola, P. Corvisiero, J. Cruz, A. D'Onofrio, A. Formicola, Z. Fülop, G. Gervino, L. Gialanella, A. Guglielmetti, C. Gustavino, G. Gyurky, G. Imbriani, A.P. Jesus, M. Junker, A. Ordine, J.V. Pinto, P. Prati, J.P. Ribeiro, V. Roca, D. Rogalla, C. Rolfs, M. Romano, C. Rossi-Alvarez, F. Schuemann, E. Somorjai, O. Straniero, F. Strieder, F. Terrasi, H.P. Trautvetter, S. Zavatarelli, Nucl. Phys. A 706 (2002) 203-216.
- [67] V.M. Bystritsky, V.V. Gerasimov, A.R. Krylov, S.S. Parzhitskii, G.N. Dudkin, V.L. Kaminskii, B.A. Nechaev, V.N. Padalko, A.V. Petrov, G.A. Mesyats, M. Filipowicz, J. Wozniak, Vit.M. Bystritskii, Nucl. Instrum. Meth. A 595 (2008) 543-548.
- [68] G.J. Schmid, M. Viviani, B.J. Rice, R.M. Chasteler, M.A. Godwin, G.C. Kiang, L.L. Kiang, A. Kievsky, C.M. Laymon, R.M. Prior, R.Schiavilla, D.R. Tilley, H.R. Weller, Phys. Rev. Lett. 76 (1996) 3088-3091.
- [69] L.E. Marcucci, M. Viviani, R. Schiavilla, A. Kievsky, S. Rosati, Phys. Rev. C 72 (2005) 014001 [29 pages].
- [70] R.W. Zurmühle, W.E. Stephens, H.H. Staub, Phys. Rev. 132 (1963) 751-754.
- [71] W.E. Meyerhof, W. Feldman, S. Gilbert, W. O'Connell, Nucl. Phys. A (1969) 489-500.
- [72] F.J. Wilkinson III, F.E. Cecil, Phys. Rev. C 31 (1985) 2036-2040.
- [73] H.R. Weller, P. Colby, J. Langenbrunner, Z.D. Huang, D.R. Tilley, F.D. Santos, A. Arriaga, A.M. Eiró, Phys. Rev. C 34 (1986) 32-37.
- [74] C.A. Barnes, K.H. Chang, T.R. Donoghue, C. Rolfs, J. Kammeraad, Phys. Lett. B 197 (1987) 315-319.
- [75] J. Zhou, Y.-Y. Fu, S.-H. Zhou, H.-H. Xia, C.-B. Li, Q.-Y. Meng, Chin. Phys. C 33 (2009) 350-353.
- [76] R.E. Brown, N. Jarmie, Phys. Rev. C 41 (1990) 1391-1400.
- [77] K. Arai, S. Aoyama, Y. Suzuki, P. Descouvemont, D. Baye, Phys. Rev. Lett. 107 (2011) 132502 [5 pages].
- [78] H.J. Assenbaum, K. Langanke, Phys. Rev. C 36 (1987) 17-20.
- [79] R.L. Schulte, M. Cosack, A.W. Obst, J.L. Weil, Nucl. Phys. A 192 (1972) 609-624.
- [80] A. Krauss, H.W. Becker, H.P. Trautvetter, C. Rolfs, K. Brand, Nucl. Phys. A 465 (1987) 150-172.
- [81] U. Greife, F. Gorris, M. Junker, C. Rolfs, D. Zahnow, Z. Phys. A 351 (1995) 107-112.
- [82] K.G. McNeill, G.M. Keyser, Phys. Rev. 81 (1951) 602-606.
- [83] W.R. Arnold, J.A. Phillips, G.A. Sawyer, E.J. Stovall, Jr., J.L. Tuck, Phys. Rev. 93 (1954) 483-497.
- [84] G.R. Preston, P.F.D. Shaw, S.A. Young, Proc. Roy. Soc. A 226 (1954) 206-216.
- [85] N. Jarmie, R.E. Brown, Nucl. Instrum. Meth. B 10/11 (1985) 405-410.
- [86] M.A. Hofstee, A.K. Pallone, F.E. Cecil, J.A. McNeil, C.S. Galovich, Nucl. Phys. A 688 (2001) 527c-529c.
- [87] D.S. Leonard, H.J. Karwowski, C.R. Brune, B.M. Fisher, E. J. Ludwig, Phys. Rev. C 73 (2006) 045801 [14 pages].
- [88] V.M. Bystritsky, V.V. Gerasimov, A.R. Krylov, S.S. Parzhitskii, P.S. Anan'in, G.N. Dudkin, V.L. Kaminskii, B.A. Nechaev, V.N. Padalko, A.V. Petrov, G.A. Mesyats, M. Filipovicz, J. Wozniak, V.M. Bystritskii, Eur. Phys. J. A 36, (2008) 151-158.
- [89] A. Tumino, C. Spitaleri, A.M. Mukhamedzhanov, S. Typel, M. Aliotta, V. Burjan, M. Gimenez del Santo, G.G. Kiss, V. Kroha, Z. Hons, M. La Cognata, L. Lamia, M. Mrazek, R.G. Pizzone, S. Piskor, G.G. Rapisarda, S. Romano, M.L. Sergi, R. Spartà, Phys. Lett. B 700 (2011) 111-115; A. Tumino, private communication (2012).
- [90] A.S. Ganeev, A.M. Govorov, G.M. Osetinskii, A.N. Rakivenko, I.V. Sizov, V.S. Siksin, Sov. J. At. Energy Suppl. No. 5 (1958) 21-36.
- [91] S.E. Koonin, M. Mukerjee, Phys. Rev. C 42 (1990) 1639-1645.
- [92] W.A. Wenzel, W. Whaling, Phys. Rev. 88 (1952) 1149-1154.
- [93] A. Rinollo, S. Romano, C. Spitaleri, C. Bonomo, S. Cherubini, A. Del Zoppo, P. Figuera, M. La Cognata, L. Lamia, A. Musumarra, M.G. Pellegriti, R.G. Pizzone, C. Rolfs, D. Schümann, F. Strieder, S. Tudisco, A. Tumino, Nucl. Phys. A 758 (2005) 146c-149c.
- [94] F. Raiola, P. Migliardi, G. Gyürky, M. Aliotta, A. Formicola, R. Bonetti, C. Broggini, L. Campajola, P. Corvisiero, H. Costantini, J. Cruz, A. D'Onofrio, Z. Fülop, G. Gervino, L. Gialanella, A. Guglielmetti, G. Imbriani, C. Gustavino, A.P. Jesus, M. Junker, R.W. Kavanagh, P.G.P. Moroni, A. Ordine, J.V. Pinto, P. Prati, V. Roca, J.P. Ribeiro, D. Rogalla, C. Rolfs, M. Romano, F. Schümann, D. Schürmann, E. Somorjai, F. Strieder, F. Terrasi, H.P. Trautvetter, S. Zavatarelli, Eur. Phys. J. A 13, (2002) 377-382.
- [95] R.G.H. Robertson, P. Dyer, R.A. Warner, R.C. Melin, T.J. Bowles, A.B. McDonald, G.C. Ball, W.G. Davies, E.D. Earle, Phys. Rev. Lett. 47 (1981) 1867-1870; Erratum: Phys. Rev. Lett. 75 (1995)

- [96] J. Kiener, H.J. Gils, H. Rebel, S. Zagromski, G. Gsottschneider, N. Heide, H. Jelitto, J. Wentz, G. Baur, Phys. Rev. C 44 (1991) 2195-2208; J. Kiener, private communication (2009) [see NACRE].
- [97] P. Mohr, V. Kölle, S. Wilmes, U. Atzrott, G. Staudt, J. W. Hammer, H. Krauss, H. Oberhummer, Phys. Rev. C 50 (1994) 1543-1549.
- [98] F. Hammache, M. Heil, S. Typel, D. Galaviz, K. Sümmeler, A. Coc, F. Uhlig, F. Attallah, M. Caamano, D. Cortina, H. Geissel, M. Hellström, N. Iwasa, J. Kiener, P. Koczon, B. Kohlmeyer, P. Mohr, E. Schwab, K. Schwarz, F. Schümann, P. Senger, O. Sorlin, V. Tatischeff, J.P. Thibaud, E. Vangioni, A. Wagner, W. Walus, Phys. Rev. C 82 (2010) 065803 [11 pages].
- [99] K.M. Nollett, R.B. Wiringa, R. Schiavilla, Phys. Rev. C 63 (2001) 024003 [13 pages].
- [100] J.E. Brolley, Jr., J.L. Fowler, E.J. Stovall, Jr., Phys. Rev. 82 (1951) 502-505.
- [101] H.V. Argo, R.F. Taschek, H.M. Agnew, A. Hemmendinger, W.T. Leland, Phys. Rev. 87 (1952) 612-618.
- [102] J.P. Conner, T.W. Bonner, J.R. Smith, Phys. Rev. 88 (1952) 468473.
- [103] A. Hemmendinger, H. V. Argo, Phys. Rev. 98 (1955) 70-72.
- [104] A. Galonsky, C. H. Johnson, Phys. Rev. 104 (1956) 421-425.
- [105] S.J. Bame, Jr., J.E. Perry Jr., Phys. Rev. 107 (1957) 1616-1620.
- [106] M.D. Goldberg, J.M. Le Blanc, Phys. Rev. 122 (1961) 164-168.
- [107] A.P. Kobzev, V.I. Salatetskii, S.A. Telezhnikov, Yad. Fiz. 3 (1966) 1060-1063 [Sov. J. Nucl. Phys. 3 (1966) 774-776].
- [108] D.K. McDaniels, M. Drosg, J.C. Hopkins, J.D. Seagrave, Phys. Rev. C 7 (1973) 882-888.
- [109] E. Magiera, M. Bormann, W. Scobel, P. Heiss Nucl. Phys. A246 (1975) 413-424.
- [110] N. Jarmie, R.E. Brown, R.A. Hardekopf, Phys. Rev. C 29 (1984) 2031-2046; Erratum: Phys. Rev. C 33 (1986) 385.
- [111] R.E. Brown, N. Jarmie, G.M. Hale, Phys. Rev. C 35 (1987) 1999-2004; Erratum: Phys. Rev. C 36 (1987) 1220.
- [112] P. Navaatlí, S. Quoglionni, Phys. Rev. Lett. 108 (2012) 042503 [5 pages].
- [113] G.M. Griffiths, J.B. Warren, R.A. Morrow, P. J. Riley, Can. J. Phys. 39 (1961) 1397-1408.
- [114] S. Burzyński, K. Czerski, A. Marcinkowski, P. Zupranski, Nucl. Phys. A 473 (1987) 179-188.
- [115] C.R. Brune, R.W. Kavanagh, C. Rolfs, Phys. Rev. C 50 (1994) 2205-2218.
- [116] U. Schröder, A. Redder, C. Rolfs, R.E. Azuma, L. Buchmann, C. Campbell, J.D. King, T.R. Donoghue, Phys. Lett. B 192 (1987) 55-58.
- [117] Y. Tokimoto, H. Utsunomiya, T. Yamagata, M. Ohta, Y.-W. Lui, R.P. Schmitt, S. Typel, Y. Aoki, K. Ieki, K. Katori, Phys. Rev. C63 (2001) 035801 [20 pages].
- [118] T. Kajino, Nucl. Phys. A 460 (1986) 559-580.
- [119] T. Neff, Phys. Rev. Lett. 106 (2011) 042502 [4 pages].
- [120] U. Schröder, S. Engstler, A. Krauss, K. Neldner, C. Rolfs, E. Somorjai, K. Langanke, Nucl. INstrum. Meth. B 40/41 (1989) 466-469.
- [121] W.H. Geist, C.R. Brune, H.J. Karwowski, E.J. Ludwig, K.D. Veal, G.M. Hale, Phys. Rev. C 60 (1999) 054003 [9 pages]; Erratum: Phys. Rev. C 67 (2003) 059904(E).
- [122] H. Costantini, A. Formicola, M. Junker, R. Bonetti, C. Broggini, L. Campajola, P. Corvisiero, A. D'Onofrio, A. Fubini, G. Gervino, L. Gialanella, U. Greife, A. Guglielmetti, C. Gustavino, G. Imbriani, A. Ordine, P.G. Prada Moroni, P. Prati, V. Roca, D. Rogalla, C. Rolfs, M. Romano, F. Schümann, O. Straniero, F. Strieder, F. Terrasi, H.P. Trautvetter, S. Zavatarelli, Phys. Lett. B 482 (2000) 43-49.
- [123] M. Aliotta, F. Raiola, G. Gyürky, A. Formicola, R. Bonetti, C. Broggini, L. Campajola, P. Corvisiero, H. Costantini, A. D'Onofrio, Z. Fülpöp, G. Gervino, L. Gialanella, A. Guglielmetti, C. Gustavino, G. Imbriani, M. Junker, P.G. Moroni, A. Ordine, P. Prati, V. Roca, D. Rogalla, C. Rolfs, M. Romano, F. Schümann, E. Somorjai, O. Straniero, F. Strieder, F. Terrasi, H.P. Trautvetter, S. Zavatarelli, Nucl. Phys. A 690 (2001) 790-800.
- [124] M. La Cognata, C. Spitaleri, A. Tumino, S. Typel, S. Cherubini, L. Lamia, A. Musumarra, R.G. Pizzone, A. Rinollo, C. Rolfs, S. Romano, D. Schürmann, F. Strieder, Phys. Rev. C72 (2005) 065802 [12 pages].
- [125] S. Engstler, A. Krauss, K. Neldner, C. Rolfs, U. Schröder, K. Langanke, Phys. Lett. B 202 (1988) 179-184.
- [126] P. Prati, C. Arpesella, F. Bartolucci, H.W. Becker, E. Bollotti, C. Broggini, P. Corvisiero, G. Fiorentini, A. Fubini, G. Gervino, F. Gorris, U. Greife, C. Gustavino, M. Junker, C. Rolfs, W.H. Schulte, H.P. Trautvetter, D. Zahnow, Z. Phys. A 350 (1994) 171-176.
- [127] T. W. Bonner, J. P. Conner, A. B. Lillie, Phys. Rev. 88 (1952) 473-476.

- [128] R.G. Jarvis, D. Roaf, Proc. R. Soc. Lond. A 218 (1953) 432-438.
- [129] J.L. Yarnell, R.H. Lovberg, W.R. Stratton, Phys. Rev. 90 (1953) 292-297.
- [130] G. Freier, H. Holmgren, Phys. Rev. 93 (1954) 825-826.
- [131] W.E. Kunz, Phys. Rev. 97 (1955) 456-462.
- [132] Electrostatic accelerator charged-particle nuclear reaction group, Atom. Ener. Sci. Tech. (1977) 129-134 (in Chinese); EXFOR/IAEA cites the authors as Li Zhichang, Yang Jingang, Ding Xunliang.
- [133] W. Möller, F. Besenbacher, Nucl. Instrum. Meth. 168 (1980) 111-114.
- [134] W. Gruebler, V. König, A. Ruth, P.A. Schmelzbach, R.E. White, P. Marmier, Nucl. Phys. A 176 (1971) 636-644.
- [135] L. Stewart, J.E. Brolley, Jr., L. Rosen, Phys. Rev 119 (1960) 1649-1653.
- [136] F.C. Barker, Phys. Rev. C 75 (2007) 027601 [3 pages].
- [137] N.-M. Wang, V. Novatskii, G.M. Osetinskii, N.-K. Chien, I.A. Chepurchenko, Yad. Fiz. 3 (1966) 1064-1068 [Sov. J. Nucl. Phys. 3 (1966) 777-781].
- [138] A.D. Bacher, T.A. Tombrello, unpublished (1966) as quoted in: J.B. Marion, D.M. Van Patten (Eds.), Nuclear Research with Low-energy Accelerator (Academic Press, New York, 1967) p. 195.
- [139] M.R. Dwarakanath, H. Winkler, Phys. Rev. C 4 (1971) 1532-1540.
- [140] M.R. Dwarakanath, Phys. Rev. C 9 (1974) 805-808.
- [141] R.E. Brown, F.D. Correll, P.M. Hegland, J.A. Koepke, C.H. Poppe, Phys. Rev. C 35 (1987) 383-392.
- [142] A. Krauss, H.W. Becker, H.P. Trautvetter, C. Rolfs, Nucl. Phys. A 467 (1987) 273-290.
- [143] M. Junker, A. D'Alessandro, S. Zavatarelli, C. Arpesella, E. Bellotti, C. Broggini, P. Corvisiero, G. Fiorentini, A. Fubini, G. Gervino, U. Greife, C. Gustavino, J. Lambert, P. Prati, W.S. Rodney, C. Rolfs, F. Strieder, H.P. Trautvetter, D. Zahnow, Phys. Rev. C 57 (1998) 2700-2710.
- [144] C. Arpesella, E. Bellotti, C. Broggini, P. Corvisiero, G. Fiorentini, A. Fubini, G. Gervino, U. Greife, C. Gustavino, M. Junker, J. Lambert, P. Prati, W.S. Rodney, C. Rolfs, H.P. Trautvetter, D. Zahnow, S. Zavatarelli, Phys. Lett. B 389 (1996) 452-456.
- [145] R. Bonetti, C. Broggini, L. Campajola, P. Corvisiero, A. D'Alessandro, M. Dessalvi, A. D'Onofrio, A. Fubini, G. Gervino, L. Gialanella, U. Greife, A. Guglielmetti, C. Gustavino, G. Imbriani, M. Junker, P. Prati, V. Roca, C. Rolfs, M. Romano, F. Schuemann, F. Strieder, F. Terrasi, H.P. Trautvetter, S. Zavatarelli, Phys. Rev. Lett. 82 (1999) 5205-5208.
- [146] N. Kudomi, M. Komori, K. Takahisa, S. Yoshida, K. Kume, H. Ohsumi, T. Itahashi, Phys. Rev. C 69 (2004) 015802 [13 pages].
- [147] A. Csótó, K. Langanke, Nucl. Phys. A 646 (1999) 387-396.
- [148] S. Winkler, H. Krauss, K. Grün, T. Rauscher, H. Oberhummer, H. Abele, G. Staudt, J. Phys. G Nucl. Partic. 18 (1992) L147-L152.
- [149] H.D. Holmgren, R.L. Johnston, Phys. Rev. 113 (1959) 1556-1559.
- [150] P.D. Parker, R.W. Kavanagh, Phys. Rev. 131 (1963) 2578-2582.
- [151] K. Nagatani, M.R. Dwarakanath, D. Ashery, Nucl. Phys. A 128 (1969) 325-332.
- [152] H. Kräwinkel, H.W. Becker, L. Buchmann, J. Görres, K.U. Kettner, W.E. Kieser, R. Santo, P. Schmalbrock, H.P. Trautvetter, A. Vlieks, C. Rolfs, J.W. Hammer, R.E. Azuma, W.S. Rodney, Z. Phys. A 304 (1982) 307-332.
- [153] R.G.H. Robertson, P. Dyer, T.J. Bowles, R.E. Brown, N. Jarmie, C.J. Maggiore, S.M. Austin, Phys. Rev. C 27 (1983) 11-17.
- [154] T.K. Alexander, G.C. Ball, W.N. Lennard, H. Geissel, H.-B. Mak, Nucl. Phys. A 427 (1984) 526-544.
- [155] J.L. Osborne, C.A. Barnes, R.W. Kavanagh, R.M. Kremer, G.J. Mathews, J.L. Zyskind, P.D. Parker, A.J. Howard, Nucl. Phys. A 419 (1984) 115-132.
- [156] M. Hilgemeier, H.W. Becker, C. Rolfs, H.P. Trautvetter, J. W. Hammer, Z. Phys. A 329 (1988) 243-254.
- [157] B.S. Nara Singh, M. Hass, Y. Nir-El, G. Haquin, Phys. Rev. Lett. 93 (2004) 262503 [4 pages].
- [158] D. Bemmerer, F. Confortola, H. Costantini, A. Formicola, Gy. Gyürky, R. Bonetti, C. Broggini, P. Corvisiero, Z. Elekes, Zs. Fülpöp, G. Gervino, A. Guglielmetti, C. Gustavino, G. Imbriani, M. Junker, M. Laubenstein, A. Lemut, B. Limata, V. Lozza, M. Marta, R. Menegazzo, P. Prati, V. Roca, C. Rolfs, C. Rossi Alvarez, E. Somorjai, O. Straniero, F. Terrasi, H.P. Trautvetter, Phys. Rev. Lett. 97 (2006) 122502 [5 pages].
- [159] T.A.D. Brown, C. Bordeanu, K.A. Snover, D.W. Storm, D. Melconian, A.L. Sallaska, S.K.L. Sjue, S. Triambak, Phys. Rev. C 76 (2007) 055801 [12 pages].
- [160] F. Confortola, D. Bemmerer, H. Costantini, A. Formicola, Gy. Gyürky, P. Bezzon, R. Bonetti, C. Broggini, P. Corvisiero, Z. Elekes, Zs. Fülpöp, G. Gervino, A. Guglielmetti, C. Gustavino, G. Imbriani,

- M. Junker, M. Laubenstein, A. Lemut, B. Limata, V. Lozza, M. Marta, R. Menegazzo, P. Prati, V. Roca, C. Rolfs, C. Rossi Alvarez, E. Somorjai, O. Straniero, F. Strieder, F. Terrasi, H.P.Trautvetter, Phys. Rev. C 75 (2007) 065803 [4 pages].
- [161] Gy. Gyürky, F. Confortola, H. Costantini, A. Formicola, D. Bemmerer, R. Bonetti, C. Broggini, P. Corvisiero, Z. Elekes, Zs. Fülop, G. Gervino, A. Guglielmetti, C. Gustavino, G. Imbriani, M. Junker, M. Laubenstein, A. Lemut, B. Limata, V. Lozza, M. Marta, R. Menegazzo, P. Prati, V. Roca, C. Rolfs, C. Rossi Alvarez, E. Somorjai, O. Straniero, F. Strieder, F. Terrasi, H.P. Trautvetter, Phys. Rev. C 75 (2007) 035805 [8 pages].
- [162] H. Costantini, D. Bemmerer, F. Confortola, A. Formicola, Gy. Gyürky, P. Bezzon, R. Bonetti, C. Broggini, P. Corvisiero, Z. Elekes, Zs. Fülop, G. Gervino, A. Guglielmetti, C. Gustavino, G. Imbriani, M. Junker, M. Laubenstein, A. Lemut, B. Limata, V. Lozza, M. Marta, R. Menegazzo, P. Prati, V. Roca, C. Rolfs, C. Rossi Alvarez, E. Somorjai, O. Straniero, F. Strieder, F. Terrasi, H.P. Trautvetter, Nucl. Phys. A 814 (2008) 144-158.
- [163] A. Di Leva, L. Gialanella, R. Kunz, D. Rogalla, D. Schürmann, F. Strieder, M. De Cesare, N. De Cesare, A. D'Onofrio, Z. Fülop, G. Gyürky, G. Imbriani, G. Mangano, A. Ordine, V. Roca, C. Rolfs, M. Romano, E. Somorjai, F. Terrasi, Phys. Rev. Lett. 102 (2009) 232502 [4 pages]; Erratum: Phys. Rev. Lett. 103 (2009) 159903.
- [164] C. Bordeanu, Gy. Gyürky, Z. Halász, T. Szűcs, G.G. Kiss, Z. Elekes, J. Farkas, Zs. Fülop, E. Somorjai, Nucl. Phys. A 908 (2013) 1-11.
- [165] A. Kontos, E. Uberseder, R. deBoer, J. Görres, C. Akers, A. Best, M. Couder, M. Wiescher, Phys. Rev. C 87 (2013) 065804 [9 pages].
- [166] Z.E. Switkowski, J.C.P. Heggie, D.L. Kennedy, D.G. Sargood, F.C. Barker, R.H. Spear, Nucl. Phys. A 331 (1979) 50-60.
- [167] S. Bashkin, R.R. Carlson, Phys. Rev. 97 (1955) 1245-1249.
- [168] R. Ostojić, K. Subotić, B. Stepančić, Nuovo Cim. 76 A (1983) 73-82.
- [169] R. Bruf, O. Arkis, H. Bucka, P. Heide, in: F. Käppeler, K. Wissak, Nuclei in the Cosmos, Inst. Phys. Publ., Bristol, 1993, 169-174.
- [170] T. Paradellis, unpublished (1999), quoted by [177] as ref. 25.
- [171] J.J. He, S.Z. Chen, S.W. Xu, J. Hu, X.W. Ma, L.Y. Zhang, S.Q. Hou, X.Q. Yu, N.T. Zhang, S.B. Ma, Y.H. Zhang, X.H. Zhou, H.S. Xu, G.Q. Xiao, W.L. Zhan, C.E. Rolfs, M. Wiescher, R.J. deBoer, T. Kajino, M. Kusakabe, G. Lan, Proceedings of Science (NIC XII, 2012) 005; J.J. He, Anomaly in the $^6\text{Li}(p,\gamma)^7\text{Be}$ reaction at low energies, VIII Tours Symposium on Nuclear Physics and Astrophysics, Sept. 2-7, 2012, Lenzkirch-Saig, unpublished.
- [172] J.B. Warren, T.K. Alexander, G.B. Chadwick, Phys. Rev. 101 (1956) 242-245.
- [173] R.M. Prior, M.C. Spraker, A.M. Amthor, K.J. Keeter, S.O. Nelson, A. Sabourov, A. Tonchev, M. Ahmed, J.H. Kelley, D.R. Tilley, H.R. Weller, H.M. Hofmann, Phys. Rev. C 70 (2004) 055801 [8 pages].
- [174] F.E. Cecil, D. Ferg, H. Liu, J.C. Scorby, J.A. McNeil, P.D. Kunz, Nucl. Phys. A 539 (1992) 75-96.
- [175] J.J. He, priv. comm. (2013). See Note added in-proof.
- [176] F.C. Barker, Aust. J. Phys. 33 (1980) 159-176.
- [177] K. Arai, D. Baye, P. Descouvemont, Nucl. Phys. A 699 (2002) 963-975.
- [178] J.B. Marion, G. Weber, F.S. Mozer, Phys. Rev. 104 (1956) 1402-1407.
- [179] W. Gemeinhardt, D. Kamke, Chr. von Rhöneck, Z. Phys. 197 (1966) 58-74.
- [180] U. Fasoli, D. Toniolo, G. Zago, Phys. Lett. 8 (1964) 127-128.
- [181] H. Spinka, T. Tombrello, H. Winkler, Nucl. Phys. A 164 (1971) 1-10.
- [182] C.R. Gould, R.O. Nelson, J.R. Williams, J.R. Boyce, Nucl. Sci. Eng. 55 (1974) 267-272.
- [183] C.-S. Lin, W.-S. Hou, M. Wen, J.-C. Chou, Nucl. Phys. A 275 (1977) 93-99.
- [184] A.J. Elwyn, R.E. Holland, C.N. Davids, L. Meyer-Schützmeister, F.P. Mooring, W. Ray, Jr., Phys. Rev. C 20 (1979) 1984-1992.
- [185] T. Shinozuka, Y. Tanaka, K. Sugiyama, Nucl. Phys. A 326 (1979) 47-54.
- [186] J.U. Kwon, J.C. Kim, B.N. Sung, Nucl. Phys. A 493 (1989) 112-123.
- [187] S. Engstler, G. Raimann, C. Angulo, U. Greife, C. Rolfs, U. Schröder, E. Somorjai, B. Kirch, K. Langanke, Z. Phys. A 342 (1992) 471-482; Phys. Lett. B 279 (1992) 20-24.
- [188] O. Fiedler, P. Kunze, Nucl. Phys. A 96 (1967) 513-520.
- [189] A. Tumino, C. Spitaleri, A. Di Pietro, P. Figuera, M. Lattuada, A. Musumarra, M. G. Pellegriti, R. G. Pizzone, S. Romano, C. Rolfs, S. Tudisco, S. Typel, Phys. Rev. C 67 (2003) 065803 [7 pages].
- [190] J. Cruz, Z. Fülop, G. Gyürky, F. Raiola, A. Di Leva, B. Limata, M. Fonseca, H. Luis, D. Schürmann, M. Aliotta, H. W. Becker, A.P. Jesus, K.U. Kettner, J.P. Ribeiro, C. Rolfs, M. Romano, E. Somorjai, F. Strieder, Phys. Lett B 624 (2005) 181-185.

- [191] J. Cruz, H. Luis, M. Fonseca, Z. Fülop, G. Gyürky, F. Raiola, M. Aliotta, K.U. Kettner, A.P. Jesus, J.P. Ribeiro, F.C. Barker, C. Rolfs, *J. Phys. G Nucl. Partic.* 35 (2008) 014004 [4 pages].
- [192] L. Lamia, C. Spitaleri, R.G. Pizzzone, E. Tognelli, A. Tumino, S. degl'Innocenti, P.G. Prada Moroni, M. La Cognata, L. Pappalardo, M.L. Segri, *Astrophys. J.* 768 (2013) 65 [8 pages].
- [193] R.R. Perry, B. Mainsbridge, J. Rickards, *Nucl. Phys.* 45 (1963) 586-592.
- [194] V. Riech, *Phys. Lett.* 6 (1963) 267-268.
- [195] D. Zahnow, C. Angulo, C. Rolfs, S. Schmidt, W.H. Schulte, E. Somorjai, *Z. Phys. A* 351 (1995) 229-236.
- [196] M. Spraker, R.M. Prior, M.A. Godwin, B.J. Rice, E.A. Wulf, J.H. Kelly, D.R. Tilley, H.R. Weller, *Phys. Rev. C* 61 (1999) 015802 [6 pages].
- [197] R.M. Chasteler, H.R. Weller, D.R. Tilley, R.M. Prior, *Phys. Rev. Lett.* 72 (1992) 3949-3952.
- [198] M.A. Godwin, R.M. Chasteler, C.M. Laymon, R.M. Prior, D.R. Tilley, H.R. Weller, *Phys. Rev. C* 53 (1996) R1-R4.
- [199] K.I. Hahn, C.R. Brune, R.W. Kavanagh, *Phys. Rev. C* 53 (1996) 1273-1277.
- [200] M.A. Godwin, C.M. Laymon, R.M. Prior, D.R. Tilley, H.R. Weller, *Phys. Rev. C* 56 (1997) 1605-1612.
- [201] J.M. Sampaio, A.M. Eiró, I.J. Thompson, *Nucl. Phys. A* 688 (2001) 518-520.
- [202] Y. Cassagnou, J.M.F. Jeronymo, G.S. Mani, A. Sadeghi, P.D. Forsyth, *Nucl. Phys.* 33 (1962) 449-457; Erratum: *Nucl. Phys.* 41 (1963) 176.
- [203] G.S. Mani, R. Freeman, F. Picard, A. Sadeghi, D. Redon, *Nucl. Phys.* 60 (1964) 588-592.
- [204] C. Rolfs, R.W. Kavanagh, *Nucl. Phys. A* 455 (1986) 179-188.
- [205] J.F. Harmon, *Nucl. Instrum. Meth. B* 40/41 (1989) 507-509.
- [206] M. Lattuada, R.G. Pizzzone, S. Typel, P. Figuera, D. Miljanić, A. Musumarra, M.G. Pellegriti, C. Rolfs, C. Spitaleri, H.H. Wolter, *Astrophys. J.* 562 (2001) 1076-1080.
- [207] J. Cruz, M. Fonseca, H. Luis, R. Mateus, H. Marques, A.P. Jesus, J.P. Ribeiro, O.M.N.D. Teodoro, C. Rolfs, *Nucl. Instrum. Meth. B* 267 (2009) 478-481.
- [208] G. Raimann, B. Bach, K. Grüne, H. Herndl, H. Oberhummer, S. Engstler, C. Rolfs, H. Abele, R. Neu, G. Staudt, *Phys. Lett. B* 249 (1990) 191-194.
- [209] Y. Yamashita, *Nucl. Phys. A* 582 (1995) 270-282.
- [210] R.G. Pizzzone, C. Spitaleri, L. Lamia, C. Bertulani, A. Mukhamedzanov, L. Blokhintsev, V. Burjan, S. Cherubini, Z. Hons, G.G. Kiss, V. Kroha, M. La Cognata, C. Li, J. Mrazek, Š. Piskoř, S.M.R. Puglia, G.G. Rapisarda, S. Romano, M.L. Sergi, A. Tumino, *Phys. Rec. C* 83 (2011) 045801 [8 pages].
- [211] P. Paul, N.G. Puttaswamy, D. Kohler, *Phys. Rev. B* 164 (1967) 1332-1342.
- [212] G. Hardie, B. W. Filippone, A.J. Elwyn, M. Wiescher, R.E. Segel, *Phys. Rev. C* 29 (1984) 1199-1206.
- [213] G. Gyürky, Z. Fülop, E. Somorjai, G. Kiss, C. Rolfs, *Eur. Phys. J. A* 21 (2004) 355-358.
- [214] J.H. Keley, E. Kwan, J.E. Purcell, C.G. Sheu, H.R. Weller, *Nucl. Phys. A* 880 (2012) 88-195.
- [215] P. Descouvemont, *Nucl. Phys. A* 584 (1995) 532-546.
- [216] R.W. Kavanagh, *Nucl. Phys.* 15 (1960) 411-420.
- [217] P.D. Parker, *Phys. Rev.* 150 (1966) 851-856.
- [218] R.W. Kavanagh, T.A. Tombrello, J.M. Mosher, D.R. Goosman, *Bull. Am. Phys. Soc.* 14 (1969) 1209.
- [219] F.J. Vaughn, R.A. Chalmers, D. Kohler, L.F. Chase, Jr., *Phys. Rev. C* 2 (1970) 1657-1665.
- [220] B.W. Filippone, A.J. Elwyn, C.N. Davids, D.D. Koetke, *Phys. Rev. Lett.* 50 (1983) 412-416.
- [221] B.W. Filippone, A.J. Elwyn, C.N. Davids, D.D. Koetke, *Phys. Rev. C* 28 (1983) 2222-2229.
- [222] F. Hammache, G. Bogaert, P. Aguer, C. Angulo, S. Barhoumi, L. Brillard, J. F. Chemin, G. Claverie, A. Coc, M. Hussonnois, M. Jacotin, J. Kiener, A. Lefebvre, J.N. Scheurer, J.P. Thibaud, E. Virassamynaïken, *Phys. Rev. Lett.* 80 (1998) 928-931.
- [223] C. Wiezorek, H. Kräwinkel, R. Santo, L. Waldek, *Z. Phys. A* 282 (1977) 121-123.
- [224] M. Hass, C. Broude, V. Fedoseev, G. Goldring, G. Huber, J. Lettry, V. Mishin, H.J. Ravn, V. Sebastian, L. Weissman, ISOLDE Collaboration, *Phys. Lett. B* 462 (1999) 237-242.
- [225] F. Hammache, G. Bogaert, P. Aguer, C. Angulo, S. Barhoumi, L. Brillard, J. F. Chemin, G. Claverie, A. Coc, M. Hussonnois, M. Jacotin, J. Kiener, A. Lefebvre, C. Le Naour, S. Ouichaoui, J.N. Scheurer, V. Tatischeff, J.P. Thibaud, E. Virassamynaïken, *Phys. Rev. Lett.* 86 (2001) 3985-3988.
- [226] F. Strieder, L. Gialanella, G. Gyürky, F. Schümann, R. Bonetti, C. Broggini, L. Campajola, P. Corvisiero, H. Costantini, A. D'Onofrio, A. Formicola, Z. Fülop, G. Gervino, U. Greife, A. Guglielmetti, C. Gustavino, G. Imbriani, M. Junker, P.G.P. Moroni, A. Ordine, P. Prati, V. Roca, D. Rogalla, C. Rolfs, M. Romano, E. Somorjai, O. Straniero, F. Terrasi, H.P. Trautvetter, S. Zavatarelli, *Nucl. Phys. A* 696 (2001) 219-230.

- [227] L.T. Baby, C. Bordeanu, G. Goldring, M. Hass, L. Weissman, V.N. Fedoseyev, U. Köster, Y. Nir-El, G. Haquin, H.W. Gäggeler, R. Weinreich, Phys. Rev. C 67 (2003) 065805 [14 pages].
- [228] A.R. Junghans, E.C. Mohrmann, K.A. Snover, T.D. Steiger, E. G. Adelberger, J.M. Casandjian, H.E. Swanson, L. Buchmann, S.H. Park, A. Zyuzin, A.M. Laird, Phys. Rev. C 68 (2003) 065803 [21 pages].
- [229] F. Schümann, S. Typel, F. Hammache, K. Süßerer, F. Uhlig, I. Böttcher, D. Cortina, A. Förster, M. Gai, H. Geissel, U. Greife, E. Grosse, N. Iwasa, P. Koczoń, B. Kohlmeyer, R. Kulessa, H. Kumagai, N. Kurz, M. Menzel, T. Motobayashi, H. Oeschler, A. Ozawa, M. Płoskoń, W. Prokopowicz, E. Schwab, P. Senger, F. Strieder, C. Sturm, Z.-Y. Sun, G. Surówka, A. Wagner, W. Walus, Phys. Rev. C 73 (2006) 015806 [13 pages].
- [230] A.R. Junghans, K.A. Snover, E.C. Mohrmann, E.G. Adelberger, L. Buchmann, Phys. Rev. C 81 (2010) 012801(R) [4 pages].
- [231] T. Motobayashi, N. Iwasa, Y. Ando, M. Kurokawa, H. Murakami, J. Ruan (Gen), S. Shimoura, S. Shirato, N. Inabe, M. Ishihara, T. Kubo, Y. Watanabe, M. Gai, R. H. France, III, K. I. Hahn, Z. Zhao, T. Nakamura, T. Tenanishi, Y. Futami, K. Furutaka, Th. Delbar, Phys. Rev. Lett. 73 (1994) 2680-2683.
- [232] S. Typel, J. Phys. G Nucl. Partic. 35 (2008) 014003 [8 pages].
- [233] P. Descouvemont, D. Baye, Nucl. Phys. A 567 (1994) 341-353.
- [234] P. Descouvemont, Phys. Rev. C 70 (2004) 065802 [10 pages].
- [235] G. Tabacaru, A. Azhari, J. Brinkley, V. Burjan, F. Carstoiu, C. Fu, C.A. Gagliardi, V. Kroha, A.M. Mukhamedzhanov, X. Tang, L. Trache, R.E. Tribble, S. Zhou, Phys. Rev. C 73 (2006) 025808 [6 pages].
- [236] Navrátil, R. Roth, S. Quaglioni, Phys. Lett B 704 (2011) 379-383.
- [237] L. Buchmann, J. M. D'Auria, P. McCorquodale, Astrophys. J. 324 (1988) 953-965.
- [238] W.E. Meyerhof, N.W. Tanner, C.M. Hudson, Phys. Rev. 115 (1959) 1227-1237.
- [239] W.F. Hornyak, C.A. Ludemann, M.L. Roush, Nucl. Phys. 50 (1964) 424-449.
- [240] W. Auwärter, V. Meyer, Nucl. Phys. A 242 (1975) 129-140.
- [241] Y.H. Park, B.N. Sung, C.B. Moon, J.W. Kwon, J.C. Kim, H.C. Bhang, W.H. Chung, S.W. Cho, New Physics (Sae Mulli, Korean Phys. Soc.) 29 (1989) 430-435.
- [242] D. Zahnow, C. Angulo, M. Junker, C. Rolfs, S. Schmidt, W. H. Schulte, E. Somorjai, Nucl. Phys. A 589 (1995) 95-105.
- [243] F.C. Barker, Nucl. Phys. A 697 (2002) 915-934.
- [244] J.A. Neuendorffer, D.R. Inglis, S.S. Hanna, Phys. Rev. 82 (1951) 75-80.
- [245] G. Weber, L.W. Davis, J.B. Marion, Phys. Rev. 104 (1956) 1307-1313.
- [246] G.M. Hudson, G.B. Crinean, D.T. Kelly, B.M. Spicer, Nucl. Phys. A 184 (1972) 175-192.
- [247] A.J. Sierk, T.A. Tombrello, Nucl. Phys. A 210 (1973) 341-354.
- [248] D. Zahnow, C. Rolfs, S. Schmidt, H.P. Trautvetter, Z. Phys. A 359 (1997) 211-218.
- [249] C.R. Brune, W.H. Geist, H.J. Karwowski, E.J. Ludwig, K.D. Veal, Phys. Rev. C 57 (1998) 3437-3446.
- [250] T. Rauscher, K. Grün, H. Krauss, H. Oberhummer, 'Potential resonances in ${}^9\text{Be}(\text{p}, \text{d}) {}^8\text{Be}$ and ${}^9\text{Be}(\text{p}, \alpha) {}^6\text{Li}$ at thermonuclear energies', Wien (1991) unpublished.
- [251] R.B. Day, R.L. Walker, Phys. Rev. 85 (1952) 582-585.
- [252] J.B. Marion, J. S. Levin, Phys. Rev. 115 (1959) 144-149.
- [253] H.R. Bliden, G.M. Temmer, K.L. Warsh, Nucl. Phys. 49 (1963) 209-238.
- [254] T. Yanabu, S. Yamashita, S. Kakigi, D.-C. Nguyen, K. Takimoto, Y. Yamada, K. Ogino, J. Phys. Soc. Japan 19 (1964) 1818-1823.
- [255] S. Morita, T. Tohei, T. Nakagawa, T. Hasegawa, H. Ueno, C.C. Hsu, Nucl. Phys. 66 (1965) 17-24.
- [256] Q.-G. Wen, C.-B. Li, S.-H. Zhou, Q.-Y. Meng, J. Zhou, X.-M. Li, S.-Y. Hu, Y.-Y. Fu, C. Spitaleri, A. Tumino, R.G. Pizzone, G.G. Rapisarda, Phys. Rev. C 78 (2008) 035805 [7 pages].
- [257] J.H. Gibbons, R.L. Macklin, Phys. Rev. 137 (1965) B1508-B1509.
- [258] L. Van der Zwan, K. W. Geiger, Nucl. Phys. A 152 (1970) 481-494.
- [259] K.W. Geiger, L. van der Zwan, Nucl. Instrum. Meth. 131 (1975) 315-321.
- [260] D. Schmidt, R. Böttger, H. Klein, R. Nolte, Physikalisch-Technische Bundesanstalt Braunschweig Report PTB-N-7, PTB-N-8 (1992).
- [261] P.R. Wrean, C.R. Brune, R.W. Kavanagh, Phys. Rev. C 49 (1994) 1205-1213.
- [262] R. Kunz, S. Barth, A. Denkter, H.W. Drotleff, J.W. Hammer, H. Knee, A. Mayer, Phys. Rev. C 53 (1996) 2486-2495.
- [263] S. Cierjacks, F. Hinterberger, G. Schmalz, D. Erdbe, P. van Rossen, B. Leugers, Nucl. Instrum. Meth. 169 (1980) 185-198.

- [264] H.M. Kuan, M. Hasinoff, W.J. O'Connell, S.S. Hanna, Nucl. Phys. A 151 (1970) 129-153.
- [265] M. Wiescher, R.N. Boyd, S.L. Blatt, L.J. Rybarcyk, J.A. Spizuoco, R.E. Azuma, E.T. H. Clifford, J.D. King, J. Görres, C. Rolfs, A. Vlieks, Phys. Rev. C 28 (1983) 1431-1442.
- [266] A.P. Tonchev, S.O. Nelson, K. Sabourov, B.T. Crowley, K. Joshi, H.R. Weller, J.H. Kelley, R.M. Prior M. Spraker, N. Kalantar-Nayestanaki, Phys. Rev. C 68 (2003) 045803 [12 pages]. *Note:* Eq.(15) of this reference contains trivial and non-trivial typographical errors.
- [267] W.E. Burcham, J.M. Freeman, Philosoph. Mag. 41 (1950) 337-348.
- [268] A.B. Brown, C.W. Snyder, W.A. Fowler, C.C. Lauritsen, Phys. Rev. 82 (1951) 159-181.
- [269] J.G. Jenkin, L.G. Earwaker, E.W. Titterton, Nucl. Phys. 50 (1964) 516-524.
- [270] J. Szabó, J. Csikai, M. Várnagy, Nucl. Phys. A 195 (1972) 527-533.
- [271] N.A. Roughton, M.R. Fritts, R.J. Peterson, C.S. Zaidins, C.J. Hansen, At. Data Nucl. Data 23 (1979) 177-194.
- [272] M. Youn, H.T. Chung, J.C. Kim, H.C. Bhang, K.-H. Chung, Nucl. Phys. A 533 (1991) 321-332.
- [273] F. Knape, H. Bucka, P. Heide, in: F. Käppeler, K. Wissak (Eds.), Proc. Second Int. Symp. on Nuclear Astrophysics: Nuclei in the Cosmos, Karlsruhe, Germany, July 6-10, 1992 (IOP Publ., Bristol, 1993), pp. 175-180.
- [274] C. Angulo, S. Engstler, G. Raimann, C. Rolfs, W.H. Schulte, E. Somorjai, Z. Phys. A 345 (1993) 231-242.
- [275] L. Lamia, S.M.R. Puglia, C. Spitaleri, S. Romano, M. G. Del Santo, N. Carlin, M. Gameiro Munhoz, S. Cherubini, G.G. Kiss, V. Kroha, S. Kubono, M. La Cognata, C.-B. Li, R.G. Pizzone, Q.-G. Wen, M.L. Sergi, A. Szanto de Toledo, Y. Wakabayashi, H. Yamaguchi, S.-H. Zhou Nucl. Phys. A 834 (2010) 655c-657c.
- [276] S.M.R. Puglia, S. Romano, M.G. Del Santo, L. Lamia, C. Spitaleri, N. Carlin, S. Cherubini, M. Gulino, V. Kroha, S. Kubono, M. La Cognata, C. Li, R.G. Pizzone, M.G. Munhoz, W. Qungang, G.G. Rapisarda, M. L. Sergi, E. Somoryai, F.A. Souza, A. Szanto de Toledo, S. Tudisco, A. Tumino, Y. Wakabayashi, H. Yamaguchi, Mem. S. A. It. Suppl. 14 (2010) 43-46.
- [277] L. Lamia, S. Romano, N. Carlin, S. Cherubini, V. Crucillà, M.M. De Moura, M.G. Del Santo, M.G. Munhoz, M. Gulino, R. Ligouri Neto, M. La Cognata, F. Mudo, R.G. Pizzone, S.M.R. Puglia, M.L. Sergi, F.A. Souza, C. Spitaleri, A.A.P. Suaide, E. Szanto, A. Szanto de Toledo, S. Tudisco, A. Tumino, Nucl. Phys. A 787 (2007) 309c-314c.
- [278] M. Freer, N.L. Achour, C. Angulo, N.L. Ashwood, D.W. Bardayan, S. Brown, W.N. Catford, K.A. Chipps, N. Curtis, P. Demaret, C. Harlin, B. Laurent, J.D. Malcolm, M. Milin, T. Munoz-Britton, N.A. Orr, S.D. Pain, D. Price, R. Raabe, N. Soić, J.S. Thomas, C. Wheldon, G. Wilson, V.A. Ziman, Phys. Rev. C 85 (2012) 014304 [7 pages]; M. Freer, private communication (2012).
- [279] T. Rauscher, G. Raimann, Phys. Rev. C 53 (1996) 2496-2504.
- [280] T. Huus, R.B. Day, Phys. Rev. 91 (1953) 599-605.
- [281] R.G. Allas, S.S. Hanna, L. Meyer-Schützmeister, R.E. Segel, Nucl. Phys. 58 (1964) 122-144.
- [282] R.E. Segel, S.S. Hanna, R.G. Allas, Phys. Rev. 139 (1965) B818-B830.
- [283] J.H. Kelley, R.S. Canon, S.J. Gaff, R.M. Prior, B.J. Rice, E.C. Schreiber, M. Spraker, D.R. Tilley, E.A. Wulf, H.R. Weller, Phys. Rev. C 62 (2000) 025803 [6 pages].
- [284] J.M. Davidson, H.L. Berg, M.M. Lowry, M.R. Dwarakanath, A.J. Sierk, P. Batay-Csorba, Nucl. Phys. A 315 (1979) 253-268.
- [285] H.W. Becker, C. Rolfs, H.P. Trautvetter, Z. Phys. A 327 (1987) 341-355.
- [286] L. Lamia, C. Spitaleri, V. Burjan, N. Carlin, S. Cherubini, V. Crucilla, M.G. Munhoz, M. G. Del Santo, M. Gulino, Z. Hons, G.C. Kiss, V. Kroha, S. Kubono, M. La Cognata, C. Li, J. Mrazek, A. Mukhamedzanov, R.G. Pizzone, S.M.R. Puglia, Q. Wen, G.G. Rapisarda, C. Rolfs, S. Romano, M.L. Sergi, E. Somorjai, F.A. Souza, A. S. de Toledo, G. Tabacaru, A. Tumino, Y. Wakabayashi, H. Yamaguchi, S.-H. Zhou, J. Phys. G: Nucl. Par. Phys. 39 (2012) 015106 [23 pages].
- [287] R. E. Segel, B. J. Bina, Phys. Rev. 124 (1961) 814-817.
- [288] B.D. Anderson, M.R. Dwarakanath, J.S. Schweitzer, A.V. Nero, Nucl. Phys. A 233 (1974) 286-296.
- [289] L. Van der Zwan, K.W. Geiger, Nucl. Phys. A 246 (1975) 93-103.
- [290] T.R. Wang, R.B. Vogelaar, R.W. Kavanagh, Phys. Rev. C 43 (1991) 883-896; Erratum: Phys. Rev. C 44 (1992) 1226.
- [291] M. Niecke, M. Niemeier, R. Weigel, H. Wirzba-Lorenz, Nucl. Phys. A 289 (1977) 408-424.
- [292] C.L. Bailey, W.R. Stratton, Phys. Rev. 77 (1950) 194-196.
- [293] R.N. Hall, W.A. Fowler, Phys. Rev. 77 (1950) 197-204.
- [294] W.A. S. Lamb, R.E. Hester, Phys. Rev. 107 (1957) 550-553.
- [295] J.L. Vogl, Radiative capture of protons by C¹² and C¹³ below 700 keV, PhD thesis, California Inst. Tech (1963) unpublished.

- [296] C. Rolfs, R.E. Azuma, Nucl. Phys. A 227 (1974) 291-308.
- [297] D.F. Hebbard, J.L. Vogl, Nucl. Phys. 21 (1960) 652-675.
- [298] N. Burtebaev, S.B. Igamov, R.J. Peterson, R. Yarmukhamedov, D.M. Zazulin, Phys. Rev. C 78 (2008) 035802 [11 pages].
- [299] M. Dufour, P. Descouvemont, Phys. Rev. C 56 (1997) 1831-1839.
- [300] K. Langanke, O.S. Van Roosmalen, W.A. Fowler, Nucl. Phys. A 435 (1985) 657-668.
- [301] P. Dyer, C.A. Barnes, Nucl. Phys. A 233 (1974) 495-520.
- [302] A. Redder, H.W. Becker, C. Rolfs, H.P. Trautvetter, T.R. Donoghue, T.C. Rinckel, J.W. Hammer, K. Langanke, Nucl. Phys. A 462 (1987) 385-412.
- [303] R.M. Kremer, C.A. Barnes, K.H. Chang, H.C. Evans, B.W. Filippone, K.H. Hahn, L.W. Mitchell, Phys. Rev. Lett. 60 (1988) 1475-1478.
- [304] J.M.L. Ouellet, M.N. Butler, H.C. Evans, H.W. Lee, J.R. Leslie, J.D. MacArthur, W. McLatchie, H.-B. Mak, P. Skensved, J.L. Whitton, X. Zhao, T.K. Alexander, Phys. Rev. C 54 (1996) 1982-1998.
- [305] G. Roters, C. Rolfs, F. Strieder, H.P. Trautvetter, Eur. Phys. J. A 6 (1999) 451-461.
- [306] L. Gialanella, D. Rogalla, F. Strieder, S. Theis, G. Gyürki, C. Agodi, R. Alba, M. Aliotta, L. Campajola, A. Del Zoppo, A. D'Onofrio, P. Figuera, U. Greife, G. Imbriani, A. Ordine, V. Roca, C. Rolfs, M. Romano, C. Sabbarese, P. Sapienza, F. Schümann, E. Somorjai, F. Terrasi, H.P. Trautvetter, Eur. Phys. J. A 11 (2001) 357-370.
- [307] R. Kunz, M. Jaeger, A. Mayer, J.W. Hammer, G. Staudt, S. Harissopoulos, T. Paradellis, Phys. Rev. Lett. 86 (2001) 3244-3247.
- [308] M. Fey, Im Brennpunkt der Nuclearen Astrophysik: Die Reaktion $^{12}\text{C}(\alpha, \gamma) ^{16}\text{O}$, PhD Thesis, Institut für Strahlenphysik, Universität Stuttgart (2004), unpublished.
- [309] D. Schürmann, A. Di Leva, L. Gialanella, D. Rogalla, F. Strieder, N. De Cesare, A. D'Onofrio, G. Imbriani, R. Kunz, C. Lubritto, A. Ordine, V. Roca, C. Rolfs, M. Romano, F. Schümann, F. Terrasi, H.P. Trautvetter, Eur. Phys. J. A 26 (2005) 301-305.
- [310] M. Assunção, M. Fey, A. Lefebvre-Schuhl, J. Kiener, V. Tatischeff, J.W. Hammer, C. Beck, C. Boukari-Pelissie, A. Coc, J.J. Correia, S. Courtin, F. Fleurot, E. Galanopoulos, C. Grama, F. Haas, F. Hammache, F. Hannachi, S. Harissopoulos, A. Korichi, R. Kunz, D. LeDu, A. Lopez-Martens, D. Malcherek, R. Meunier, Th. Paradellis, M. Rousseau, N. Rowley, G. Staudt, S. Szilner, J.P. Thibaud, J. L. Weil, Phys. Rev. C 73 (2006) 055801 [19 pages].
- [311] H. Makii, Y. Nagai, T. Shima, M. Segawa, K. Mishima, H. Ueda, M. Igashira, T. Ohsaki, Phys. Rev. C 80 (2009) 065802 [16 pages].
- [312] D. Schürmann, A. Di Leva, L. Gialanella, R. Kunz, F. Strieder, N. De Cesare, M. De Cesare, A. D'Onofrio, K. Fortak, G. Imbriani, D. Rogalla, M. Romano, F. Terrasi, Phys. Lett B (2011) 557-561; D. Schürmann, private communication (2012).
- [313] R. Plag, R. Reifarth, M. Heil, F. Käppeler, G. Rupp, F. Voss, K. Wisshak, Phys. Rev. C 86 (2012) 015805 [9 pages].
- [314] K.U. Kettner, H.W. Becker, L. Buchmann, J. Görres, H. Kräwinkel, C. Rolfs, P. Schmalbrock, H.P. Trautvetter and A. Vlieks, Z. Phys. A 308 (1982) 73-94.
- [315] R. Kunz, $^{12}\text{C}(\alpha, \gamma) ^{16}\text{O}$ – Die Schlüsselreaktion im Heliumbrennen der Sterne, PhD thesis, Univ. Stuttgart (2002) unpublished.
- [316] C. Matei, L. Buchmann, W.R. Hannes, D.A. Hutcheon, C. Ruiz, C.R. Brune, J. Caggiano, A.A. Chen, J. D'Auria, A. Laird, M. Lamey, ZH. Li, WP. Liu, A. Olin, D. Ottewell, J. Pearson, G. Ruprecht, M. Trinczek, C. Vockenhuber, C. Wrede, Phys. Rev. Lett 97 (2006) 242503 [4 pages].
- [317] L.R. Buchmann, C.A. Barnes, Nucl. Phys. A 777 (2006) 254-290.
- [318] D. Schürmann, L. Gialanella, R. Kunz, F. Strieder, Phys. Lett. B 711 (2012) 35-40.
- [319] D.R. Tilley, H.R. Weller, C.M. Cheves, Nucl. Phys. A 564 (1993) 1-183.
- [320] M. Gai, Experimental determination of the $^{12}\text{C}(\alpha, \gamma) ^{16}\text{O}$ rates, VIII Tours Symposium on Nuclear Physics and Astrophysics, Sept. 2-7, 2012, Lenzkirch-Saig, unpublished; see also Proc. Int. Workshop on Thermonuclear Reaction Rates for Astrophysics Applications, Athens, Nov. 24-25, 2011: http://libra.inp.demokritos.gr/THERRAA/presentations_workshop.html
- [321] R.E. Azuma, L. Buchmann, F.C. Barker, C. A. Barnes, J.M. D'Auria, M. Dombsky, U. Giesen, K.P. Jackson, J.D. King, R.G. Korteling, P. McNeely, J. Powell, G. Roy, J. Vincent, T.R. Wang, S.S.M. Wong, P.R. Wrean, Phys. Rev. C 50 (1994) 1194-1216.
- [322] P. Tischhauser, R.E. Azuma, L. Buchmann, R. Detwiler, U. Giesen, J. Görres, M. Heil, J. Hinserfeld, F. Käppeler, J.J. Kolata, H. Schtz, A. Shotter, E. Stech, S. Vouzoukus, M. Wiescher, Phys. Rev. Lett. 88 (2002) 072501 [4 pages].
- [323] R.H. France III, E.L. Wilds, J.E. McDonald, M. Gai, Phys. Rev C 75 (2007) 065802 [7 pages].
- [324] P. Tischhauser, A. Couture, R. Detwiler, J. Görres, C. Ugalde, E. Stech, M. Wiescher, M. Heil, F.

- Käppeler, R.E. Azuma, L. Buchmann, Phys. Rev. C 79 (2009) 055803 [12 pages].
- [325] X.D. Tang, K.E. Rehm, I. Ahmad, C.R. Brune, A. Champagne, J.P. Greene, A. Hecht, D. J. Henderson, R.V.F. Janssens, C.L. Jiang, L. Jisonna, D. Kahl, E.F. Moore, M. Notani, R.C. Pardo, N. Patel, M. Paul, G. Savard, J.P. Schiffer, R.E. Segel, S. Sinha, A.H. Wuosmaa, Phys. Rev. C 81 (2010) 045809 [14 pages].
- [326] N. Oulebsir, F. Hammanche, P. Roussel, M.G. Pellegriti, L. Audouin, D. Beaumel, A. Bouda, P. Descouvemont, S. Fortier, L. Gaudefroy, J. Kiener, A. Lefebvre-Schahl, V. Tatischeff, Phys. Rev. C 85 (2012) 035804 [8 pages].
- [327] R.E. Hester, W.A.S. Lamb, Phys. Rev. 121 (1961) 584-586.
- [328] J.D. King, R.E. Azuma, J.B. Vise, J. Görres, C. Rolfs, H.P. Trautvetter, A. E. Vlieks, Nucl. Phys. A 567 (1994) 354-376.
- [329] G. Genard, P. Descouvemont, G. Terwagne, J. Phys.: Conf. Ser. 202 (2010) 012015 [4 pages].
- [330] E.J. Woodbury, W.A. Fowler, Phys. Rev. 85 (1952) 51-57.
- [331] J.P. Seagrave, Phys. Rev. 85 (1952) 197-203.
- [332] H.H. Woodbury, R.H. Day, A.V. Tollestrup, Phys. Rev. 92 (1953) 1199-1206.
- [333] R.W. Detenbeck, J.C. Armstrong, A.S. Figuera, J.B. Marion, Nucl. Phys. 72 (1965) 552-576.
- [334] W. Biesiot, Ph.B. Smith, Phys. Rev. C 24 (1981) 2443-2457.
- [335] C. Pruneau, M.B. Chatterjee, C. Rangacharyulu, C. St-Pierre, Can. J. Phys. 63 (1985) 1141-1147,
- [336] F. Zijderland, C. van der Leun, Nucl. Phys. A 460 (1986) 181-200.
- [337] A.M. Mukhamedzhanow, A. Azhari, V. Burjan, C.A. Gagliardi, V. Kroha, A. Sattarov, X. Tang, L. Trache, R.E. Tribble, Phys. Rev. C 66 (2002) 027602 [4 pages].
- [338] K.K. Sekharan, A.S. Divatia, M.K. Mehta, S.S. Kerekatte, K.B. Nambiar, Phys. Rev. 156 (1967) 1187-1190.
- [339] C.N. Davids, Nucl. Phys. A 110 (1968) 619-636.
- [340] J.K. Bair, F.X. Haas, Phys. Rev. C 7 (1973) 1356-1364.
- [341] H.W. Drotleff, A. Denker, H. Knee, M. Soiné, G. Wolf, J.W. Hammer, U. Greife, C. Rolfs, H.P. Trautvetter, Astrophys. J. 414 (1993) 735-739.
- [342] C.R. Brune, I. Licot, R.W. Kavanagh, Phys. Rev. C 48 (1993) 3119-3121.
- [343] S. Harissopoulos, H.W. Becker, J.W. Hammer, A. Lagoyannis, C. Rolfs, F. Strieder, Phys. Rev. C 72 (2005) 062801 (R) [5 pages].
- [344] M. Heil, R. Detwiler, R.E. Azuma, A. Couture, J. Daly, J. Görres, F. Käppeler, R. Reifarth, P. Tischhauser, C. Ugalde, M. Wiescher, Phys. Rev. C 78 (2008) 025803 [17 pages].
- [345] M. Dufour, P. Descouvemont, Phys. Rev. C 72 (2005) 015801 [7 pages].
- [346] S. Kubono, K. Abe, S. Kato, T. Teranishi, M. Kurokawa, X. Liu, N. Imai, K. Kumagai, P. Strasser, M. H. Tanaka, Y. Fuchi, C.S. Lee, Y.K. Kwon, L. Lee, J.H. Ha, Y.K. Kim, Phys. Rev. Lett. 90 (2003) 062501 [4 pages].
- [347] N. Keeley, K.W. Kemper, D.T. Khoa, Nucl. Phys. A 726 (2003) 159-172.
- [348] E.D. Johnson, G.V. Rogachev, A.M. Mukhamedzhanov, L.T. Baby, S. Brown, W. Cluff, A.M. Crisp, E. Diffenderfer, V.Z. Goldberg, B.W. Green, T. Hanners, C.R. Hoffman, K.W. Kemper, O. Momotyuk, P. Peplowski, A. Pipidis, R. Reynolds, B.T. Roeder, Phys. Rev. Lett. 97 (2006) 192701 [4 pages].
- [349] M.G. Pellegriti, F. Hammache, P. Roussel, L. Audouin, D. Beaumel, P. Descouvemont, S. Fortier, L. Gaudefroy, J. Kiener, A. Lefebvre-Schuhl, M. Stanoiu, V. Tatischeff, M. Vilimay, Phys. Rev. C 77 (2008) 042801 (R) [5 pages].
- [350] B. Guo, Z.H. Li, M. Lugaro, J. Buntain, D.Y. Pang, Y.J. Li, J. Su, S.Q. Yan, X.X. Bai, Y.S. Chen, Q.W. Fan, S.J. Jin, A.I. Karakas, E.T. Li, Z.C. Li, G. Lian, J.C. Liu, X. Liu, J.R. Shi, N.C. Shu, B.X. Wang, Y.B. Wang, S. Zeng, W.P. Liu, Astrophys. J. 756 (2012) 193 [10 pages].
- [351] M. La Cognata, C. Spitaleri, O. Trippella, G.G. Kiss, G.V. Rogachev, A.M. Mukhamedzhanov, M. Avila, G.L. Guarado, E. Koschchiy, A. Kuchera, L. Lamia, S.M. Puglia, S. Romano, D. Santiago, R. Spartà, Phys. Rev. Lett. 109 (2012) 232701 [5 pages].
- [352] T.E. Chupp, R.T. Kouzes, A.B. McDonald, P.D. Parker, T.F. Wang, A. Howard, Phys. Rev. C 31 (1985) 1023-1025.
- [353] P. Decrock, Th. Delbar, W. Galster, M. Huyse, P. Leleux, I. Licot, E. Liénard, P. Lipnik, C. Michotte, P. Van Duppen, J. Vanhorenbeek, J. Vervier, Phys. Lett. B 304 (1993) 50-54.
- [354] P.V. Magnus, E.G. Adelberger, A. García, Phys. Rev. C 49 (1994) R1755-R1758.
- [355] P.B. Fernandez, E.G. Adelberger, A. García, Phys. Rev. C 40 (1989) 1887-1900.
- [356] M.S. Smith, P.V. Magnus, K.I. Hahn, R.M. Curley, P.D. Parker, T.F. Wang, K.E. Rehm, P.B. Fernandez, S.J. Sanders, A. García, E.G. Adelberger, Phys. Rev. C 47 (1993) 2740-2750.
- [357] T. Motobayashi, T. Takei, S. Kox, C. Perrin, F. Merchez, D. Rebreyend, K. Ikei, H. Murakami, Y.

- Ando, N. Iwasa, M. Kurokawa, S. Shirato, J. Ruan (Gen), T. Ichihara, T. Kubo, N. Inabe, A. goto, S. Kubono, S. Shimoura, M. Ishihara, Phys. Lett. B 264 (1991) 259-264.
- [358] J. Kiener, A. Lefebvre, P. Auger, C.O. Bacri, R. Bimbot, G. Bogaert, B. Borderie, F. Clapier, A. Coc, D. Disdier, S. Fortier, C. Grunberg, L. Kraus, L. Linck, G. Pasquier, M.F. Rivet, F.St. Laurent, C. Stephan, L. Tassan-Got, J.P. Thibaud, Nucl. Phys. A 552 (1993) 66-81.
- [359] P. Decrock, M. Gaelens, M. Huyse, G. Reusen, G. Vancracynest, P. Van Duppen, J. Wauters, T, Delbar, W. Galster, P. Leluex, I. Licot, E. Liénard, P. Lipnik, C. Michotte, J. Vervier, H. Oberhummer, Phys. Rev. C 48 (1993) 2057-2067.
- [360] P. Descouvemont, Nucl. Phys. A 646 (1999) 261-273.
- [361] W.A.S. Lamb, R.E. Hester, Phys. Rev. 108 (1957) 1304-1307.
- [362] R.E. Pixley, "The reaction cross section of nitrogen 14 for protons between 220 keV and 600 keV", Ph.D. thesis, California Institute of Technology (1957), unpublished,
- [363] D.F. Hebbard, G.M. Bailey, Nucl. Phys. 49 (1963) 666-685.
- [364] U. Schröder, H.W. Becker, G. Bogaert, J. Görres, C. Rolfs, H.P. Trautvetter, R.E. Azuma, C. Campbell, J.D. King, J. Vise, Nucl. Phys. A 467 (1987) 240-260; corrected for summing effects (see citeTR05).
- [365] H.P. Trautvetter, private communication (2005).
- [366] A. Formicola, G. Imbriani, H. Constantini, C. Angulo, D. Bemmerer, R. Bonetti, C. Broggini, P. Corvisiero, J. Cruz, P. Descouvemont, Z. Fülpöp, G. Gervino, A. Guglielmetti, C. Gustavino, G. Gyürky, A.P. Jesus, M. Junker, A. Lemut, R. Menegazzo, P. Prati, V. Roca, C. Rolfs, M. Romano, C. Rossi Alvarez, E. Schümann, E. Somorjai, O. Straniero, F. Strieder, T. Terrasi, H.P. Trautvetter, A. Vomiero, S. Zavatarelli, Phys. Lett. B 591 (2004) 61-68.
- [367] G. Imbriani, H. Costantini, A. Formicola, A. Vomiero, C. Angulo, D. Bemmerer, R. Bonetti, C. Broggini, F. Confortola, P. Corvisiero, J. Cruz, P. Descouvemont, Z. Fülpöp, G. Gervino, A. Guglielmetti, C. Gustavino, Gy. Gyürky, A.P. Jesus, M. Junker, J.N. Klug, A. Lemut, R. Menegazzo, P. Prati, V. Roca, C. Rolfs, M. Romano, C. Rossi-Alvarez, F. Schümann, D. Schürmann, E. Somorjai, O. Straniero, F. Strieder, F. Terrasi, H.P. Trautvetter, Eur. Phys. J. A 25 (2005) 455-466.
- [368] R.C. Runkle, A.E. Champagne, C. Angulo, C. Fox, C. Iliadis, R. Longland, J. Pollanen, Phys. Rev. Lett. 94 (2005) 082503 [4 pages]; A.E. Champagne, private communication (2005).
- [369] D. Bemmerer, F. Confortola, A. Lemut, R. Bonetti, C. Broggini, P. Corvisiero, H. Costantini, J. Cruz, A. Formicola, Zs. Fülpöp, G. Gervino, A. Guglielmetti, C. Gustavino, Gy. Gyürky, G. Imbriani, A. Jesus, M. Junker, B. Limata, R. Menegazzo, P. Prati, V. Roca, C. Rolfs, D. Rogalla, M. Romano, C. Rossi Alvarez, F. Schümann, E. Somorjai, O. Straniero, F. Strieder, F. Terrasi, H.P. Trautvetter, Nucl. Phys. A 779 (2006) 297-317.
- [370] A. Lemut, D. Bemmerer, F. Confortola, R. Bonetti, C. Broggini, P. Corvisiero, H. Costantini, J. Cruz, A. Formicola, Zs. Fülpöp, G. Gervino, A. Guglielmetti, C. Gustavino, Gy. Gyürky, G. Imbriani, A.P. Jesus, M. Junker, B. Limata, R. Menegazzo, P. Prati, V. Roca, D. Rogalla, C. Rolfs, M. Romano, C. Rossi Alvarez, F. Schümann, E. Somorjai, O. Straniero, F. Strieder, F. Terrasi, H.P. Trautvetter, Phys. Lett. B 634 (2006) 483-487.
- [371] M. Marta, A. Formicola, Gy. Gyürky, D. Bemmerer, C. Broggini, A. Caciolli, P. Corvisiero, H. Costantini, Z. Elekes, Zs. Fülpöp, G. Gervino, A. Guglielmetti, C. Gustavino, Gy. Gyürky, G. Imbriani, M. Junker, R. Kunz, A. Lemut, B. Limata, C. Mazzocchi, R. Menegazzo, P. Prati, V. Roca, C. Rolfs, M. Romano, C. Rossi Alvarez, E. Somorjai, O. Straniero, F. Strieder, F. Terrasi, H.P. Trautvetter, A. Vomiero, Phys. Rev. C 78 (2008) 022802(R) [4 pages].
- [372] C. Angulo, P. Descouvemont, Nucl. Phys. A 690 (2001) 755-768.
- [373] A.M. Mukahmedzhanov, P. Bém, B.A. Brown, V. Burjan, C. Gagliardi, V. Kroha, J. Novák, F.M. Nunes, Š. Piskoř, F. Pirlepesov, E. Šimečková, R. Tribble, J. Vincour, Phys. Rev. C 67 (2003) 065804 [7 pages]; Publisher's Note: Phys. Rev C 68 (2003) 019901.
- [374] D.B. Duncan, J.E. Perry, Phys. Rev. 82 (1951) 809-813.
- [375] G. W. Phillips, P. Richard, D.O. Elliott, F.F. Hopkins, A.C. Porter, Phys. Rev. C 5 (1972) 297-306.
- [376] H.M. Kuan, D.G. Shirk, S. Fiarmann, Phys. Rev. C 15 (1977) 569-572.
- [377] J. Grinevicture, D. Holderson, J. Phys. G: Nucl. Part. Phys. 35 (2008) 055201 [13 pages].
- [378] C. Rolfs, W. S. Rodney, Nucl. Phys. A 235 (1974) 450-459.
- [379] D. Bemmerer, A. Caciolli, R. Bonetti, C. Broggini, F. Confortola, P. Corvisiero, H. Costantini, Z. Elekes, A. Formicola, Zs. Fülpöp, G. Gervino, A. Guglielmetti, C. Gustavino, Gy. Gyürky, M. Junker, B. Limata, M. Marta, R. Menegazzo, P. Prati, V. Roca, C. Rolfs, C. Rossi Alvarez, E. Somorjai, O. Straniero, J. Phys. G Nucl. Partic. 36 (2009) 045202 [10 pages].
- [380] P.J. LeBlanc, G. Imbriani, J. Görres, M. Junker, R. Azuma, M. Beard, D. Bemmerer, A. Best, C. Broggini, A. Caciolli, P. Corvisiero, H. Constantini, M. Couder, R. deBoer, Z. Elekes, S. Falahat,

- A. Formicola, Zs. Fülop, G. Gervino, A. Guglielmetti, G. Gustavino, Gy. Gyürky, F. Käppeler, A. Kontos, R. Kuntz, H. Leiste, A. Lemut, Q. Li, B. Limata, M. Marta, C. Mazzocchi, R. Menegazzo, S. O'Brien, A. Palumbo, P. Prati, C. Rolfs, C. Rossi Alvarez, E. Somarjai, E. Stech, O. Straniero, F. Strieder, W. Tan, F. Terrasi, H.P. Trautvetter, E. Uberseder, M. Wiescher, Phys. Rev. C 82 (2010) 055804 [10 pages]; Erratum: Phys. Rev. C 84 (2011) 019902(E).
- [381] A. Caciolli, C. Mazzocchi, V. Capogrosso, D. Bemmerer, C. Broggini, P. Corvisiero, H. Constantini, Z. Elkers, A. Formicola, Zs. Fülop, G. Gervino, A. Guglielmetti, G. Gustavino, Gy. Gyürky, G. Imbriani, M. Junker, A. Lemut, M. Marta, R. Menegazzo, S. Palmerini, P. Prati, V. Roca, C. Rolfs, C. Rossi Alvarez, E. Somarjai, O. Straniero, F. Strieder, F. Terrasi, H.P. Trautvetter, A. Vomiero, Astron. Astrophys. 533 (2011) A66 [6 pages].
- [382] D.F. Hebbard, Nucl. Phys. 15 (1960) 289-315.
- [383] A.M. Mukhamedzhanov, P. Bém, V. Burjan, C.A. Gagliardi, V.Z. Goldberg, Z. Hons, M. La Cognata, V. Kroha, J. Mrázek, J. Novák, Š. Piskoř, R. G. Pizzone, A. Plunkett, S. Romano, E. Šimečková, C. Spitaleri, L. Trache, R. E. Tribble, E. Veselý, J. Vincour, Phys. Rev. C 78 (2008) 015804 [8 pages].
- [384] F.B. Hagedorn, Phys. Rev. 108 (1957) 735-743.
- [385] S. Gorodetzky, J.C. Adloff, F. Brochard, P. Chevallier, D. Disdier, Ph. Gorodetzky, R. Modjtahed-Zadeh, F. Scheibling, Nucl. Phys., A 113 (1968) 221-232.
- [386] G. Imbriani, R.J. deBoer, A. Best, M. Couder, G. Gervino, J. Görres, P.J. LeBlanc, H. Leiste, A. Lemut, E. Stech, F. Strieder, E. Uberseder, M. Wiescher, Phys. Rev. C 85 (2012) 065810 [6 pages]; Erratum: Phys. Rev. C 86 (2012) 039902.
- [387] A. Schardt, W.A. Fowler, C.C. Lauritsen, Phys. Rev. 86 (1952) 527-535.
- [388] J.L. Zyskind, P.D. Parker, Nucl. Phys. A 320 (1979) 404-412.
- [389] A. Redder, H.W. Becker, H. Lorenz-Wirzba, C. Rolfs, P. Schmalbrock, H.P. Trautvetter, Z. Phys. A 305 (1982) 325-333.
- [390] M. La Cognata, S. Romano, C. Spitaleri, S. Cherubini, V. Crucillà, M. Gulino, L. Lamia, R.G. Pizzone, A. Tumino, R. Tribble, C. Fu, V.Z. Goldberg, A.M. Mukhamedzhanov, D. Schmidt, G. Tabacaru, L. Trache, B.F. Irgaziev, Phys. Rev. C 76 (2007) 065804 [15 pages].
- [391] S. Bashkin, R.R. Carlson, R.A. Douglas, Phys. Rev 114 (1959) 1543-1551.
- [392] M. La Cognata, V.Z. Goldberg, A.M. Mukhamedzhanov, C. Spitaleri, R. Tribble, Phys. Rev. C 80 (2009) 012801(R) [5 pages].
- [393] F. C. Barker, Phys. Rev. C 78 (2008) 044611 [5 pages].

Note added in-proof: The details of Ref. [175] are now available, for which see J.J. He, S.Z. Chen, C.E. Rolfs, S.W. Xu, J. Hu, X.W. Ma, M. Wiescher, R.J. deBoer, T. Kajino, M. Kusakabe, L.Y. Zhang, S.Q. Hou, X.Q. Yu, N.T. Zhang, G. Lian, Y.H. Zhang, X.H. Zhou, H.S. Xu, G.Q. Xiao, W.L. Zhan, Phys. Lett. B 725 (2013) 287-291.